NASA CR-123998
SAI 71-559-LJ

ELECTRON TRANSPORT AND SPACE SHIELDING HANDBOOK

FINAL REPORT

by

D. C. Shreve and J. A. Lonergan

Prepared for

NATIONAL AERONAUTICS AND SPACE ADMINISTRATION

14 November 1971

CONTRACT NAS-826753

SCIENCE APPLICATIONS, LA JOLLA, CALIFORNIA
ALBUQUERQUE • ANN ARBOR • ARLINGTON • BOSTON • CHICAGO • HUNTSVILLE • LOS ANGELES
PALO ALTO • ROCKVILLE • SUNNYVALE • TUCSON

P.O. Box 2351, 1250 Prospect Street, La Jolla, California 92037

NASA CR-
SAI 71-559-LJ

FINAL REPORT

ELECTRON TRANSPORT AND SPACE SHIELDING HANDBOOK

by

D. C. Shreve and J. A. Lonergan

SCIENCE APPLICATIONS, INC.
P. O. Box 2351
1250 Prospect Street
La Jolla, California 92037

Prepared for

NATIONAL AERONAUTICS AND SPACE ADMINISTRATION

14 November 1971

CONTRACT NAS-826753

NASA CR-
SAI 71-559-LJ

FINAL REPORT

ELECTRON TRANSPORT AND SPACE SHIELDING HANDBOOK

by

D. C. Shreve and J. A. Lonergan

SCIENCE APPLICATIONS, INC.
P. O. Box 2351
1250 Prospect Street
La Jolla, California 92037

Prepared for

NATIONAL AERONAUTICS AND SPACE ADMINISTRATION

14 November 1971

CONTRACT NAS-826753

TABLE OF CONTENTS

TABLE OF CONTENTS (Cont.)

LIST OF FIGURES

LIST OF FIGURES (Cont.)

LIST OF FIGURES (Cont.)

LIST OF FIGURES (Cont.)

LIST OF FIGURES (Cont.)

LIST OF FIGURES (Cont.)

LIST OF TABLES

LIST OF TABLES (Cont.)

ABSTRACT

This report discusses the transport of electrons through material, with emphasis on space radiation problems. Brief reviews of the electron radiation environment and electron transport properties are presented. Parametric representations of the electron transmitted fraction, energy spectrum, angular distribution, backscatter coefficient, and energy deposition are given as functions of electron energy and target material. Parametric equations for thick-target bremsstrahlung are presented. Calculations of the transport of isotropically incident electrons relevant to space applications are shown. Comparisons of parametric representation with data, photon attenuation coefficients, electron energy deposition data, flux-to-dose conversion relations, and formalism applicable to space shielding problems are presented.

FOREWORD

The work described here was done at Science Applications, Inc., under NASA Contract NAS826753. Mr. Martin Burrell, Space Sciences Laboratory, Marshal Space Flight Center, was Project Manager.

SUMMARY

This report presents a comprehensive discussion of the transport properties of the electrons encountered in the space enrivonment. The purpose of the report is to provide a single source of information to make calculations of the electron-induced radiation on, or within, a spacecraft.

The electron environment is briefly discussed to allow the user to make estimates of the radiation fields encountered in different regions of space. The properties of electron transport are discussed in detail and parametric formulas for the transmitted fraction, angular distribution, energy spectrum, and energy deposition are presented for the penetrating primary electrons. Parametric formulas are also presented for the fraction of electron energy converted into bremsstrahlung, the angular distribution of the transmitted bremsstrahlung energy, and the differential energy spectrum of the bremsstrahlung radiation.

Calculations using the parametric formulas are presented for isotropic electron incidence which are useful for space applications. Examples of calculations of the radiation transmitted through various thicknesses of material are presented for typical electron environments.

The entire discussion has been written in such a manner as to assume no prior experience with electron radiation on the part of the user. The parametric representations and resulting calculations provide a tool whereby the user can quickly and without the aid of a computer estimate the radiation levels behind arbitrary amounts of effective shielding on the interior of a spacecraft. Example problems are provided as guides in the methods of solving space radiation problems.

Comparisons of the parametric formulas to experimental data, a discussion of photon attenuation, conversion factors for flux to dose for electrons and photons, and the formalism and approximations used in solving complicated space shielding problems are presented.

1. INTRODUCTION

For the past 60 years or so scientists have known that radiation exists outside of the earth's atmosphere. Some of the most important discoveries of modern physics have been obtained by studying these radiations. With the advent of rocketborne experiments, it was discovered that large regions of space surrounding the earth contained intense fluxes of energetic protons and electrons trapped in the earth's magnetic field.[1, 2] These regions of trapped radiation presented an exciting opportunity to study the nature and extent of the geomagnetic field, the nature of the earth's surroundings, the nature of trapped plasmas, and many other interesting problems. Considerable effort has been,and continues to be,expended to understand the spacial extent of the radiation fields, their time variations in connection with the solar cycle, the nature of the trapping mechanism, the decay rate of injected particles, and so forth. All of these problems relate to a basic understanding of the nature of the radiation fields.

From a pragmatic point of view the regions of trapped radiation present a shielding problem to scientists and space engineers who plan to put men and equipment into space. This report will deal with the problem of determining the radiation transport through shields for the electron component of the trapped radiation fields.

1.1 PURPOSE OF REPORT

The purpose of this report is to provide methods for estimating the dose that might be absorbed behind an effective shield in a space electron environment. The methods are intended to be as simple as possible to implement, considering the inherent complexities of electron transport and bremsstrahlung production. Parametric expressions of the transport results required for the solution of space shielding problems are presented. It is assumed that the reader is familiar with the problems of space radiation and with radiation physics in general, but no assumptions are made about his knowledge of any of the details of electron or photon transport. All the information required to use the results presented here is included; however, this is not a textbook on radiation transport. No attempt is made to provide physical or mathematical justification for the methods. Final results of transport calculations are compared with experimental data in a few instances only to indicate the accuracy of the methods. This report is also intended to provide a convenient reference to aid in the solution of electron and photon transport problems which might arise from sources other than space

radiation. The methods presented here are known to be accurate for the 50-keV to 5-MeV electron energy range. Extrapolations to higher or lower energies are appropriate in some cases, but the user must provide his own estimate of the accuracy of such procedures.

1.2 METHOD OF PRESENTATION

The organization of this report reflects our goal in making the transport information accessible to a wide range of users whose experience and familiarity with radiation physics are varied. We have concentrated the introductory information in the second and third sections where the trapped radiation environment in space is described, and the phenomenology associated with electron transport and bremsstrahlung production is discussed in general terms. Someone familiar with this technical area need not read these sections in order to make use of the information in subsequent sections. Precise methods for calculating radiation transport problems are discussed in Section Four. These methods, coupled with the experimental data, form the basis for the parametric modeling.

The parametric representations of electron transport and photon production properties are presented and discussed in Section Five. This essentially summarizes the technology in precise analytic form. Formulas are provided to calculate the results of transport interactions for most radiation shielding and dose deposition problems in the energy range for which these formulas are valid.

In Section Six the parametric representations are translated into a form that can be used for the solution of space shielding problems. Quantities peculiar to space problems are defined in terms of the formulas presented in Section Five. Section Six includes sample calculations for typical or frequently occurring situations. The emphasis is placed on the calculation of integral quantities such as dose.

Specific topics which warrant more discussion than is reasonable to include in the text are given in three appendices. In the first appendix the parametric representation of bremsstrahlung production is compared with experimental data. This work is new and it was thought that a discussion of its source and a comparison with experimental data were needed in order to meet the wide use that can be made of it. In Appendix B extensive tabular data on the energy deposition by electrons in aluminum are presented. These data are included to provide a convenient reference for the user. The quantity, dose, and related concepts are defined in Appendix C. Here the relationships between electron and photon fluxes and dose are presented explicitly.

1.3 ENGINEERING APPLICATIONS

There are several ways this report can be applied to space radiation problems. The curves and tables presented in Section Six can be used along with shield sectoring data and the integral electron fluxes to obtain quick estimates of the dose rates at given points in B-L space or for integrations over circular orbits. This method is illustrated at the end of Section Six. Also, the present parametric representation of electron transport could easily be incorporated into complex geometry computer programs to obtain total electron and bremsstrahlung fluxes throughout the spacecraft for isotropic source electron fluxes. These results, along with those of the electron environment computer code TRECO[3] could then establish the instantaneous fluxes for particular orbits. Finally, the results of orbital integrations could also be used to establish average fluxes and average doses for particular orbits.

2. ELECTRON ENVIRONMENT IN SPACE

2.1 VAN ALLEN BELTS AND THE MAGNETOSPHERE

The only region of space where electrons contribute significantly to the total radiation environment is in the magnetosphere around the earth (and in similar domains around some other planets). Fields of electrons were discovered by Van Allen[1] in 1958, when radiation counters were saturated by unexpectedly high fluxes encountered in a satellite mission designed to measure cosmic radiation. Since that discovery, many experiments have been performed to measure the spatial and temporal properties of this radiation. High electron fluxes were found to be distributed in toroidal belts about the earth's magnetic dipole axis. A pictorial description of the electron flux intensity distribution during mid-1964 is shown in Fig. 2.1. In this figure the dark regions indicate an increased concentration of electrons. There are two peaks in the electron flux on the radial profile along the magnetic equatorial plane. This is the origin of the terminology for the Inner and Outer zones, but it is applicable only for energetic electrons. Protons and low-energy electrons exhibit a more uniform spatial behavior.

Electrons are trapped in the Van Allen belts by the magnetic field of the earth. The particles follow helical paths about field lines. As the electrons move toward the poles along such a path, the magnetic field intensity will increase to a point where the electrons reverse their direction and return toward the equator.[4] In a static magnetic field electrons will neither gain nor lose energy. Consequently, electrons will pass through the equatorial plane and again be reflected in the other hemisphere. This motion of electrons oscillating between mirror points located symmetrically about the equatorial plane is illustrated in Fig. 2.2. In addition to the helical and oscillatory motions, the electrons undergo a slow drift in the easterly direction. This motion is due to the non-uniformity of the magnetic field over the helical path. Typical periods for these motions are: (1) microseconds for a single gyration about a field line, (2) seconds for a bounce between mirror points, and (3) minutes to drift around the earth. Because these periods are so different, the motions are mathematically separable to a first approximation and have been treated by several authors.[4,5]

2.2 B-L COORDINATES

Because of the spatial correlations between the earth's magnetic field and the distribution of trapped radiation, McIlwain[6] was able to develop a

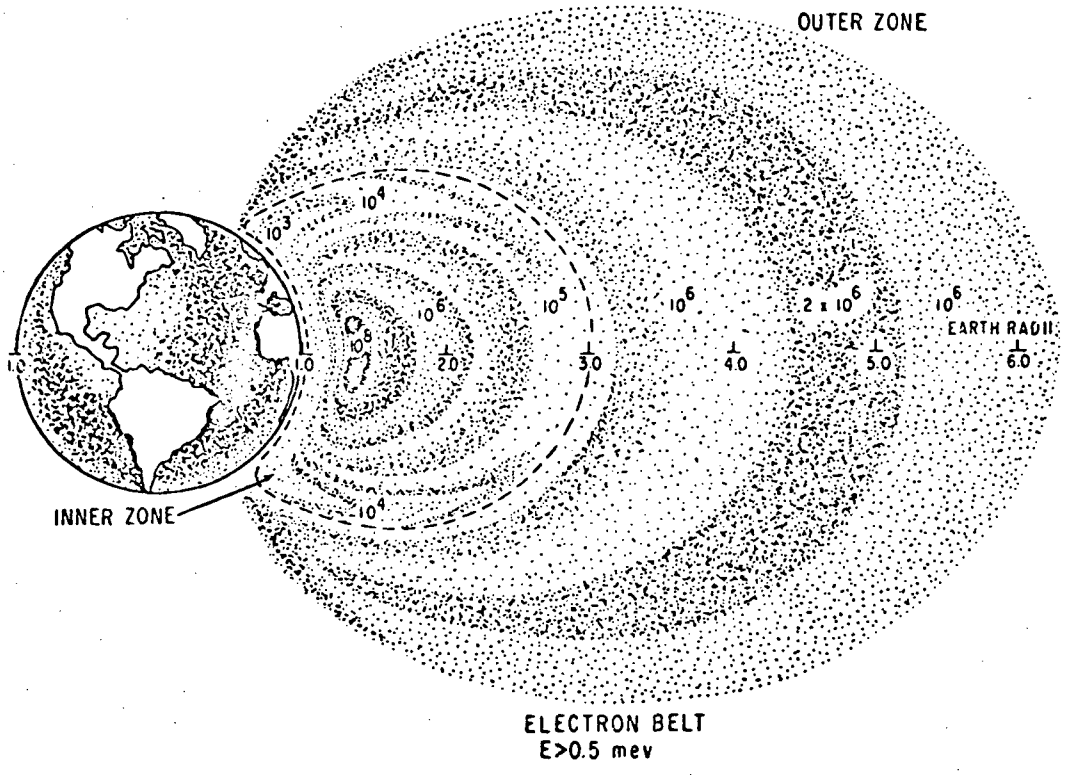

TRAPPED RADIATION ZONES

Figure 2.1. A model of the earth's electron radiation belts (from Aerospace Medicine, Dec. 1969, p. 1442)

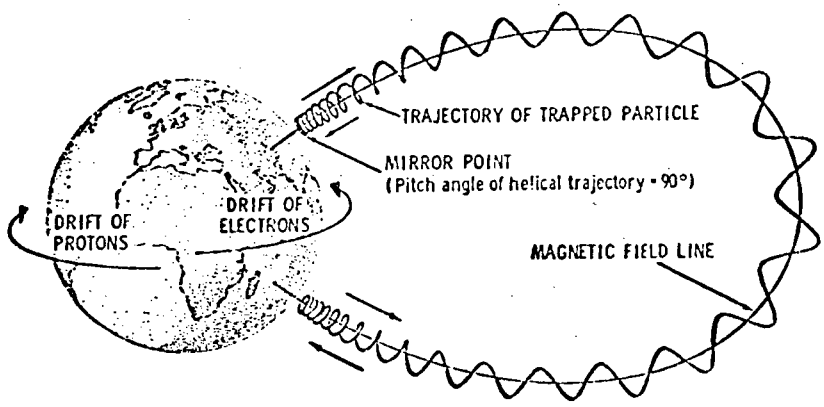

Figure 2. 2. Schematic illustration of electron motion in the earth's magnetic field (From Ref. 7, p. 169)

convenient set of coordinates that are commonly used in discussions of the Van Allen belt. The coordinates in this system are: B, the field intensity and L, a parameter which identifies a surface upon which all particles that drift on a given field line will remain. To get a feel for this parameter if we assume the earth's magnetic field to be a perfect dipole, L would then be the radial distance in the equatorial plane to the magnetic lines of force. A precise numerical definition is given in Ref. 6. This coordinate system is shown in Fig. 2.3. A surface of constant L resembles a tire casing fitted to the earth. A surface of constant B is a prolate spheroid everywhere perpendicular to the lines of force. To help illustrate this system, the surfaces and regions indicated in Fig. 2.3 are projected into B-L coordinates in Fig. 2.4.

For a pure dipole magnetic field, the relation between the radius from the earth's center to a particular point in space and the corresponding L value depends on the geomagnetic latitude λ through the equation[8]

$$L = R/\cos^2\lambda \qquad (2.1)$$

The corresponding magnetic field B is obtained from the relation

$$B = M(4-3\cos^2\lambda)^{1/2}/R^3 \qquad (2.2)$$

where $M = 0.311653$ (Gauss R_E^3) and R is the distance from the center of the earth to the space point measured in R_E. (R_E is the earth's radius.)

2.3 SPATIAL DISTRIBUTION OF TRAPPED ELECTRONS

The spatial distribution of the trapped radiation intensity is shown in Fig. 2.1. cated. In general, the intensity is highest in the equatorial plane and decreases as the latitude increases toward the poles. This results from the trapping mechanism which places the mirror points for electrons with large pitch angles (see Sect. 2.5) near the equator while electrons with smaller pitch angles will reverse their direction at higher latitudes. At the poles the intensity of the radiation vanishes.

The radiation belts are not exactly symmetric about the earth, as might be implied from the previous discussion. Because the center of the earth's magnetic dipole is displaced from the geometric center of the earth and tilted from the axis of rotation, magnetic fields are not even axially symmetric about the earth's surface. An important consequence of this asymmetry is a region off the coast of Brazil where surfaces of constant B reach their lowest altitudes. The region is known as the South Atlantic anomaly and is significant because at this point trapped radiation from nuclear devices or from natural causes reaches its lowest altitude.

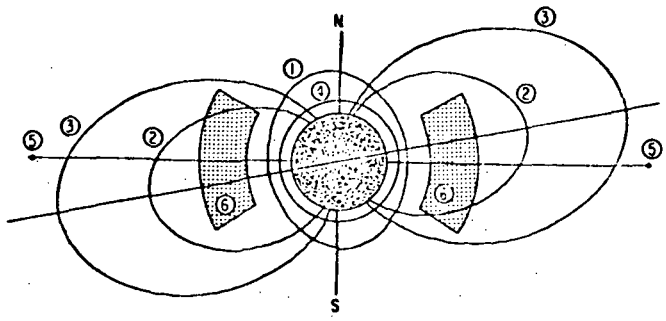

Figure 2.3. An illustration of the geomagnetic coordinate system. The following examples are shown: (1) a line of constant magnetic field intensity; (2) a line of constant L, L = 4; (3) a line of constant L, L = 6; (4) a polar orbit; (5) a synchronous orbit; (6) an orbit with an apogee of R = 3, a perigee of R = 2, and an inclination of 30° to the geographic equator. (From Aerospace Medicine, Dec. 1969, p. 1443)

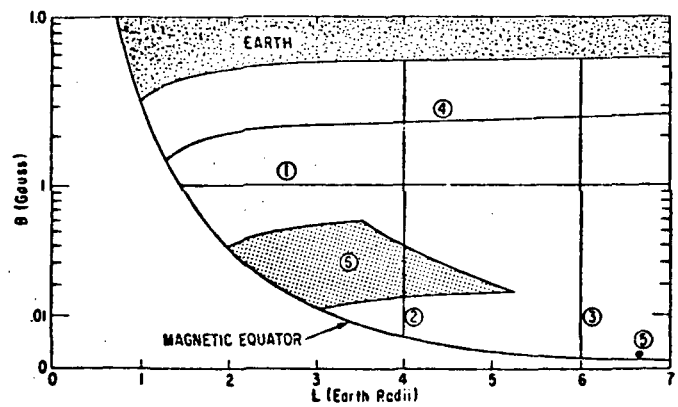

Figure 2.4. Cases (1) through (6), Fig. 2.3 illustrated in B-L magnetic coordinates. (From Aerospace Medicine, Dec. 1969, p. 1444)

In addition to the asymmetry caused by the variations in the earth's magnetic field there is a significant asymmetry caused by the interaction of the solar wind and magnetosphere. The solar wind compresses the magnetosphere on the side of the earth facing the sun and extends it on the night side of the earth. The asymmetry from this source is pronounced in the outer trapping regions and fairly minor in the inner regions.

2.4 ELECTRON ENERGY SPECTRA

The shape of the energy spectra of trapped electrons normalized to 1 particle/cm^2 above 0.5 MeV is, to first order, independent of B but dependent on L. There may actually be a B dependence of the energy spectra, but with the data presently available a B dependence cannot be separated from existing experimental uncertainties. The L dependence is indicated in Fig. 2.5, where the energy spectrum for L = 2.0, 3.5, and 6.0, are plotted. These spectra are also tabulated for convenience in Table 2.1, where N(E, 0.5) is the energy spectrum (per MeV) of electrons. This quantity is normalized so that

$$\int_{0.5}^{\infty} N(E,0.5)dE = 1 \qquad (2.3)$$

The curves were taken from Vette's AE2 environment model[9] which will be discussed in more detail below. To indicate the spread in the data, the differential flux of electrons at L = 3.5 is plotted with the satellite data in Fig. 2.6.

2.5 PITCH ANGLE AND ANGULAR DISTRIBUTION

The angular distribution of trapped electrons is best described in terms of the pitch angle. This is the angle an electron makes with the lines of force about which the electron is circulating. A pitch angle of 90° implies that the electron is moving perpendicular to the lines of force. Trapped electrons have pitch angles of 90° at the mirror points where they are reflected. A pitch angle of 0° implies that the electron is moving parallel to the lines of force and is, therefore, not circulating about those lines. Such electrons will not be mirrored and are consequently not trapped. In fact, there is a range of equatorial pitch angles about 0°, for which the electrons are mirrored at such low altitudes that they are lost in the atmosphere. This range of pitch angles for which electrons fail to be trapped defines "the loss cone." The angular distribution of electrons is known to change due to variations in the magnetic fields during magnetic storms and to other perturbations, but the pitch angle distribution will diffuse to a steady state in a few days. In Fig. 2.7, this behavior is indicated. The flux is plotted versus a parameter $x = (1 - B_0/B)^{1/2}$ which is the value of the cosine of the equatorial pitch angle for a particle which mirrors at a field intensity of B. If an electron is lost at an altitude corresponding to B then the range

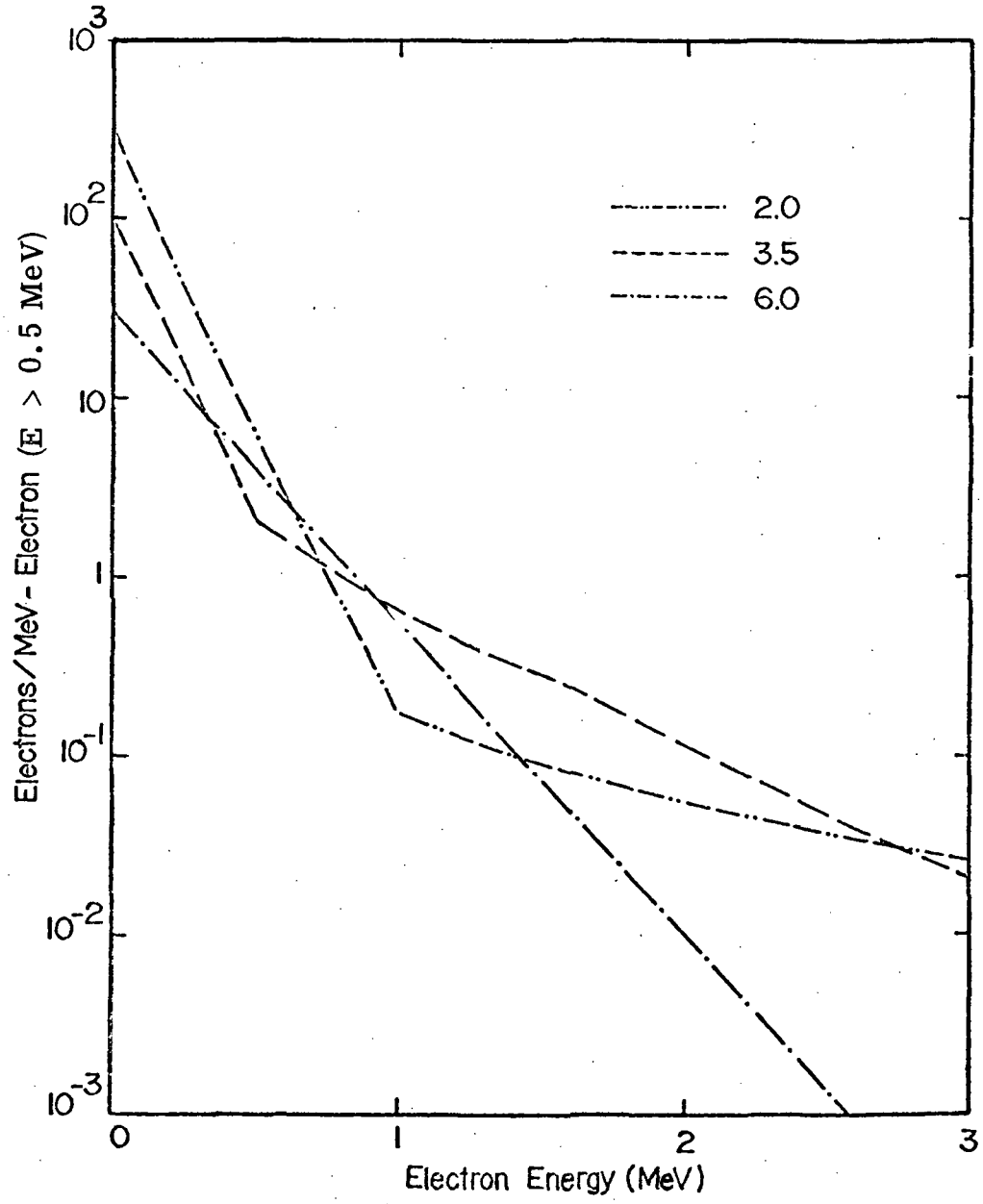

Figure 2.5. The electron energy spectra for the following values of L, 2.0, 3.5 and 6.0 (From Ref. 9)

TABLE 2.1. ELECTRON ENERGY SPECTRA FROM AE2;
(ELECTRON/MeV - ELECTRON GREATER THAN 500 keV)

E	L = 2.0 N(E, .50)	L = 3.5 N(E, .50)	L = 6.0 N(E, .50)
0.	0.267E 03	0.650E 03	0.492E 02
0.25	0.411E 02	0.514E 01	0.108E 02
0.50	0.634E 01	0.211E 01	0.399E 01
0.75	0.970E 00	0.115E 01	0.147E 01
1.00	0.196E 00	0.577E 00	0.542E 00
1.25	0.116E 00	0.462E 00	0.200E 00
1.50	0.909E-01	0.261E 00	0.736E-01
1.75	0.737E-01	0.173E 00	0.271E-01
2.00	0.597E-01	0.113E 00	0.100E-01
2.25	0.484E-01	0.696E-01	0.368E-02
2.50	0.392E-01	0.488E-01	0.136E-02
2.75	0.318E-01	0.311E-01	0.500E-03
3.00	0.258E-01	0.198E-01	0.184E-03
3.25	0.209E-01	0.126E-01	0.679E-04
3.50	0.169E-01	0.801E-02	0.250E-04
3.75	0.137E-01	0.510E-02	0.922E-05
4.00	0.111E-01	0.324E-02	0.340E-05
4.25	0.902E-02	0.206E-02	0.125E-05
4.50	0.731E-02	0.131E-02	0.461E-06
4.75	0.592E-02	0.836E-03	0.170E-06
5.00	0.480E-02	0.532E-03	0.626E-07
5.25	0.389E-02	0.339E-03	0.231E-07
5.50	0.316E-02	0.216E-03	0.850E-08
5.75	0.256E-02	0.137E-03	0.313E-08
6.00	0.207E-02	0.873E-04	0.115E-08
6.25	0.168E-02	0.556E-04	0.425E-09
6.50	0.136E-02	0.354E-04	0.157E-09
6.75	0.110E-02	0.225E-04	0.577E-10
7.00	0.895E-03	0.143E-04	0.213E-10

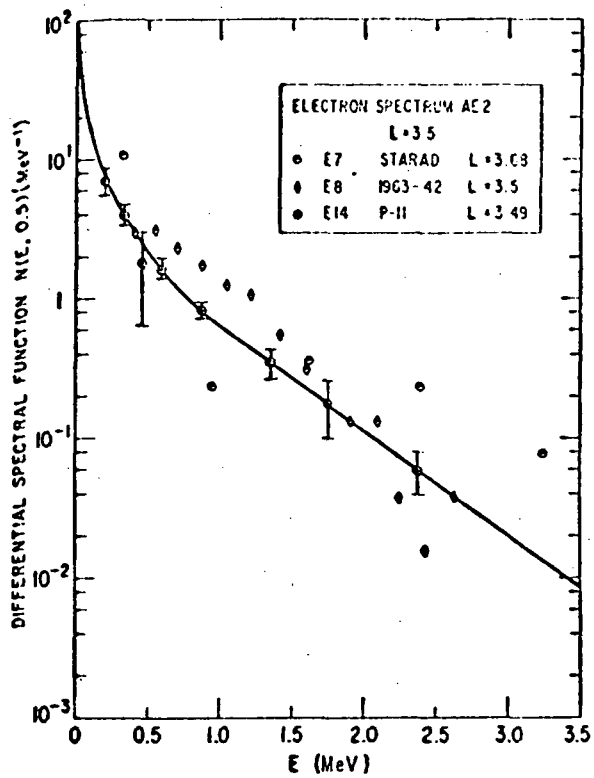

Figure 2.6. A comparison of the AE2 spectrum at L = 3.5 with satellite data (From Ref. 9)

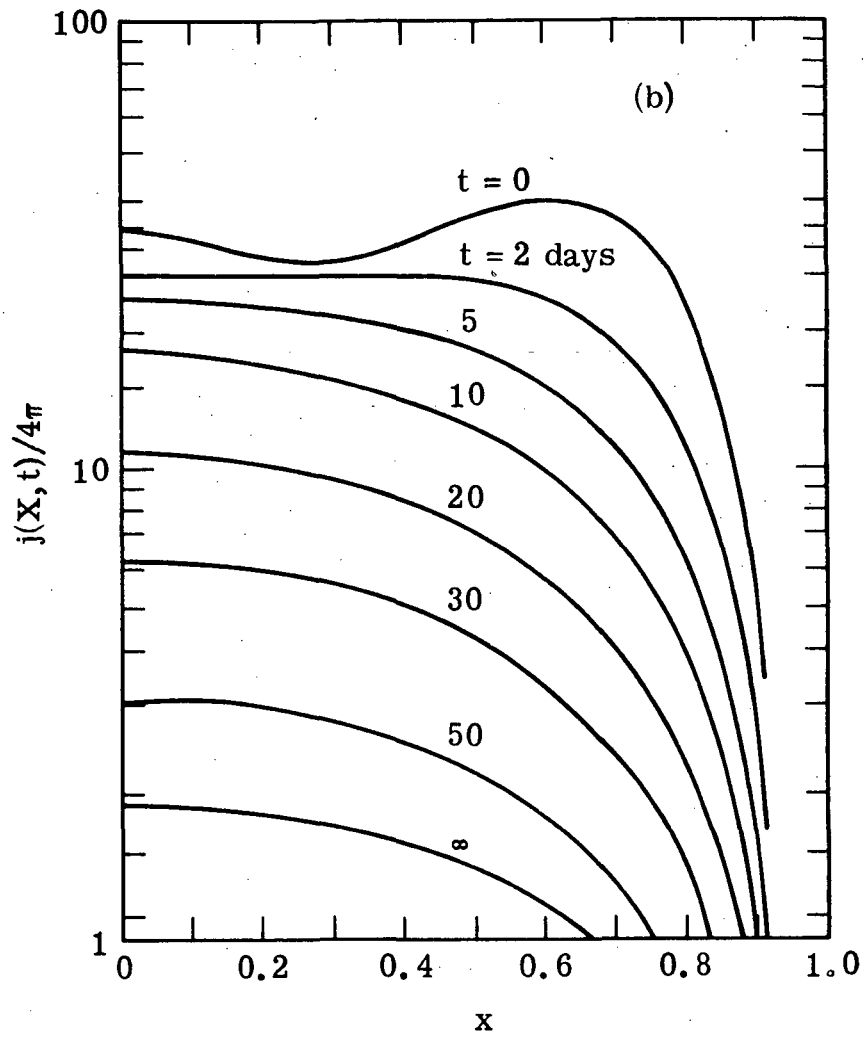

Figure 2.7. Decay of some initial particle fluxes to the steady state caused by pitch-angle diffusion. The flux is plotted as a function of the coordinate $x = (1-B_0/B)^{1/2}$, where B_0 is the field intensity at the intersection of the L-surface in which the electron lies in the magnetic equatorial plane.

of allowable pitch angles at the geomagnetic equator α_o is $90^o > \alpha_o > \cos^{-1} x$. For most dose calculations, the flux distribution labeled ∞ in Fig. 2.7 best indicates the angular distribution.

2.6 ARTIFICIAL RADIATION INJECTION

The artificial injection of electrons by nuclear detonation has altered the energy spectra by the introduction of many high energy electrons. This effect was most pronounced at low values of L near the injection point but all the inner zones were affected to some extent. The data shown in Fig. 2.5 were measured in 1964--two years after the Starfish event. In these data there is still a large contribution due to artificially trapped electrons. In Fig. 2.8, the spectrum at L = 1.2, measured a few months after the artificial injection, is compared with the spectrum measured two years later. The decay of the high energy component is evident.

The decay of the abnormally high flux levels accompanying the detonation of nuclear devices is L-dependent. The behavior is indicated in the curves for 2-MeV electrons in Fig. 2.9.

Recent evidence indicates that there are no natural sources of inner zone electrons for energies greater than approximately 700 keV.[10] This means that the higher energy electrons are the residue of Starfish. It is reasonable to assume that they will continue to decay at the same rate as they have over the past 5 or 6 years. There seems to be no direct effect of solar activity on this decay. Therefore, by 1969, the inner zone electron contours for energies > 1 MeV should be decreased by about a factor of 12. The lower energy electrons seem to have reached their natural background levels by late 1966. The E > 0 energy contours have remained about the same as in 1964, and the E > 0.5 MeV have dropped about a factor of 6. Until a new electron model is generated, these are the best estimates that can be given.

2.7 TIME VARIATIONS

Electron radiation fields in space are not stable in time. There are fluctuations in the spatial distribution that are due to a variety of sources. The more systematic effects are caused by the rotation of the earth relative to the sun. This rotation causes diurnal effects in the spatial flux distribution measured relative to the earth since the radiation will tend to remain fixed to the field contours and will consequently fluctuate with local time. However, these effects are small compared to the fluctuations caused by solar magnetic storm activity. Prior to a solar flare, magnetic activity can cause the flux in the inner zone to change by as much as factors of 2 or 3. In the outer zone, the flux might change by more than an order of magnitude. These fluctuations are illustrated in Fig. 2.10, where electrons (>1.6 MeV) are plotted versus time for several values of L. In the center of this figure, K_p, which is a

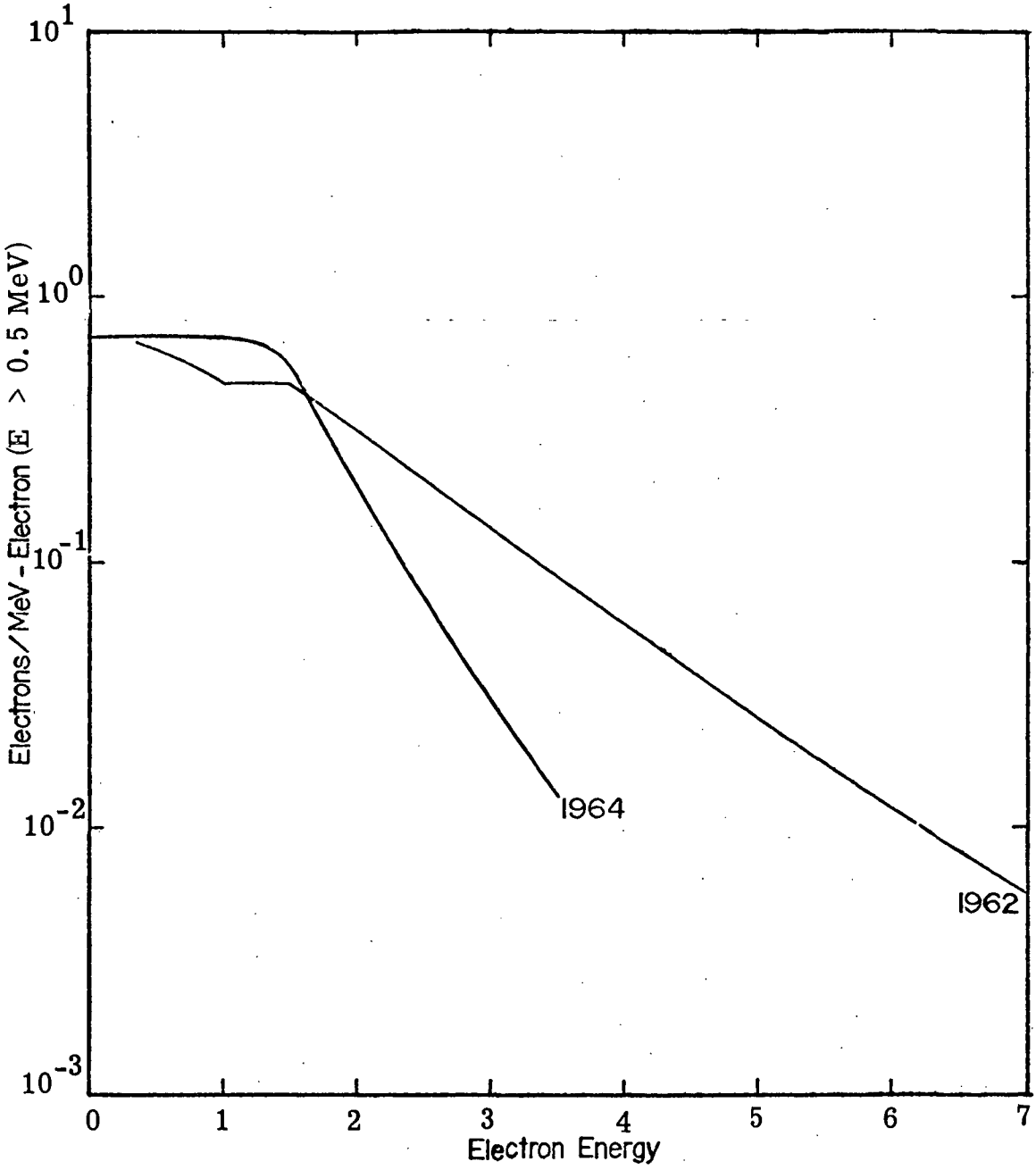

Figure 2.8. Electron energy spectrum at L = 1.2 measured two months after the Starfish event (1962) and two years later (1964)

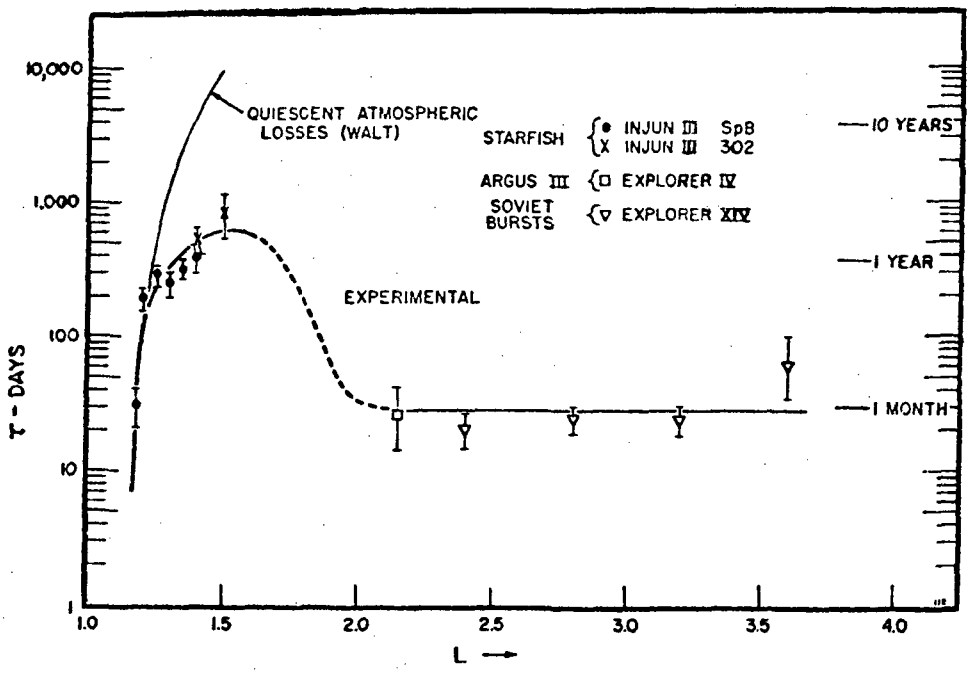

Figure 2.9. The L dependence of observed values of the apparent mean lifetime of ~2-MeV electrons from two U.S. and two USSR nuclear detonations at high altitudes (From Ref. 9)

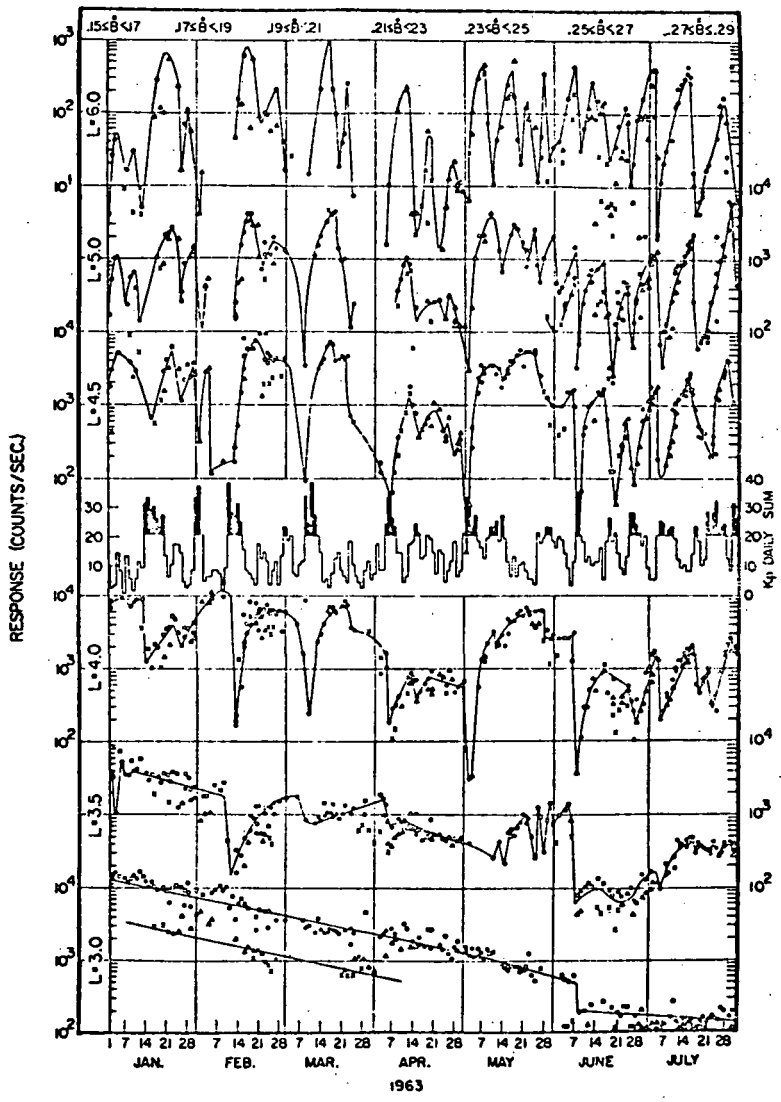

Figure 2.10. Injun 3 observations of the intensity of electrons E > 1.6 MeV at low altitudes over a seven-month period

measure of the magnetic activity, is plotted. The correlation between magnetic activity and electron flux variation is obvious. There are also long term variations in the trapped electron radiation belts associated with the 11-year solar cycle. These changes are most pronounced in the outer belt where, during periods of solar maximum, the fluxes of energetic electrons can be increased by an order of magnitude compared with solar minimum conditions. The position of the maximum electron flux also changes during the solar cycle. During periods of solar maximum the position is closer to the earth being at about $L = 3$ to $L = 4$. At solar minimum, the position of the maximum ranges from $L = 4$ to $L = 5$.

2.8 MODELS OF THE ELECTRON ENVIRONMENT

Data measured aboard satellites since 1958 have been collected and assimilated in a systematic fashion by NASA. Vette, et al., [9, 11, 12] have developed models of the radiation environment that have been computerized and are available to interested users. These models are being updated as more measurements become available. This has been particularly important during the last decade while the artificially injected radiation has been dissipating. The Vette codes can be used to read out the radiation environment along any path specified by the user. Vette's AE2 electron distribution model which is used in this report is considered to be outdated at the present time due to the decay of the artificially injected electrons. A new model environment (AE4) is soon to be released (1972). They can also integrate the flux along the path of a specified orbit to yield the total flux exposure during a mission. These models and the accompanying system of codes are virtually the only places where all the data on space radiation have been assembled.

3. ELECTRON TRANSPORT PROPERTIES

3.1 INTRODUCTION

In this section we discuss the general features of electron transport. Since electrons interact with matter in a significantly different manner than do other radiations (such as protons, neutrons, and heavier charged particles) it is instructive to point out the relationship between the basic interaction mechanisms and the effect these processes have on the properties of the transport of electrons through bulk media. It is important to understand the diffusive properties of electron penetration that are very unlike the sharply defined quantities such as range and stopping power associated with protons and heavier particles. On the other hand, unlike photons, electrons are not attenuated exponentially as they pass through matter. Consequently, there is no highly reliable first order analysis that can be used to determine the penetration of electrons. However, some properties of the electron transport have smooth, predictable behaviors so that analyses of specific problems can be made if the analyst is willing to expend the effort needed to correlate these properties with the problem of interest. The effort involves assembling the parametric representations presented here and using them correctly where they apply.

3.2 INTERACTION MECHANISMS

Electrons will interact with matter in essentially three different ways. (1) They will scatter from other electrons causing the target electron to recoil. This is called Møller scattering,[13] and the recoiling electron is known as a knock-on electron. Møller scattering applies to the interaction of one free electron with another free electron, but it is used to approximate the interaction of a free electron with an electron bound to an atom; (2) an electron can scatter from the atomic nucleus. In this case, known as Rutherford scattering,[14] the electron loses very little of its initial energy to the nucleus but may be scattered in any direction. Often, in electron-nucleus interactions the acceleration imposed on the electron in order to change its direction will result in a photon being emitted in the process. In this case the photon and scattered electron share virtually all the energy of the incident electron; (3) the electron may interact with the whole atom leaving some of its energy with the atom. This energy is converted to either photons, ejected electrons, or heat, usually by a complicated series of interactions in the atom.

In the process of slowing down from an initial energy of 1 MeV to thermal energies in matter an electron will undergo on the average more than 100,000 interactions. Since all three of the cases mentioned above are possible, the energy and direction of any incident or secondary electron at an intermediate point in the slowing down process is not unique. The large number of intereactions and the wide range of possible final states after any single interaction result in the complication of electron transport. On the other hand, since there is such a large number of interactions involved, electron transport can be treated in a statistical manner yielding smooth distributions which can be used to characterize electron transport with a rather high degree of confidence.

Below 10 MeV or so, electron-electron scattering is the main mechanism for energy loss by energetic electrons.[15] Depending on the scattering angle an incident electron can lose any amount of its initial energy in one collision. However, it is assumed that an electron never loses more than half its initial energy. Though an incident electron can lose all its initial energy in a straight-on nonrelativistic collision, in that case the target electron recoils in the forward direction with the initial energy of the incident electron. Since there is no way of distinguishing between the two electrons, such an interaction is counted as no collision. If we extend this argument it is not difficult to see why at least one electron will have half or more of the incident electron energy after a nonrelativistic collision. So, if it is always assumed that the incident electron is the more energetic of the two recoiling electrons, then it always has at least half the incident energy. When the incident electron has a kinetic energy of the order of 500 keV or more then relativistic effects alter the energy distribution. The relativistic effects can be pictured by imagining the electron increasing its mass as the energy increases above a few hundred keV. The relativistic effective mass increase can be stated quantitatively by the following expression:[16]

$$\frac{m}{m_o} = 1 + \frac{E}{m_o c^2} \tag{3.1}$$

where m/m_o is the ratio of the effective mass to the rest mass and E is the electron kinetic energy in MeV. This ratio is plotted in Fig. 3.1 over the transition region from nonrelativistic energies to relativistic energies. Relativity affects the transport properties by weighting the angular distribution of scattered particles in the forward direction. In general, electron angular distributions tend to become isotropic after the electron loses from a fifth to a third of its initial energy.[17] Because of the relativistic effects, the depth at which this occurs increases with energy.

The electron-electron collisions dominate the energy loss distribution. In spite of the fact that there is a rather wide range of energies that an

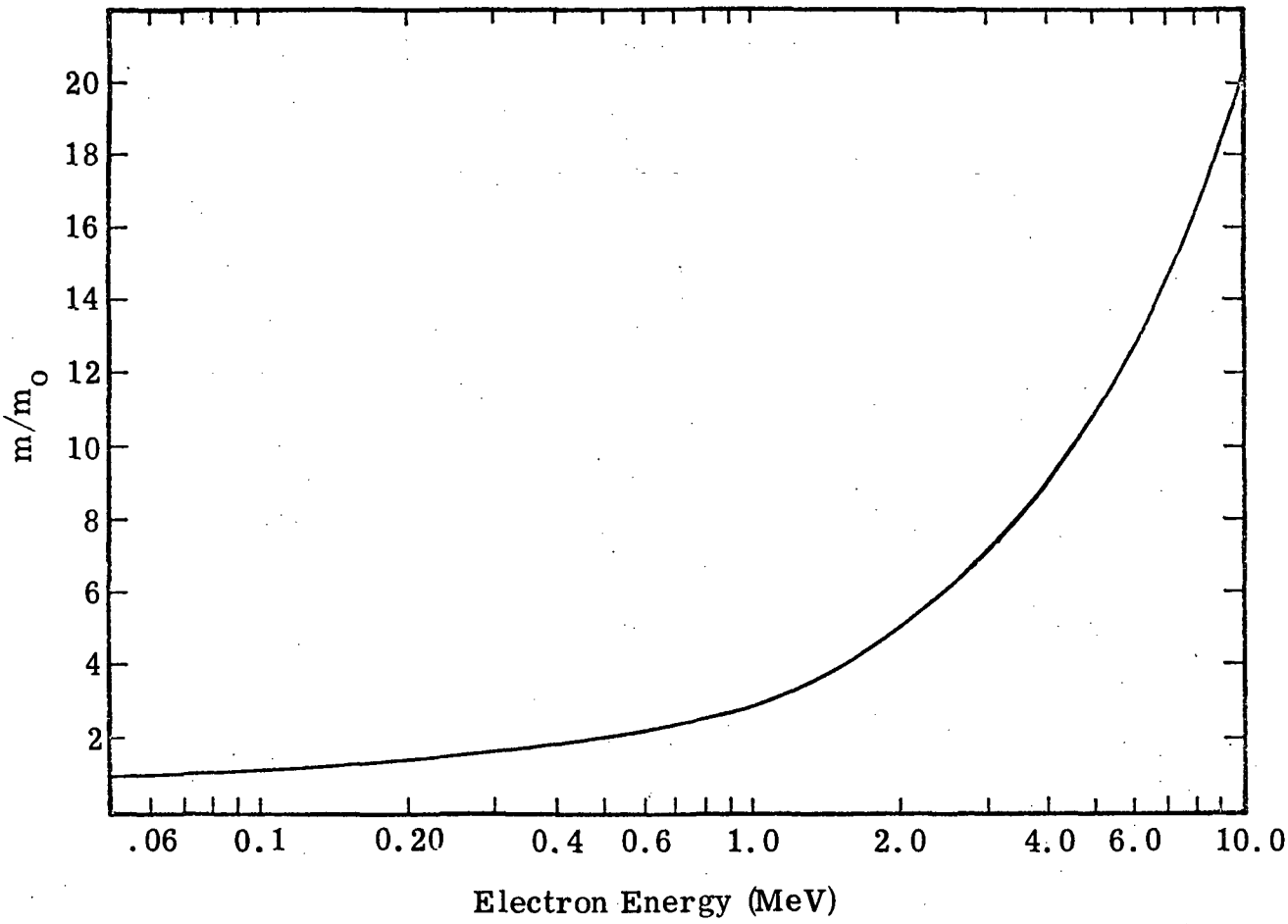

Figure 3.1. Ratio of effective relativistic mass to the rest mass

electron can lose in a single collision, the average energy lost after a few thousand collisions is not subject to large fluctuations. Quantitatively, if the path length the electron actually traverses is greater than a few percent of the path length nominally required to stop the electron, then the energy of the electron after traversing that path length is predictable to within 10 percent with better than 90 percent confidence. (Path length here refers to the actual distance traveled on the slab as distinguished from the depth of penetration.) The fluctuations in energy loss per unit path length have been studied by Landau[18] and are given by a distribution function bearing this Russian physicist's name.

Electron-nucleus collisions do not transfer a significant amount of energy to the recoiling nucleus. If energy is lost in these interactions it is typically converted into electromagnetic energy through the bremsstrahlung process. In general, the bremsstrahlung process does not play an important role at electron energies below 10 MeV. For example, if 10-MeV electrons are incident on aluminum the bremsstrahlung process accounts for 8 percent of the energy loss; in gold it accounts for 33 percent. The bremsstrahlung adds a low energy tail to an essentially Gaussian final energy distribution for electrons penetrating a given thickness of material. This effect is illustrated in Fig. 3.2. The photon distributions will be discussed in more detail below.

The important effect that the electron-nucleus interactions have on electron transport is that they change the direction of the electron from the incident direction enough so that after a small number of such collisions (relative to the number of collisions required to stop the electron) the directional distribution of the electrons approaches isotropy. Directional dispersion has the significant effect of making the depth of penetration of electrons into matter shorter than the path length they travel. Electrons execute a random walk as they penetrate matter, eventually proceeding in every direction with essentially equal probability. To illustrate the effect of directional dispersion on the transport properties consider the energy distribution of monoenergetic electrons incident on a slab of material and penetrating to a specific depth. If there were no directional dispersion the energy distribution might look like the solid line in Fig. 3.2 since the depth would be always equal to the path length. However, in actual fact directional dispersion implies that the electrons reaching a given depth arrive there after traversing a variety of different path lengths. Consequently, the energy distribution of these electrons might look more like the dashed curve in Fig. 3.2. The directional dispersion caused by the electron-nucleus collisions broadens the energy loss versus depth of penetration distribution and thus complicates the properties of electron transport.

The energy loss to the excitation of entire atoms is not important to electron transport until the electron energy gets down to the order of a few tens of keV's. At these lower energies the electrons begin to transfer their energy to the whole atomic structure putting the bound electrons in excited states. These states decay by a variety of modes which eventually leave the sea of bound electrons and nuclei with increased thermal energy

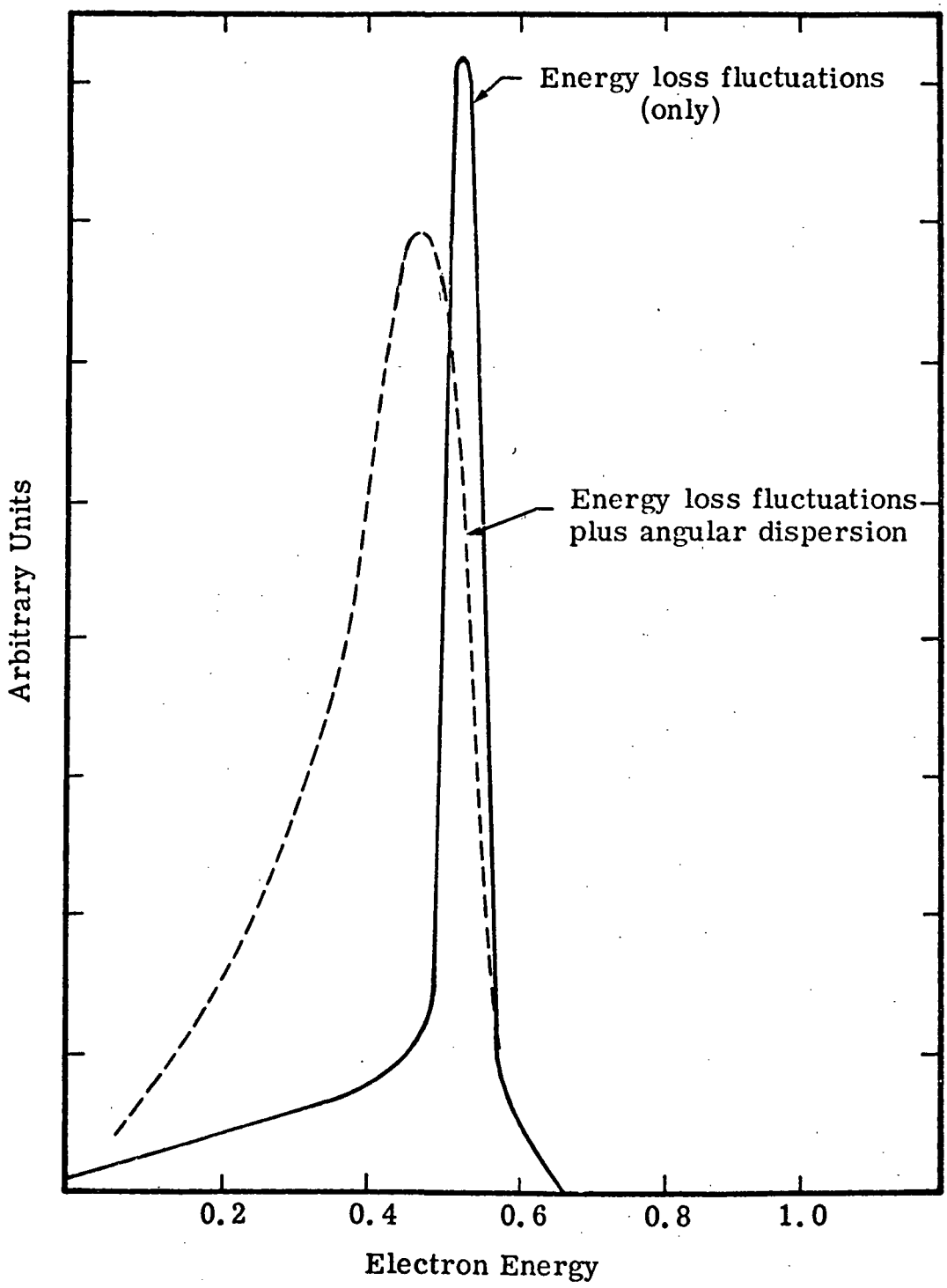

Figure 3.2. Effects of energy spreading mechanisms

which heats the material. Some of the excited states will decay by photon emission radiating in the visible and infrared regions. In addition, there are some other interactions which affect the atomic and molecular structures that are not important to the electron transport properties, but are significant to a description of radiation damage mechanisms.

3.3 ELECTRON TRANSPORT PROPERTIES

The previous section discussed the mechanisms with which electrons interact with matter and how they relate to the transport properties of electrons. In this section the transport properties will be discussed explicitly since they are the observable results of electron interactions with matter. Specifically, transport properties are defined here as those quantities which are observed and readily measured when energetic electrons are directed at bulk media. These are the properties that are determined and manipulated in shield designs. The specific properties defined are the transmitted fraction, range, backscatter coefficient, transmitted spectra, angular distribution, energy deposition, bremsstrahlung production, and bremsstrahlung spectra. These quantities are discussed with regard to their overall significance and their dependence on energy and atomic number.

3.3.1 Transmitted Fraction

Assume that a beam of monoenergetic electrons is incident on a slab of material at right angles to the plane of the slab. The transmitted fraction is defined as the number of electrons penetrating through a thickness of material per incident electron. Throughout, the assumption is made that the "thickness of material" and "depth of penetration" are the same. The difference in the expressions is that thickness of material implies a slab of a given thickness and depth of penetration implies depth into a semi-infinite medium. The transmission fraction and other properties are different due to backscattering in the latter case but this difference is assumed to be negligible in this discussion. The transmitted fraction is a function of the incident electron energy, the atomic number of the material, and the depth of penetration. Throughout this discussion, depth will be defined in units of mass per unit area e.g., g/cm^2 since most of the electron transport quantities can be scaled in this unit regardless of density. This unit of length is defined in the following expression:

$$x(g/cm^2) = \rho(g/cm^3)z(cm)$$

where ρ is the material density and z is the thickness.

The shape of a typical transmission curve, i.e., the transmitted fraction as a function of depth, is shown in Fig. 3.3. These curves correspond to 1-MeV electrons incident on aluminum and gold targets. The general shapes of the transmitted fraction are also found at other energies and in other materials.

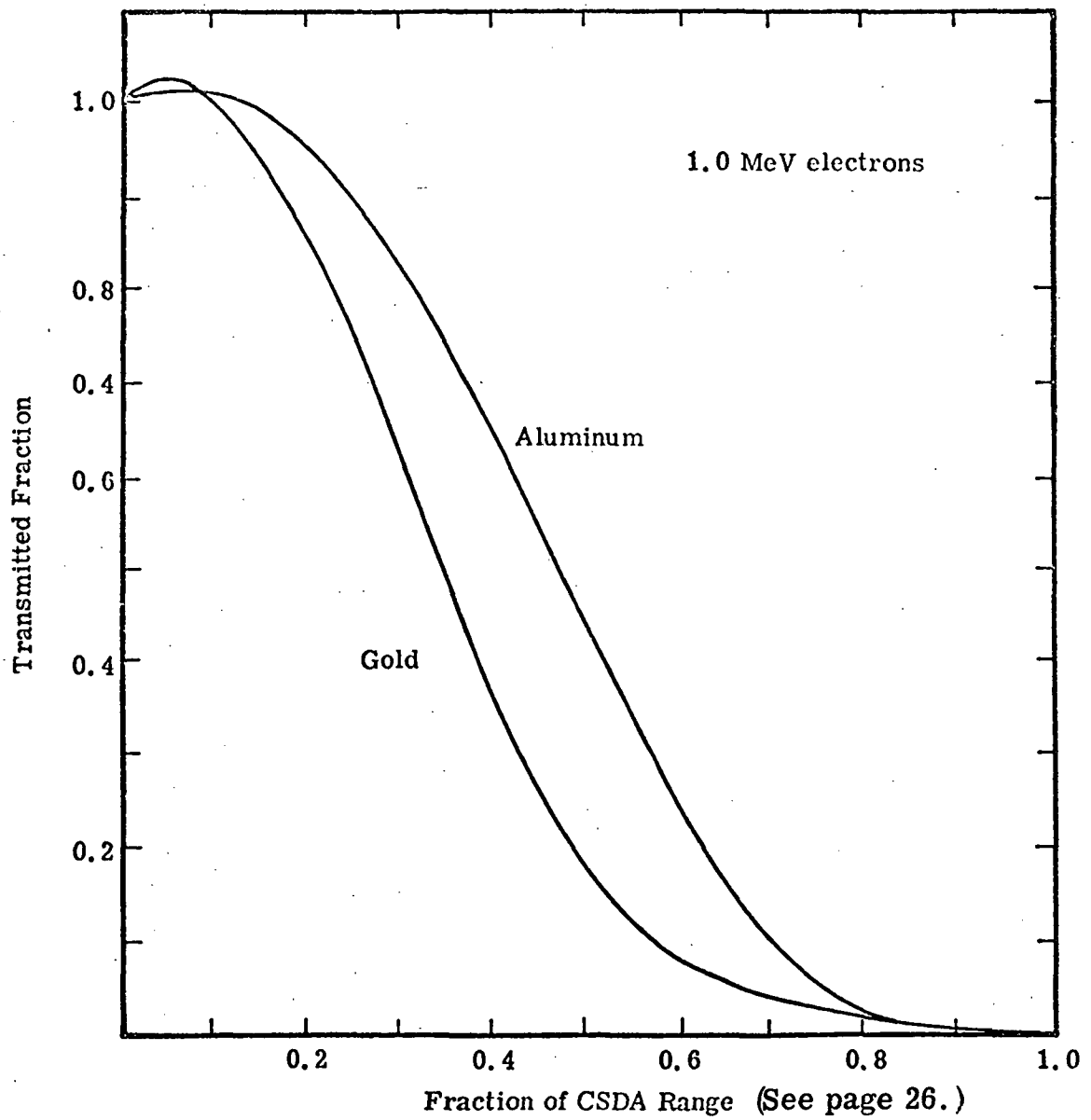

(See page 26.)

Figure 3.3. Comparison of aluminum and gold transmission fractions

Note that the transmitted fraction exceeds one after penetrating a few tenths of a g/cm^2. This is typical and is the result of the flow of knock-on electrons recoiling in the forward direction after electron-electron collisions. To first order, the transmitted fraction is independent of incident electron energy when the material thickness is measured in terms of the csda range (see Sect. 3.3.2). A second order effect due to relativistic considerations would indicate a tendency to push the penetration to larger depths. This effect is essentially cancelled, however, by the increase in the energy loss due to bremsstrahlung production at higher energies. As is seen in Fig. 3.3 the transmitted fraction decreases more rapidly as a function of thickness for high Z targets than low Z targets. The decreased penetration is attributable to the increased angular dispersion at higher atomic number. This effect is enhanced by the increased bremsstrahlung production at higher energy (see Fig. 3.3).

3.3.2 Range

The range is a single number which relates an electron of a given energy to a depth of penetration in a given material. It is a very useful concept for bounding electron shield problems. However, its precise definition is complicated by the fact that electrons of a given energy will not penetrate to a single depth. This effect is called range straggling. Electrons are in contrast to protons and heavier ions which have well defined depths of penetration (range straggling is only a small perturbation for protons and heavy ions). Typical distributions are displayed in the transmission curves of Fig. 3.3. Because of the usefulness of the concept, several ranges have been defined for electrons. The continuous slowing down approximation (csda) range is defined by the expression for an electron of energy E

$$R_o = \int_0^E (dE'/dx)^{-1} \, dE' \quad , \tag{3.2}$$

where dE'/dx is the average rate of energy loss along the electron path length (stopping power). In this approximation the range is defined to be the length required to stop the electron, assuming the average stopping power dE'/dx to be without fluctuations. For this reason it is sometimes referred to as the average path length. A comparison of the values of R_o as a function of electron energy for Al and Au is shown in Fig. 3.4.

Another range defined to facilitate comparisons of experimental measurements of electron penetration is the extrapolated range, R_{ex} (sometimes called the practical range). The extrapolated range, R_{ex}, is the depth at

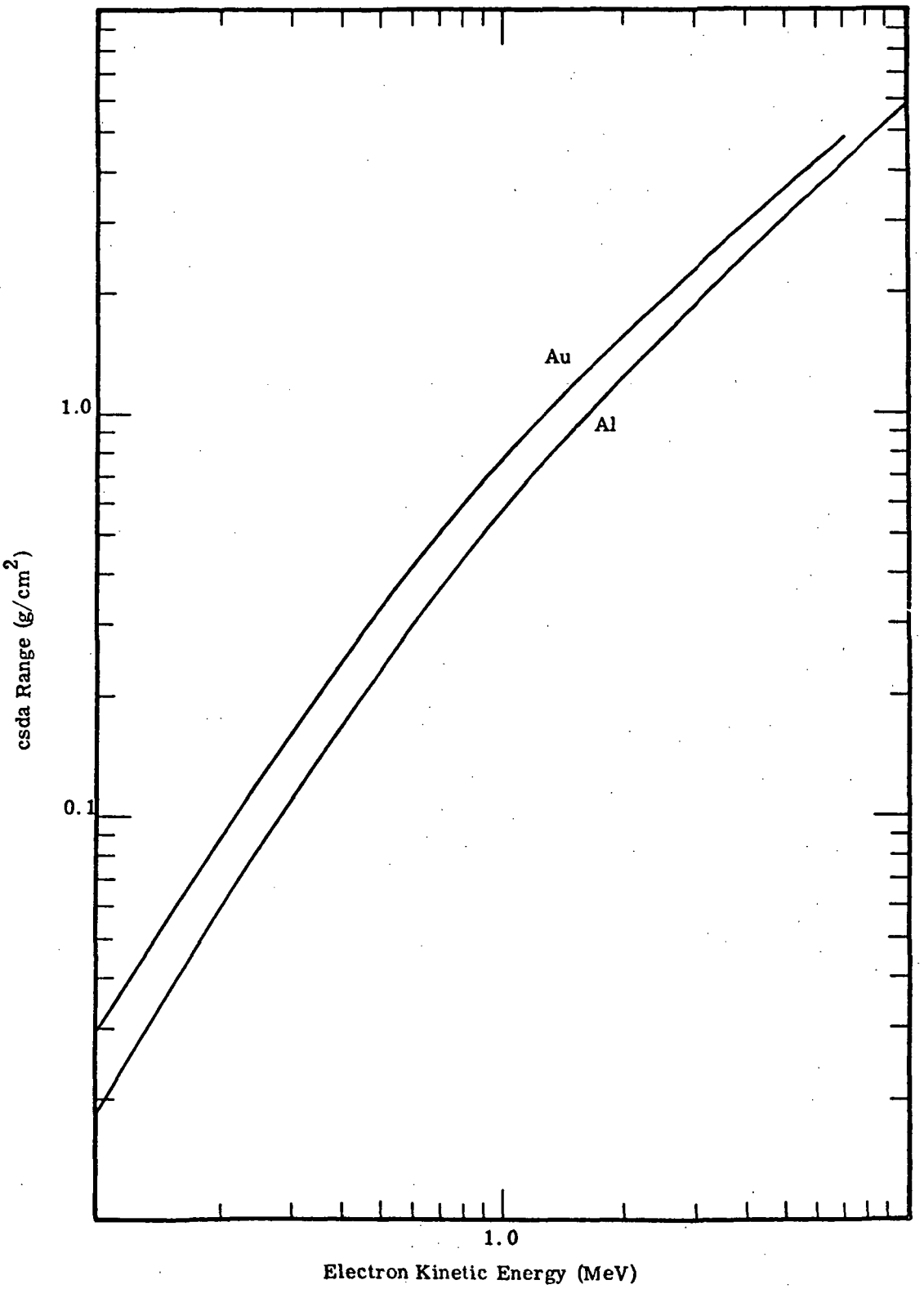

Figure 3.4. Comparison of continuous slowing down approximation range in Al and Au vs electron energy

which a straight line tangent to the transmission curve, at the point where the transmission fraction is 1/2, is extrapolated to zero transmission. This definition is illustrated in Fig. 3.5. The extrapolated range is not simply related to R_o but is roughly of the order of 30-40 percent less than R_o. An expression for the relationship is given in Section Five. The csda range is, to first order, proportional to energy and independent of atomic number. A rough estimate of the stopping power is 2 MeV per g/cm^2, so that the range of a 1-MeV electron is roughly 0.5 g/cm^2 in any material (except for hydrogen). The extrapolated range R_{ex} tends to become increasingly smaller than R_o as the atomic number increases.

One of the convenient uses of the range concept is that the properties of electron transport can be discussed universally and rather accurately in terms of range, thereby eliminating the need to reference the energy or atomic number except to discuss bremsstrahlung production. In the remainder of this section, references to the range will imply the continuous slowing down approximation range.

3.3.3 Backscatter Coefficient

Electrons incident on a surface will mainly penetrate the surface but some will be scattered and emerge in the backward direction. The fraction of incident electrons that do so is defined as the backscatter coefficient.

In the case of normal incidence the backscatter coefficient is very dependent on the atomic number, increasing from about 5 percent in beryllium for 1-MeV electrons to 30 percent for 1-MeV electrons in gold. The energy dependence of the backscatter coefficient is weaker, varying by a factor of six in aluminum as the energy is increased from 1.0 MeV to 10 MeV.[19] The energy spectrum of backscattered electrons tends to be harder (more energetic electrons) when scattered from low atomic number materials. This is because the electron-electron collisions degrade the electron energy while the electron-nuclear collisions cause the backscattering. Since there are more electrons per nucleus in high atomic number materials, there is more energy loss per backscatter collision.

3.3.4 Transmitted Energy Spectrum

As discussed above, the energy spectrum of electrons penetrating to a given depth is primarily broadened by the angular dispersion of electrons penetrating matter. This effect is illustrated in Fig. 3.6. Spectra are shown for 1-MeV electrons after penetrating thicknesses of aluminum corresponding to 0.2 and 0.56 of the csda range. A characteristic feature of these spectra is that for normal electron incidence highest energy electrons correspond to an energy loss equal to that calculated assuming no angular dispersion; that is, the thickness equals the path length. This results in a high energy cutoff in the transmitted spectra. The distribution of energies below that

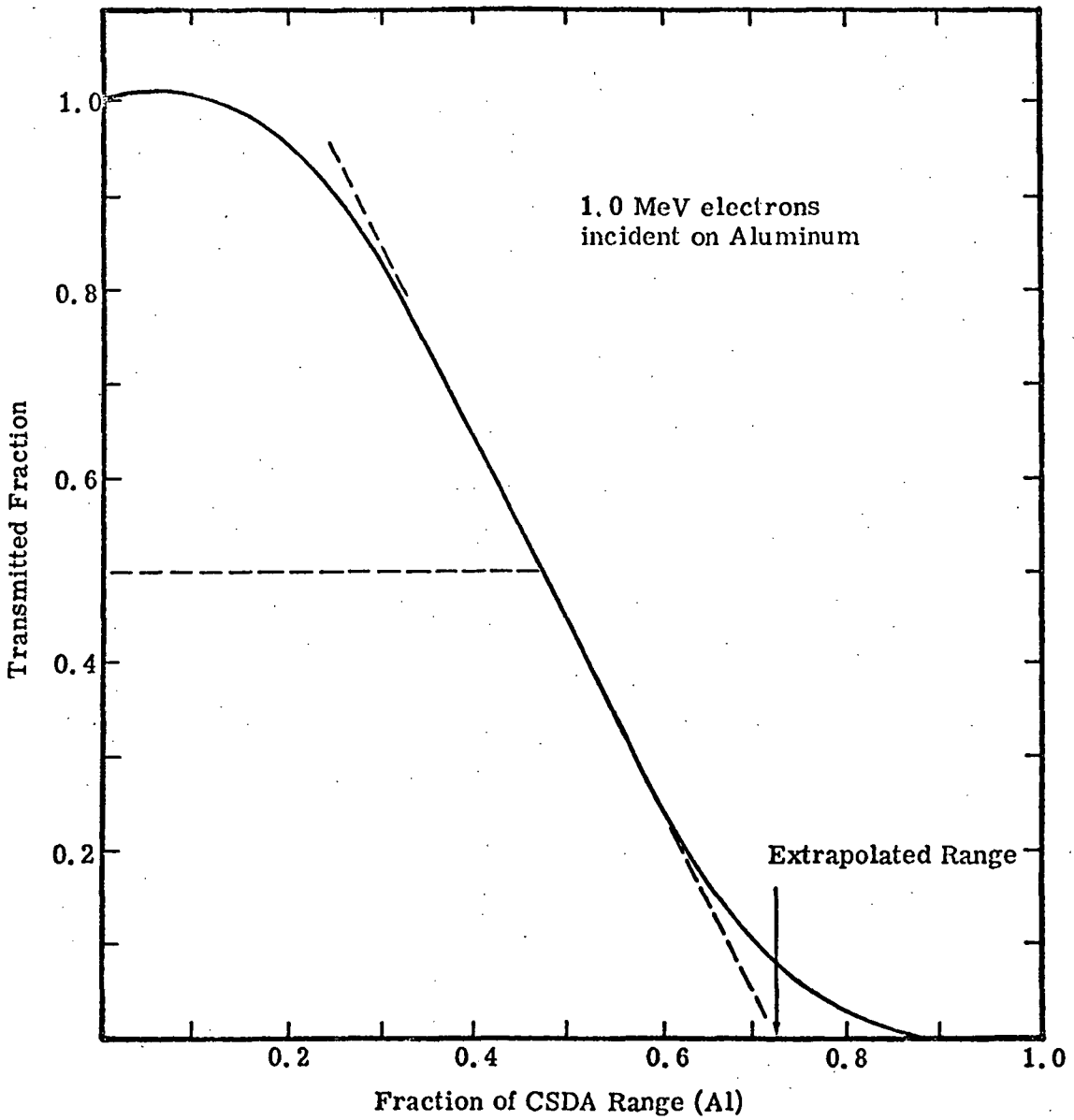

Figure 3.5. Illustrative definition of extrapolated range

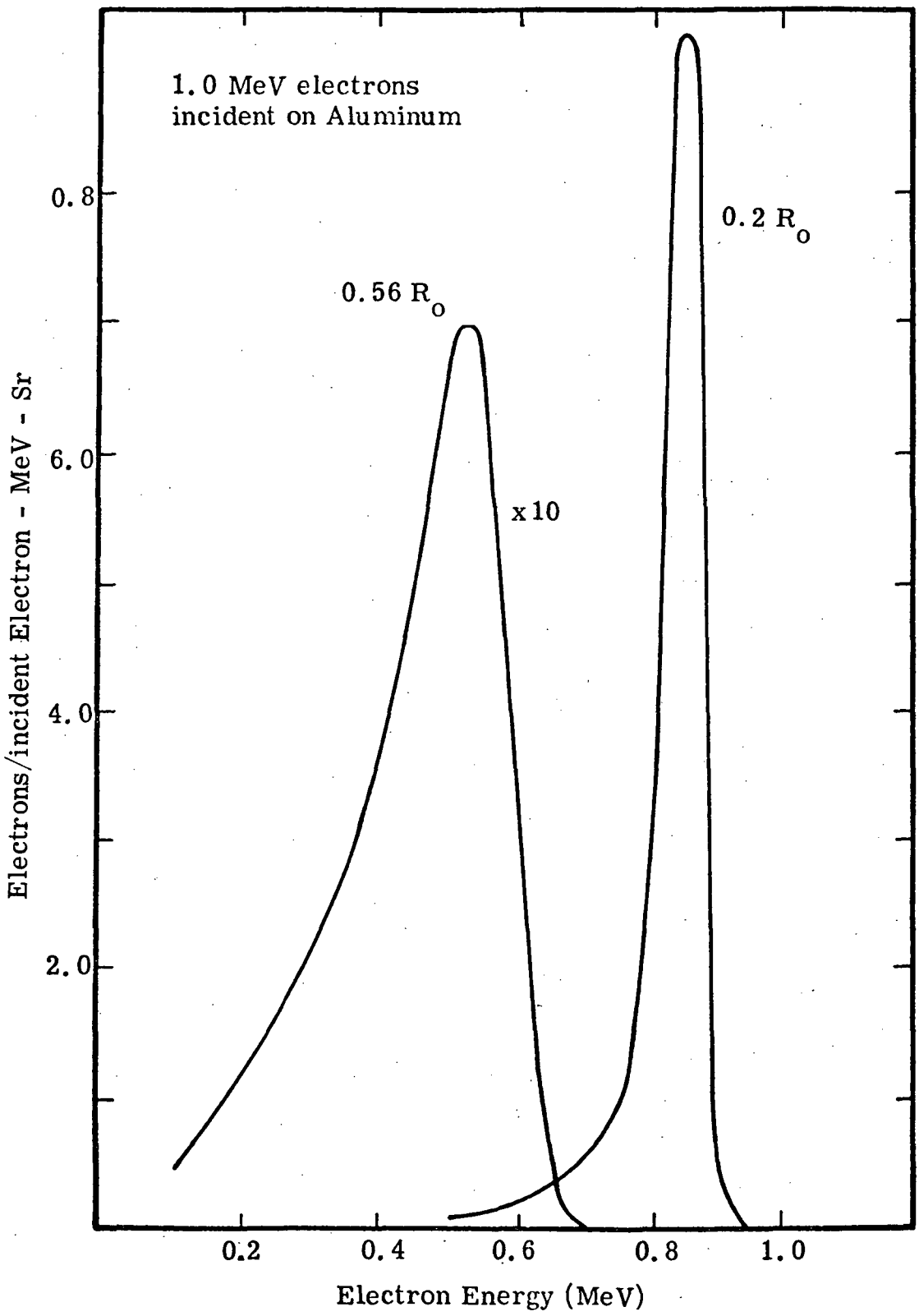

Figure 3.6. Comparison of transmitted energy spectra for normally incident electron for two thicknesses of aluminum. Electrons are emitted along the incident beam direction.

point results from the combined effects of angular dispersion and energy loss fluctuations. The general features of these transmitted spectra are independent of atomic number and energy (when they are scaled to the range). However, there is a tendency toward more smearing as the atomic number is increased.

3.3.5 Angular Distribution

The angular distribution of electrons after penetrating a given thickness of material is nearly Gaussian for very thin depths of the order of 0.05 range or less[20] and becomes almost a cosine current distribution (isotropic flux) at thicknesses of the order of 0.2 range or greater. That the distribution approaches a cosine shape at a few tenths of a range and does not change as the thickness is increased is due to the fact that at these depths the angular dispersion has succeeded in making the internal distribution of electrons essentially isotropic. Angular distributions for electrons penetrating thicknesses of aluminum corresponding to 0.10 and 0.5 ranges are shown in Fig. 3.7. The energy and atomic number dependences of the angular distribution are reflected in the thickness at which the cosine-like shape sets in and dominates. This occurs at smaller thicknesses for lower energies and higher atomic numbers.[17] The thickness region over which these variations are observed is approximately 0.15 to 0.30 of the range. Again, a quantitative parameterization of the angular distribution is given in similar to Section 5.

3.3.6 Energy Deposition

The deposition of energy by electrons as they penetrate into material is characterized by an initially low value which increases with depth to about 0.3 range where it reaches a maximum and decreases to zero at the end of the range.[21, 22] The deposition by 2-MeV electrons penetrating aluminum is shown as a function of depth in Fig. 3.8. The dependence of this property on energy and atomic number is again (and for the same reasons) dependence of the angular distribution on these quantities. As the energy is lowered and/or the atomic number is increased the energy deposition profile varies less rapidly with depth.

3.4 BREMSSTRAHLUNG PRODUCTION

When a charged particle is accelerated it emits energy in electromagnetic radiation.[20] The amount of energy emitted depends on the magnitude of the acceleration. In the process of stopping in matter charged particles s uffer many decelerations and emit this radiation called bremsstrahlung (breaking radiation). For protons and other heavy charged particles the individual decelerations experienced in stopping are relatively small and, consequently, little bremsstrahlung is emitted. Electrons, which have a rest mass about 1840 times smaller than protons, but the same electric charge, experience much more drastic accelerations in their interactions with atomic nuclei and hence will produce much more bremsstrahlung than heavier charged particles.

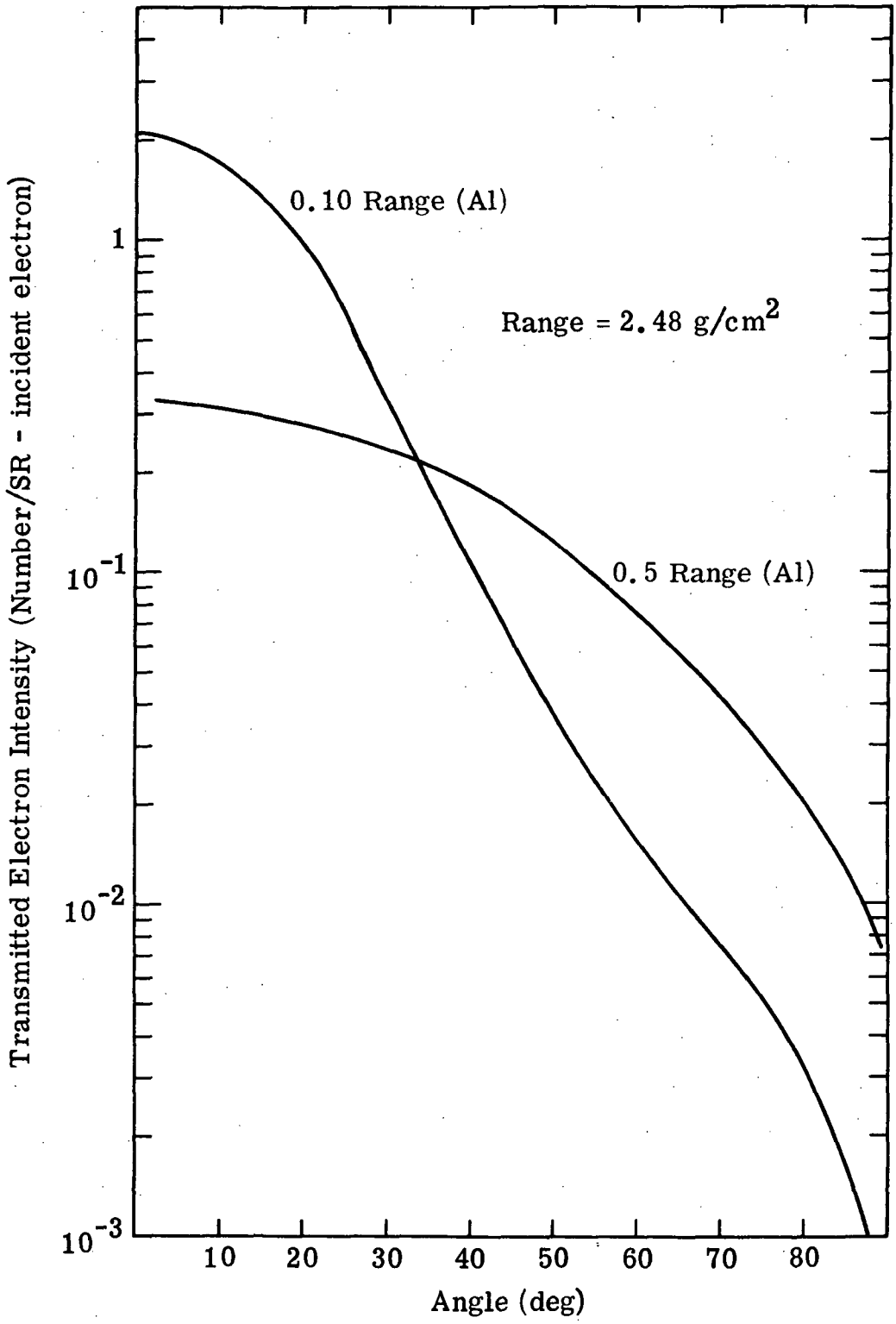

Figure 3.7. Angular distribution of 4.0 MeV electrons penetrating two slabs of aluminum at right angles (23)

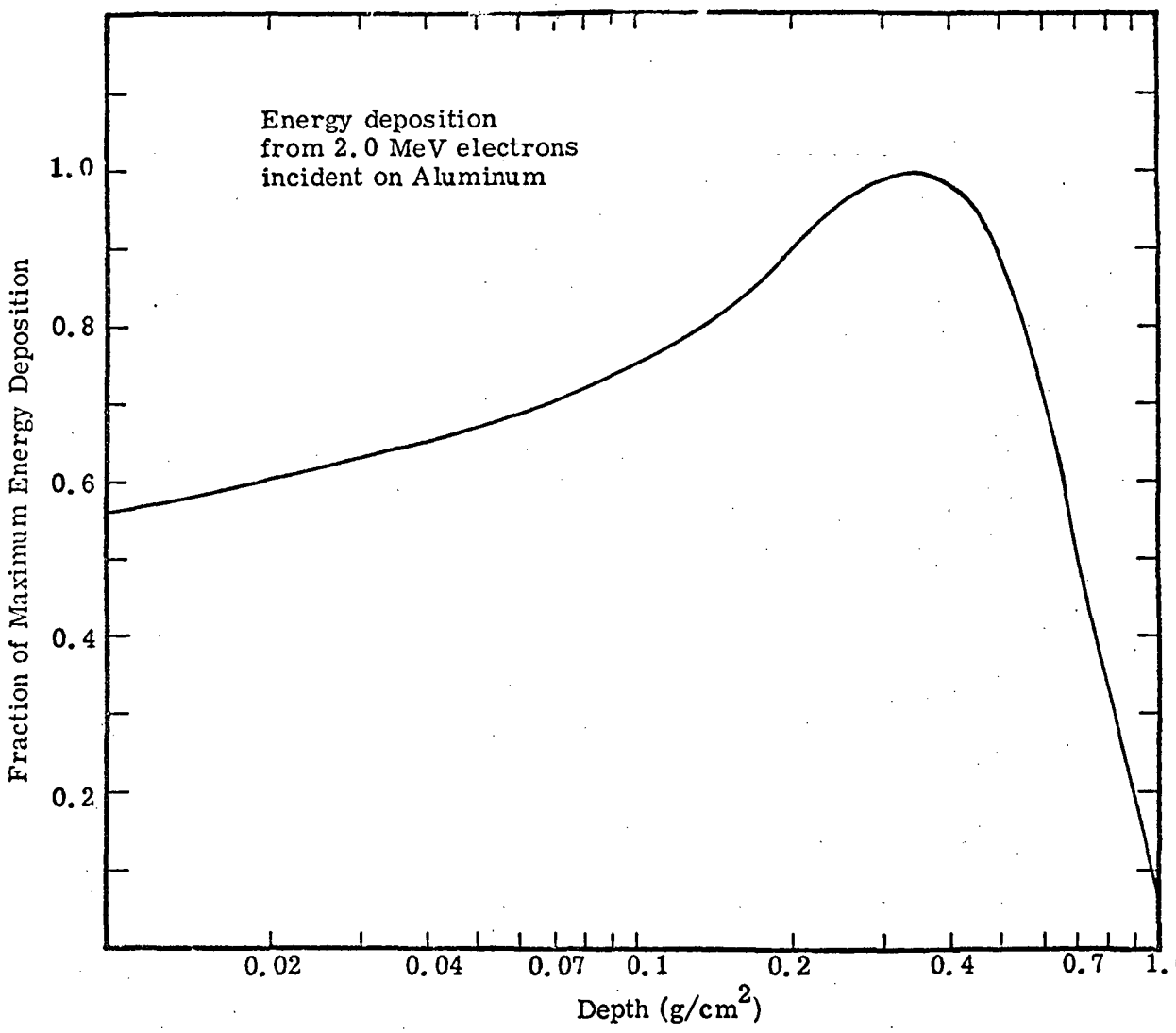

Figure 3.8. Energy deposition fraction as a function of depth.

The production of bremsstrahlung by electrons is a very important shielding consideration. This process is usually responsible for the dose that is delivered to points behind shields thick enough to stop most of the electrons. This is due to two facts: (1) the amount of energy converted to bremsstrahlung becomes significant as the electron energy and the target atomic number are increased, [15,24] and (2) a mean free path for photons (which corresponds to a shield thickness required to reduce the photon intensity by 1/e) is on the order of ten greater than the ranges of electrons of the same energy. [25] Consequently, shields are often designed sufficiently thick to stop electrons, but not to adequately attenuate bremsstrahlung which requires much heavier shields. The radiation hazard is then caused in these cases by the bremsstrahlung production.

The cross section for the production of bremsstrahlung by electrons incident on atomic nuclei is proportional to the square of the atomic number Z of the target material in the Born approximation. [26] The electron-electron collision rate which determines the rate of energy loss is proportional to the atomic number of the target. This indicates that the number of nuclei an electron encounters in slowing down to rest in bulk media will be proportional to 1/Z. Bremsstrahlung, which is produced mainly by the interaction of electrons with atomic nuclei, will be approximately proportional to the atomic number of the stopping material.

Actually, the effects of the angular dispersion caused by multiple scattering with atomic nuclei tend to lessen this Z dependence. This occurs because in high atomic number materials the electrons suffer large deflections sooner in the energy loss process. Since the bremsstrahlung production cross section is proportional to the square of the electron's energy at any given point in the stopping process and the bremsstrahlung cross section for relativistic electrons is strongly peaked in the direction of the electron's motion, a larger fraction of the photon intensity will be radiated into larger angles for high Z targets.

The angular distribution of the bremsstrahlung emitted from thick targets reflects the angular distribution of the electrons in the first few tenths of the electron range. In light materials the electrons at these depths are much more forward peaked than in heavy elements. Consequently, the bremsstrahlung angular distribution is more forward peaked in light elements.

3.4.1 Thin Target Bremsstrahlung

The differential cross section $(d^2\sigma/dkd\Omega)$ for the production of bremsstrahlung by an atomic nucleus falls off as the photon energy increases and is very strongly peaked around the direction of the electron. Figures 3.9 and 3.10 show the differential cross sections for the production of bremsstrahlung by 1-MeV electrons on Al and Au targets. [27] The energy spectra can be approximated over most of the photon energy range by (1-k/E)/k per MeV where k is the photon energy and E is the kinetic energy of the incident electron.

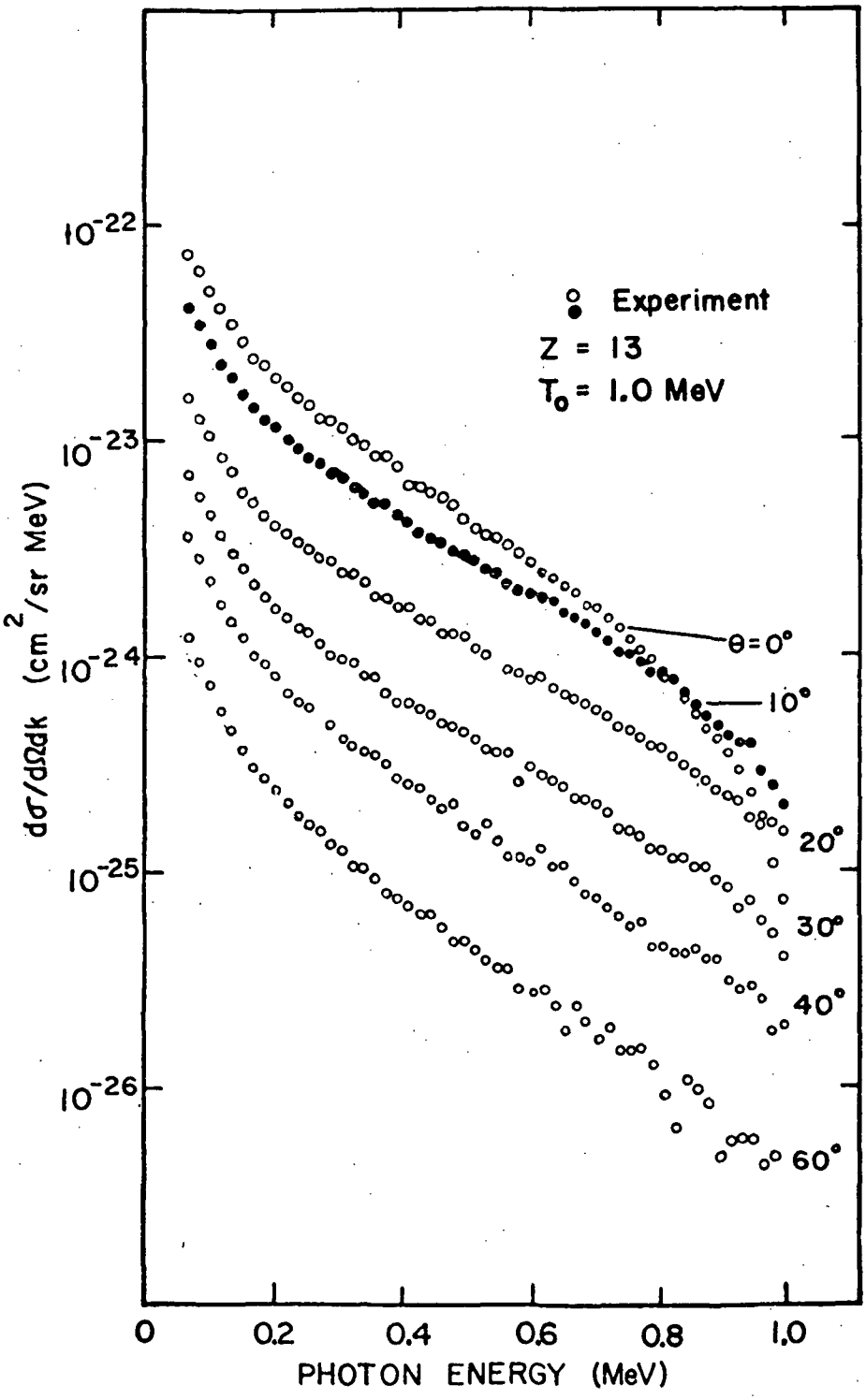

Figure 3.9. Bremsstrahlung differential cross sections for 1.0-MeV electrons on Al (from Ref. 27)

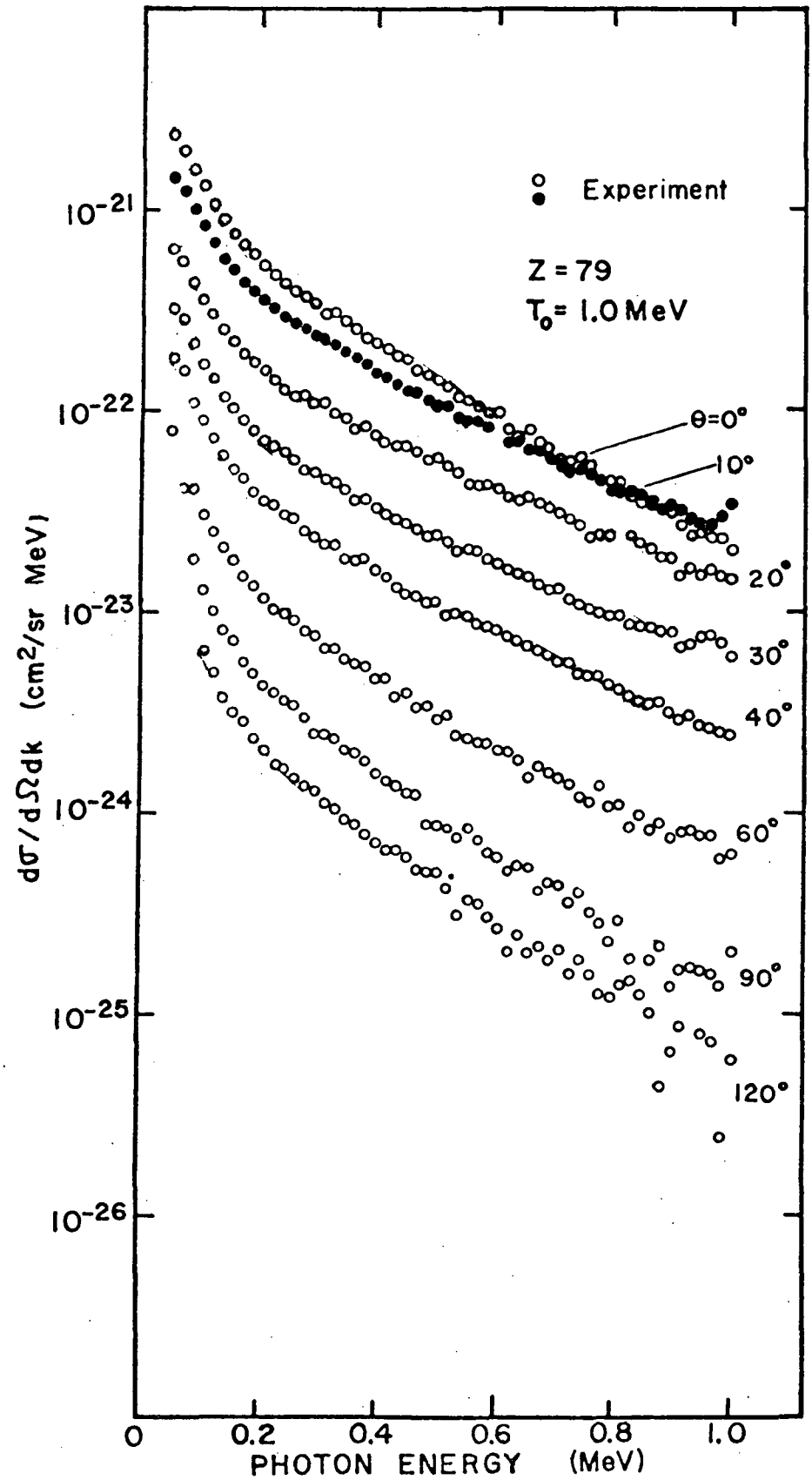

Figure 3.10. Bremsstrahlung differential cross sections for 1.0-MeV electrons on Au (From Ref. 22)

Figure 3.9 shows that the angular distribution of the cross section for fixed photon energy decreases by about a factor of 10 in the first 25 degrees and continues to decrease almost exponentially as the angle increases. The extent to which the differential cross section is forward peaked becomes more pronounced as the energy of the electron increases.

3.4.2 Thick Target Bremsstrahlung

For all practical situations one will be dealing with thick-target bremsstrahlung where the effect of the dispersion of the electrons as they penetrate the material will smear the thin-target distribution over a larger angular spread. The energy spectrum will also be increased for low-energy photons as the electrons lose energy in the material. Examples of the thick-target bremsstrahlung intensity yields for 1-MeV electrons incident on targets Al and Au are shown in Figs. 3.11 and 3.12.[28] It should be noted that the intensity (photon number times photon energy) is plotted in these graphs.

To first order, the shapes of the energy spectra are independent of electron energy and atomic number when plotted vs k/E, the ratio of photon to electron energy. Because of the energy-angle correlation of the electrons in the early penetration stages, the shape of the spectrum is angularly dependent. The effect of this correlation is to make the spectrum harder in the direction of the electron motion than at nonzero angles with respect to the incident beam direction. This effect, as will be seen in Figs. 3.11 and 3.12 is more pronounced in low Z material than in high Z material. At angles greater than 90 degrees, that is in the backward direction, there is a noted increase in the number of low energy photons. This occurs because in thick targets the bremsstrahlung is generated close to the surface on which the electrons are incident. Low energy photons are readily attenuated by the target material and must pass through much more material to emerge in the forward direction than in the backward direction. Consequently, the soft portion of the spectrum is more prevalent at backward angles. Low energy photons are more readily attenuated by high Z materials so that the thick target bremsstrahlung intensity spectra from aluminum extends to lower photon energies before it drops off than for higher Z materials.

In the foregoing discussion the transport properties of monoenergetic electrons incident at right angles on bulk media has been described. In the more practical case where electrons with a spectrum of energies will be incident on bulk media from a variety of directions the problem of predicting results is more complicated. In general, the procedure is to build up the final transport results by superimposing the properties discussed for monoenergetic-monodirectional beams. The effect of many incident energies and directions is to wash out what structure exists in the transport properties. That is, the dependence on energy, thickness, and atomic number becomes smoother and weaker. Quantitative numbers for these cases can be extracted from the formulations discussed in Section 5.

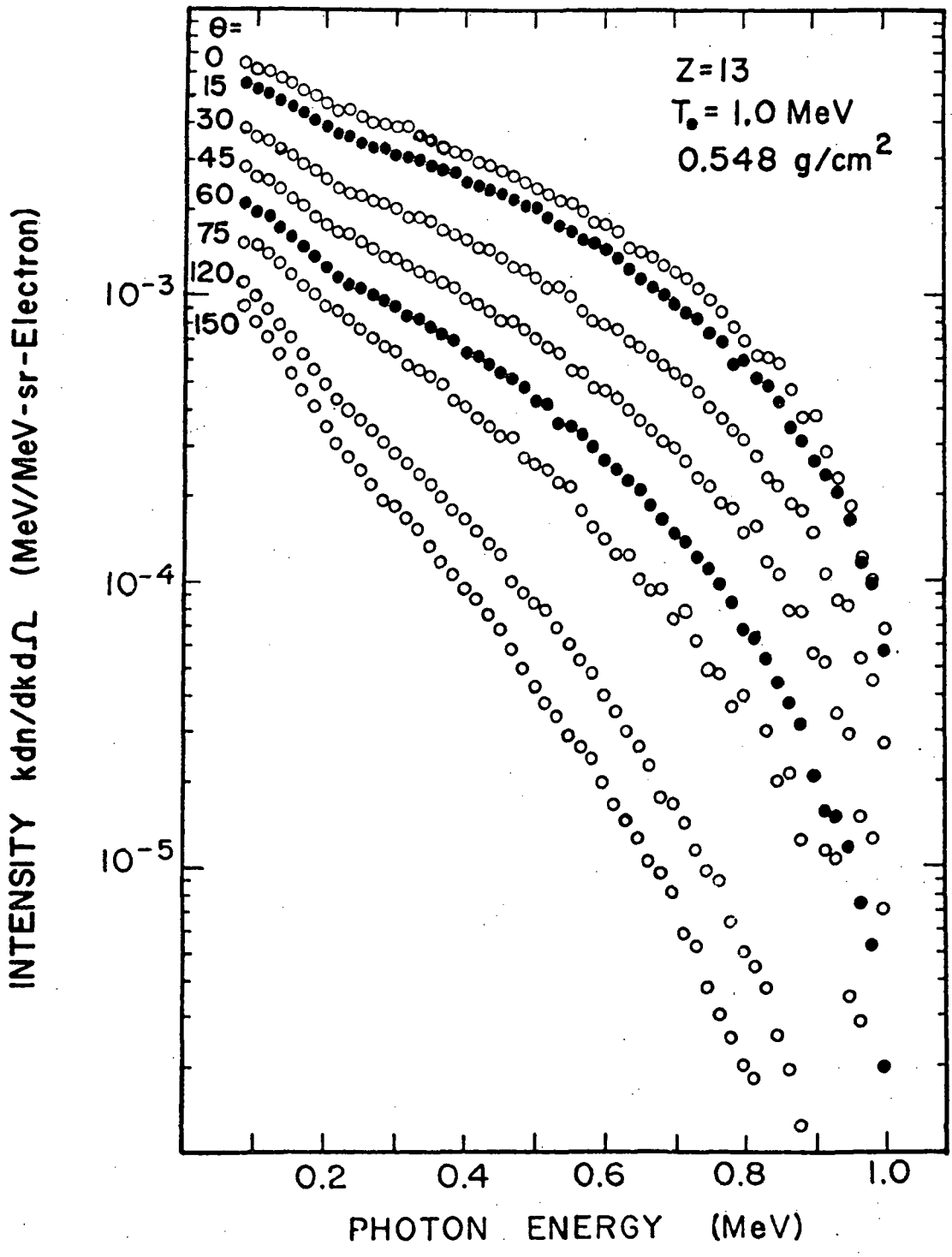

Figure 3.11. Bremsstrahlung differential intensity spectra for 1.0-MeV electrons on a thick Al target (From Ref. 28)

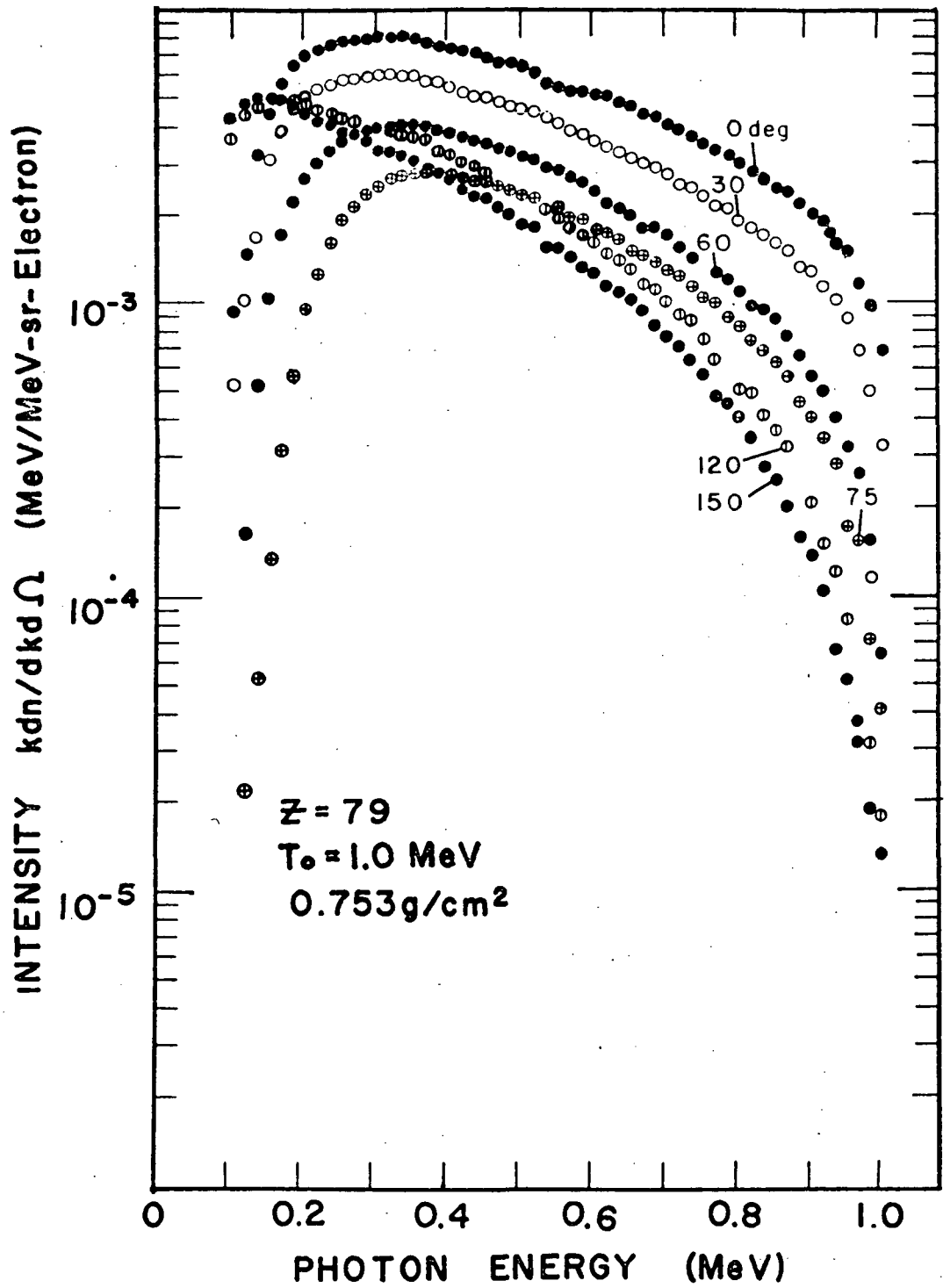

Figure 3.12. Bremsstrahlung differential intensity spectra for 1.0-MeV electrons on a thick Au target (From Ref. 28)

4. ACCURATE METHODS OF CALCULATING TRANSPORT PROPERTIES

There have been several excellent review articles concerned with the basic properties of electron transport.[14, 29, 30] This section is not meant to supplant or duplicate these articles. Its purpose is simply to serve as an introduction to the theoretical treatment of electron transport. The interested reader can find details of the theories in the review articles or more detailed descriptions of their application to transport problems in other works. This section contains short descriptions of the interaction cross sections, theories of multiple interactions, and methods of using these theories in transport calculations.

4.1 INTERACTION CROSS SECTIONS

The basic force between electrons and other charged particles is the Coulomb interaction. This force is the only interaction in the field of atomic and nuclear physics which is completely understood. The Dirac theory of the electron[31] and the field theories of quantum electrodynamics put the properties of electrons on an exact mathematical basis. The basic interaction cross sections can be calculated using these theories.

4.1.1 Elastic Nuclear Scattering

The elastic scattering of electrons from nuclei can be calculated for a bare, point nucleus and a spinless electron according to the Rutherford nonrelativistic scattering theory.[14] Modifications introduced by the spin of the electron have been incorporated in the Mott relativistic theory of elastic scattering.[32] Another effect on elastic scattering is the screening by atomic electrons of the nuclear Coulomb potential for large impact parameters. This has been taken into account in a number of approximate ways by various authors.[20, 33-35] The results of calculations of the cross section for elastic scattering using these corrections agree with experimental data. An excellent review article by Mots, Olsen and Koch presents the relevant formulas for electron-nuclear scattering.[36]

4.1.2 Electron-Electron Scattering

The scattering of electrons from electrons is formally different from the scattering of electrons by nuclei because of the Pauli principle. Møller has derived the cross section for the elastic scattering of electrons by free electrons.[13] Because the incident and atomic electrons are indistinguishable, after the collision the higher energy electron is treated as the incident particle. A comparison of the electron-electron cross section with experimental

data is presented in the review article by Birkhoff [14] and shows good agreement. The fact that the electrons are bound to atoms complicates the electron-electron collision considerably. The physical processes are understood, but the numerical complication involved in an exact calculation of the cross section makes such an endeavor impractical for atoms heavier than hydrogen at this time. Approximate methods have been developed and are discussed by Birkhoff. [14]

4.1.3 Bremsstrahlung Production

Bremsstrahlung can be produced in the scattering of electrons from atomic nuclei or to a lesser extent in scattering from atomic electrons. The interaction matrix element was first calculated [26] using the Born approximation. This approximation assumes that the incoming and outgoing electron wave functions can be treated as plane waves. For cases where both incoming and outgoing electrons have high energies, that is,

$$V_i >> \frac{2\pi Z}{137} c \qquad (4.1)$$

and

$$V_f >> \frac{2\pi Z}{137} c$$

where V_i and V_f are the electrons' initial and final velocities, the approximation is valid, and reasonable results are obtained. [37] For low-energy electrons in the outgoing channel (corresponding to high photon energies) the approximation breaks down and the theory may underestimate the cross section by orders of magnitude.

Calculations of the bremsstrahlung cross section using Dirac wave functions for the electron and partial wave expansions for the Coulomb field have been performed. [38, 39, 40] These calculations do not yield analytic formulas however, and require extensive numerical procedures to obtain results. For this reason these calculations have not been used extensively.

4.2 AVERAGE QUANTITIES

Although the basic cross sections for electrons are well known, it is difficult to apply them directly to electron transport properties since an electron undergoes so many interactions in the process of slowing down. A 1-MeV electron experiences about 10^5 interactions in stopping. It would thus become very time consuming to attempt to follow the electron as it slows down interaction by interaction. Approximations have been developed to treat the average properties of electron transport which are applicable to short path lengths. The formulation of energy straggling due to electron-electron collisons has been developed by Landau [18] and improved by Blunck and

Leisegang.[41] Directional dispersion has been approximated by a number of authors.[20, 35, 42, 43] The theories which are most commonly used for multiple nuclear scattering are the theories due to Moliere,[20] and Goudsmit and Saunderson.[35] Reviews of the various theories are given by Birkhoff,[14] Scott,[43] and Zerby and Keller.[30]

4.3 APPLICATION OF AVERAGE PROPERTIES TO THICK TARGETS

The theories of the average behavior of electrons penetrating matter are typically valid for the passage of electrons through amounts of material which are small compared to the electron range. There have been many attempts to solve the problem of the penetration of electrons and the production of bremsstrahlung in bulk media. Some of these attempts make use of various approximations to reduce the problem to a point where analytic or semi-analytic solutions are possible.[17, 44-47] However, these approximations limit the application of the analytic solutions either to a very high electron energies or very small angles, which in turn limits their usefulness in space radiation problems. Other methods of solution that are not based on limiting assumptions on the electron energy or electron angle employ either a numerical summation of the contribution of scattering in multilayered shields,[48, 49] a moments method type of calculation,[22, 48] or Monte Carlo solutions.[51, 53] All these methods rely on rather lengthy computer calculations to obtain solutions.

4.3.1 Moments Methods Calculations

The moments method was developed to solve the Boltzman transport equation for electrons by Spencer and Fano.[22] The method employs a semianalytical solution to the transport equation in which the energy, angular, and spatial dependence of the flux are described by a series of polynomial expansions. Electron-electron collisions involving small energy transfers are treated according to a continuous slowing-down model which assumes that the form of the cross sections for these collisions is unimportant as long as the correct stopping power is obtained. The stopping power is the average energy loss per unit path length and is the result of many electrons making many collisions. In the moments method the relativistic Møller cross section is assumed to be valid down to a very small fractional energy loss which is defined so as to give the correct total stopping power. Typically, moments method calculations can be practically performed in infinite homogeneous media. For this reason their application to problems related to space radiation has been limited.

4.3.2 Monte Carlo Calculations

The second method of accurately solving electron transport problems is through the use of Monte Carlo techniques. Theoretically, Monte Carlo calculations can follow each individual electron through every collision as the electrons are slowed down and scattered through the target foil. In practice,

this is not feasible due to the large number of collisions involved. Instead, theories describing various segments of the transport problem are used to group together large numbers of collisions. The computation proceeds by considering successive spatial intervals with the resulting distributions determined by a conventional random sampling based on the suitable multiple scattering theories.[35] Berger and Seltzer [53] have written a Monte Carlo code ETRAN, in which the angular deflections can be computed by the methods of Goudsmit and Saunderson, Moliere, and Fermi's Gaussian distribution. The spectrum resulting from energy loss is determined by the modified Landau energy straggling distribution or from a continuous slowing down model. Collisions involving large energy transfers can be considered separately from the continuous slowing down model, and secondary electrons and photons are produced and transported through the target sample. In general calculations based on ETRAN have shown good agreement with experimental results.

The principal disadvantage of the Monte Carlo electron transport calculations is that they require a considerable amount of computer time. Because of the stochastic nature of the method the accuracy is directly dependent on the number of particle histories that are run and hence the computer time required. Another disadvantage of ETRAN is that in its present form it is only capable of performing calculations in homogeneous slab material. However, Buxton and others have modified ETRAN so that it is capable of making calculations in multimaterial laminations of slabs.[54]

4.3.3 Discrete Ordinates

Recently Bartine et al.,[55] have employed the method of discrete ordinates to perform electron transport calculations. This method has been used in neutron and gamma ray transport successfully for some time. In this method an analytical solution to the Boltzman transport equation is obtained through the use of approximations in the representations of the angular, spatial, and energy scales. Briefly, these variables are grouped into a finite number of increments which cover the range of interest. By then expanding the angular dependent flux and cross sections as a series of suitable functions (usually Legendre expansion) the Boltzman equation can be reduced to a set coupled equations. By a judicious choice of discrete angular structure the number of equations is reduced to those corresponding to a few terms in the expansion. Each of the equations is then solved numerically using iterative techniques. The advantage is that an analytical solution is obtained everywhere the spatial mesh is defined so that accurate results can be obtained at deep penetrations where it is costly in computer time to obtain good statistical accuracy using Monte Carlo methods. The disadvantage of the technique in general is that the savings in computer time is significant for one-dimensional problems only. By one dimension it is implied that only one linear dimension is varied. Infinite slabs, spherical shells, and infinite cylinders are examples of one-dimensional configurations. In discrete ordinates calculations the angular distribution of the flux is calculated, but this is still a one-dimensional

configuration if only one spatial dimension is varied. Another disadvantage of the application of discrete ordinates approach to electron transport is that the techniques have not been fully developed. The present accurate methods of incorporating the cross sections cause the computer time required for a given calculation to be comparable with Monte Carlo calculations. Bartine et al., have used the continuous slowing down approximation with success at low atomic number but with some uncertainty in heavy elements. The discrete ordinates method seems to have a lot of potential and hopefully the work that just started in the last year or two will lead to as useful a tool in electron transport as discrete ordinates has proven to be in neutron and gamma-ray transport problems.

5. PARAMETRIC REPRESENTATION OF TRANSPORT PROPERTIES

5.1 INTRODUCTION

In practical problems in which it is necessary to make a quick determination of the radiation dose delivered to a point partially shielded from a radiation source, it is very useful to have an inexpensive means of obtaining reasonably accurate results. In particular, in the space environment it is often necessary to establish the dose level due to both electrons and associated secondary photons at points inside a spacecraft. Just as frequently the initial estimate becomes the burden of an engineer or scientist whose professional interests are related to the experiment or person being placed in space and may have only a passing familiarity with the properties of electron transport and bremsstrahlung production. One simple method of calculating electron transport properties makes use of parametric representations which express the results of experimental data or accurately calculated results. The method by passes the mathematical complications inherent in a rigorous analysis which incorporates all of the intermediate processes.

This section will present such parametric formulas for the electron and photon transport properties. Many of these formulas have been obtained in the past by others and are collected here for completeness while some have been generated by the authors.

For ease of access, these formulas are presented with a minimum of explanation or justification. A detailed comparison of the parameterization for bremsstrahlung production which is new, with experimental data and results generated with Monte Carlo calculations are presented in Appendix A.

5.2 PARAMETERIZATION OF ELECTRON TRANSPORT PROPERTIES

In this section, formulas which describe the property specified are displayed. As mentioned above, many of these formulas are the result of the efforts of other workers. Those which are presented have been selected because they best represent the experimental data with which we have been able to compare them.

5.2.1 Transmitted Number Fraction

The number of electrons penetrating through a given depth within a material per incident electron is defined as the transmitted number fraction.

Ebert et al., [56] have measured this quantity for normally incident electrons in the energy range 4 to 12 MeV and have suggested the following parametric representation.

$$T_F(E, Z, T) = \exp\left[-\alpha\left(\frac{T}{R_{ex}}\right)^{\beta}\right] \quad \left(\frac{\text{electrons}}{\text{incident electron}}\right) \tag{5.1}$$

where

$$\alpha = (1 - 1/\beta)^{1-\beta}$$

$$\beta = \left[\frac{387\ E}{Z(1 + 7.5 \times 10^{-5}\ ZE^2)}\right]^{1/4}$$

the quantity, T is the penetration depth in (g/cm^2).

Mar [57] has suggested a parametric representation for the transmitted number fraction based on the results of Monte Carlo calculations for electrons with energies between 0.4 and 10 MeV as

$$T_F(E, Z, T) = \exp\left[-\left(\frac{0.634\ E\ Z^{-0.23}}{T^{0.848}}\right)^{-\gamma(Z)}\right] \tag{5.2}$$

where

$$\gamma(Z) = 7.0(Z - 3.25)^{-0.24}$$

and E is the initial kinetic energy in MeV.

The transmitted fraction for electrons incident on aluminum has been calculated by Watts and Burrell [58] using ETRAN. [59] The results of these calculations are tabulated in Appendix B as a function of incident electron angle, energy and slab thickness.

5.2.2 Range

There are two commonly used definitions of range, one is the extrapolated range, the other is the continuous slowing-down approximation (csda) range. The extrapolated range is more easily determined from experimental data. The following expression is due essentially to Katz and Penfold [60] with some modifications by Ebert et al., [56]

$$R_{ex}(E, Z) = 0.565\left(\frac{125}{Z + 112}\right)E - 0.423\left(\frac{175}{Z + 162}\right)(g/cm^2) \quad E > 2.5\ \text{MeV}$$

$$= 0.38\ E^A \qquad (g/cm^2) \qquad E < 2.5\ \text{MeV} \tag{5.3}$$

where

$$A = (1.265 - 0.095 \ell n\, E)(1.7 - 0.273 \ell n\, Z)$$

Here E is the electron kinetic energy in MeV and Z is the atomic number.

The continuous slowing-down approximation range is more easily calculated than is the extrapolated range and has come into rather wide use because of the very convenient tabulation of this quantity by Berger and Seltzer.[15] Watts and Burrell[58] have suggested the following parametric fit for the csda range in aluminum.

$$R_o(g/cm^2) = (1.33 - 0.019E)\left(\sqrt{0.2713\, E^2 + 0.0121} - 0.11\right) \qquad (5.4)$$

which is accurate to within 2 percent for energies between 0.3 MeV and 10 MeV. For other elements R_o for aluminum can be multiplied by 2.08 Z/A to obtain the csda range for element Z to within about 15 percent in the same energy region. From the data of Ebert et al.,[56] and Bergers tabulation, we have derived the following relationship between the extrapolated and csda ranges

$$(R_{ex}/R_o) = 1.21 - 0.208 \ell n\, Z + 0.0242\, E \qquad (5.5)$$

which is valid for electron energies between 250 keV and 12 MeV. This formula agrees with the experimental data to within 5 percent for elements of atomic number of 13 or higher and within 10 percent for carbon.

5.2.3 Backscatter Coefficient

The backscatter coefficient is defined as the fraction of electrons incident on an infinitely thick target that are scattered in the backward direction. The following expression was derived by Tabata[19] from data he measured and is valid for $Z > 6$.

$$\eta(E, Z) = 1.28 \exp\left[-11.9\, Z^{-0.65}(1 + 0.103\, Z^{0.37}\, E^{0.65})\right] \qquad (5.6)$$

The backscatter coefficients for aluminum have been generated by Watts and Burrell[58] using the Monte Carlo code ETRAN.[59] The results of these calculations are tabulated in Appendix B as a function of the incident electron angle and energy and slab thickness.

5.2.4 Transmitted Energy Spectrum

The energy spectra of electrons penetrating a depth (T/R_o), that is, penetrating through a thickness of some fraction of the continuous slowing down range, have been fit. The experimental data measured by Lonergan

et al.,[23] Costello et al.,[61] and Rester et al.,[62] were used as the base from which the following parametric representation was derived:

$$S(E, E_o, T, Z) = \frac{1}{N} \left\{ \exp\left(-\left(\frac{E - E_p}{W} \right)^2 \right) + C \frac{E}{1 + \exp\left(\frac{E - E_p}{W} \right)} \right\} \qquad (5.7)$$

$$\left(\frac{\text{electrons out}}{\text{MeV total electrons out}} \right)$$

where

$$E_p = E_o[1 - T/R_o]$$

$$N = W\sqrt{\pi} + C\left[\frac{W^2\pi^2}{12} + \frac{3}{2} E_p^2 \right]$$

$$W = 0.05\sqrt{Z}(T/R_o)$$

$$C = (T/R_o)^2\sqrt{Z}$$

where E_o is the energy of the incident electrons in MeV and E is the energy of the degraded electrons. This function is normalized so that integrating it over E from 0 to E_o yields unity

$$1 = \int_o^{E_o} S(E, E_o, R)\, dE$$

The absolute number of emergent electrons as a function of E is obtained by weighting $S(E, E_o, T, Z)$ by the transmitted fraction.

The energy transmitted through slabs of aluminum has also been calculated by Watts and Burrell[58] using ETRAN.[59] They define a quantity called the energy transmission coefficient which:

Energy Transmission Coefficient = energy current transmitted/
energy current incident

where current is defined in Chapter 6. The energy transmission coefficient is tabulated in Appendix B as a function of incident electron angle and energy and slab thickness. Also tabulated as a function of these same parameters is the energy reflection coefficient for aluminum which is defined as

Energy Reflection Coefficient = energy current reflected/
energy current incident

5.2.5 Angular Distribution

The angular distribution of electrons integrated over all electron energies (differential electron current) penetrating a slab after striking it normally has been fit in two regions. If the slab thickness is less than approximately 1/3 the extrapolated range, a Gaussian distribution fits the data reasonably well:

$$\phi(E, Z, T) = \left(\frac{K}{\sqrt{\pi}}\right)\exp(-K^2\theta^2) \qquad (5.8)$$

where $\left(\frac{\text{electrons}}{\text{Sr}}\right)$

$$K^2 = E^2/[\,0.1212\,T\,Z^{0.88}\,\ell n\,(T/0.00105)\,]$$

where E is the kinetic electron energy in MeV, T is in g/cm^2, and θ is in radians. However, if the slab is thicker than 1/3 the extrapolated range, the distribution merges into a thickness-independent form given by Bethe, Rose, and Smith[63] as

$$\phi = 0.23\,(0.717 + \cos\theta_n)\cos\theta_n \cdot \left(\frac{\text{electrons}}{\text{Sr}}\right) \qquad (5.9)$$

This expression is normalized so that the integral of ϕ over the hemisphere of the outgoing electrons yields unity. The absolute number of electrons emerging in a given direction per incident electron is obtained by weighting ϕ with the transmitted fraction for the appropriate slab thickness, where θ_n refers to the polar angle relative to the normal to the plane from which the electrons are emerging. It is important to note that θ_n is not referenced to the incident electron direction. Experimental data[23,62] indicate that for thick targets ($T/R_{ex} > 1/3$) the angular distribution is independent of the incident electron direction.

5.2.6 Energy Deposition

The energy deposited by electrons as they penetrate a material has been calculated with ETRAN,[59] a Monte Carlo electron transport code. Watts and Burrell[58] have made parametric fits to these results for two cases. The first is for a broad monodirectional beam, normally incident on a semi-infinite slab of material and is given by

$$\rho_\perp(E,X) = \exp\left(\sum_{c=1}^{4} A_i\, X^{i-1}\right) \qquad (5.10)$$

where $\rho_\perp$ is the energy deposition in (MeV/g unit current) and:

$$A_1 = 0.913\,\exp(-0.963\,E) + 0.021\,E + 0.215$$

$$A_2 = 5.0 - 0.49\ E$$

$$A_3 = 57.6\ (E - 5.0)/(E + 30)$$

$$A_4 = -1.6\ E^{0.837}$$

The second case is for a half space isotropic incident flux of electrons, which is an isotropic distribution in one hemisphere and normalized so that an integration of the flux over that hemisphere yields unity. In this case the energy deposition is parameterized as

$$\rho_{iso}(E,X) = \exp\left(\sum_{1}^{5} A_i X^{i-1}\right) \tag{5.11}$$

where ρ_{iso} is the energy deposition in (MeV/g unit half-space isotropic flux) and

$$A_1 = 0.52 + 0.098\ E^{-1.47}$$

$$A_2 = \exp\ (-0.82\ E) - 1.0$$

$$A_3 = -2.5\ [\exp\ (-1.022\ E) + 1.0]$$

$$A_4 = 3.25\ \exp\ (-0.323\ E) + 5.8$$

$$A_5 = -15.44 + 1.55\ E - 0.0786\ E^2$$

where X is the depth of penetration in units of R_o.

The energy deposition coefficients $\rho_\perp$ and ρ_{iso} for aluminum which were calculated to provide the data base for the parametric fit are tabulated in Appendix B. The quantity θ is tabulated for beams incident at several angles relative to the normal of a semi-infinite plane.

5.2.7 Non-Normal Electron Incidence

The parametric representation of the preceding sections deals with electrons normally incident on a target. It has been found experimentally [64] that for targets thicker than about three-tenths of the csda range, non-normal electron incidence shifts the energy spectra slightly down in energy, hardly affects the relative angular distribution of the emitted radiation, and decreases the transmitted fraction $T_F(E, Z, T)$ by a factor that is approximately given by the cosine of the angle between the direction of the incident electron and the target normal raised to some power which depends on the target thickness and initial electron energy. As an approximation one can assume that the energy spectrum and angular distribution are unaffected and write the transmitted fraction for non-normal electron incidence as

$$T_F(E, Z, T, \theta) = T_F(E, Z, T, O) \left[\cos \theta\right]^a \tag{5.12}$$

where X is given for Al as

$$a = \left[0.41 + 3.7\ (T/Ro)^2 + \left[0.14\left(\frac{T}{R_o}\right) - 0.039\right]E\right]$$

Here T is the slab thickness in g/cm^2, R_o is the continuous slowing down approximation range defined in Section 5.2.2 and $T_F(E, Z, T, O)$ is the transmitted fraction for normal incidence defined in Section 5.2.1.

5.3 PARAMETERIZATION OF BREMSSTRAHLUNG PRODUCTION

Electrons slowing down in matter emit electromagnetic radiation which is typically more penetrating than the electrons themselves and hence must be considered in radiation shielding calculations. The photons which are created in the bremsstrahlung process emerge in all directions with respect to the direction of the original electron and have energies ranging from zero up to the kinetic energy of the electron. For a complete description of the production of bremsstrahlung one must consider both the angular and energy dependence of the photons as functions of the electron energy, the target material, and the direction of both the electron and photon. Often, however, useful information can be obtained from integral quantities. Presented in this section are formulas that relate both integral and differential quantities to the electron energy, target material, initial electron direction relative to the material orientation, and direction of the final photon.

5.3.1 Total Electron Energy Converted to Bremsstrahlung

When an electron stops, part of its initial kinetic energy is converted into bremsstrahlung. The amount of energy converted into bremsstrahlung depends strongly on the initial energy of the electron and the atomic number of the stopping material.

Convenient tables of the stopping powers and ranges of electrons in various elements calculated by Berger and Seltzer,[15] and more recently by L. Pages, et al.,[24] include values for the fraction of the electron energy which is converted into bremsstrahlung. Examples of these calculated fractions plotted vs the incident electron energy are shown in Fig. 5.1 for carbon, aluminum, iron, tin, and gold. Figure 5.2 shows the calculated fraction vs the target atomic number for 1 MeV electrons. Over the energy region $0.1 < E < 10$ MeV, the fraction $F(E, Z)$ of the electron energy E which is converted into bremsstrahlung can be parameterized as

$$F(E, Z) = 5.71 \times 10^{-4}\ Z^{1.145}\ E^{\sigma(Z)} \left(\frac{\text{MeV photon}}{\text{MeV electron}}\right) \tag{5.13}$$

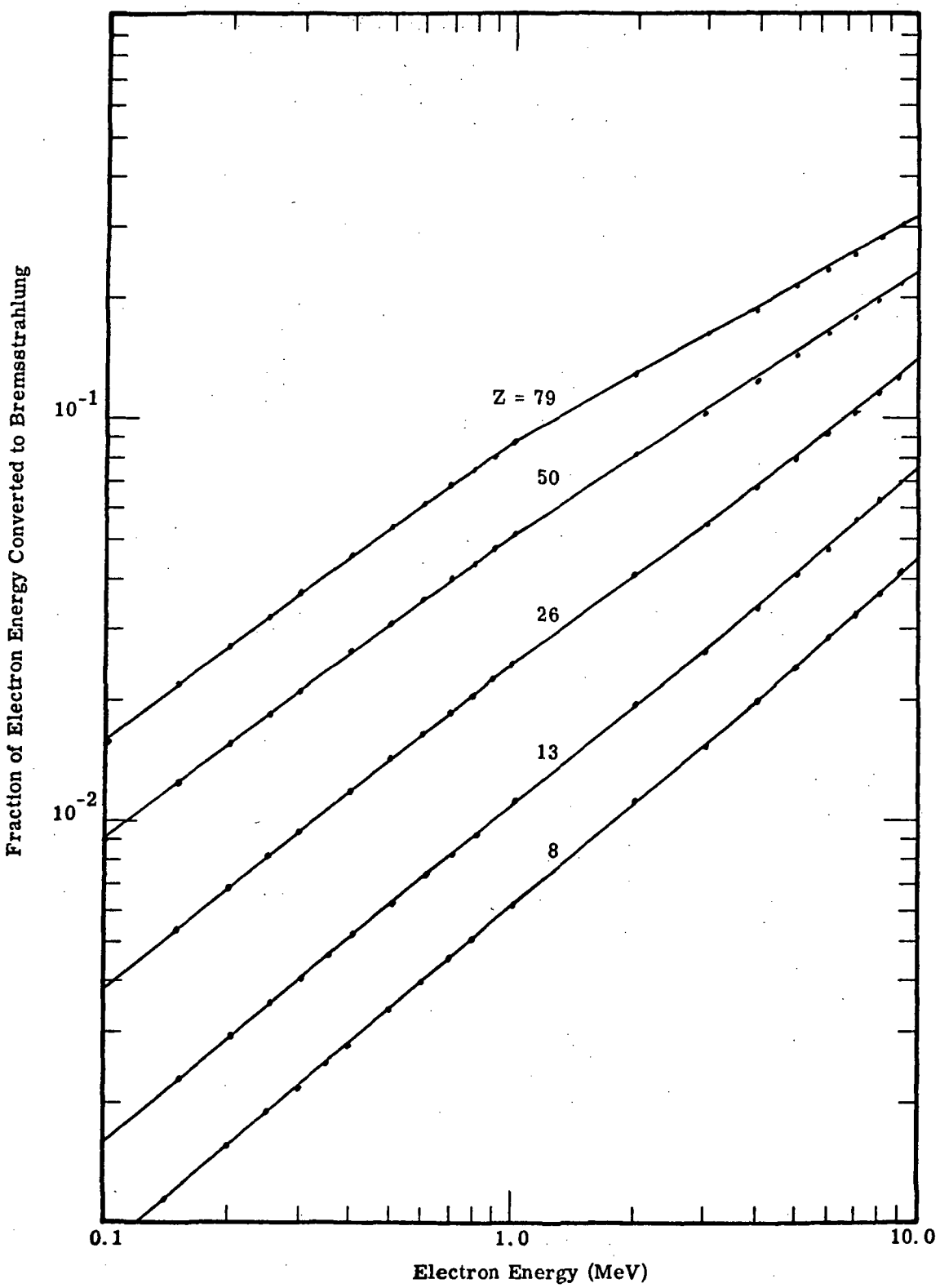

Figure 5.1. Calculated fraction of electron energy converted into bremsstrahlung (points) (Ref. 24) and parametric representation (solid lines) for different atomic numbers vs incident electron energy

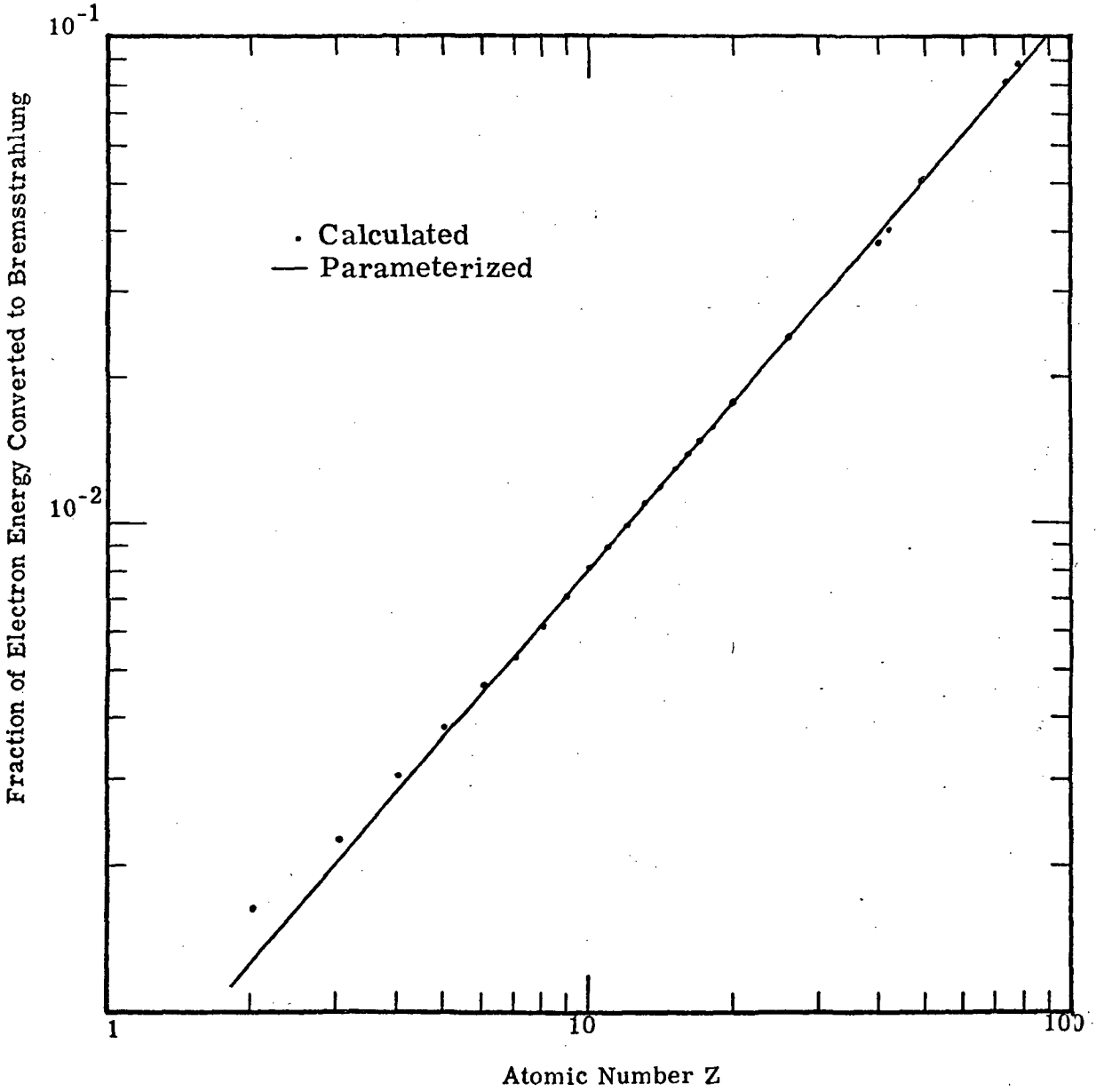

Figure 5.2. Fraction of 1 MeV electrons converted into bremsstrahlung vs target atomic number. Dots are calculated values due to L. Pages et al. (Ref. 24). The solid line is the parametric representation.

where Z is the atomic number of the stopping material and E is the initial kinetic energy of the electron in MeV. The function $\sigma(Z)$ can be parameterized as

$$\sigma(Z) = \begin{cases} 0.79 - 5 \times 10^{-4}\, Z + 6.4 \times 10^{-2} \exp(-Z^2/466) & ;\quad 0.1 < E < 1 \\ 0.79 - 2.68 \times 10^{-3}\, Z + 8.4 \times 10^{-2} \exp(-Z^2/831) & ;\quad 1 < E < 10 \end{cases} \tag{5.14}$$

over these energy regions. The solid lines in Fig. 5.1 are the parameterized values of F(E, Z). The total energy converted to bremsstrahlung I_T will be given in this parameterization as

$$I_T\,(E, Z) = F(E, Z)\, E = 5.71 \times 10^{-4}\, Z^{1.156}\, E^{\sigma+1} \left(\frac{\text{photon} \cdot \text{MeV}}{\text{electron}}\right), \tag{5.15}$$

Approximate estimates of the total electron energy converted into bremsstrahlung can be obtained assuming $1.145 \approx 1$ and $\sigma \approx 1$ so that I_T becomes:

$$I_T\,(E, Z) = 6 \times 10^{-4}\, ZE^2$$

It should be pointed out that the values listed above are total energy converted to bremsstrahlung. A fraction of the bremsstrahlung energy will be absorbed in the stopping material and will not emerge from shielding material. The total bremsstrahlung energy which emerges from thick targets for normally incident electrons is discussed in the next section.

5.3.2 Total Bremsstrahlung Energy Radiated from Thick Targets

Because of absorption in the target, the observed bremsstrahlung emerging from a thick target (one which is thick enough to stop the electrons) will be less than that produced by the incident electrons.

A comparison of the measured[28] values of the total bremsstrahlung energy radiated for normally incident electrons and calculated values of I_T for Al is shown in Fig. 5.3. It is seen that the measured values fall considerably below the calculated values; differing by a factor of three at 0.2 MeV and a factor of 1.8 at 2.8 MeV. Some of this discrepancy may be due to the backscatter of electrons which decreases with increasing electron energy, but the main contribution is due to the absorption of photons in the target which decreases rapidly as the average photon energy increases. The measured total radiated energy for electrons normally incident on targets of Be, Al, Fe, Sn, and Au is shown in Fig. 5.4. The targets in these experiments were just thick enough to stop all of the incident electrons. These experimental values have been parameterized by Dance[28] as

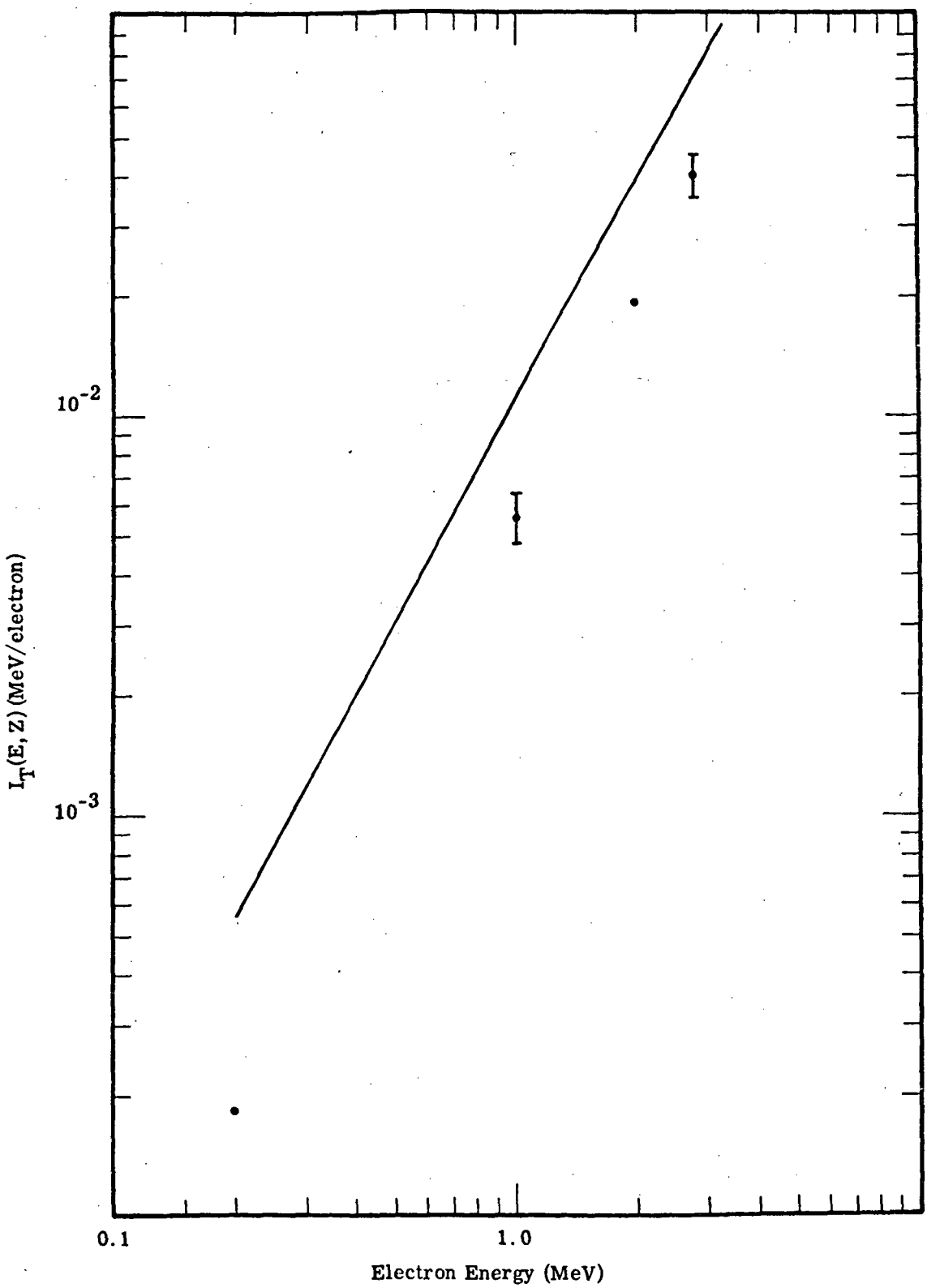

Figure 5.3. Comparison of calculated total energy converted into bremsstrahlung (solid curve) (Ref. 24) and measured total bremsstrahlug emitted from a thick A1 target (points) (Ref. 28).

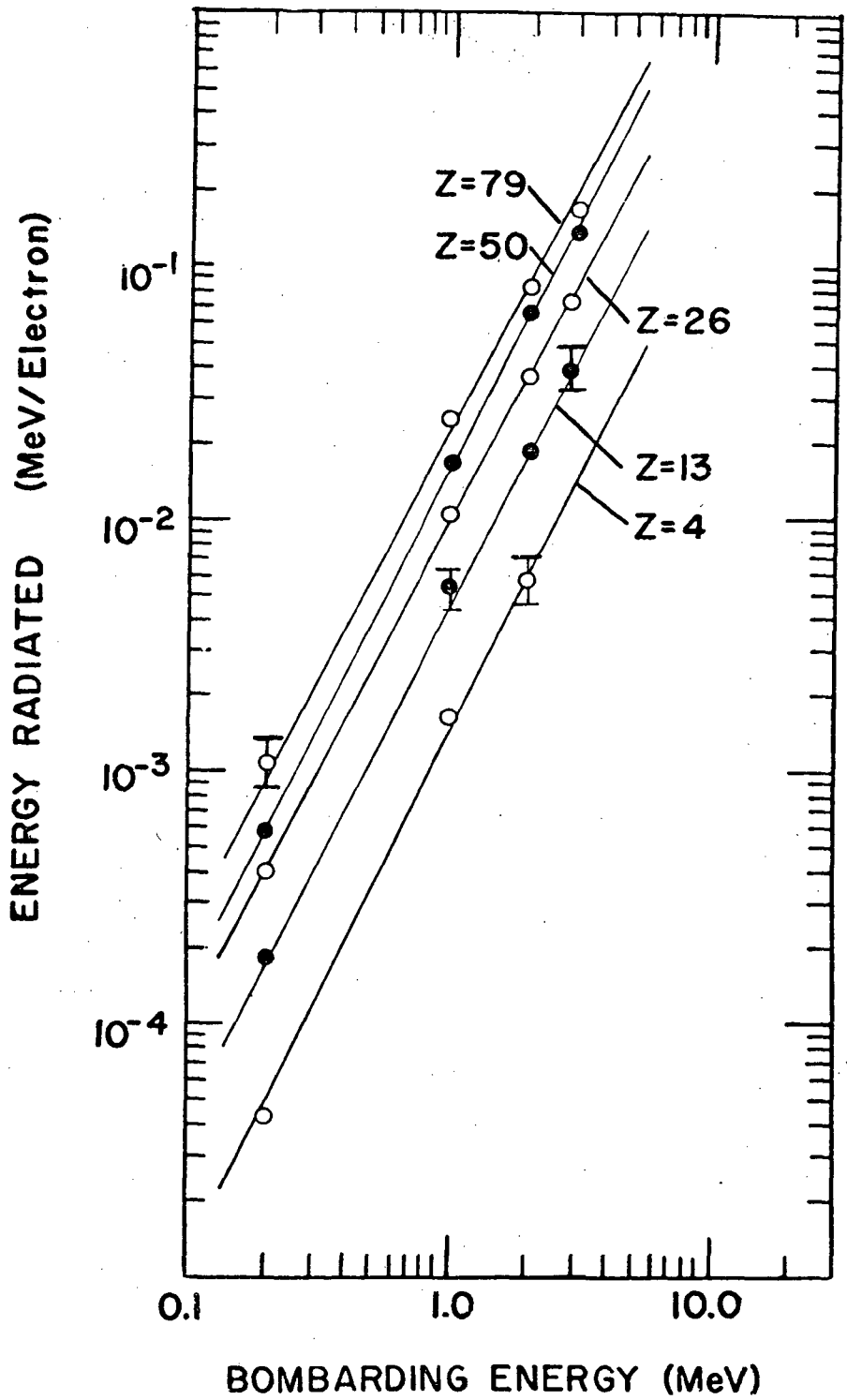

Figure 5.4. Energy radiated from thick targets of Be, Al, Fe, Sn, and Au as a function of bombarding energy, E. The respective lower cutoff photon energies for E = 0.2, 1.0, 2.0, and 2.8 MeV. Experimental lower cutoffs are 36 keV, 50 keV, 133 keV, and 171 keV respectively. (From Ref. 28)

$$I_T^r(E, Z) = C(Z) Z E^{A(Z)} \quad \text{(MeV/electron)} \tag{5.16}$$

where the values of C(Z) and A(Z) are given in Table 5.1

TABLE 5.1. VALUES OF PARAMETERS C(Z) AND A(Z) FOR EQ. 5.16

Z	C x 10^4	A(Z)
4	3.53	2.16
13	3.51	2.02
26	3.85	1.91
50	3.24	2.07
79	2.96	1.90

5.3.3 Bremsstrahlung Energy Radiated as a Function of Photon Angle

In some applications it is necessary to have some information about the angular distribution of the bremsstrahlung energy which is radiated from a target. Angular distributions of the bremsstrahlung energy radiated from thick targets (integrated over the photon energy from some nominal lower cutoff value) for 1 and 2 MeV electrons normally incident on targets of Be, Al, Fe, Sn, and Au are shown in Figs. 5.5 and 5.6.[28] The relative angular distributions of forward going radiation $I_f(E, Z, \theta)$ are shown in Figs. 5.7 and 5.8 where the data have been plotted vs $E^{1/2}\theta$ and the zero-degree data have been normalized to unity. It is seen that to a fair approximation the relative angular distributions depend only on Z when plotted in this coordinate system. The data for the forward going radiation have been parameterized as

$$I_f(E, Z, \theta) = I_0(E, Z) \left\{ 0.8 \exp\left(-\sqrt{E}\theta / K_1(Z)\right) + 0.2 \exp\left(-E\theta^2/2320\right) \right\} \left(\frac{\text{MeV}}{\text{Sr} \cdot \text{electron}}\right) \tag{5.17}$$

where θ is the angle between the direction of the electron and the photon in degrees and E is the kinetic energy of the incident electron in MeV. The Z dependence of the forward going bremsstrahlung energy is contained in the terms I_0 and K_1. The quantities $I_0(E, Z)$, the bremsstrahlung radiated into a unit differential solid angle at zero degrees, and K(Z) a measure of the

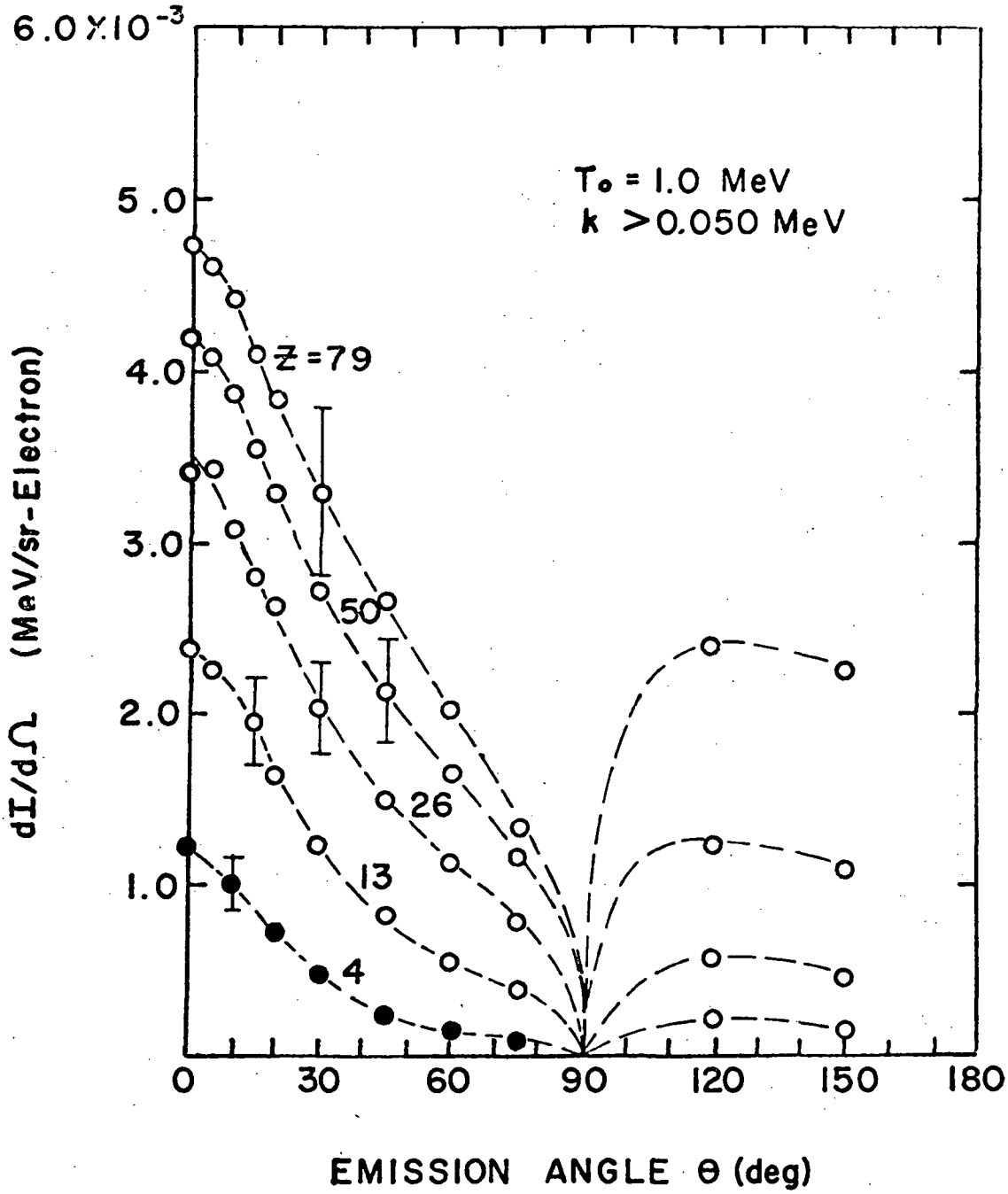

Figure 5.5. Angular distributions of bremsstrahlung intensities, integrated over photon energy, $k > 0.050$ MeV, for 1.0 MeV electrons on thick targets of Be, Al, Fe, Sn, and Au. (From Ref. 28)

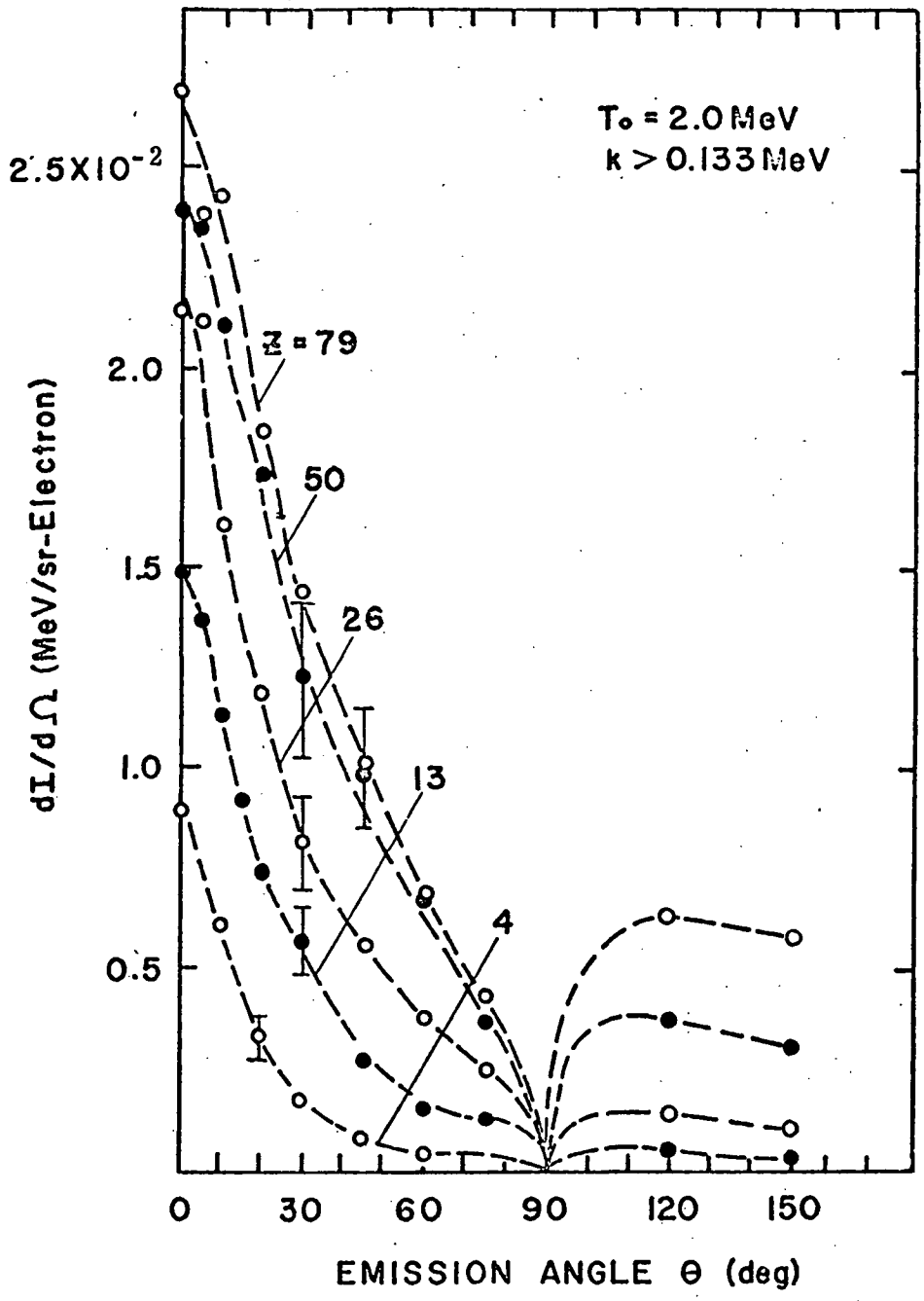

Figure 5.6. Angular distributions of bremsstrahlung intensities, integrated over photon energy, k>0.133 MeV, for 2.0 MeV electrons on thick targets of Be, Al, Fe, Sn, and Au. (From Ref. 28)

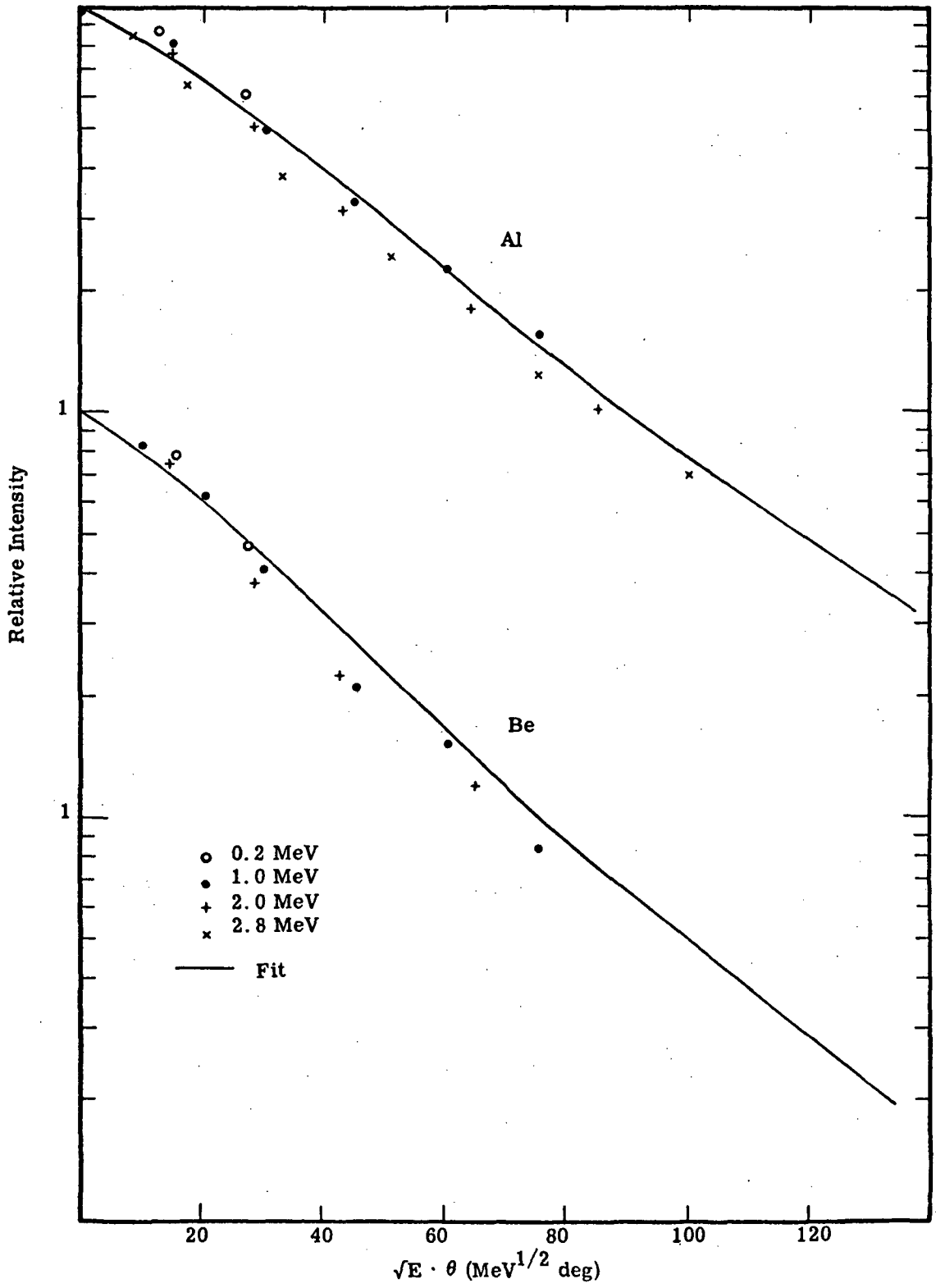

Figure 5.7. Relative angular distribution for forward hemisphere bremsstrahlung intensity plotted vs $\sqrt{E} \cdot \theta$ for targets of Al and Be. The different symbols refer to different incident electron energies. The solid line corresponds to the parameterization discussed in the text, (Eq. 5.17). All of the curves have been normalized to unity at $\theta = 0$ degrees.

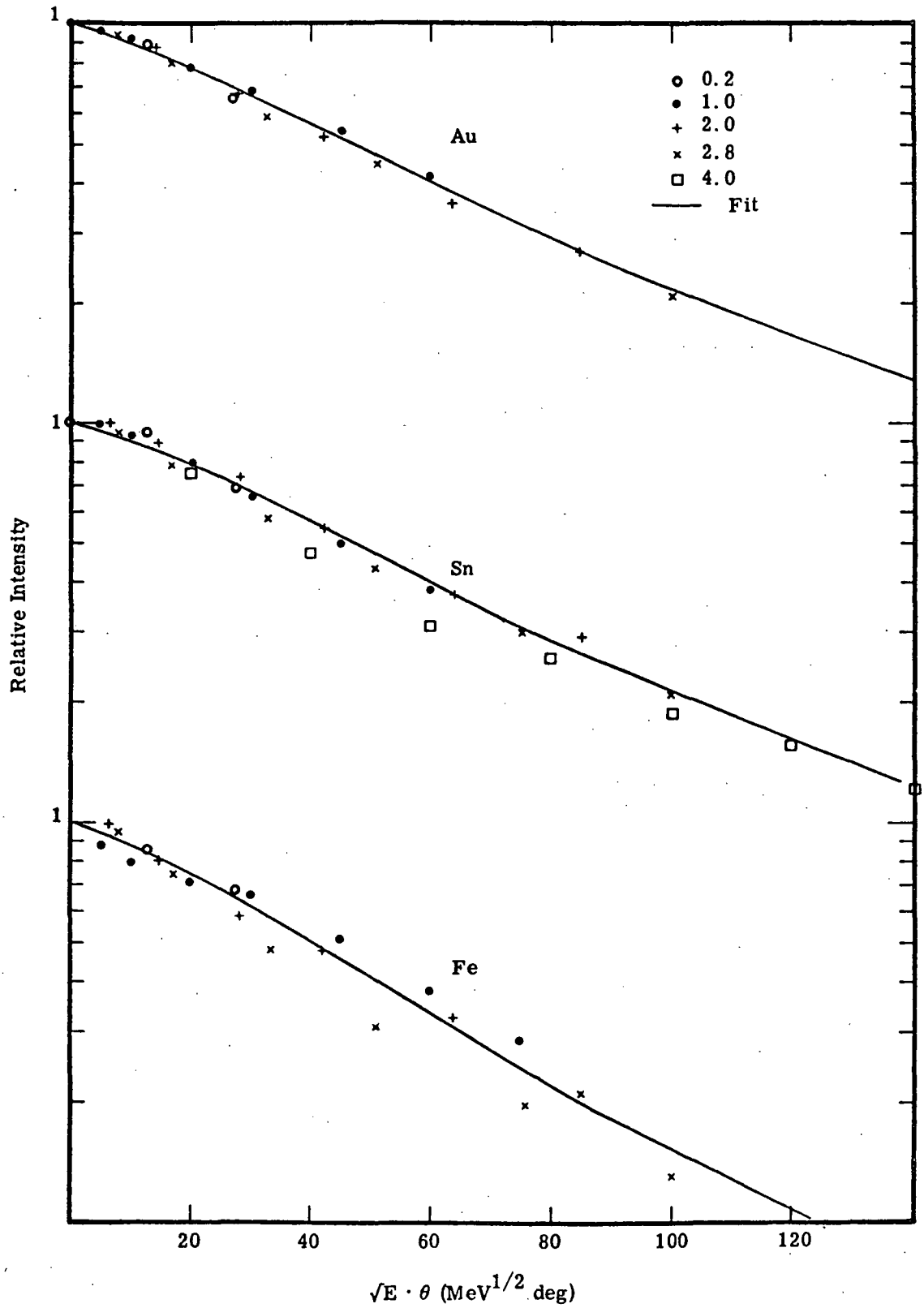

Figure 5.8. Relative angular distribution for forward hemisphere bremsstrahlung intensity plotted vs $\sqrt{E} \cdot \theta$ for targets of Fe, Au, and Sn. The different symbols refer to different incident electron energies. The solid line corresponds to the parameterization discussed in the text, (Eq. 5.17). All of the curves have been normalized to unity at θ = 0 degrees.

rate at which the bremsstrahlung energy falls off with angle are parameterized as

$$I_o(E, Z) = A_T(Z)E^{\beta(Z)} \quad \left(\frac{\text{MeV}}{\text{Sr electron}} \right) \tag{5.18}$$

and

$$K_1(Z) = 76 - 43 \exp(-Z^2/695) \quad . \tag{5.19}$$

The values of $A_T(Z)$ and $\beta(Z)$ in the expression for $I_o(E, Z)$ are listed in Table 5.2 for several elements from Z = 4 to 79.

TABLE 5.2. VALUES OF A_T AND β FOR EQ. 5.18

Z	A_T	β
4	1.2×10^{-3}	2.89
13	2.4×10^{-3}	2.59
26	3.5×10^{-3}	2.43
50	4.2×10^{-3}	2.40
79	5.1×10^{-3}	2.17

The solid curves in Figs. 5.7 and 5.8 are the parametric representations of Eq. 5.17.

5.3.4 Bremsstrahlung Intensity as a Function of Photon Energy and Photon Angle

For calculations where accurate dose estimates are necessary or where the energy spectrum of the incident bremsstrahlung is needed, one must know not only the angular distribution of the emitted radiation but also its energy spectrum.

5.3.4.1 Parameterization of Normal Incidence Data

Most of the available experimental data on bremsstrahlung production are for electron beams normally incident on thick targets of elementally pure materials. Examples of the bremsstrahlung intensity as a function of photon angle and energy are shown in Figs. 5.9 and 5.10,[28] where the bremsstrahlung intensities produced by 1-MeV electrons on Al and Au targets are displayed. It will be noticed that the spectra for Au are harder (i.e. they contain more high energy photons) than the spectra for Al at the same angles and that for both cases the spectra become softer as one increases the photon

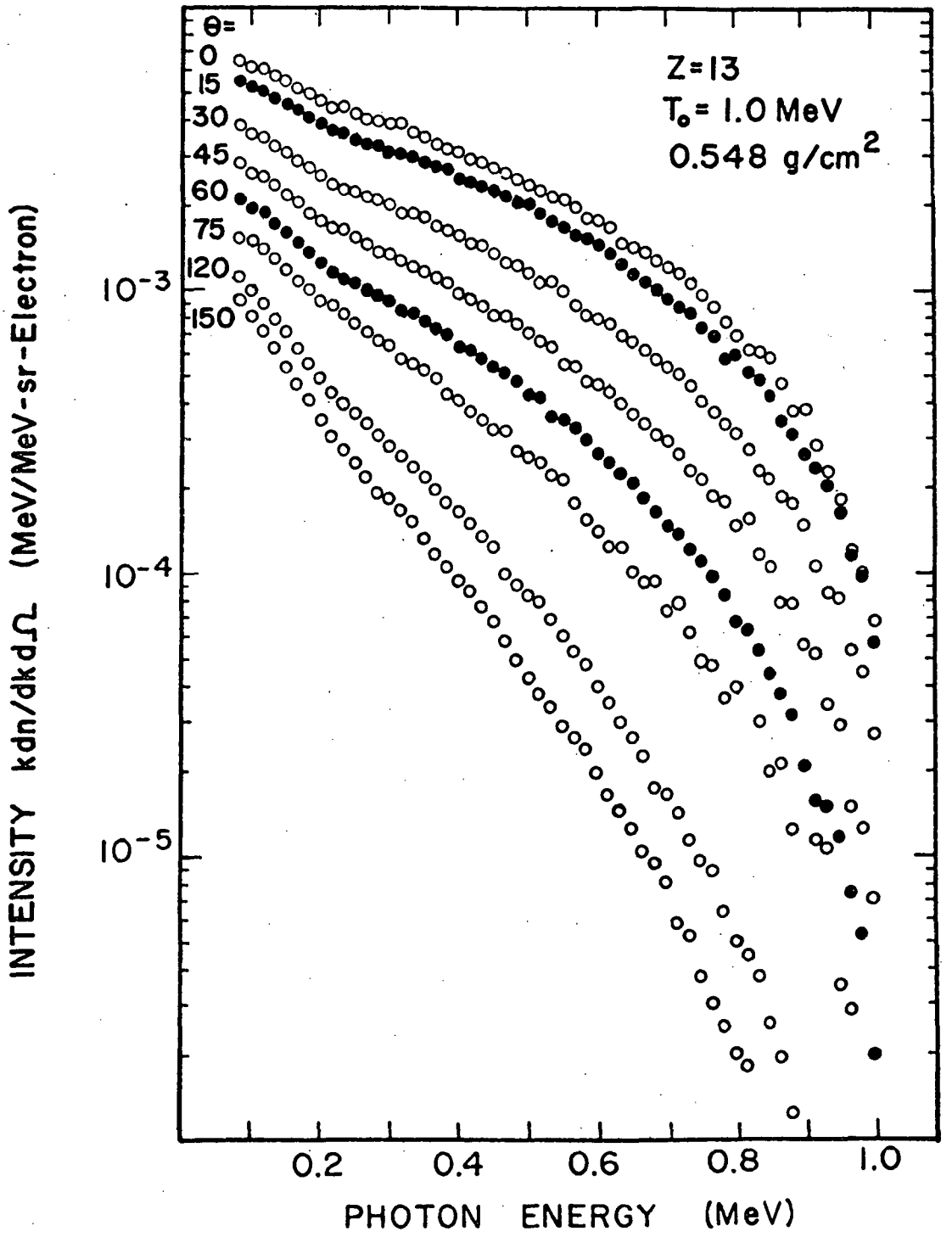

Figure 5.9. Bremsstrahlung differential intensity spectra for 1.0 MeV electrons on a thick Al target. (From Ref. 28)

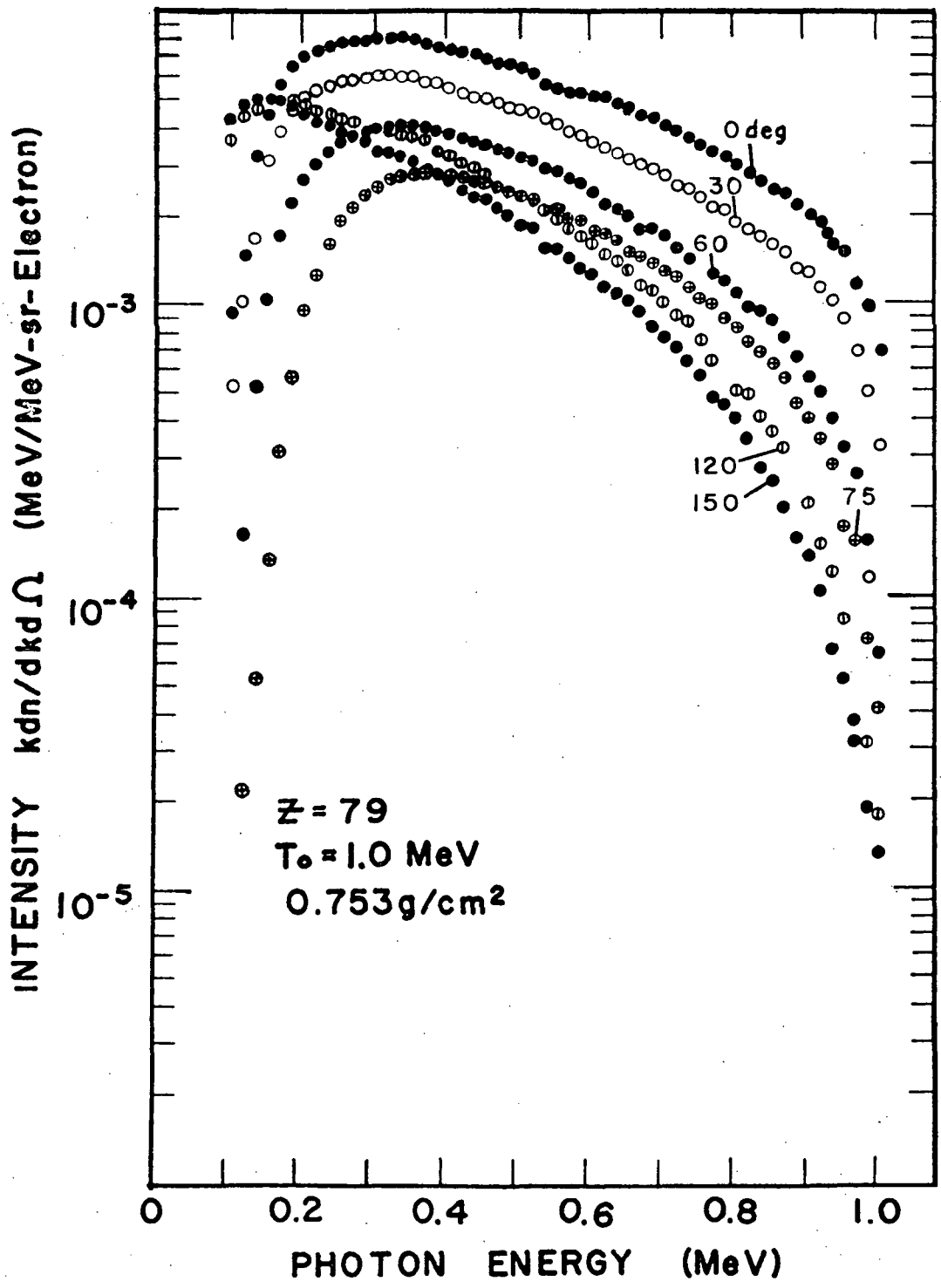

Figure 5.10. Bremsstrahlung differential intensity spectra for 1.0 MeV electrons on a thick Au target. (From Ref. 28)

angle. The bremsstrahlung intensity data have been parameterized as a source term and an attenuation term with

$$I(E,k,\theta,Z) = I_S(E,k,\theta,Z)A_T(k,\theta,Z) \tag{5.20}$$

where k is the photon energy. The attenuation term is calculated in this parameterization by assuming that the electrons produce a point source of bremsstrahlung at a penetration depth of 0.2 times their range. The attenuation is then calculated using mass attenuation coefficients (see Section 5.4). The attenuation term thus is given for normally incident electrons by the expression

$$A_T(k,\theta,Z) = \begin{cases} e^{-\mu(k,Z)(T - 0.2\,R_o)/\cos\theta} & \theta<\pi/2 \\ e^{-\mu(k,Z)\,0.2\,R_o/|\cos\theta|} & \theta>\pi/2 \end{cases} \tag{5.21}$$

where T is the thickness of the material in g/cm^2, R_o is the csda range of the electrons and $\mu(k,Z)$ is the mass attenuation coefficient in units of (cm^2/g) for photons of energy k in a material of atomic number Z. It is known that although the electrons emit bremsstrahlung along their entire path length most of the bremsstrahlung is emitted near the front surface of the material. The simple treatment of the attenuation term should therefore be reasonable. Also, errors introduced by this parameterization of the attenuation will tend to be compensated in the parameterization of the source term.

The source term $I_S(E,k,\theta,Z)$ has been parameterized as a function of electron energy E, photon energy k, photon emission angle θ, and target atomic number Z. It was found that all of the individual photon energy spectra could be fit very well (i.e., with errors less than 10 percent) by a three-parameter function of the form

$$I_S = Ae^{-B\cdot k/E}(1-k/E)^C \tag{5.22}$$

Expressing the parameters A, B, and C as functions of E,θ, and Z the parameterization was accomplished by noting that the shapes of the differential bremsstrahlung intensity spectra (with the attenuation term removed) formed a smoothly varying family of curves when plotted vs the ratio of the photon to electron energies. This is illustrated in Fig. 5.11. The numbers on the figure are arbitrary and simply label the different curves. A single curve of Fig. 5.11 represents several energy spectra for different target materials, electron bombarding energies, and photon measurement

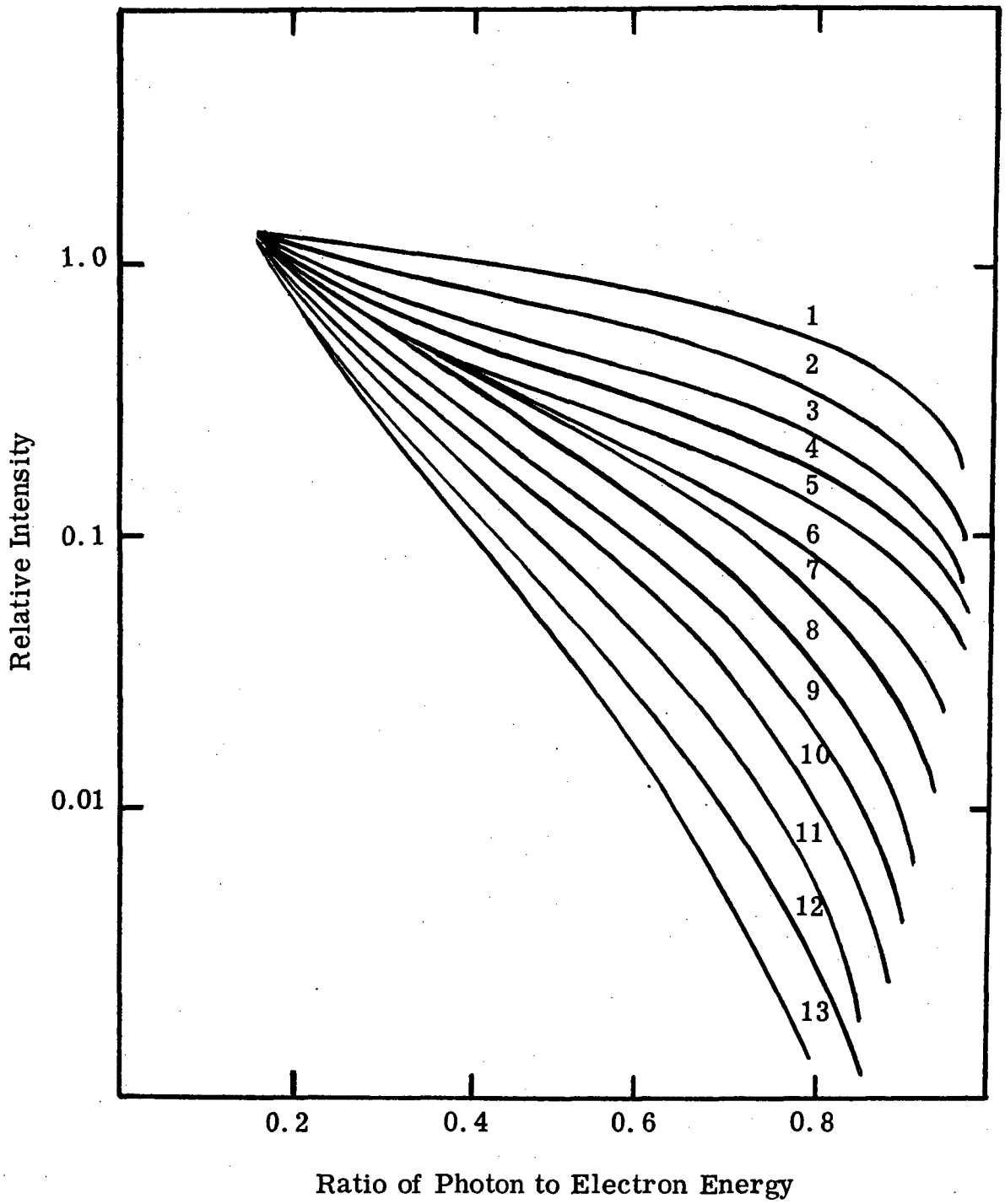

Figure 5.11. Family of bremsstrahlung intensity curves (corrected for attenuation term) for values of Z ranging from 13 to 79, E from 0.2 to 4 MeV and, θ from 0 to 150 degrees. (From data of Ref. 23, 28) The numbers on the figure are arbitrary and simply label the curves. Each curve represents the shape of the differential photon intensity spectrum at different electron energies on different target materials.

angles. The curve labeled 6, for example, is a fairly good approximation to the shape of bremsstrahlung intensity spectrum for the following situations:

Kinetic Electron Energy (MeV)	Target	Photon Observation Angle (deg)
1	Fe	60
1	Au	120
2	Fe	45
2	Sn	60
2.8	Al	30
2.8	Fe	40
2.8	Sn	45
4	Sn	40
8	Sn	60

The functional forms of A, B, and C thus obtained are given as

$$A(E,\theta,Z) = [A'(E,\theta) + a(E,Z) + b(E,Z)\cdot\theta] \times 10^{-2}$$

$$A'(E,\theta) = 0.4\,E^2 \exp(-E\theta^2/575) + 0.82\,(0.925\,E^{1.45} + 0.39\sqrt{E})\left(1 - \frac{\sqrt{E}\cdot\theta}{450}\right)$$

$$a(E,Z) = (0.34\,Z^{0.4} - 1.6)\sqrt{E}$$

$$b(E,Z) = [0.004 - 0.06\exp(-Z^2/695)]E^2/60 \quad . \qquad (5.23)$$

$$B(E,\theta,Z) = [1.41+1.41\times10^{-4}(\theta')^2]\,[0.4+0.6\exp(-(E-1.5)^2/7.6)]$$

$$\theta' = \alpha(E,Z)\cdot\theta + \beta(E,Z)$$

$$\alpha(E,Z) = 0.78\left(\frac{10.5\,E}{Z^{0.6}}\right)^{0.15}$$

$$\beta(E,Z) = \frac{33(1.15\times10^{-2}\,Z - 0.3 + E)^{0.36}}{(0.709 + 4.35\times10^{-4}\,Z^2)}$$

and

$$C(E,\theta,Z) = 0.95 + 0.35 \cos\left(\pi\left(\frac{\theta'' + 50}{100}\right)\right) - D(Z)$$

$$\theta'' = \theta' + D\theta(Z)$$

$$D(Z) = 0.245 \exp\left(-(Z-72)^2/1470\right)$$

$$D\theta(Z) = 36 \exp\left(-(Z-68)^2/830\right)$$

In these equations E is the electron kinetic energy in MeV, θ is the photon observation angle in degrees and k is the photon energy in MeV. Comparisons of the parametric representation and the bremsstrahlung data below 3 MeV are presented in Appendix A.

Undoubtedly, other, perhaps simpler, parametric representations could be derived. The above representation in no way is claimed to be the simplest representation. As is seen from the comparisons of the data, however, the parameterization gives a good representation of the data over most of the energies and atomic numbers for which it is valid.

5.3.5 Parameterization of Non-normal Incidence Data

The extension from the parameterization of normal incidence data, which are symmetric about the beam axis, to non-normal incidence data which show no complete symmetry about any axis could be quite difficult. Since it is known that the high energy portion of the bremsstrahlung is created very near the incident face of the material and it is suspected that the majority of the bremsstrahlung is also created close to the incident face of the material, an approximate treatment of non-normal incidence electrons is used in this parameterization. All of the bremsstrahlung is assumed to be created at a point 0.2 times the range of the electron in the direction of the original electron motion. (The value of 0.2 was obtained by trial and error in obtaining fits to the normal incidence data.) The angular and energy dependence of the bremsstrahlung produced at this point is assumed to be independent of the electron's original direction relative to the surface of the material and is given by the source term $I_0(E,k,\theta,Z)$ of Eq. 5.20. The difference between normal and non-normal incidence is assumed to be taken up in the attenuation term $A_T(k,\theta,Z)$ of Eq. 5.20. The situation is sketched in Fig. 5.12. Here the electron enters the material at an angle θ with respect to the normal of the material, travels 0.2R in the material and emits a photon which travels in a direction θ_γ with respect to the normal to the target. The attenuation term in this case will be

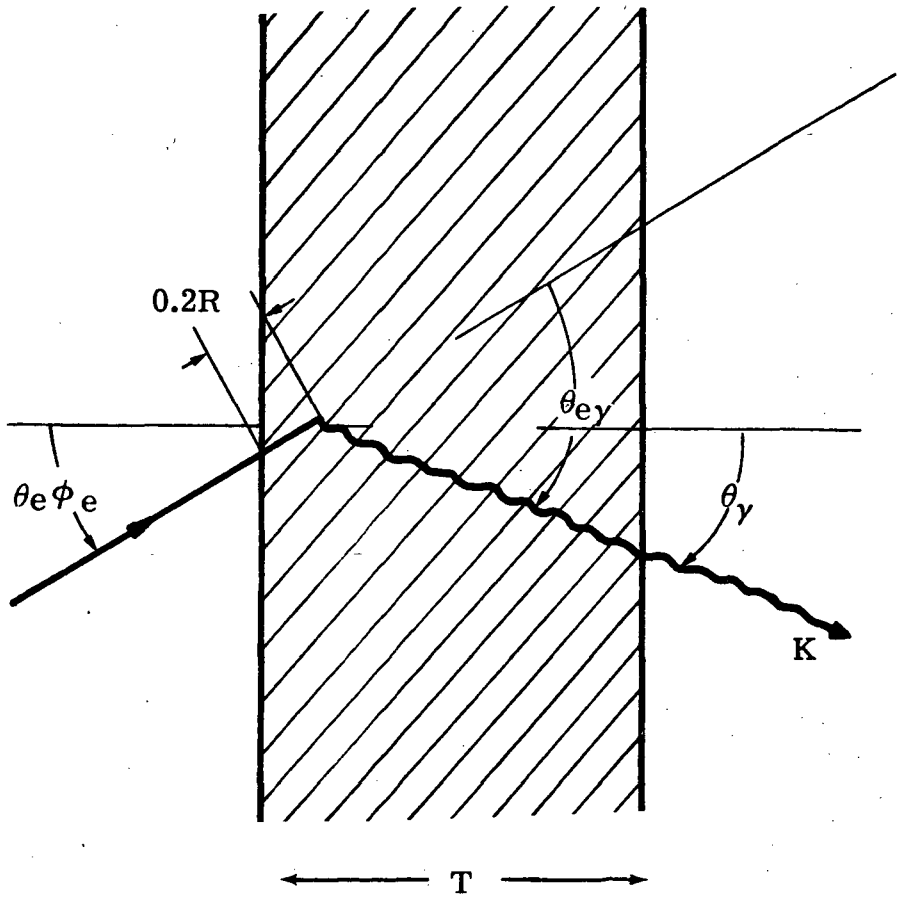

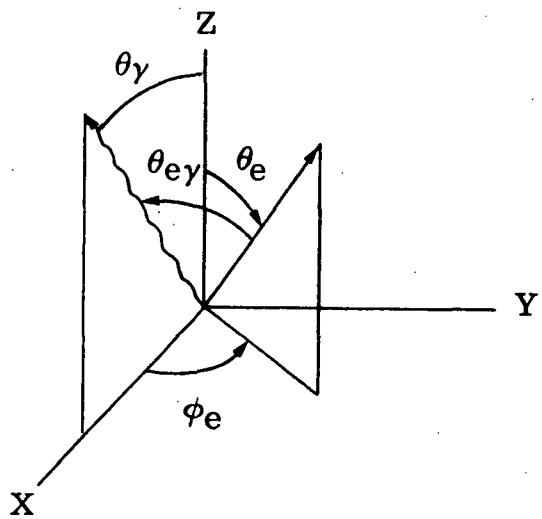

Figure 5.12. Geometry for the calculation of bremsstrahlung attenuation assumed in the parameterization of non-normal electron incidence

$$A_T(k, Z, \theta_e, \theta_\gamma, T) = \exp\left[\frac{-\mu(k) \cdot (T - 0.2R_o \cos\theta_e)}{\cos\theta_\gamma}\right] \qquad \theta_\gamma < \pi/2 \tag{5.24}$$

$$= \exp\left[\frac{-\mu(k) \cdot 0.2R_o \cos\theta_e}{|\cos\theta_\gamma|}\right] \qquad \theta_\gamma > \pi/2$$

where T is the target thickness, R_o is the csda range, $\mu(k)$ is the mass attenuation coefficient for photons of energy k in a material Z, and θ_γ is shown in the figure.

The angle between the direction of the electron and photon, $\theta_{e\gamma}$ is given by the relation

$$\cos\theta_{e\gamma} = \cos\theta_e \cos\theta_\gamma + \sin\theta_e \sin\theta_\gamma \cos\varphi_e \tag{5.25}$$

where the photon is assumed to emerge in xz plane. A comparison of the parameterized bremsstrahlung intensities and experimental data[64] is shown in Figs. 5.13 and 5.14 for 1-MeV electrons incident on Al and Au targets at 30 degrees and 45 degrees with respect to the normal, respectively. It is seen that there are some fairly large discrepancies at low energies for angles greater than $\pi/2$ between the electron and photon. This might be expected since the simple model neglects the fact that the low-energy bremsstrahlung is created throughout the target. It is felt that these discrepancies will contribute little error to the analysis of the bremsstrahlung created by isotropic electron fluxes since the electron fluxes are weighted by cos θ in the integration over the direction of the incident electrons and the highest secondary intensities are in the direction of the incident electron. A comparison of the bremsstrahlung intensities calculated for monoenergetic half-space isotropic electrons incident on Al using Monte Carlo methods[65] and the parameterization presented here is shown in Fig. 5.15. The agreement is quite good.

5.3.6 Limits of Bremsstrahlung Parameterization

Although the formula presented for the bremsstrahlung produced in thick targets is continuous in E, k, θ, and Z there are practical limitations on its use. There are limitations as to target material, target thickness, electron energy, photon energy, and photon angle. The present representation of thick target bremsstrahlung was intended to be useful for dealing with the electron environment encountered in space. Extrapolations to other uses should be done with caution.

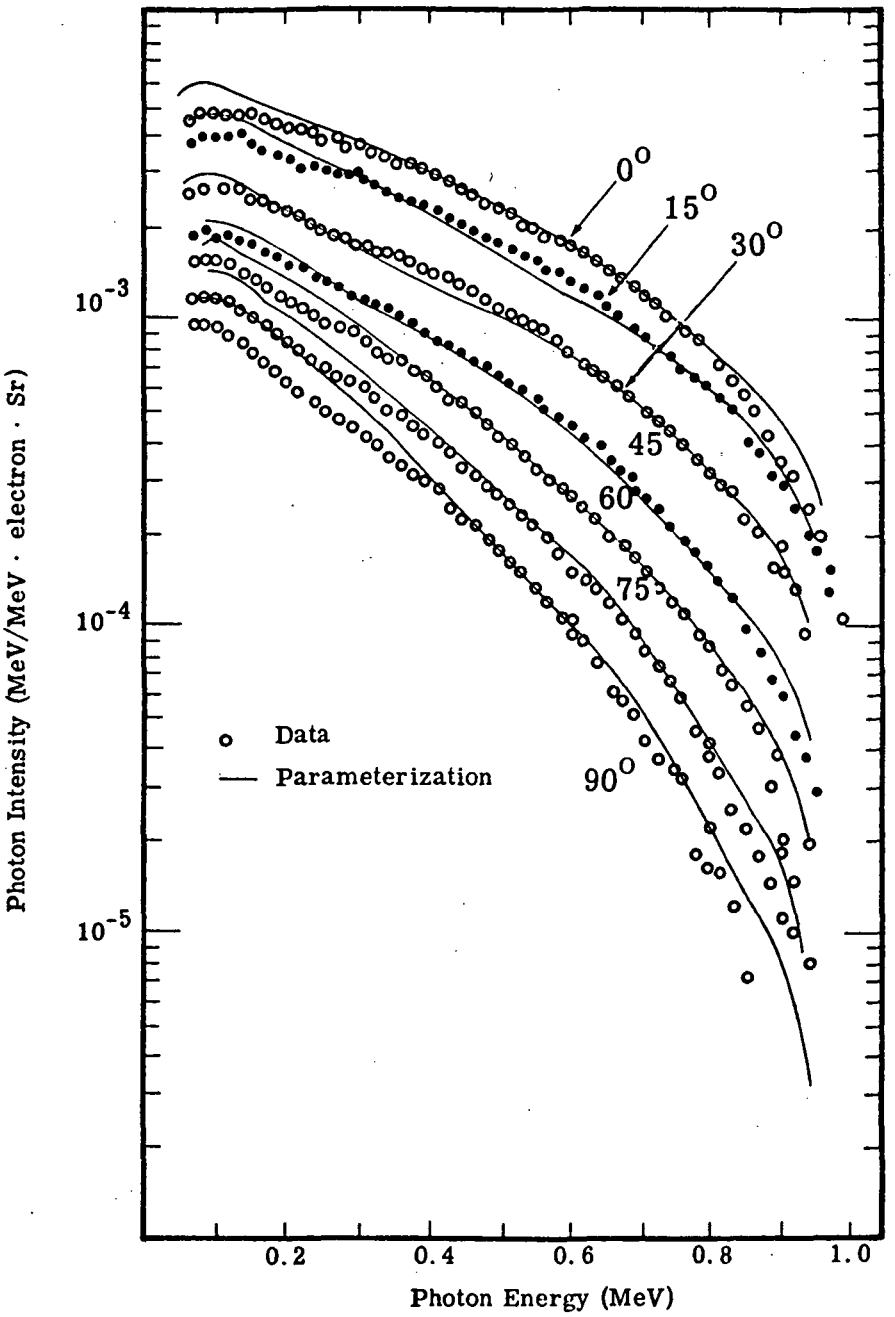

Figure 5.13. Comparison of parametric fits for non-normal electron incidence with experimental data for 1 MeV electrons on Al (Ref. 64). The angle between the electron direction and the Al target normal is 30°. The angles listed on the figure are the angles between the electron and photon directions.

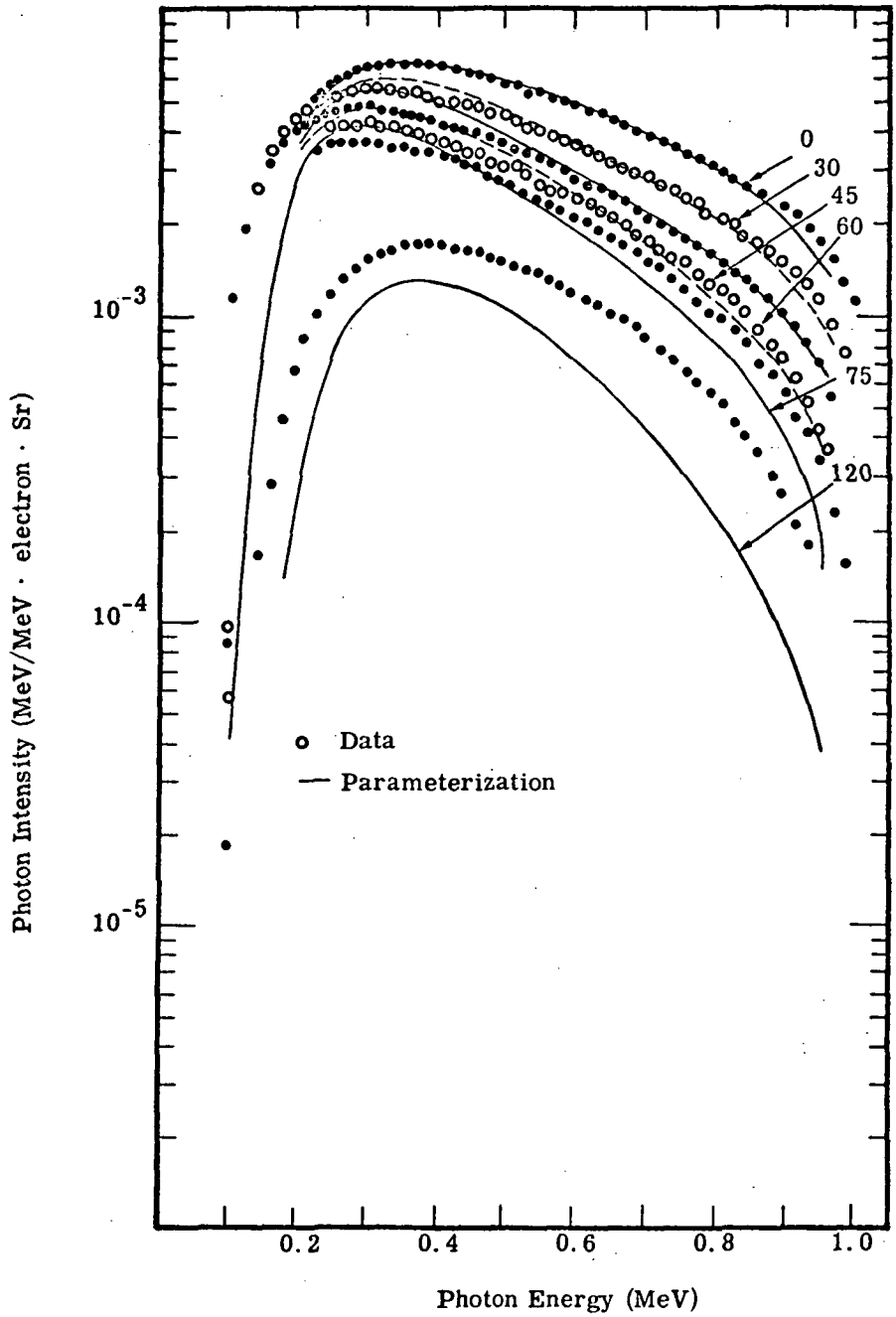

Figure 5.14. Comparison of parametric fits to non-normal electron incidence with experimental data (Ref. 64) for 1 MeV electrons on Au. The angle between the direction of the electrons and the target normal is 45^{o}. The angles listed on the figure are the angles between the electron and photon directions.

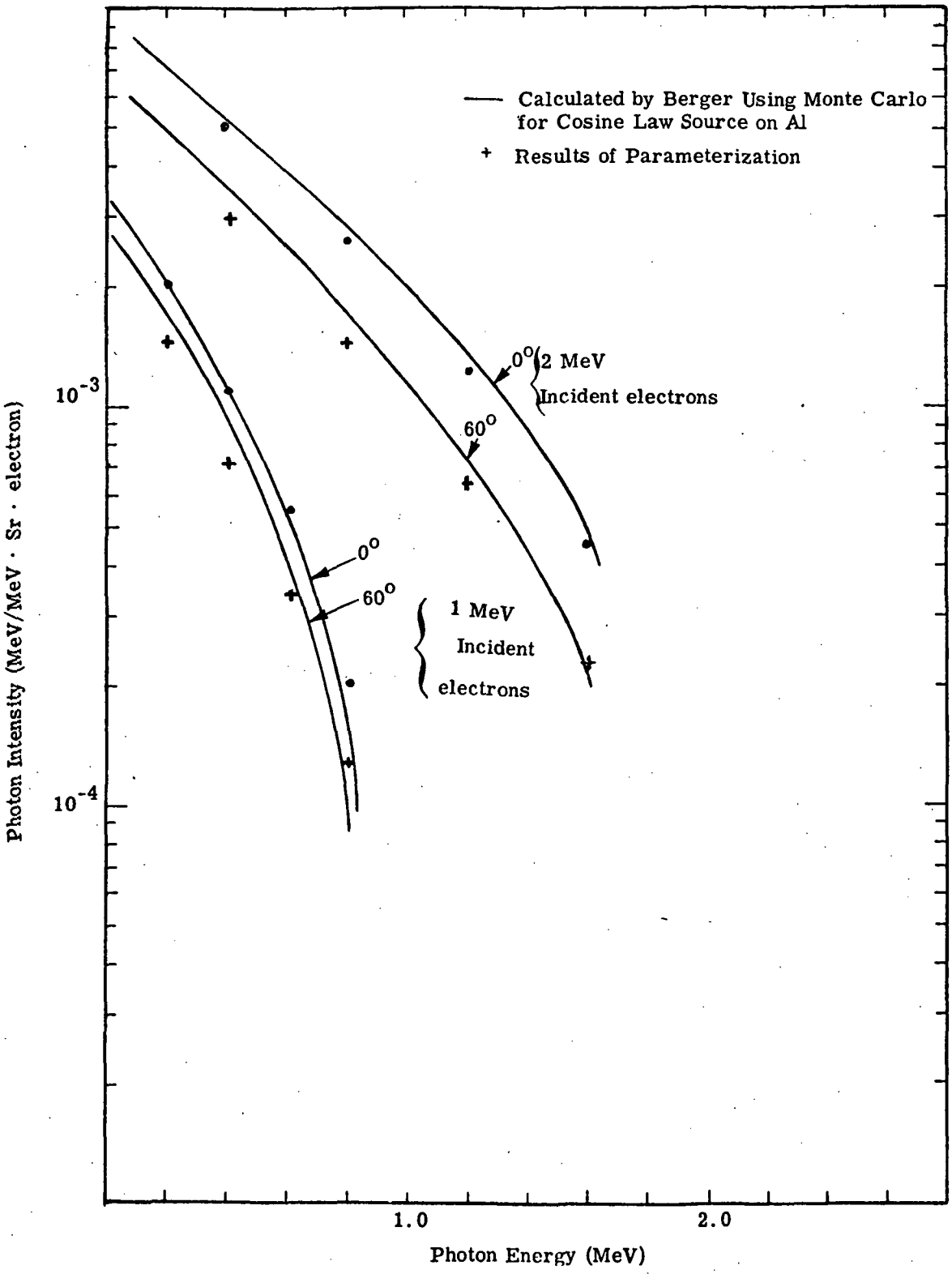

Figure 5.15. Comparison of bremsstrahlung calculated for monoenergetic isotropic electrons incident on one side of an Al target by Monte Carlo techniques (solid lines) (Ref. 65) and by the parameterization (dots and crosses) for 1 and 2 MeV electrons.

5.3.6.1 Limitations on Target Material

The parametric representation presented above is based on data for elementally pure targets with atomic numbers ranging from Z = 4 to 79. Extrapolations to below Z = 4 may be dangerous since the bremsstrahlung production rate is changing so rapidly in this region. However, this should not be serious in space shielding studies, since one is not likely to be using shields of hydrogen, helium, or lithium. A much more severe limitation is the restriction to elementally pure targets. The results of the present study are difficult to extend to shields of chemical compounds since the angular distribution of the bremsstrahlung radiation follows the electron angular distribution at small penetration depths which depends on the density of electrons. However, the bremsstrahlung production rate depends on the nuclear charge. Also, multilayered shields are not covered by the present parameterization unless the first layer is about 0.6 of the electron range. In this case the bremsstrahlung may be considered to be produced entirely in the first layer.

5.3.6.2 Limitations on Target Thickness

The parameterization is based upon data which were obtained for target thicknesses equal to the range of the incident electrons. For targets thinner than this, the dose due to bremsstrahlung is usually unimportant in comparison with the dose caused by the incident electrons. Extension to thicker targets will only involve the attenuation of the photons. Therefore, this restriction should not be a severe limitation for space shielding applications but may cause difficulties in other applications.

5.3.6.3 Limitations on Photon Emission Angle

In the interest of simplicity, the backward angle photon data were given very small weighting in the fitting procedure. This is justified because these photons are not nearly as intense as the forward going photons and they produce only a small fraction of the penetrating intensity, even for isotropically incident electrons. In space applications where bremsstrahlung is important the point where the dose is needed will be completely surrounded by material. The discrepancies introduced by assuming an isotropic electron source are probably much larger than the errors introduced in the parameterization of the backward component of the bremsstrahlung intensity.

5.3.6.4 Limitations on Electron Energy

The parameterization presented above agrees well with the thick target bremsstrahlung data for electrons in the 1- to 3-MeV energy region. The fits obtained for 0.2-MeV electrons are poor, with discrepancies on the order of 30 percent. Above 4-MeV there is little experimental data, and the parameterization over much of the region of Z is uncertain by an unknown amount. However, the 8-MeV electron data[23] on Sn agree well with the parameterization.

5.4 PHOTON ATTENUATION

Photons that are produced in the bremsstrahlung process interact with matter in a different way than electrons. In this section the main photon interaction mechanisms are outlined briefly and the problem of photon attenuation through shields is discussed.

5.4.1 Interaction Mechanisms

There are three main interaction mechanisms by which photons interact with atomic electrons in matter; the photoelectric effect which dominates at low photon energies (< 50 keV), the Compton effect which is important at intermediate energies, and pair production which dominates at high photon energies (>5 MeV).

5.4.1.1 Photoelectric Effect

The photoelectric effect occurs when a photon transfers essentially all of its energy to an atomic electron. To conserve both energy and momentum in such an interaction, there must be a third body nearby which will share some of the momentum. Usually this third body is the atomic nucleus. The closer the electron is to the nucleus, the more probable is the interaction. This explains why the most tightly bound electrons (the K electrons) are more likely to be affected in photo-absorption than less tightly bound electrons and also why the probability of photo-absorption increases with the atomic number of the atom.

Empirically, it is found that the photo-absorption cross section per electron is approximately proportional to Z^4/k^3, where Z is the atomic number of the material and k is the energy of the photon.[16] The photo-absorption cross section is found to increase in this manner as the energy of the photon decreases until a critical point at which the photon energy is not sufficient to eject the inner-most electrons. At this point (K edge) the absorption cross section drops abruptly by about a factor of from 5 to 10. As the photon energy is decreased further, the cross section again increases as $1/k^3$ until another series of discontinuities arise. The energies of these discontinuities correspond to the energies necessary to remove electrons from the L orbit. Other series of discontinuities are seen at still lower energies corresponding to the energies necessary to remove electrons from the outermost orbits. These discontinuities in the absorption cross section are illustrated in Fig. 5.16.

The electron that absorbs the photon (photoelectron) typically will be ejected from the atom. It will then interact with other electrons causing ionization, bremsstrahlung, etc., until it stops or leaves the material.

5.4.1.2 Compton Scattering

Compton scattering corresponds to situations where the photon scatters from an essentially free electron. Since this process does not depend on the

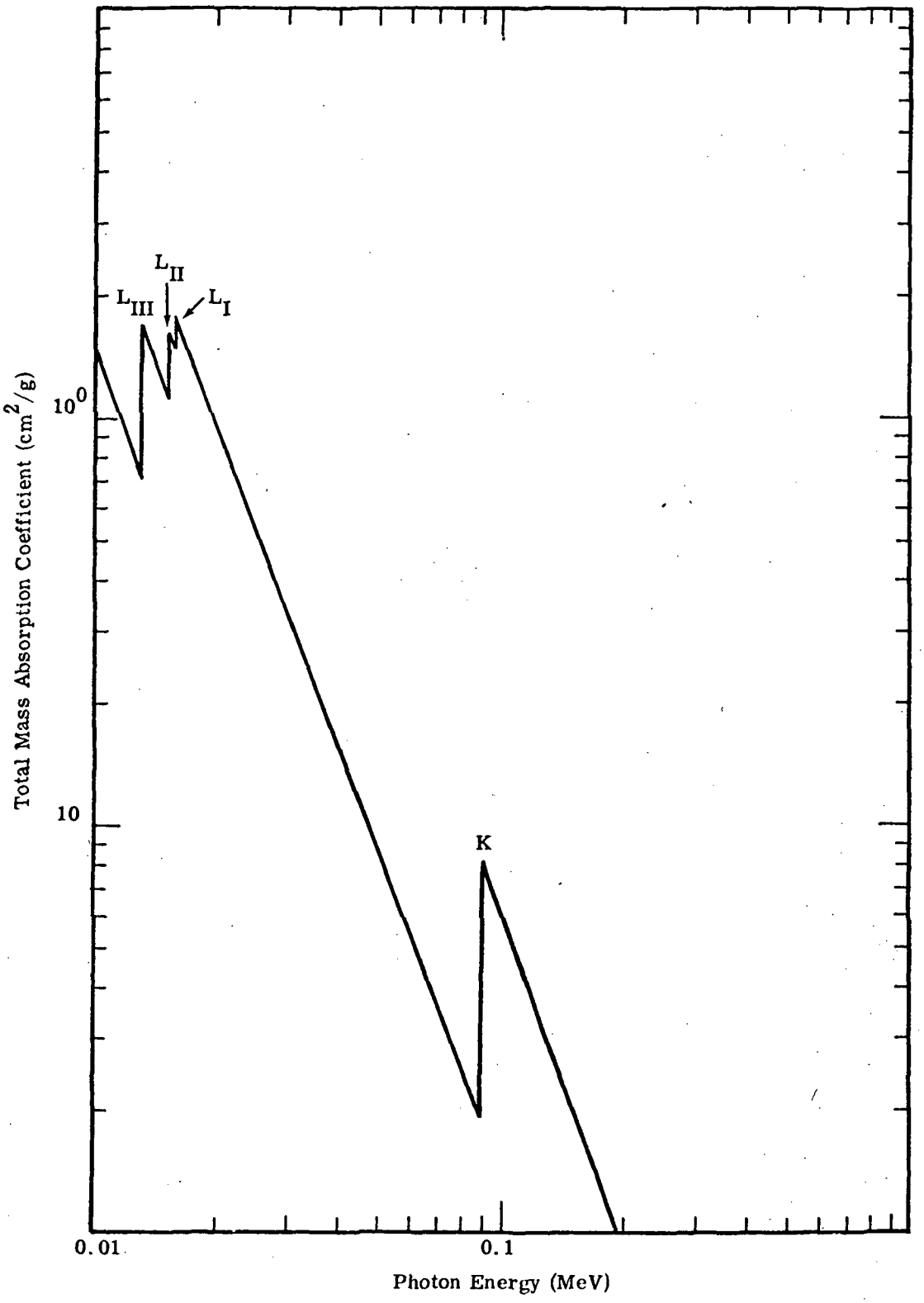

Figure 5.16. Total mass absorption coefficients for Pb illustrating the K and L absorption edges. (Data from Ref. 66)

presence of an atomic nucleus, it will depend only on the number of electrons a photon encounters. When the path length is measured in g/cm^2, the number of electrons per path length is essentially independent of the material so the Compton absorption coefficient, when expressed in cm^2/g, is essentially independent of atomic number.

In Compton scattering the energy of the photon is decreased and its direction is changed. The energy (in MeV) of the scattered photon, k', is related to incident energy (in MeV), k, and the angle of scattering, θ, through the relationship

$$k' = \frac{k}{1 + \frac{k}{m_o c^2}(1-\cos\theta)} \quad \text{(MeV)} \tag{5.26}$$

where $m_o c^2$ is the rest mass of an electron ($m_o c^2 = 0.511$ MeV). The maximum energy transferred to an electron E_c occurs when $\theta = \pi$ and is given by the relation

$$E_c = k - \frac{k}{\left(1 + \frac{2k}{m_o c^2}\right)} \quad \text{(MeV)} \tag{5.27}$$

5.4.1.3 Pair Production

The third important interaction mechanism is pair production. Photons with energies greater than twice the rest mass of the electron ($k > 1.02$ MeV) may encounter the field of a charged particle and disappear, creating an electron-positron pair. The kinetic energy of the electron-positron pair approximately equals the energy of the original photon minus the rest mass of the pair.

Usually pair production takes place in the field of an atomic nucleus. The nucleus receives some momentum but little energy.[16] If pair production takes place in the field of an electron (triplet production) the electron and electron-positron will all share the photon energy. Triplet production occurs only rarely, however.

In the process of stopping, the positron produced in pair production can encounter an electron, which results in annihilation of the pair, giving rise to two photons. If the positron is at rest when it annihilates, the photons will each have an energy of 0.511 MeV. If the positron annihilates in flight, the photons will share the kinetic energy of the positron. Each of these photons may, if their energy is high enough, create electron-positron pairs giving

rise to another set of annihilation photons. If the initial photon has enough energy this process could occur many times, giving rise to many secondary photons; a phenomenon known as a shower.

Unlike the other photon interaction mechanisms pair production increases with increasing photon energy. There is no closed form expression for the pair production cross section in the energy region of interest here (1.02 to 10 MeV), but values obtained by numerically integrating analytical expressions for the cross section are provided for aluminum (see Table 5.3). The pair production cross section varies closely with the square of the atomic number so that the cross sections for other elements can be computed by multiplying the aluminum cross section by $Z^2/169$.

TABLE 5.3. PAIR PRODUCTION CROSS SECTIONS FOR ALUMINUM

Photon Energy (MeV)	Pair Production Cross Section (b/atom)
1.5	7.69×10^{-3}
2.0	3.03×10^{-2}
3.0	8.64×10^{-2}
4.0	1.40×10^{-1}
5.0	1.87×10^{-1}
6.0	2.29×10^{-1}
8.0	2.99×10^{-1}
10.0	3.57×10^{-1}

5.4.1.4 Other Processes

There are several other gamma-ray interaction processes which affect the transport of photons through matter. These are Rayleigh (coherent) scattering from atomic electrons, two photon Compton scattering, photonuclear reaction with atomic nuclei and elastic and inelastic scattering from atomic nuclei. Rayleigh scattering occurs at low photon energies where photoelectric absorption is large. Rayleigh scattering does not significantly change the direction or energy of the photons and is consequently ignored in most photon transport calculations. Photonuclear absorption has a very small cross section compared to atomic process.

The thresholds of photonuclear absorption are typically around 6-8 MeV with a few exceptions such as ^{2}H(2.2 MeV) and ^{9}Be (1.66 MeV) and play no part in the transport of photons below 5 MeV. The cross sections for the other process are also very small in comparison to these for the dominant processes.

5.4.2 Photon Attenuation Coefficients

In practical problems, one is concerned with the amount of the original photon intensity transmitted through the material. This depends on the geometry of the problem, the types of shields, the quantity one is measuring behind the shield, etc. These considerations make the transport of photons a fairly complicated problem, which typically is treated by sophisticated transport computer codes.

5.4.2.1 Narrow Beam Mass Attenuation Coefficients

If a narrow beam of monoenergetic photons is incident on a shield and a collimated detector is placed behind the shield, (see Fig. 5.17) the transmitted intensity of photons decreases exponentially as the thickness of the shield is increased. The unscattered intensity behind the shield is given by

$$I(T) = I_o e^{-\mu T} \tag{5.28}$$

where I_o is the incident intensity, T is the thickness of the shield, and μ is termed the narrow beam or total attenuation coefficient. If the thickness of the shield is measured in units such as g/cm^2 (thickness (cm) x density, ρ, (g/cm^2)), then the appropriate units of μ/ρ are cm^2/g. The quantity μ/ρ is referred to as the mass attenuation coefficient. The attenuation coefficient represents the probability per unit path length that any interaction (photoelectric, Compton, or pair production) will occur. The attenuation coefficient is related to the total microscopic interaction cross section through the relationship

$$\frac{\mu}{\rho}(cm^2/g) = \sigma_T \frac{N_o}{A} ZM \tag{5.29}$$

where

σ_T is the total cross section (cm^2/electron)

ρ is the density (g/cm^3)

N_o is Avogadro's number $(\frac{\#\ molecules}{mole})$

Z is the atomic number of the material,

M is the number of atoms of material Z per molecule,

and A is the atomic weight (g/mole).

The mass attenuation coefficients for various materials as functions of photon energy are tabulated in many places.[66-68] Table 5.4 is a copy of the mass attenuation coefficients presented in the "Compendium of Radiation Shielding."[67]

5.4.3 Parameterization of Total Absorption Coefficients

For convenience in using the bremsstrahlung production parameterization, the total mass attenuation coefficients, $\mu/\rho(k, Z)$, have also been parameterized. The photoelectric mass attenuation coefficient has been parameterized for photon energies above the K absorption edge as

$$\frac{\mu_{pe}}{\rho}(k, Z) = \frac{3.71 \times 10^{-10} Z^{5.212} k^{-(4.4\, Z^{-0.1142})}}{A} \quad (cm^2/g) \quad , \qquad (5.30)$$

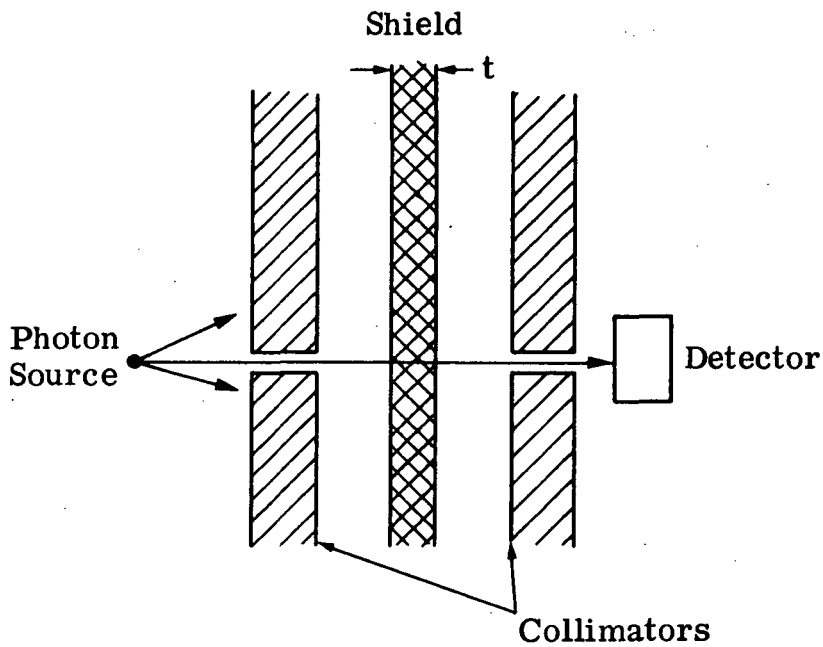

Figure 5.17. Illustration of narrow beam attenuation geometry

TABLE 5.4. VALUES OF THE MASS ATTENUATION COEFFICIENT μ/ρ[cm^2/g], EXCLUDING RAYLEIGH (COHERENT) SCATTERING AND THE PHOTONUCLEAR EFFECT, FOR A NUMBER OF ELEMENTS (FROM REF. 67)

Photon energy [MeV]	$_{1}$H	$_{4}$Be	$_{6}$C	$_{7}$N	$_{8}$O	$_{11}$Na	$_{12}$Mg	$_{13}$Al
0.01	0.385	0.536	2.16	3.57	5.58	15.1	20.3	25.8
0.015	0.376	0.268	0.721	1.09	1.62	4.37	5.98	7.66
0.02	0.369	0.206	0.387	0.541	0.754	1.88	2.56	3.24
0.03	0.357	0.171	0.230	0.276	0.335	0.639	0.839	1.03
0.04	0.346	0.159	0.193	0.212	0.236	0.355	0.437	0.514
0.05	0.335	0.152	0.179	0.187	0.199	0.254	0.298	0.334
0.06	0.326	0.147	0.170	0.175	0.181	0.209	0.236	0.255
0.08	0.309	0.139	0.158	0.160	0.163	0.170	0.183	0.189
0.10	0.294	0.132	0.149	0.150	0.152	0.152	0.161	0.162
0.15	0.265	0.119	0.134	0.134	0.134	0.131	0.136	0.134
0.2	0.243	0.109	0.122	0.123	0.123	0.118	0.122	0.120
0.3	0.211	0.0945	0.106	0.106	0.107	0.102	0.106	0.103
0.4	0.189	0.0847	0.0953	0.0953	0.0954	0.0914	0.0943	0.0921
0.5	0.173	0.0773	0.0870	0.0870	0.0871	0.0834	0.0861	0.0840
0.6	0.160	0.0715	0.0805	0.0805	0.0806	0.0771	0.0796	0.0777
0.8	0.140	0.0628	0.0707	0.0707	0.0707	0.0677	0.0699	0.0682
1.0	0.126	0.0565	0.0635	0.0636	0.0636	0.0609	0.0628	0.0613
1.5	0.103	0.0459	0.0517	0.0517	0.0518	0.0496	0.0512	0.0500
2	0.0875	0.0393	0.0445	0.0444	0.0445	0.0428	0.0442	0.0431
3	0.0691	0.0313	0.0356	0.0357	0.0359	0.0348	0.0361	0.0353
4	0.0581	0.0267	0.0305	0.0308	0.0310	0.0304	0.0316	0.0311
5	0.0505	0.0235	0.0271	0.0275	0.0278	0.0276	0.0288	0.0284
6	0.0450	0.0212	0.0247	0.0251	0.0255	0.0256	0.0268	0.0266
8	0.0375	0.0182	0.0216	0.0221	0.0227	0.0232	0.0245	0.0244
10	0.0325	0.0163	0.0196	0.0203	0.0209	0.0218	0.0231	0.0232
15	0.0254	0.0136	0.0170	0.0178	0.0187	0.0203	0.0217	0.0220
20	0.0215	0.0123	0.0158	0.0167	0.0177	0.0197	0.0213	0.0217
30	0.0175	0.0110	0.0147	0.0159	0.0170	0.0196	0.0214	0.0220
40	0.0154	0.0104	0.0144	0.0157	0.0170	0.0199	0.0218	0.0225
50	0.0142	0.0102	0.0143	0.0156	0.0170	0.0203	0.0223	0.0231
60	0.0133	0.0100	0.0143	0.0157	0.0172	0.0207	0.0227	0.0236
80	0.0124	0.00993	0.0144	0.0160	0.0176	0.0213	0.0235	0.0244
100	0.0119	0.00993	0.0146	0.0162	0.0179	0.0219	0.0242	0.0251

TABLE 5.4. (CONTINUED)

Photon energy [MeV]	$_{14}$Si	$_{15}$P	$_{16}$S	$_{18}$Ar	$_{19}$K	$_{20}$Ca	$_{26}$Fe	$_{29}$Cu
0.01	33.6	40.2	50.3	63.8	80.1	95.6	172.0	223.0
0.015	9.97	12.0	15.2	19.5	24.6	29.6	55.7	73.3
0.02	4.20	5.10	6.42	8.27	10.5	12.6	25.1	33.0
0.03	1.31	1.55	1.95	2.48	3.14	3.82	7.88	10.6
0.04	0.635	0.731	0.891	1.11	1.39	1.67	3.46	4.71
0.05	0.396	0.441	0.524	0.630	0.777	0.925	1.84	2.50
0.06	0.292	0.318	0.367	0.420	0.512	0.595	1.13	1.52
0.08	0.207	0.215	0.238	0.252	0.296	0.334	0.550	0.718
0.10	0.173	0.175	0.189	0.189	0.216	0.237	0.342	0.427
0.15	0.140	0.138	0.145	0.136	0.150	0.159	0.184	0.208
0.2	0.125	0.122	0.127	0.117	0.128	0.133	0.139	0.148
0.3	0.107	0.104	0.108	0.0979	0.106	0.109	0.107	0.108
0.4	0.0954	0.0928	0.0958	0.0868	0.0938	0.0966	0.0921	0.0919
0.5	0.0870	0.0846	0.0873	0.0789	0.0852	0.0877	0.0829	0.0821
0.6	0.0804	0.0781	0.0806	0.0729	0.0786	0.0809	0.0761	0.0752
0.8	0.0706	0.0685	0.0707	0.0639	0.0689	0.0709	0.0664	0.0654
1.0	0.0634	0.0617	0.0635	0.0574	0.0619	0.0636	0.0596	0.0586
1.5	0.0517	0.0502	0.0517	0.0468	0.0505	0.0519	0.0486	0.0478
2	0.0447	0.0436	0.0448	0.0406	0.0439	0.0451	0.0425	0.0419
3	0.0367	0.0358	0.0371	0.0338	0.0366	0.0377	0.0361	0.0359
4	0.0324	0.0317	0.0329	0.0302	0.0328	0.0340	0.0331	0.0332
5	0.0297	0.0292	0.0304	0.0280	0.0306	0.0318	0.0315	0.0318
6	0.0279	0.0275	0.0287	0.0267	0.0292	0.0304	0.0306	0.0309
8	0.0257	0.0255	0.0268	0.0252	0.0277	0.0289	0.0299	0.0307
10	0.0246	0.0245	0.0259	0.0245	0.0270	0.0284	0.0299	0.0310
15	0.0235	0.0237	0.0252	0.0242	0.0269	0.0284	0.0309	0.0324
20	0.0234	0.0236	0.0253	0.0246	0.0274	0.0291	0.0322	0.0341
30	0.0239	0.0243	0.0262	0.0257	0.0287	0.0308	0.0347	0.0370
40	0.0246	0.0251	0.0271	0.0267	0.0300	0.0321	0.0367	0.0393
50	0.0252	0.0258	0.0279	0.0276	0.0311	0.0333	0.0384	0.0412
60	0.0256	0.0264	0.0286	0.0284	0.0319	0.0343	0.0397	0.0426
80	0.0268	0.0275	0.0299	0.0297	0.0335	0.0359	0.0418	0.0449
100	0.0276	0.0283	0.0308	0.0307	0.0346	0.0371	0.0432	0.0466

TABLE 5.4. (CONTINUED)

Photon energy [MeV]	$_{42}$Mo	$_{50}$Sn	$_{53}$I	$_{74}$W	$_{82}$Pb	$_{92}$U	Absorption edges
0.01	84.0	139.0	158.0	91.2	132.0	173.0	
0.015	26.8	44.3	53.4	136.0	112.0	60.3	
0.02	11.7	20.1	24.7	63.7	83.4	68.5	L_3-edge
0.03	28.3	41.5	7.98	21.5	27.9	39.6	L_2-, L_1-edges
0.04	13.0	18.4	22.3	9.86	13.1	18.7	
0.05	6.97	9.94	12.3	5.39	7.17	10.4	
0.06	4.25	6.15	7.55	3.30	4.47	6.45	
0.08	1.92	2.95	3.52	7.66	2.12	3.04	
0.10	1.05	1.64	1.91	4.29	5.62	1.71	
0.15	0.399	0.597	0.673	1.50	1.99	2.47	K-edge
0.2	0.228	0.311	0.349	0.738	0.969	1.23	
0.3	0.131	0.155	0.168	0.302	0.385	0.484	
0.4	0.101	0.110	0.116	0.180	0.221	0.273	
0.5	0.0858	0.0911	0.0936	0.129	0.154	0.185	
0.6	0.0766	0.0790	0.0807	0.103	0.120	0.140	
0.8	0.0663	0.0655	0.0660	0.0772	0.0856	0.0963	
1.0	0.0576	0.0571	0.0574	0.0639	0.0689	0.0754	
1.5	0.0467	0.0459	0.0459	0.0487	0.0509	0.0538	
2	0.0414	0.0408	0.0409	0.0433	0.0450	0.0470	
3	0.0365	0.0366	0.0369	0.0401	0.0416	0.0435	
4	0.0348	0.0355	0.0359	0.0399	0.0415	0.0434	
5	0.0343	0.0353	0.0359	0.0406	0.0424	0.0443	
6	0.0343	0.0357	0.0364	0.0416	0.0435	0.0455	
8	0.0351	0.0370	0.0378	0.0440	0.0460	0.0481	
10	0.0363	0.0387	0.0397	0.0466	0.0487	0.0509	
15	0.0396	0.0428	0.0441	0.0527	0.0553	0.0578	
20	0.0425	0.0464	0.0479	0.0581	0.0611	0.0641	
30	0.0473	0.0520	0.0539	0.0663	0.0701	0.0739	
40	0.0507	0.0560	0.0581	0.0720	0.0760	0.0804	
50	0.0534	0.0591	0.0614	0.0764	0.0806	0.0854	
60	0.0555	0.0615	0.0640	0.0798	0.0843	0.0893	
80	0.0587	0.0653	0.0678	0.0848	0.0899	0.0950	
100	0.0611	0.0678	0.0705	0.0881	0.0936	0.0993	

where A is the atomic weight of the target.

This parameterization does not consider the abrupt decreases at the K and L edges and, hence, greatly overestimates the attenuation for photon energies below the K absorption edge. Since the highest energy K edge is below 100 keV, even for heavy elements, where the absorption is large, this limitation of the parameterization is not important in space radiation shielding problems.

The Compton mass attenuation coefficient has been parameterized as

$$\frac{\mu_c}{\rho}(k, Z) = \frac{0.0484 - 0.00532k + 0.091\, e^{-k/0.63}}{0.85\, Z^{0.072}} \quad (cm^2/g) \tag{5.31}$$

and the pair production mass attenuation coefficient as

$$\frac{\mu_{pair}}{\rho}(k, Z) = 8.06 \times 10^{-4} \log_{10}(k+4) Z^2/A \quad (cm^2/g) \tag{5.32}$$

$$\text{for } k > 1.022 \text{ MeV}$$

$$\frac{\mu_{pair}}{\rho} = 0 \qquad \text{for } k < 1.022 \text{ MeV} \quad .$$

The total mass attenuation coefficient μ_a is equal to the sum of the three absorption coefficients

$$\frac{\mu_a(k, Z)}{\rho} = \frac{\mu_{pe}}{\rho} + \frac{\mu_c}{\rho} + \frac{\mu_{pair}}{\rho} \quad . \tag{5.33}$$

A comparison of the parameterized mass attenuation coefficients and the values presented in Siegbahm is shown for Al and Sn in Fig. 5.18. It is seen that the parametric fits to the coefficients are accurate to about 5 percent from the K absorption edge to about 2 to 3 MeV where the deviations increase to about 10 percent.

It should be pointed out that the uncertainty introduced in the bremsstrahlung intensity from the uncertainty in the mass attenuation coefficient can be large for low-energy photons since the percent uncertainty in the attenuation is given by

$$\% \text{ error in } A_T = |e^{\pm \epsilon \mu x} - 1| \times 100 \quad , \tag{5.34}$$

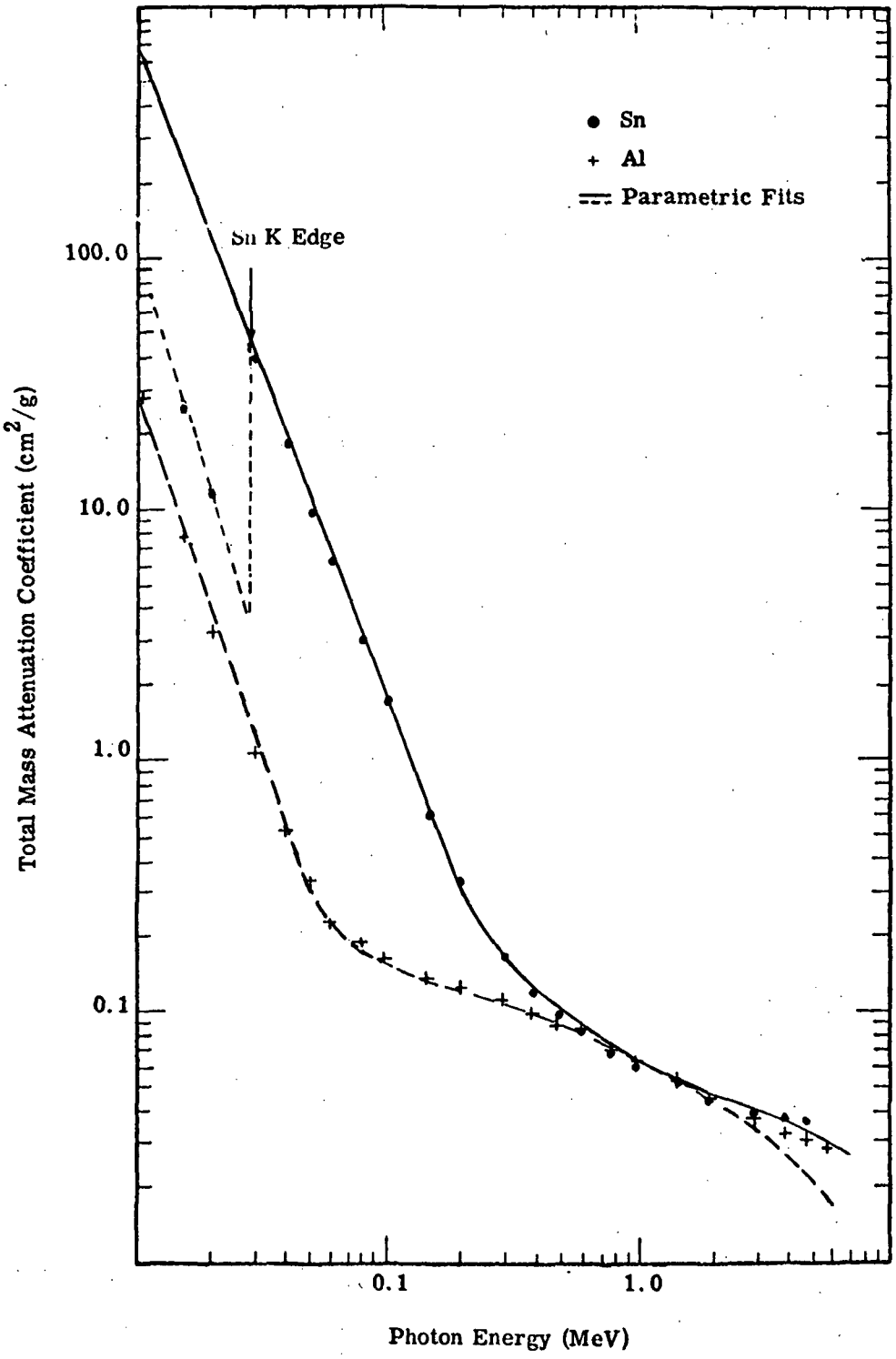

Figure 5.18. Examples of parametric fits for total mass attenuation coefficients. Dots and crosses are data from Siegbahm for Sn and Al, respectively. Lines represent parametric fits. The parametric fits greatly over estimate the attenuation coefficients for energies lower than the K edge. (Points from Ref. 66)

where ϵ is the fractional error in the parameterization and μx is the product of the mass attenuation coefficient and the thickness. For a 2 g/cm^2 Sn target, the error introduced by the parameterization would be about 80 percent at 0.06 MeV assuming a 5 percent error in μ, and less than a 1 percent error at 2 MeV assuming a 10 percent error in μ. For accurate calculations at low photon energies one should obviously use tabulated or accurately calculated values of μ. In general the spectrum of electron generated photons that can be expected in the space environment will peak at or near several hundred keV and fall off sharply below 100 keV and above 5 MeV. Consequently, the errors in dose calculations encountered by using the parameterized form of the mass attenuation coefficient will be small. The high energy photons will be only slightly attenuated by typical space shields so that a large uncertainty in the attenuation will not result in large uncertainty in the flux. Also, low energy photons account for only a small fraction of the dose and fairly large uncertainties in the low energy component do not result in large uncertainties in the total dose.

5.4.4 Broad Beam Attenuation

In space shielding problems one deals with spatially distributed sources of gamma rays which surround the point of interest. One of the mechanisms for the removal of photons from a narrow beam of gamma radiation is Compton scattering. This mechanism changes the direction of the photons and lowers their energies which removes them from consideration in a narrow beam geometry, but does not remove them from consideration in a distributed source geometry. Radiation which is scattered in the shielding material, but not absorbed, can contribute to the dose. This is illustrated in Fig. 5.19 which shows a sketch of possible photon paths in a segment of shield. Photons which originally were directed away from the detector can have their directions changed in the shield so they enter the detector. Figure 5.20 is a schematic of the relationship between the dose behind a shield and the shield thickness. Also shown in Fig. 5.20 is the dose due to the unscattered radiation. In situations such as this it is common to define buildup factors which correct for the effect of scattered radiation. The total detector response D (number of photons, energy fluence, or energy deposited by the radiation) will be given by a relationship of the sort

$$D = B D_0 \quad , \tag{5.35}$$

where B is the buildup factor and D_0 is the detector response to the unscattered portion of the radiation.

The values of the buildup factors depend on many things, such as the geometric configuration of the original gamma-ray source, the configuration of the attenuating medium, the geometric relationship of the source and detector to one another and to the attenuating medium, the angular distribution

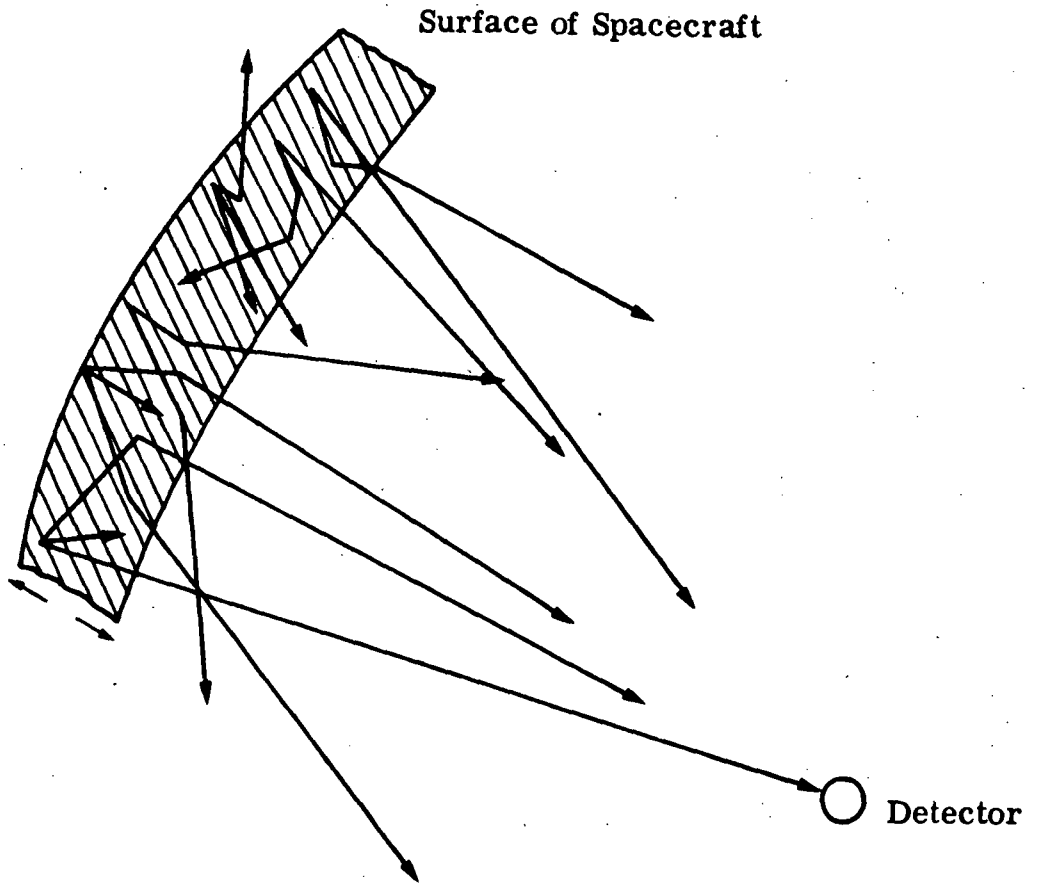

Figure 5.19. Possible paths of photons as they are transported through a section of space craft shielding

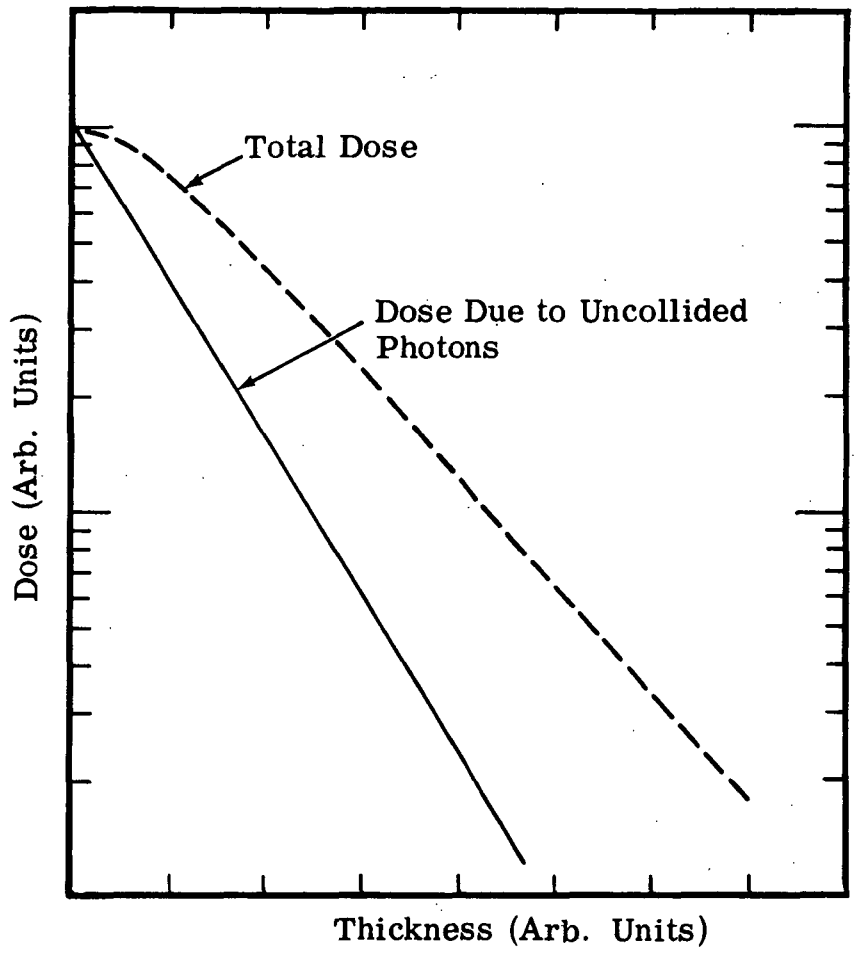

Figure 5.20. Contribution of scattered flux to total dose behind a shield for broad beam geometry

of the gamma-ray source, the composition of the medium, and the quantity being measured by the detector (e.g., number, energy fluence or dose).

5.4.5 Buildup Factors

Dose, energy fluence, and number buildup factors have been calculated for different source geometries, source angular distributions, and shield geometries.[69] The number buildup factor is defined as the ratio of the total number of photons, N_T, which pass through the detector (volume of interest) to the number of unscattered photons N_{uc}. The total number is the sum of the scattered N_s and unscattered photons N_{uc} so the number buildup factor is

$$B_N = \frac{N_s + N_{uc}}{N_{uc}} \quad . \tag{5.36}$$

The energy fluence buildup factor is slightly more complicated than the number buildup factor. It is defined as the total photon intensity divided by the unscattered photon intensity where intensity is defined as the number of photons with an energy k times this energy. If $dN_S/dk' \, dk'$ is the number of photons scattered into the detector with energies between k' and $k' + dk'$ then the energy fluence buildup factor will be given by

$$B_E = \frac{k\, N_{uc} + \int_0^k dk' \; k' \frac{dN_s}{dk'}}{k\, N_{uc}} \tag{5.37}$$

where k is original photon energy and k' is the energy of the scattered radiation. Both the number buildup factor and the energy fluence buildup factor are independent of the type of detector. A more useful quantity in some applications is the energy deposited in the detector relative to that which is deposited by the uncollided flux of photons. This quantity is termed the dose buildup factor and is, of course, dependent on the material of the detector or volume of interest. The dose buildup factor for photons of energy k is defined as

$$B_D = \frac{k\, N_{uc}\, \mu_a(Z,k) + \int_0^k dk' \mu_a(Z,k') k' \frac{dN_s}{dk'}}{k\, N_{uc}\, \mu_a(Z,k)} \quad , \tag{5.38}$$

where $\mu_a(Z,k)$ is the energy absorption coefficient for photons of energy k in a material of atomic number Z.

It might appear from these definitions that one must solve the entire photon transport problem to obtain buildup factors for each geometrical situation. If this were the case the use of buildup factors would actually complicate any given problem. The usefulness of buildup factors results from the fact that they vary more slowly as functions of atomic mass and photon energy than the attenuation term. Interpolations are therefore easier and more reliable for buildup factors than for the corresponding attenuation terms. Also, buildup factors for complicated geometries can be approximated in some cases by buildup factors calculated for simple geometries. Buildup factors for some simple geometries are given in the next section.

5.4.5.1 Calculated Buildup Factors

Buildup factors have been calculated for several simple geometries and source angular distributions. The most commonly calculated geometries include:

1. A point isotropic source in an infinite medium
2. A broad parallel beam in an infinite medium
3. A broad parallel beam incident on a semi-infinite medium
4. A broad parallel beam incident on a slab of material
5. A plane of isotropic sources in an infinite medium
6. A plane of isotropic sources on slabs of material

These six cases are illustrated schematically in Fig. 5.21. The buildup factors for these cases will be discussed below.

Point Isotropic Source - Infinite Medium – The buildup factors most commonly employed are calculated for a point isotropic source in an infinite medium. The detector is assumed to be isotropic and separated from the source by a distance r (g/cm^2). The dose is given for this case by the equation

$$D(k, r, Z) = \kappa \frac{S \cdot k \cdot \mu_a \cdot B_D(\mu r) e^{-\mu r}}{4\pi r^2} , \qquad (5.39)$$

where κ is the conversion factor from MeV/g to Rad

$$\kappa = 1.6 \times 10^{-8} \left(\frac{\text{Rad g}}{\text{MeV}} \right) . \qquad (5.40)$$

S is the source strength in photons/time, k is the photon energy (MeV), μ_a is the mass absorbtion coefficient for the detector material (cm^2/g) (typically assumed to be tissue) μ (cm^2/g) is the mass attenuation coefficient for the shielding material. and $B_D(\mu r)$ is the dose buildup factor. Values of these buildup factors[69] are given in Table 5.5 for several materials.

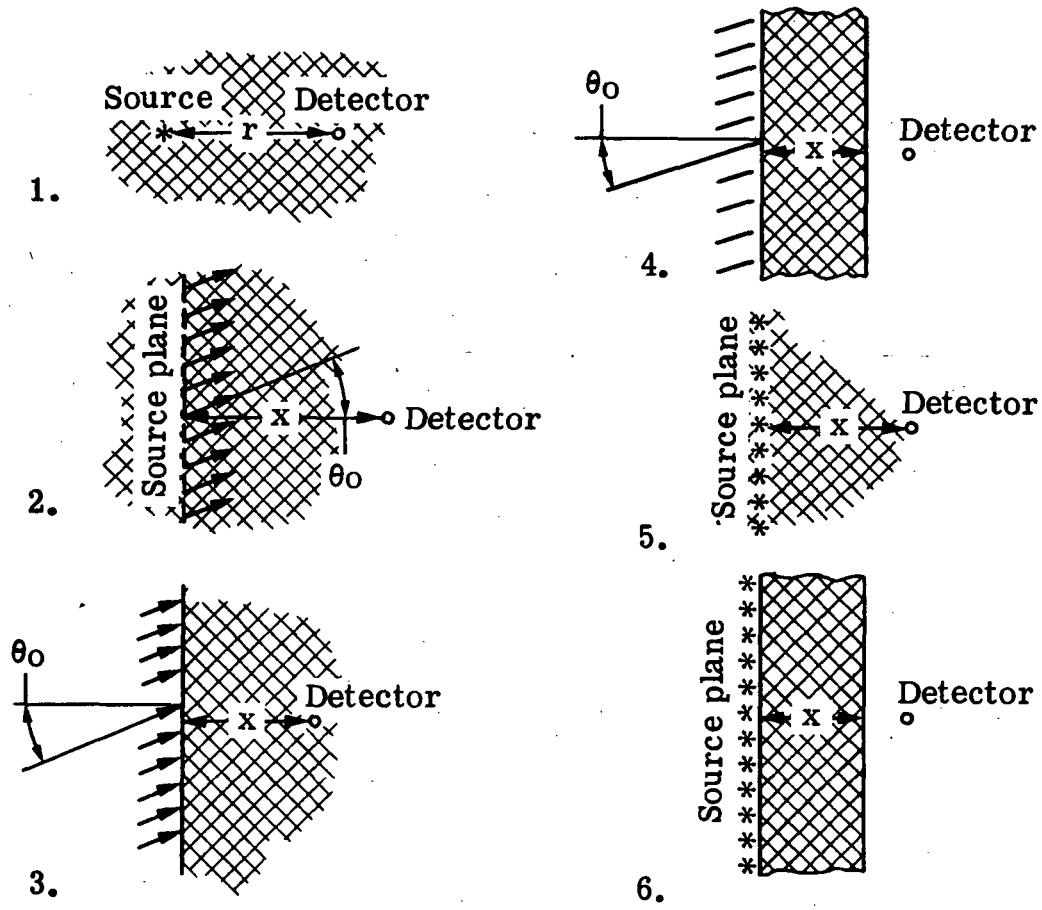

Figure 5.21. Geometries used in buildup factor calculations

TABLE 5.5. TISSUE DOSE BUILDUP FACTORS FOR A POINT ISOTROPIC SOURCE IN AN INFINITE MEDIUM (FROM REF. 69)

E_0 [MeV]	μr						
	1	2	4	7	10	15	20
				Water			
0.255	3.09	7.14	23.0	72.9	166	456	982
0.5	2.52	5.14	14.3	38.8	77.6	178	334
1.0	2.13	3.71	7.68	16.2	27.1	50.4	82.2
2.0	1.83	2.77	4.88	8.46	12.4	19.5	27.7
3.0	1.69	2.42	3.91	6.23	8.63	12.8	17.0
4.0	1.58	2.17	3.34	5.13	6.94	9.97	12.9
6.0	1.46	1.91	2.76	3.99	5.18	7.09	8.85
8.0	1.38	1.74	2.40	3.34	4.25	5.66	6.95
10.0	1.33	1.63	2.19	2.97	3.72	4.90	5.98
				Aluminum			
0.5	2.37	4.24	9.47	21.5	38.9	80.8	141
1.0	2.02	3.31	6.57	13.1	21.2	37.9	58.5
2.0	1.75	2.61	4.62	8.05	11.9	18.7	26.3
3.0	1.64	2.32	3.78	6.14	8.65	13.0	17.7
4.0	1.53	2.08	3.22	5.01	6.88	10.1	13.4
6.0	1.42	1.85	2.70	4.06	5.49	7.97	10.4
8.0	1.34	1.68	2.37	3.45	4.58	6.56	8.52
10.0	1.28	1.55	2.12	3.01	3.96	5.63	7.32
				Iron			
0.5	1.98	3.09	5.98	11.7	19.2	35.4	55.6
1.0	1.87	2.89	5.39	10.2	16.2	28.3	42.7
2.0	1.76	2.43	4.13	7.25	10.9	17.6	25.1
3.0	1.55	2.15	3.51	5.85	8.51	13.5	19.1
4.0	1.45	1.94	3.03	4.91	7.11	11.2	16.0
6.0	1.34	1.72	2.58	4.14	6.02	9.89	14.7
8.0	1.27	1.56	2.23	3.49	5.07	8.50	13.0
10.0	1.20	1.42	1.95	2.99	4.35	7.54	12.4
				Lead			
0.5	1.24	1.42	1.69	2.00	2.27	2.65	(2.73)
1.0	1.37	1.69	2.26	3.02	3.74	4.81	5.86
2.0	1.39	1.76	2.51	3.66	4.84	6.87	9.00
3.0	1.34	1.68	2.43	3.75	5.30	8.44	12.3
4.0	1.27	1.56	2.25	3.61	5.44	9.80	16.3
5.1097	1.21	1.46	2.08	3.44	5.55	11.7	23.6
6.0	1.18	1.40	1.97	3.34	5.69	13.8	32.7
8.0	1.14	1.30	1.74	2.89	5.07	14.1	44.6
10.0	1.11	1.23	1.58	2.52	4.34	12.5	39.2

Broad Parallel Beam, Normal to Source Plane – Buildup factors for broad beams have been calculated for infinite media, semi-infinite media, and slab geometries.[69, 70] The buildup factor for broad parallel beams normally incident on the source plane in infinite media are given in Table 5.6. The energy fluence buildup factors for broad parallel beams normally incident on slabs of material are given in Table 5.7. The dose calculated for a normally incident beam is given by the equation

$$D(k, X, Z) = \kappa \, S \, k \, \mu_a \, B(\mu X) e^{-\mu X} \quad , \tag{5.41}$$

where S is the source strength in photons/cm^2 and X(g/cm^2) is the separation distance between the source plane and the detector. For slab geometries X is the thickness of the slab.

Planes of Isotropic Sources; Infinite Medium – Buildup factors have been calculated for planes of isotropic sources in both infinite and slab geometries. These are termed plane isotropic buildup factors (the source here radiates current isotropically from each differential area; the flux radiated from the differential area is not isotropic, see Section 6). The plane isotropic dose buildup factors for infinite media are given in Table 5.8 while those for a slab geometry are given in Table 5.9.

The dose calculated for a plane of isotropic sources is given by the equation

$$D(k, X, Z) = \kappa \, \frac{S \, k \, \mu_a \, B(\mu X) E1(\mu X)}{2} \quad , \tag{5.42}$$

where S is the total source strength in photons/cm^2 and E1 is the first exponential integral[25] defined by the equation

$$E1(\mu X) = \int_{\mu X}^{\infty} \frac{e^{-y}}{y} \, dy \quad .$$

It is significant here that the dose falls off as $E1(\mu X)$ rather than as $e^{-\mu X}$ as it does in the other cases. The function $E1(\mu X)$ has two characteristics which are different from the simple exponential function. First, it goes to infinity as μX approaches zero. This is as it should be since the dose from an infinite, unshielded plane of isotropically emitting sources is infinite. Second, it drops off considerably faster than $e^{-\mu X}$. The buildup factors for a plane of isotropic sources can therefore be considerably larger than other buildup factors, but the product of the buildup factor and the exponential integral can be less than the corresponding value of $B\,e^{-\mu X}$ for a point isotropic source.

TABLE 5.6. TISSUE DOSE BUILDUP FACTORS FOR A NORMAL PLANE PARALLEL BEAM IN AN INFINITE MEDIUM. (FROM REF. 69)

E_0 [MeV]	μx					
	1	2	4	7	10	15
			Water			
0.5	2.63	4.29	9.05	20.0	35.9	74.9
1.0	2.26	3.39	6.27	11.5	18.0	30.8
2.0	1.84	2.63	4.28	6.96	9.87	14.4
3.0	1.69	2.31	3.57	5.51	7.48	10.8
4.0	1.58	2.10	3.12	4.63	6.19	8.54
6.0	1.45	1.86	2.63	3.76	4.86	6.78
8.0	1.36	1.69	2.30	3.16	4.00	5.47
			Iron			
0.5	2.07	2.94	4.87	8.31	12.4	20.6
1.0	1.92	2.74	4.57	7.81	11.6	18.9
2.0	1.69	2.35	3.76	6.11	8.78	13.7
3.0	1.58	2.13	3.32	5.26	7.41	11.4
4.0	1.48	1.90	2.95	4.61	6.46	9.92
6.0	1.35	1.71	2.48	3.81	5.35	8.39
8.0	1.27	1.55	2.17	3.27	4.58	7.33
10.0	1.22	1.44	1.95	2.89	4.07	6.70
			Lead			
0.5	1.24	1.39	1.63	1.87	2.08	—
1.0	1.38	1.68	2.18	2.80	3.40	4.20
2.0	1.40	1.76	2.41	3.36	4.35	5.94
3.0	1.36	1.71	2.42	3.55	4.82	7.18
4.0	1.28	1.56	2.18	3.29	4.69	7.70
6.0	1.19	1.40	1.87	2.97	4.69	9.53
8.0	1.14	1.30	1.69	2.61	4.18	9.08
10.0	1.11	1.24	1.54	2.27	3.54	7.70
			Uranium			
0.5	1.17	1.28	1.45	1.60	1.73	—
1.0	1.30	1.53	1.90	2.32	2.70	3.60
2.0	1.33	1.62	2.15	2.87	3.56	4.89
3.0	1.29	1.57	2.13	3.02	3.99	5.94
4.0	1.25	1.49	2.02	2.94	4.06	6.47
6.0	1.18	1.37	1.82	2.74	4.12	7.79
8.0	1.13	1.27	1.61	2.39	3.65	7.36
10.0	1.10	1.21	1.48	2.12	3.21	6.58

TABLE 5.7. ENERGY FLUENCE BUILDUP FACTORS – BROAD, PARALLEL BEAMS NORMALLY INCIDENT ON SLABS (REF. 69)

Material	Energy [MeV]	μx					
		0.5	1.0	2.0	4.0	8.0	16.0
Water	0.66	1.49	1.96	3.10	5.99	13.3	39.4
	1.0	1.40	1.80	2.72	5.01	10.5	25.7
	4.0	1.22	1.42	1.83	2.60	4.21	7.20
Iron	1.0	1.40	1.72	2.43	4.07	7.80	17.8
	4.0	1.20	1.36	1.72	2.50	4.17	7.45
	10.0	1.07	1.16	1.35	1.75	2.80	5.85
Tin	1.0	1.29	1.56	2.10	3.15	5.31	10.2
	4.0	1.16	1.31	1.63	2.35	4.12	9.41
	10.0	1.06	1.12	1.26	1.59	2.75	8.22
Lead	1.0	1.20	1.35	1.63	2.09	2.87	4.24
	4.0	1.11	1.23	1.44	1.98	3.28	7.46
	10.0	1.03	1.08	1.17	1.40	2.17	6.47

TABLE 5.8. TISSUE DOSE BUILDUP FACTORS – PLANE ISOTROPIC SOURCE, INFINITE MEDIUM (Ref 69)

μx	E_0 [MeV]							
	0.5	1	2	3	4	6	8	10
				Exposure in water				
1	4.74	3.34	2.57	2.23	2.02	1.80	1.66	1.57
2	8.71	5.24	3.60	3.03	2.66	2.29	2.03	1.87
4	20.6	9.98	5.87	4.55	3.94	3.12	2.73	2.46
7	50.3	19.8	9.78	7.00	5.77	4.45	3.65	3.28
10	94.5	31.9	13.9	9.52	7.62	5.67	4.60	4.04
15	205.0	56.8	21.3	13.9	10.7	7.60	6.05	5.21
				Exposure in lead				
1	1.38	1.61	1.67	1.61	1.49	1.37	1.28	1.22
2	1.55	1.92	2.11	2.03	1.86	1.66	1.47	1.38
4	1.80	2.52	2.91	2.86	2.64	2.38	2.05	1.84
7	2.14	3.30	4.11	4.27	4.21	4.09	3.53	3.06
10	2.43	4.07	5.37	5.97	6.26	6.95	6.20	5.48
15	2.73	5.15	7.40	8.86	10.9	16.7	17.8	16.1

TABLE 5.9. TISSUE DOSE BUILDUP FACTORS - PLANE ISOTROPIC SOURCE, SLAB GEOMETRY (Ref 70)

ALUMINUM

(M.F.P.)	0.5	1.0	2.0	4.0	7.0
ENERGY (MEV)					
0.05	1.457	1.730	2.203	2.940	3.663
0.10	1.780	2.576	4.265	8.290	15.260
0.30	1.738	2.621	4.490	10.220	22.040
0.50	1.702	2.410	4.213	8.847	19.720
0.70	1.687	2.382	3.683	8.076	15.690
1.00	1.624	2.288	3.473	6.482	12.150
2.00	1.539	2.051	2.823	5.104	7.373
3.00	1.481	1.858	2.622	3.846	6.153
4.00	1.464	1.771	2.427	3.593	4.513
6.00	1.388	1.610	2.046	2.884	4.164
8.00	1.304	1.514	1.909	2.492	3.768

LEAD

(M.F.P.)	0.5	1.0	2.0	4.0	7.0
ENERGY (MEV)					
0.05	1.011	1.015	1.022	1.032	1.037
0.10	1.015	1.030	1.054	1.151	1.989
0.30	1.090	1.140	1.209	1.294	1.366
0.50	1.172	1.283	1.420	1.674	1.907
0.70	1.251	1.428	1.627	2.009	2.247
1.00	1.335	1.512	1.834	2.316	2.831
2.00	1.367	1.560	1.923	2.603	4.096
3.00	1.302	1.497	1.906	2.767	3.678
4.00	1.254	1.440	1.717	2.522	4.454
6.00	1.177	1.299	1.590	2.221	3.644
8.00	1.134	1.237	1.435	1.957	3.143

WATER

(M.F.P.)	0.5	1.0	2.0	4.0	7.0
ENERGY (MEV)					
0.05	2.166	3.365	6.936	17.690	34.850
0.10	2.014	3.399	8.351	25.990	87.020
0.30	1.803	2.599	5.444	15.040	36.090
0.50	1.751	2.475	4.368	11.050	27.950
0.70	1.686	2.364	4.195	7.793	18.730
1.00	1.641	2.283	3.708	6.306	14.090
2.00	1.556	2.041	3.017	4.564	8.341
3.00	1.482	1.922	2.554	4.233	6.560
4.00	1.456	1.813	2.377	3.817	5.505
6.00	1.383	1.663	2.062	2.755	4.592
8.00	1.341	1.573	1.914	2.528	3.422

5.4.5.2 Comparison of Buildup Factors for Different Geometries

Realistic space shielding problems seldom will have the exact geometries used in most buildup factors calculations. It is useful, then, to know how well buildup factors calculated for one geometry and source angular distribution can be applied to other geometries. Figure 5.22 shows a comparison of the buildup factors calculated for 0.5 - MeV photons in water. This should be a sensitive comparison since the buildup factors are greatest for low energy photons in low Z material. It is seen that the buildup factors for a plane of isotropic sources are considerably larger than the others. The buildup factors for the other geometries are similar for penetration depths of less than two mean free paths. As was pointed out before, the plane of isotropic sources is an extreme case and often reasonable results can be obtained by using buildup factors calculated in one geometry for problems with similar geometries.

It is also instructive to compare the doses calculated for different source distributions. Figure 5.23 illustrates the different source distributions under consideration for slab geometries. Included as Case 2 is a distributed source of radiation which emits radiation into the slab as the cosine of the angle to the normal. The dose in this case is given by the equation

$$D = 2\kappa S k \mu_a B(\mu X) E2(\mu X), \tag{5.43}$$

where $E2(\mu X)$ is the second exponential integral defined as

$$E2(\mu X) = \mu X \int_{\mu X}^{\infty} \frac{e^{-y}}{y^2} dy. \tag{5.44}$$

Figure 5.24 shows the doses calculated for these five cases. (Case 2 was calculated using the buildup factors for a plane of isotropic sources and Case 4 was calculated assuming no contribution from scattering). It is apparent from this figure that the effect of the shielding depends strongly on 1.) the source normalizations and 2.) the angular distribution of the emitted radiation. This should be considered when calculating the attenuation of photons passing through complicated shields.

5.4.3 Buildup Factors for Low Energy Photons

The buildup factors given in Tables 5.5 - 5.8 are useful for photon energies above 0.5 MeV. The bremsstrahlung energy spectrum extends to energies lower than this so buildup factors for lower energies must be used. Extrapolation of the buildup factors to lower energies is dangerous since for low Z material the buildup factors given in Tables 5.5 - 5.8 increase monotonically as the photon energy decreases to 0.5 MeV. Extrapolation would lead to very high values as the energy is lowered further. Such is not the case.

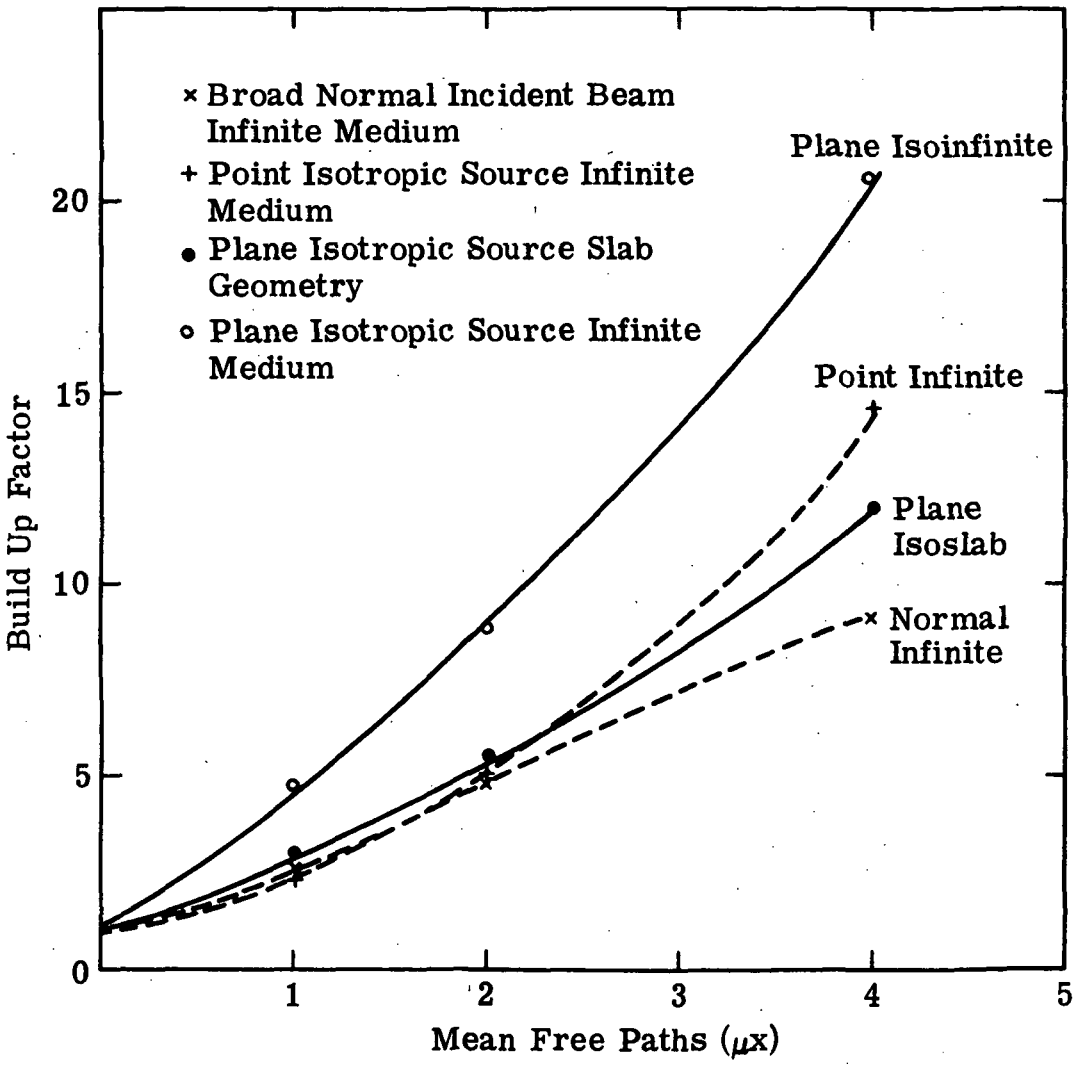

Figure 5.22. Comparison of buildup factors for 0.5 MeV photons in water

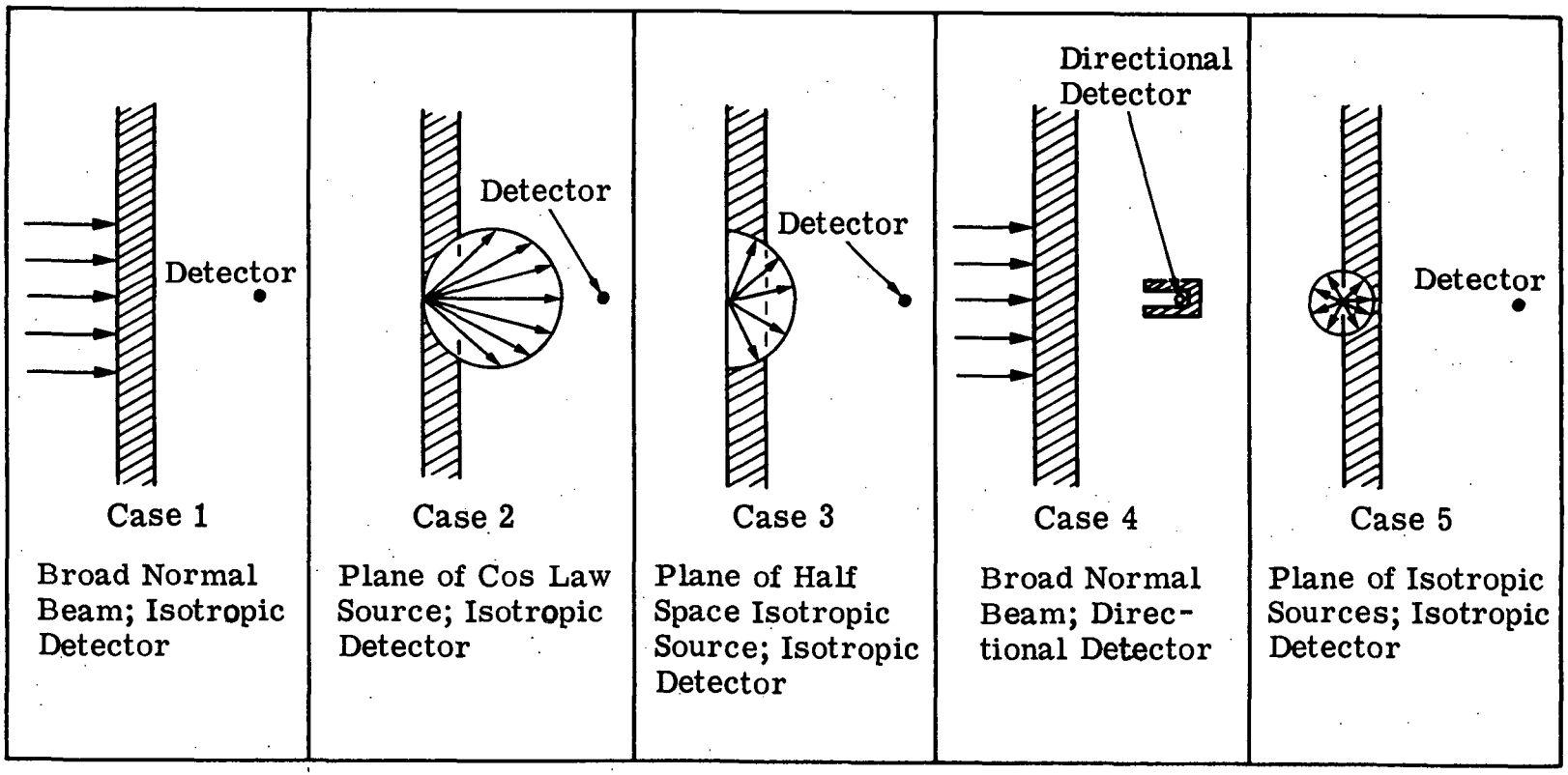

Figure 5.23. Geometries and source angular distributions for comparison of dose transmission through slabs of material. All sources are assumed to be uniformly distributed over the entire surface plane.

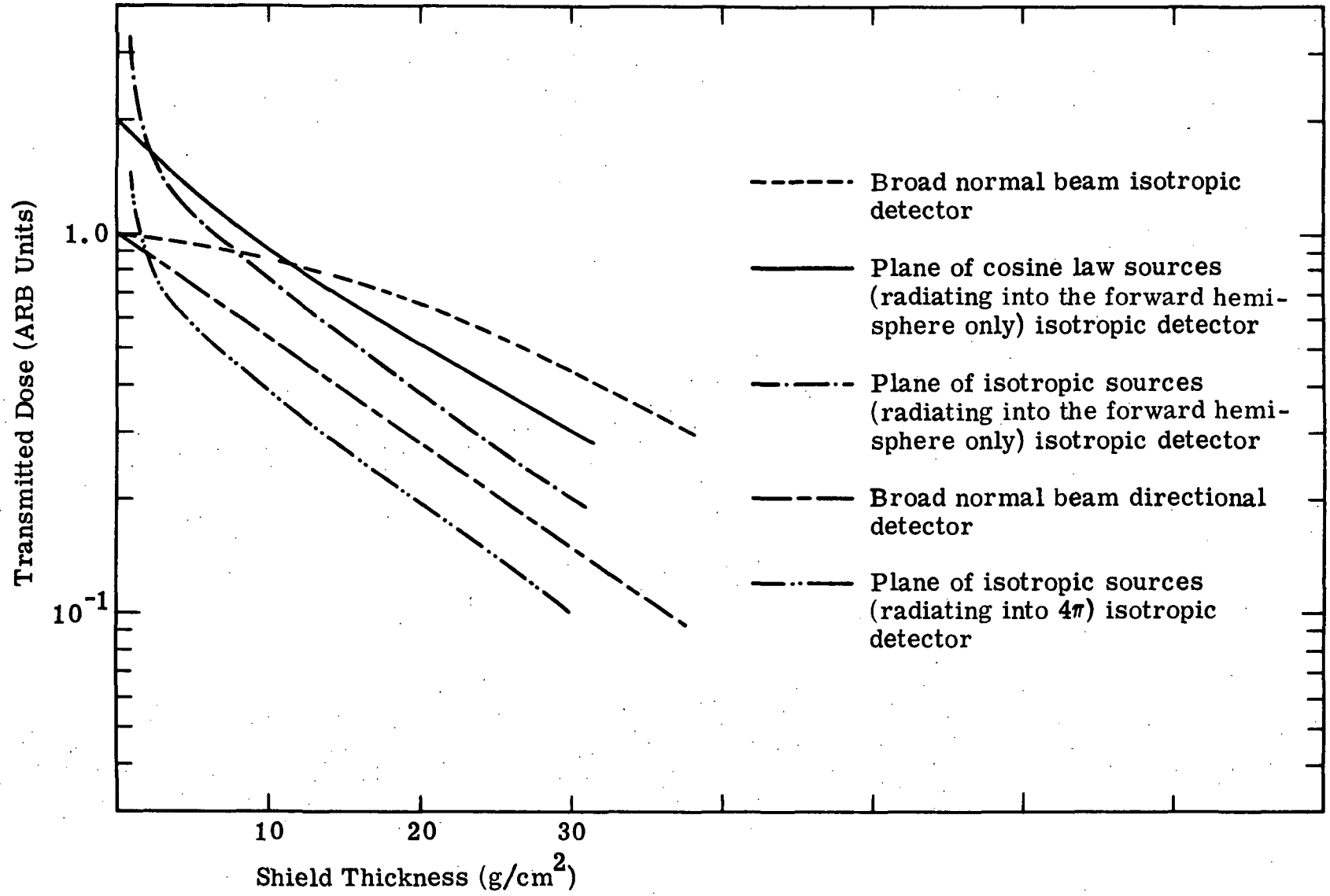

Figure 5.24. Relative doses produced by 1 MeV photons after passing through a slab from plane source for different source distributions normalized to the same total source strength

Figure 5.25 and Fig. 5.26 show the buildup factors for a plane of isotropic sources and a slab geometry for shield material of Al and Pb. These figures show the low energy dependence of the buildup factors for various slab thickness. Figure 5.26 shows the point isotropic dose buildup factors for photons in water. It is seen that for low photon energies the buildup factors decrease to a value of 1. This is easily understood since photoabsorbtion becomes larger for low photon energies. Thus as the photon energy decreases an increasing fraction of the scattered radiation is absorbed before it reaches the detector. Also shown in Fig. 5.27 is the quantity

$$\left[1 - \frac{\mu a}{\mu}\right] \quad ,$$

where μ and μ_a are, respectively, the total attenuation coefficient and the energy absorption coefficient. It is seen that this function reaches a maximum at essentially the same point as the buildup factors. This holds true for other elements as well. So one can estimate the photon energy at which the buildup factor will have its maximum value.

5.4.5.4 Buildup Factors for Multilayered Shields

Buildup factors represent the contribution to the dose (photon number, energy fluence) from scattered radiation. High Z elements are much more efficient at absorbing scattered gamma radiation than low Z elements and have correspondingly smaller buildup factors. The amount of scattered radiation which will reach the detector depends on the order of shields in a multilayered system. If a low Z shield is followed by a high Z shield much of the radiation scattered in the first shield will be absorbed in the second and the buildup factor for the entire system will be smaller than the product of the buildup factors for the two layers. If the situation is reversed and the high Z shield is followed by a low Z material the buildup factor will be higher than the product of the buildup factors for the individual layers. An estimate of the appropriate buildup factor can be obtained, if the last shield is greater than about one mean free path, by using the buildup factor for the last material, with the argument of the buildup factor being the number of mean free paths in the entire system. Thus, if the system is comprised of one mean free path of Al and one mean free path of Pb the appropriate buildup factor would be for two mean free paths of Pb.

5.4.6 Energy Spectra After Shielding Material

It was shown in the preceding section how one could estimate integral quantities such as the dose, the energy fluence, or the number fluence of photons after shielding by using buildup factors. These quantities cannot lead to an understanding of the energy spectrum of the transported radiation. In some applications it may be necessary to understand, or predict, the energy spectrum of the transported radiation. The following is a simplified solution to

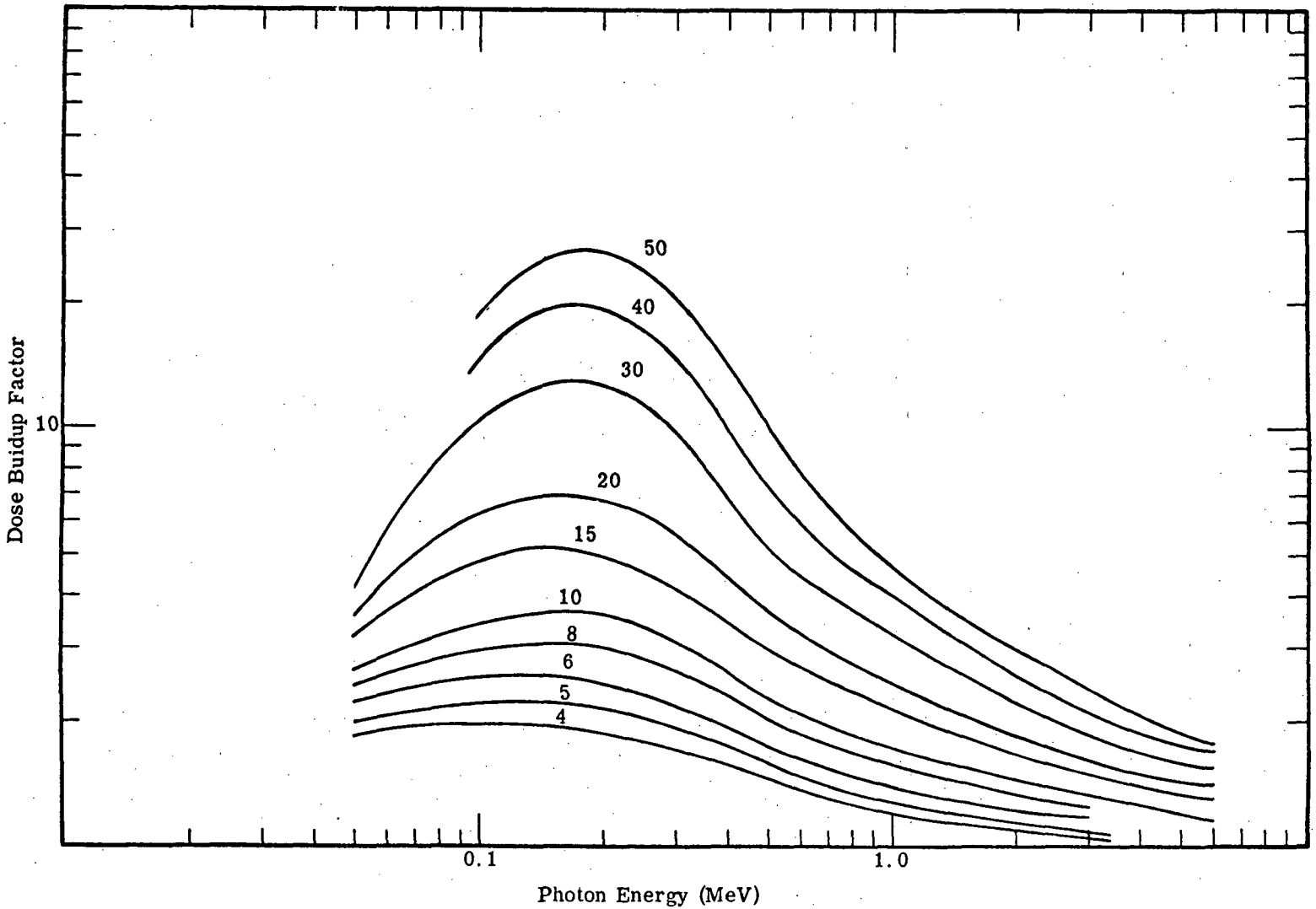

Figure 5.25. Plane of isotropic sources; slab geometry dose buildup factors for Al calculated by Watts and Burrell (Ref. 70) vs photon energy. The thickness of Al in g/cm^2 is listed for the appropriate curve.

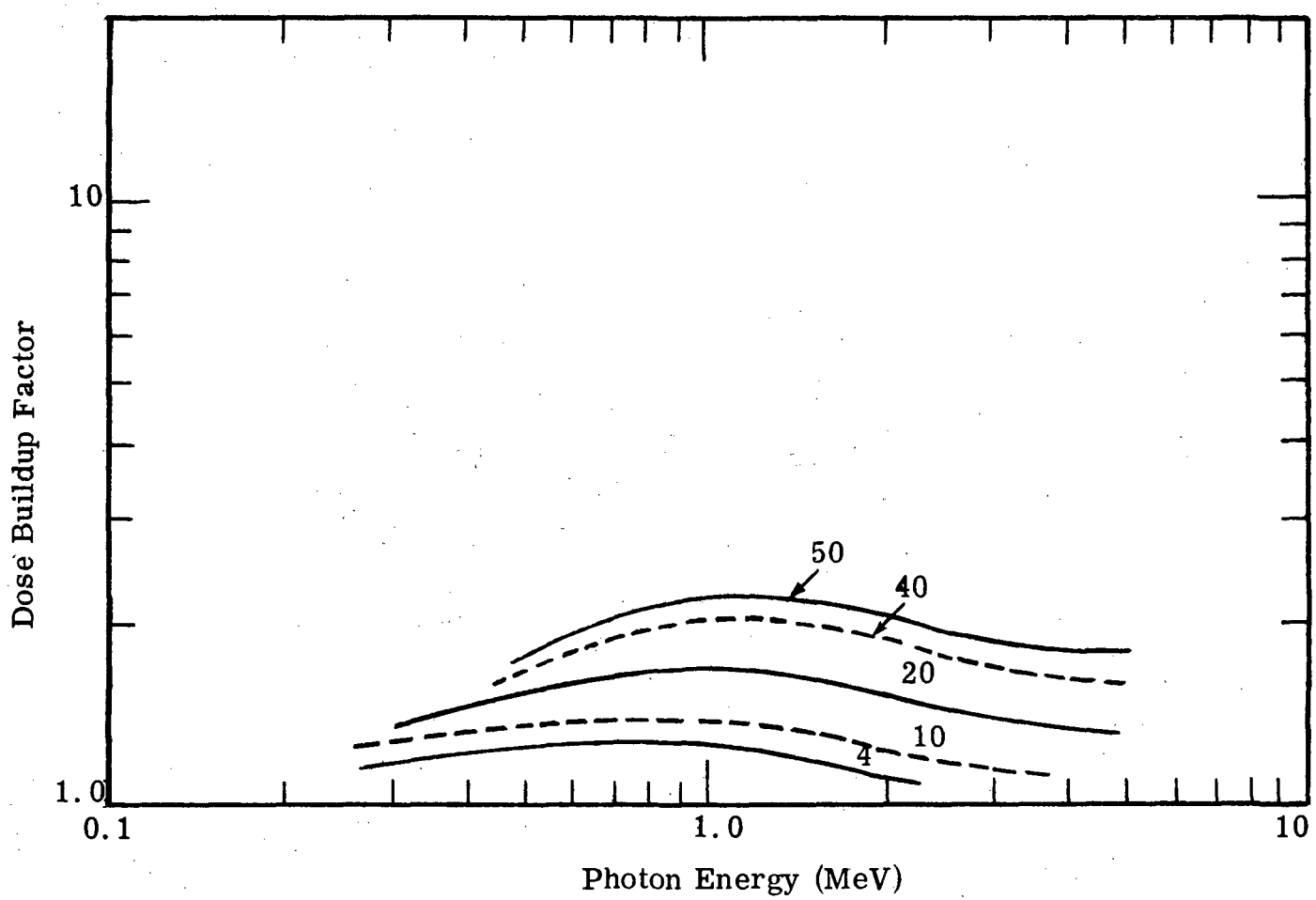

Figure 5.26. Plane isotropic dose buildup factor for Pb calculated by Watts and Burrell (Ref. 70) vs photon energy. The thickness of Pb in g/cm^2 is listed for the various curves.

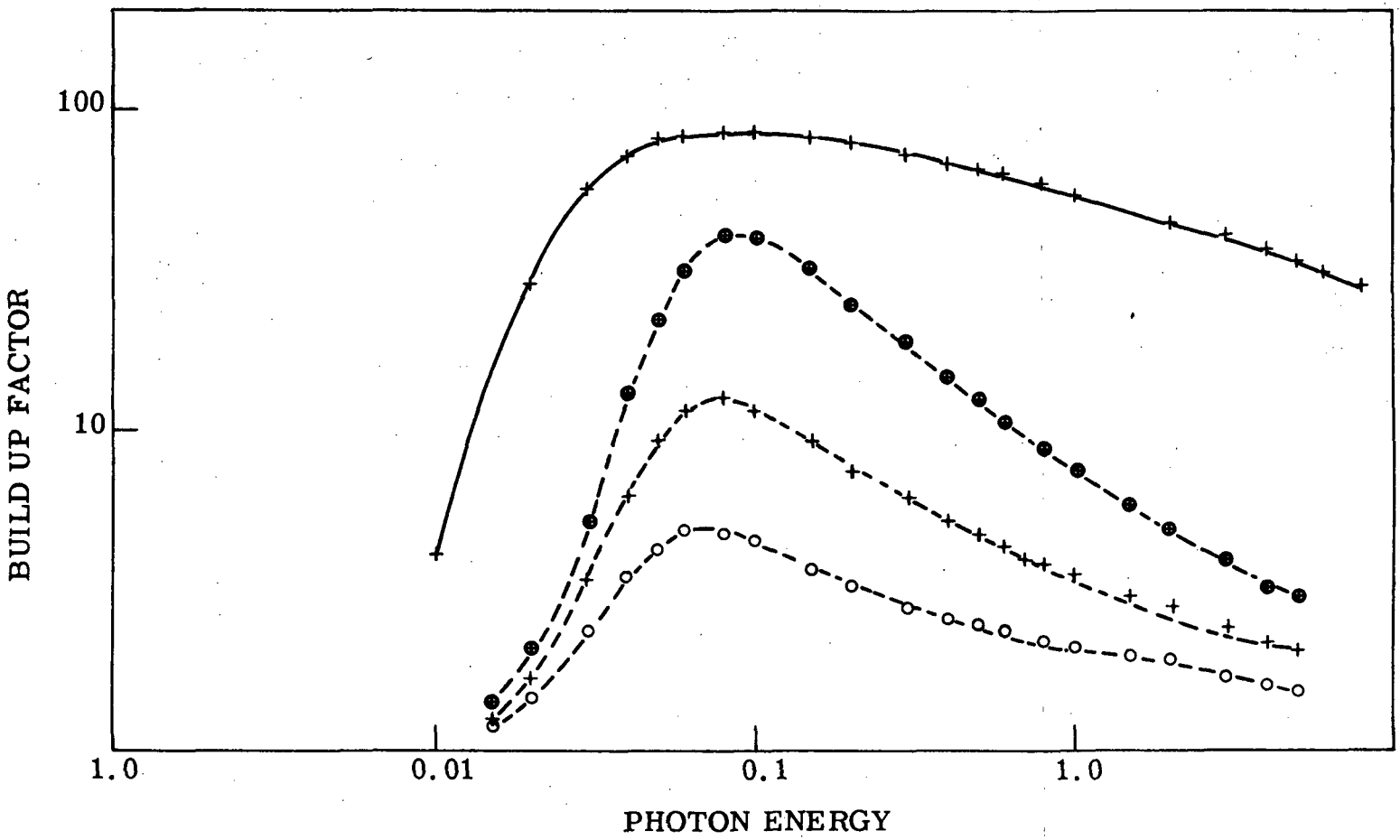

Figure 5.27. Comparison of the point isotropic dose buildup factors for low energy photons in H_2O with the quantity $\exp[(\mu-\mu_a)x]$. The coefficient μ and μ_a are the attenuation and energy absorbtion coefficients, respectively.

the problem and is not meant to give an accurate description of the transmitted energy spectrum. For accurate calculations it is necessary to use sophisticated computer codes which treat scattering to all orders.

The model presented here considers only the contribution of single Compton scattering as it affects the photons which emerge at right angles to the target. The unscattered radiation which emerges normally to the target will be given by

$$I(k,0) = I(k,0)e^{-\mu(k,Z)} \qquad \left(\frac{\text{photons} \cdot \text{MeV}}{\text{MeV} \cdot \text{Sr}}\right) , \tag{5.45}$$

where $I(k,0)$ is the intensity of the incident photons per unit solid angle normal to the plane of the shield, k is the photon energy, $\mu(k,Z)$ is the total attenuation coefficient for photons of energy k in a material Z, and T is the thickness of the material. The intensity of the scattered radiation which emerges at right angles to the plane of the target will be composed of a spectrum of energies from the initial energy k down to some minimum energy. If scattering through all angles is permitted this minimum energy will be

$$k_{min} = \frac{k}{1 + \frac{2k}{m_o c^2}} \tag{5.46}$$

while if only scattering through angles less than $\pi/2$ is permitted, the minimum energy will be a minimum energy.

$$k_{min} = \frac{k}{1 + \frac{k}{m_o c^2}} \tag{5.47}$$

The intensity spectrum of the scattered radiation in this model is given by the equation

$$I_{sc}(k',0) = \frac{N_o Z k'}{Ak} I(k,\theta) \frac{d\sigma}{dk'}(k,k')dk' \left[\frac{e^{-\mu' T} - e^{-\mu T/\cos\theta}}{+\mu - \mu\cos\theta}\right] \tag{5.48}$$

which has units of

$$\left(\frac{\text{photons} \cdot \text{MeV}}{\text{MeV} \cdot \text{Sr}}\right)$$

In this equation N_o is Avogrado number, Z is the atomic number of the shielding material, k' is the energy of the scattered photon, A is the gram molecular weight of the shielding material, $I(k,\theta)$ is the intensity spectrum of the original photon source as a function of angle θ with units of $(\frac{\text{photons} \cdot \text{MeV}}{\text{MeV} \cdot \text{Sr}})$ and $d\sigma/dk'$ is the cross section for scattering from an energy k to an energy k', and μ and μ' are the mass attenuation coefficients for photons of energies k and k', respectively. The quantities k' and θ are related through the equation

$$k' = \frac{k}{1 + \frac{k}{m_o c^2}(1-\cos\theta)} \tag{5.49}$$

and the cross section $\frac{d\sigma}{dk'}(k,k')$ is given by the Klein-Nishina formula for free electrons as[69]

$$\frac{d\sigma}{dk'}(k,k') = \frac{\pi r_o^2 m_o c^2}{k^2}\left\{\frac{k'}{k} + \frac{k}{k'} - 2m_o c^2\left(\frac{1}{k'} - \frac{1}{k}\right) + (m_o c^2)^2\left(\frac{1}{k} - \frac{1}{k'}\right)^2\right\},$$

$$(\text{cm}^2/\text{electron}) \tag{5.50}$$

where r_o is the classical electron radius (2.81785×10^{-13} cm) and $m_o c^2$ is the rest mass of the electron.

Figure 5.28 shows examples of the calculated energy spectra of the scattered component of the radiation for 2-MeV photons and Al shielding material. The angular distribution of $I(k,\theta)$ assumed for these calculations is

$$I(k,\theta) = I(k,0)\cos\theta$$

and directed into the shield.

5.4.7 Characteristic X-rays

When charged particles or photons pass through matter, they encounter atomic electrons. If the energy of the incident charged particle or photon is above the binding energy of the atomic electron, the atomic electron may be ejected from its orbit leaving the atom in an excited state. This state decays either as an electron drops into the vacancy and the atom emits a photon of fixed energy (x-ray fluorescence), or by an Auger transition in which an electron instead of a photon is ejected from the atom. Since there are many possible orbits between which the transitions can take place there

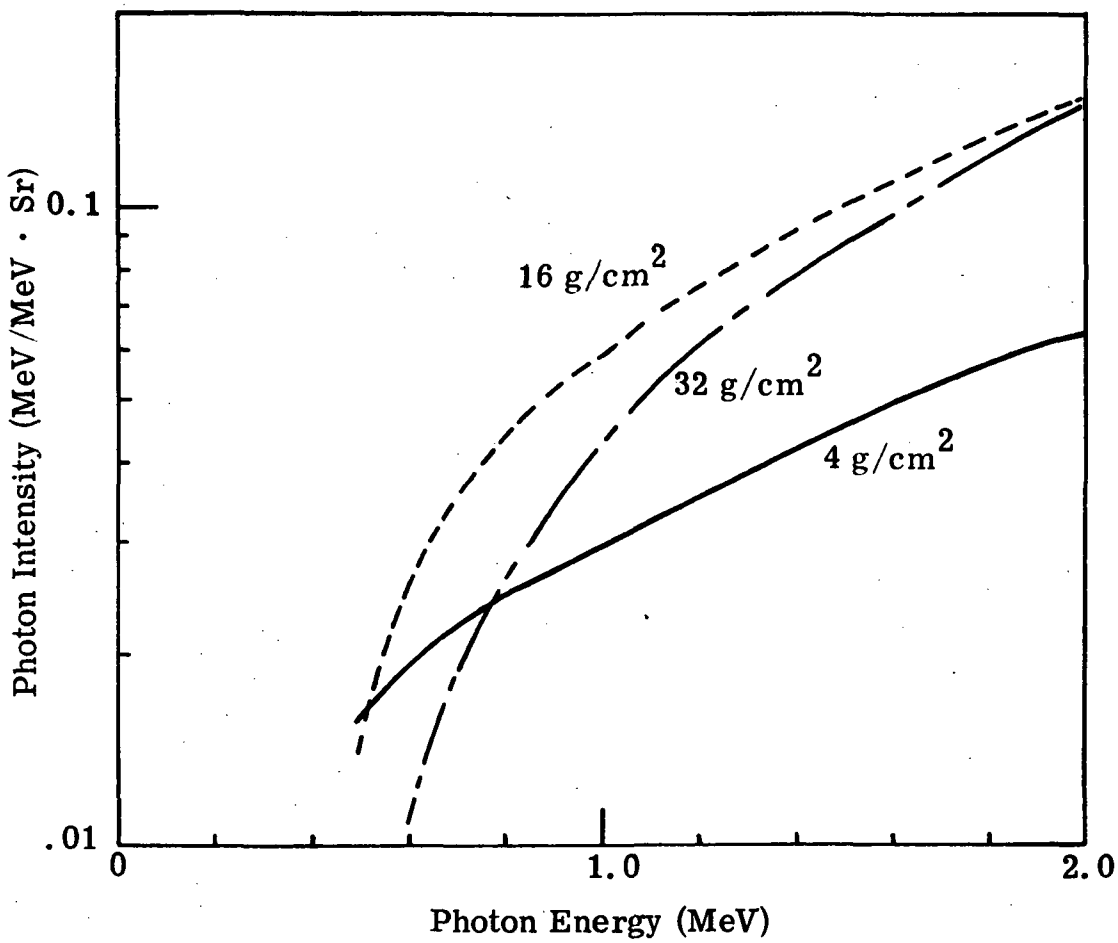

Figure 5.28. Single Compton scattering photon energy spectrum for 2 MeV half-space isotropic photons after passing through various thicknesses of Al (Eq. 5.48)

will be a number of characteristic x-rays. The series of transitions to the innermost shell of a given atom all have very nearly the same energies and are called the K x-rays. The energy of these x-rays is given by the equation

$$E_K = 0.0136\, Z^2 \quad \text{(keV)} \quad . \tag{5.51}$$

All characteristic x-rays have energies below 120 keV and hence will be readily absorbed in fairly thin shields. For example, 0.7 cm of Cu will reduce the intensity of the 69-keV x ray from W by a factor of 10^3, while it would take about 14 cm of Cu to produce the same attenuation for 1-MeV photons. An interesting point, however, is that a material is very transparent to its own characteristic x-ray. That this is the case can be seen by the fact that when an atom absorbs a K x-ray it will more than likely reradiate the same energy photon as it deexcites. Figure 5.29[70] shows a spectrum of K x-rays from Al (E_k = 1.58 keV) after passing through 1.5 mg/cm^2 of Al and Mg. It is seen that there is approximately a factor of 100 times less attenuation in the Al absorber than in the equivalent thickness Mg absorber. In applications where the greatest attenuation of the photon flux is desired, it is often necessary to use multi-layered shields of different materials to reduce the number of transmitted characteristic x-rays.

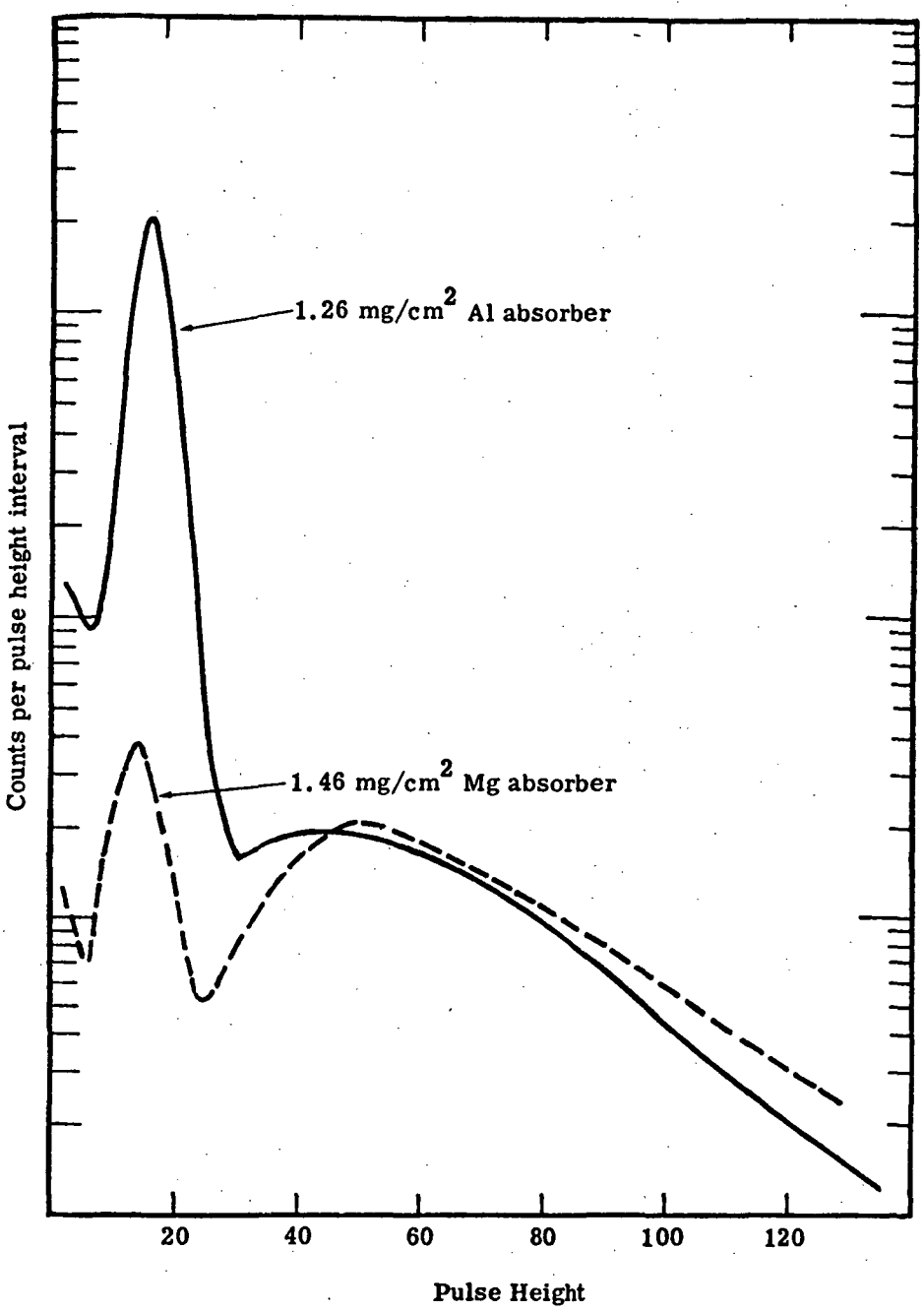

Figure 5.29. Pulse height distribution produced by K x-rays from Al after passing through a matched pair of Al and Mg filters (From Ref. 70)

6. SPACE RADIATION SHIELDING

6.1 INTRODUCTION

In the preceding chapter parametric representations of the results of electron transport experiments and calculations were presented. All the experimental results (and most of the calculated results) were obtained for monoenergetic beams of electrons incident on small areas of plane targets. Since the electron radiation encountered in the space environment is spatially distributed, omnidirectional, and has a continuous energy distribution, all outside surfaces of the spacecraft will be bombarded with electrons incident from all possible directions and kinetic energies ranging from 0 to about 7 MeV. Consequently, the results of the preceding section cannot be applied directly to space radiation problems. Integrations over the solid angle subtended by the primary electron directions, over the surface of the spacecraft, and over the electron energy spectrum must be performed to obtain results which are useful in space shielding problems. This section will present the formalism necessary to perform these integrations. It will be seen that the exact solution of the most general problem is quite complicated and in most cases is not even desired. Next, approximations for the angular distributions of primary electrons, and for the angular distributions of the electrons, and bremsstrahlung penetrating the shield material, will be introduced which greatly simplify the problem. The results of calculations for various useful quantities will then be presented for both electron penetration through the shielding material and the secondary bremsstrahlung intensity. Finally, the errors introduced by the approximations will be discussed.

6.1.1 Statement of Problem

In space shielding problems one typically wants to know the dose rate, or accumulated dose, at some point on the interior of an enclosed vehicle caused by an external radiation environment. Since the structure of the vehicle and its internal components may be quite complex, setting up a formalism to solve the problem rigorously is difficult. The formalism presented here will introduce several simplifying assumptions which reduce the problem to a manageable size. An illustration of the problem

to be solved is schematically shown in Fig. 6.1. Here, the problem is to calculate the dose at some interior point of a complex enclosure which is bombarded on all exterior surfaces by an omnidirectional flux of electrons.

There are several methods that can be used in the solution of this problem, the choice of which depends on the amount of effort one is willing to spend. The most accurate would be to consider the surface area to a depth of two or three g/cm^2 and calculate the penetrating electron and secondary bremsstrahlung radiations emerging from the interior of this surface. These radiations could then be transported to the dose point and a dose estimate obtained. However, this approach is difficult. It is more convenient to assume that all shielding materials can be considered as part of the surface since it is likely that most of the material will be concentrated in the surface region. The problem is thus reduced to the situation shown in Fig. 6.2.

The method presented here for solving this problem is to segment the interior of the shield into differential elements and assume that the thickness of the shield is small compared to the other dimensions in the problem (e.g., inches in comparison to several feet). The results of the preceding section can be used to establish the radiation pattern emerging from this surface and the portion which arrives at the dose point can then be determined. This procedure can be repeated for all other elements of the surface and the contributions summed to establish the dose at the point of interest. As will be pointed out, additional assumptions will be made since even this simplified approach can become very complex.

6.2 DEFINITIONS OF TERMS AND CONCEPTS

This section defines the quantities used to convert the results of experiments using monoenergetic, monodirectional beams of electrons incident on small areas of targets to quantities useful for space radiation shielding problems. Since problems often arise in notation, and normalization, particular attention will be paid to these quantities. In most cases the notation will conform to normal usage, but in some cases, to avoid confusion, new symbols will be introduced. These will be fully discussed where they are introduced. Definitions will be presented for each quantity. Where confusion might arise between the units for the primary and secondary radiation subscripts will be used.

6.2.1 Primary Electron Density

The primary electron number density, which is a function of electron direction and kinetic energy is defined so that

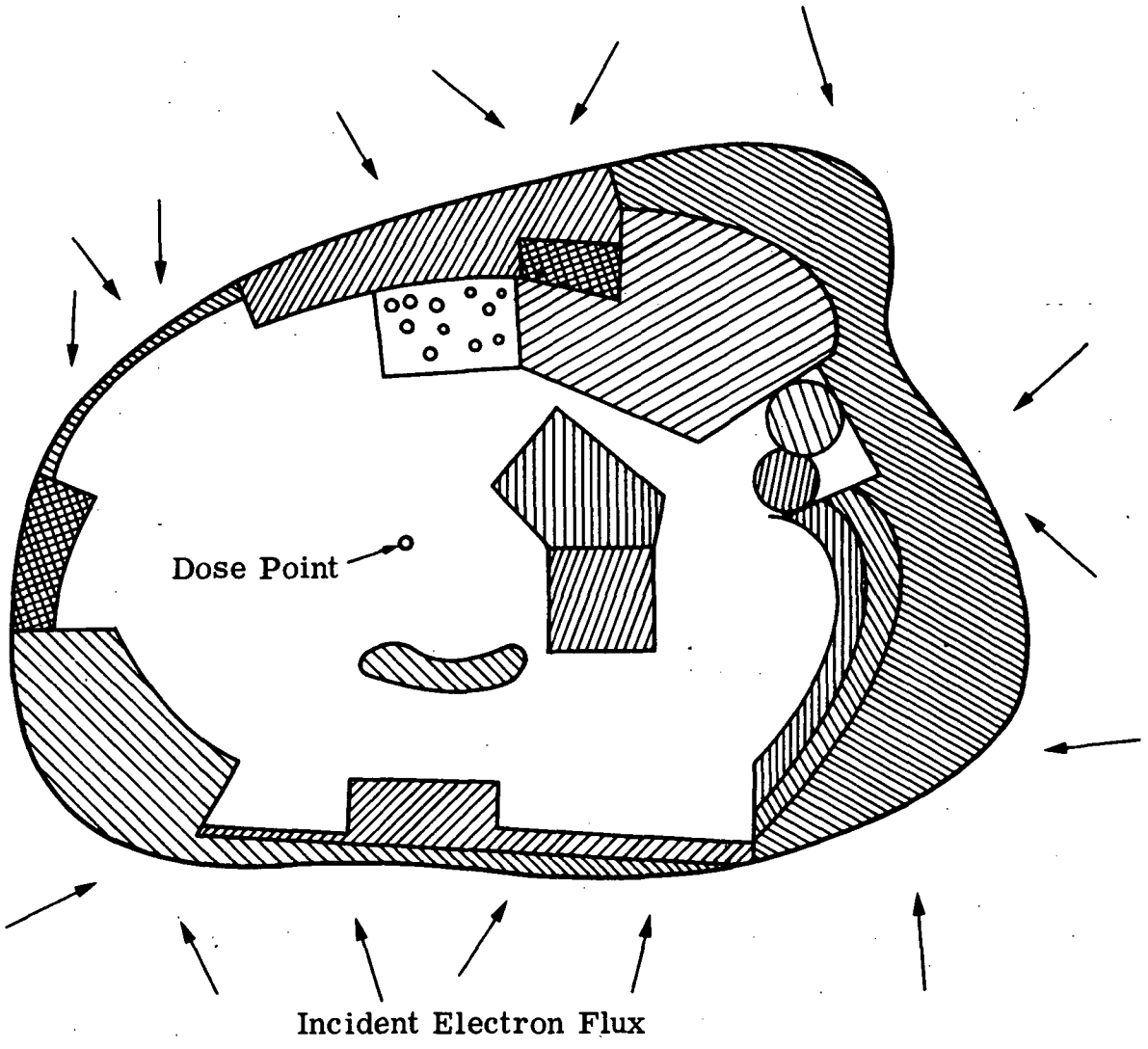

Figure 6.1 Schematic illustration of complex space shielding problem

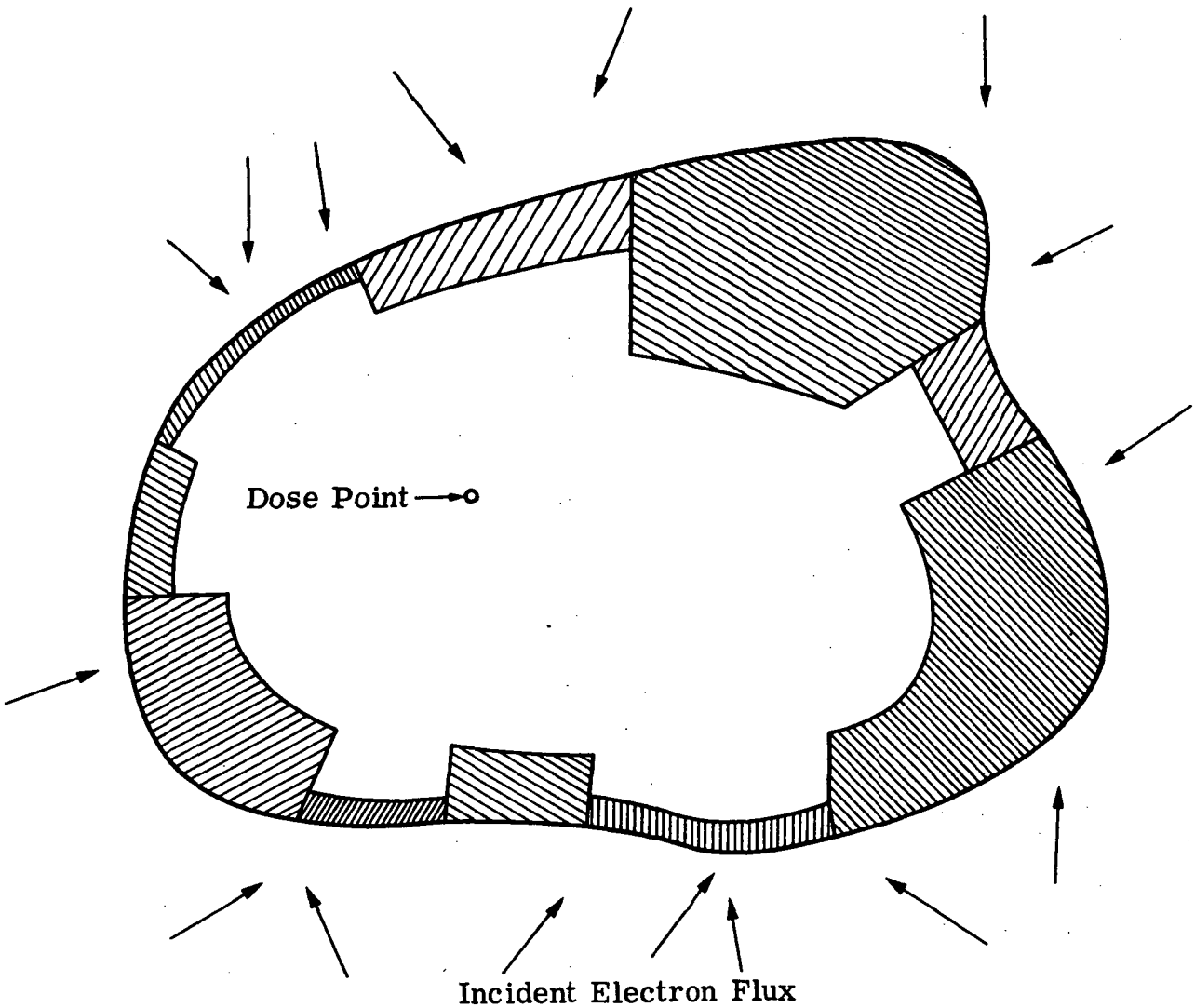

Figure 6.2 Illustration of simplified space shielding problem

$n(\bar{\Omega}, E)dE d\Omega \equiv$ The number of primary electrons per unit volume of space which have kinetic energies between E and E + dE and which are traveling within a solid angle $d\Omega$ about the direction $\bar{\Omega}$.

The units of $n(\bar{\Omega}, E)$ are

$$\left(\frac{\text{electrons}_p}{\text{MeV}_p \ \text{Sr}_p \ \text{cm}^3} \right) ,$$

where the subscript "p" refers to the primary electrons.

6.2.2 Primary Electron Flux

From the primary electron number density one can define an angularly dependent electron flux through the relation

$\varphi(\bar{\Omega}, E)dE d\Omega \equiv n(\bar{\Omega}, E) v \, dE d\Omega \equiv$ The distance traveled per unit time per unit volume by electrons which have energies in the kinetic energy interval E to E+dE and travel in the direction $\bar{\Omega}$ within the solid angle $d\Omega$.

Here v is the average velocity of the electron in the kinetic energy interval E to E+dE. There is an alternative definition of $\varphi(\bar{\Omega}, E)$ which is sometimes more useful than the definition given above. If one considers a unit differential area perpendicular to the direction $\bar{\Omega}$ then, since v is the distance traveled by electrons in the energy interval E to E+dE per unit time, the flux can be defined as

$n(\bar{\Omega}, E) v \, dE \, d\Omega = \varphi(\Omega, E) dE d\Omega$
= the number of electrons traveling within $d\Omega$ about the direction $\bar{\Omega}$ with kinetic energies between E and E and E+dE which cross a unit differential area perpendicular to $\bar{\Omega}$ per unit time.

The units of the angular primary electron flux are

$$\left(\frac{\text{electrons}_p}{\text{MeV}_p \ \text{Sr}_p \ \text{cm}^2 \ \text{sec}} \right) .$$

6.2.3 Primary Electron Current

It should be emphasized that the unit area referred to in the definition of flux is perpendicular to the direction $\bar{\Omega}$ and, hence, its orientation depends on the direction $\bar{\Omega}$. The definition of current j is similar to the definition of flux (and often confused with it) but in the definition of current the unit area is fixed in space. The angular dependent electron current at a differential unit area of surface is

$j(\bar{\Omega}, E, \mu)d\Omega dE \equiv$ The number of electrons in the kinetic energy interval E to E+dE traveling in the direction $\bar{\Omega}$ within the solid angle $d\Omega$ which cross a fixed unit differential surface area per unit time.

Here the variable μ is the cosine of the angle between the normal to the surface $\hat{n}_s$ and the electron's direction Ω. The direction of $\hat{n}_s$ is taken such that a positive current results from a flux of electrons hitting the outside of the spacecraft. That is, the unit normal vector $\hat{n}_s$ at a differential surface area is taken as being directed into the spacecraft. The current j is related to the flux φ through the equation

$$j(\bar{\Omega}, E, \mu) = \varphi(\Omega, E)\,(\hat{n}_s \cdot \hat{\Omega}) = \varphi(\bar{\Omega}, E)\mu \qquad (6.1)$$

where $\hat{\Omega}$ is a unit vector in the direction of the electron motion. The units of the electron current are the same as those of the electron flux and are:

$$\left(\frac{\text{electrons}_p}{\text{MeV}_p\ \text{Sr}_p\ \text{cm}^2\ \ \text{sec}}\right) .$$

6.2.4 Penetrating Electron and Bremsstrahlung Radiation

The penetration of electrons and the production of secondary bremsstrahlung radiation were discussed in the preceding section. The penetration probabilities for electrons and the production probability for bremsstrahlung were expressed in forms which gave the number of penetrating electrons or secondary gamma rays radiated into a particular solid angle. The parametric representation of the probability for electron penetration and bremsstrahlung production can be defined in a general way as

$P(E, E', \bar{\Omega}, \bar{\omega}, \xi, T, Z)dE'd\omega \equiv$ The number of secondary particles which emerge from a plane target with kinetic energies between E'+dE' in the direction $\bar{\omega}$ within the solid angle $d\omega$ that are produced per electron of kinetic energy E incident from the direction $\bar{\Omega}$. The variables ξ, T, and Z specify the target orientation, thickness, and atomic number, respectively.

For the bremsstrahlung production, the intensity or number of photons times their energy was parameterized. The concept of "P" for bremsstrahlung will reflect this distinction so the units of "P" are

$$\left(\frac{\text{electrons}_s}{\text{MeV}_s\ \text{Sr}_s\ \text{electron}_p}\right) \qquad \text{for penetrating electrons}$$

and

$$\left(\frac{\text{photons}_s\ \ \text{MeV}_s}{\text{MeV}_s\ \text{Sr}_s\ \text{electron}_p}\right) \qquad \text{for the bremsstrahlung intensity .}$$

The subscripts "s" refer to the units of the secondary radiation.

6.2.5 Secondary Radiation Current

The secondary radiation current j_s emitted from a differential area of the interior of the spacecraft shield which is produced by the primary current j is given by a product of the primary current times the production probability P.

$$j_s(E, E', \bar{\Omega}, \bar{\omega}, \xi, T, Z) = P(E, E', \bar{\Omega}, \bar{\omega}, \xi, T, Z) \quad j(E, \bar{\Omega}) \quad . \qquad (6.2)$$

The quantity j_s is defined such that

$j_s(E, E', \bar{\Omega}, \bar{\omega}, \xi, T, Z)\, d\Omega\, dE\, ds\, dE'\, d\omega$ = The number of secondary particles radiated into a differential solid angle $d\omega$ about the direction $\bar{\omega}$ with energies between E' and $E'+dE'$ from a fixed differential surface area ds which is bombarded with primary electrons with kinetic energies between E and $E+dE$ which are incident from the direction $\bar{\Omega}$ within the solid angle $d\Omega$. The quantities ξ, T, and Z refer to the orientation of the surface, the shield thickness, and the atomic number of the shield, respectively.

The units of j_s are

$$\left(\frac{\text{electrons}_s}{\text{cm}^2\ \text{sec}\ \text{MeV}_p\ \text{MeV}_s\ \text{Sr}_p\ \text{Sr}_s}\right) \text{ for penetrating electrons}$$

and

$$\left(\frac{\text{photons MeV}_s}{\text{cm}^2 \text{ sec MeV}_p \text{ MeV}_s \text{ Sr}_p \text{ Sr}_s} \right)$$ for the bremsstrahlung intensity .

The quantity j_s is a function of eight variables and integrations must be performed to obtain information useful to space shielding calculations.

6.2.6 Isotropic Primary Electron Flux

It is possible, in principle, to evaluate the integrals implied by the preceding formalism. This requires keeping track of the direction of the geomagnetic field in relation to the orientation of each surface element of the spacecraft for the integration over the surface ds. It also requires performing these complicated integrations for many steps along the spacecraft's trajectory to obtain results for a single orbit. Such calculations are usually not carried out in practice. Instead, assumptions are introduced which greatly reduce the complexity of the problem but still allow reasonably accurate "average" quantities to be obtained. The first of these assumptions is that the primary electron flux is isotropic (that is, the electron current incident on a differential area is distributed as $\cos \theta_n$). If the total electron flux $\Phi(E)$, energies between E and E+dE is defined by the equation

$$\Phi(E)dE = \int_{4\pi} \varphi(E, \bar{\Omega}) d\bar{\Omega}\, dE \quad , \tag{6.3}$$

where Φ has the units of

$$\left(\frac{\text{electrons}_p}{\text{MeV}_p \text{ cm}^2 \text{ sec}} \right)$$

and φ is assumed to be independent of $\vec{\Omega}$, then

$$\varphi(E) = \frac{\Phi(E)}{4\pi} \quad . \tag{6.4}$$

The quantity $\Phi(E)$ is defined such that

$\Phi(E)dE$ = the number of electrons with kinetic energies between E and E+dE which pass through a sphere of unit cross sectional area per unit time .

6.2.6.1 Incident Electron Current

It is instructive at this point to evaluate the number of electrons which strike a fixed unit surface area in terms of the isotopic omnidirectional electron flux Φ. From the definition of the electron current $j(\bar{\Omega}, E\mu)$ one sees that the number of electrons which strike a unit surface area from one side can be defined as

$J_{in}(E)dE \equiv$ the number of electrons whose energies range from E to E+dE which strike a unit differential area from one side per unit time.

and is equal to:

$$J_{in}(E) = \int_0^{2\pi} d\varphi \int_0^1 j(E, \mu) d\mu$$

$$J_{in}(E) = 2\pi \int_0^1 \varphi(E)\mu \, d\mu \qquad (6.5)$$

$$= \pi\varphi(E) = \frac{\Phi(E)}{4} \quad .$$

Thus, the number of electrons which strike a fixed unit surface from one side is equal to the isotropic omnidirectional flux divided by 4. This number will be defined as the incident electron current.

6.2.6.2 Vette's Model of the Electron Environment

In Vette's model of the electron environment the omnidirectional electron flux $\Phi(B, L, E)$ is written as a product of a function which depends on B and L and a function which depends on E and L such that

$$\Phi(B, L, E) = F(B, L)N(E, L) \quad , \qquad (6.6)$$

where $F(B, L)$ is defined as the total omnidirectional flux of electrons with energies above a cutoff energy E_o at a point in space described by the parameters B and L

$$F(B, L) = \int_{E_o}^{\infty} dE \, \Phi(B, L, E) \qquad (6.7)$$

and $N(E, L)$ is the energy spectrum of the electrons for a given L value (the electron energy spectrum is assumed to be independent of B in this model) normalized per unit electron with energy greater than E_o, that is

$$N(E, L) = \frac{\Phi(B, L, E)}{\int_{E_o}^{\infty} dE\, \Phi(B, L, E)} \quad . \tag{6.8}$$

The units of $F(B, L)$ are

$$\left(\frac{\text{electrons}_p\ (E > E_o)}{\text{cm}^2\ \text{sec}} \right)$$

where the symbol "electrons $(E > E_o$" denotes the number of electrons with energies greater than the cut off energy E_o. The units of $N(E, L)$ are

$$\left(\frac{\text{electrons}_p}{\text{MeV}_p\ \text{electron}_p (E > E_o)} \right) \quad .$$

In this model the total electron current with energies greater than E_o incident on a fixed unit area from one side is given as:

$$J_{In}^{T}(B, L) = \frac{F(B, L)}{4}$$

with units of

$$\left(\frac{\text{incident electrons}\ (E > E_o)}{\text{cm}^2\ \text{sec}} \right) \quad . \tag{6.9}$$

This quantity may be used as the source term in space shielding calculations.

6.2.7 Secondary Radiation Current for Isotropic Electron Flux

The secondary radiation current as defined in Equation 6.2 cannot be integrated simply for an isotropic electron flux since the secondary source term $P(E, E', \vec{\Omega}, \omega, \xi, T, Z)$ depends on the incident electron coordinates. The integration over incident electron solid angle can be performed numerically, however, and results can be obtained which are useful in succeeding calculations. The secondary radiation current produced by an isotropic primary electron flux incident on one side of a shield is

$$J_s(E, E', \theta_\gamma, T, Z)\, dE dE' ds\, d\omega \equiv \frac{\Phi(E)}{4} J_s^{iso}(E, E', \theta_\gamma, T, Z) dE dE' ds\, d\omega \quad , \tag{6.10}$$

where J_s^{iso} is defined as

$$J_s^{iso}(E, E', \theta_\gamma, T, Z) = \frac{1}{\pi} \int_o^{2\pi} d\varphi_e \int_o^{\pi/2} \cos\theta_e \sin\theta_e\, P(E, E', \theta_e, \theta_\gamma, T, Z) d\theta_e \, . \tag{6.11}$$

where the direction $\bar{\Omega}$ amd $\bar{\omega}$ have been replaced by the angles θ_e, φ_e and θ_γ of Figure 6.3 and $P(E, E', \theta_e, \varphi_e, \theta_\gamma, T, Z)$ is the secondary production probability. The quantity J_s^{iso} is the probability that, given a unit incident electron at a surface with energy E, a secondary particle will emerge per steradian at an angle θ_γ relative to the surface normal with energy between E' and $E'+dE'$. As was shown previously $\Phi(E)/4$ is the total electron current incident on the unit area so J_S is the total secondary current. The units of J_s^{iso} are

$$\left(\frac{\text{electrons}_s}{\text{MeV}_s\ \text{Sr}_s\ \text{incident electron}_p} \right) \quad \text{for penetrating electrons}$$

and

$$\left(\frac{\text{photons}_s\ \ \text{MeV}_s}{\text{MeV}_s\ \text{Sr}_s\ \text{incident electron}_p} \right) \quad \text{for the bremsstrahlung intensity} \quad .$$

6.2.8 Isotropic Secondary Radiation Flux

In most cases one is not concerned with the radiation emitted from a small area of the interior of the spacecraft shield, but rather one is interested in the flux or dose at some point on the interior of the spacecraft. To calculate these quantities it is useful to consider another coordinate system located at the dose point (or detector, observer, etc.). Figure 6.4 shows the geometry used in converting from a shield oriented coordinate system to a detector centered coordinate system. The detector (or dose point) is assumed to be spherical with a cross sectional area a located at a distance r from the differential area ds. The solid angle $d\omega_a$ subtended by the detector as viewed from the surface area ds is

$$d\omega_a = \frac{a}{r^2} \quad . \tag{6.12}$$

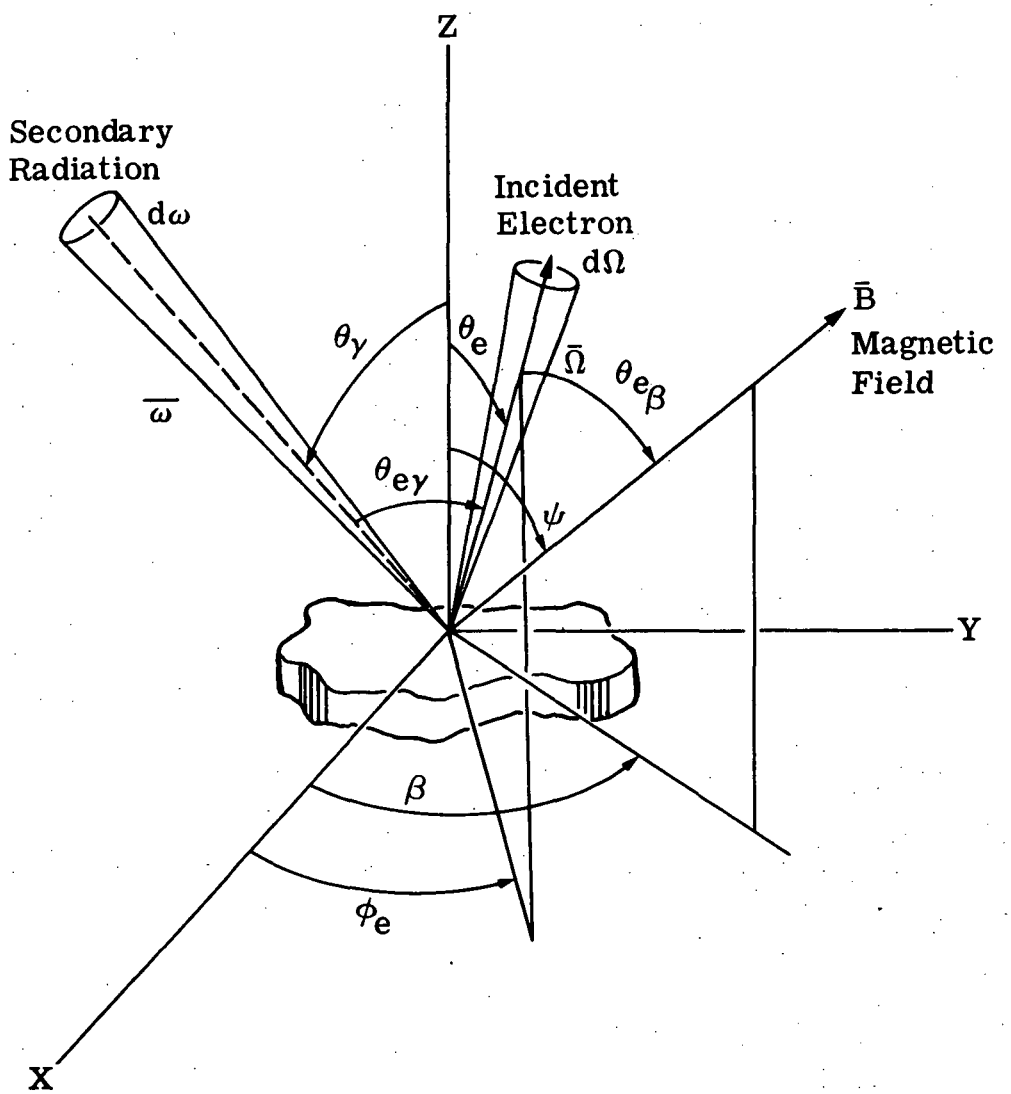

Figure 6.3. Geometry of primary electron - secondary radiation system. The incident electrons direction is given by the vector $\bar{\Omega}$ or the angles θ_e and φ_e relative to the surface normal which is in the Z axis. The direction of the magnetic field B is given by the angles ψ and β. The primary electron pitch angle is θe_β. The direction of the secondary radiation $\bar{\omega}$ is specified by the angle θ_γ. $\theta_{e\gamma}$ is the angle between the direction of the primary electron and secondary radiation.

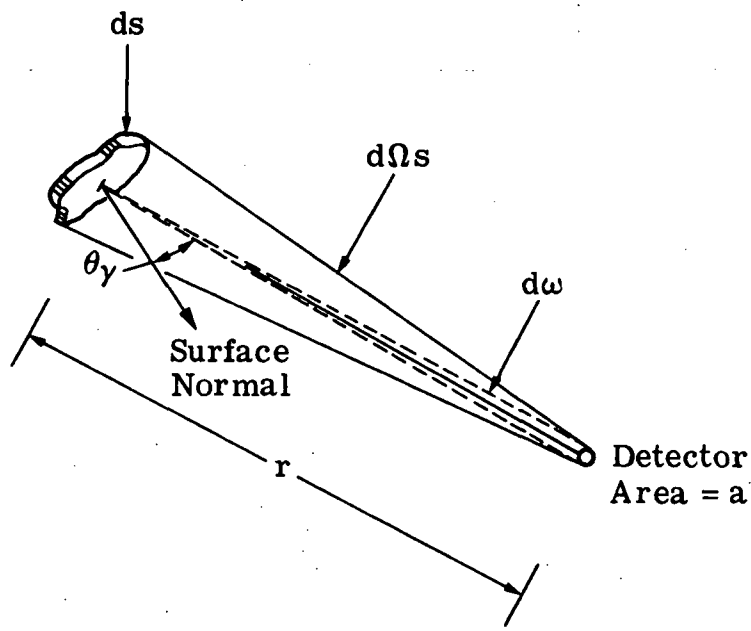

Figure 6.4. Geometry of solid angle transformation from a coordinate system located at an element of surface on the spacecraft ds to a detector centered coordinate system

The solid angle $d\Omega_s$ subtended by a differential area ds as viewed from the detector is

$$d\Omega_s = \frac{ds \cos \theta_\gamma}{r^2} \quad , \tag{6.13}$$

where θ_γ is the angle between the surface normal $\hat{n}_s$ and a unit vector in the direction between the surface area and the detector. From these definitions one can see that the product $d\omega ds$ of Eq. 6.10 can be equated to the quantity

$$d\omega\, ds = \frac{a d\Omega_s}{\cos \theta_\gamma} \tag{6.14}$$

Using this substitution, Eq. 6.10 can be modified to express the flux at the detector as

$$\varphi_s (E, E', \theta_\gamma, \bar{\xi}, T, Z)\, dE dE' a d\Omega_s = J_s (E, E', \theta_\gamma, T, Z) \frac{dE dE' a d\Omega_s}{\cos \theta_\gamma}$$

$$= \frac{\Phi(E)}{4} \frac{J_s^{iso}(E, E', \theta_\gamma, T, Z)}{\cos \theta_\gamma} dE\, dE'\, a d\Omega_s \quad , \tag{6.15}$$

where $\bar{\xi}$ defines the orientation of the differential surface area relative to some fixed coordinate system located at the detector point. The quantity φ_s is defined such that

$\varphi_s (E, E', \theta_\gamma, \bar{\xi}, T, Z)\, dE dE' a d\Omega_s \equiv$ the number of secondary particles per unit time incident from the direction $\bar{\xi}$ within the solid angle $d\Omega_s$ with energies between E' and dE' which cross a differential area a <u>perpendicular</u> to $\bar{\xi}$ which are caused by an isotropic flux of primary electrons with energies between E and E+dE incident on one

side of a surface which subtends $d\Omega_s$ as viewed from the detector.

The angle θ_γ gives the orientation of the surface relative to the direction $\bar{\xi}$. As is seen from this definition, φ_S is a flux of secondary particles.

If the quantity J_s^{iso} is assumed to depend on θ_γ as the cosine of this angle; that is, if it is assumed that

$$J_s^{iso} = (E, E', \theta_\gamma, T, Z) = J_s^{iso}(E, E', O, T, Z) \cos\theta_\gamma \qquad (6.16)$$

where $J_s^{iso}(E, E', O, T, Z)$ is the value of the secondary radiation current evaluated along the normal to the shield then it is seen for fixed values of T and Z that φ_S is independent of θ_γ or is "isotropic". The assumption implied in Eq. 6.16 is rather drastic and will be examined in detail later. The consequences of this assumption are important since the integration over the solid angle $d\Omega_S$ which was complicated by the orientation of surface ds relative to the direction $\bar{\xi}$ now becomes trivial. The problem is seen to reduce to summing contributions from shield segments each differing in thickness and composition. The units of φ_S are

$$\left(\frac{\text{electrons}_s}{\text{MeV}_s \quad \text{Sr}_s \quad \text{cm}^2 \quad \text{sec}}\right) \quad \text{for penetrations electrons}$$

and

$$\left(\frac{\text{photons}_s \ \text{MeV}_s}{\text{MeV}_s \ \text{Sr}_s \quad \text{cm}^2 \text{sec}}\right) \quad \text{for the bremsstrahlung intensity}$$

where now Sr_s refers to the solid angle as viewed from the detector point.

6.2.9 Dose Rate Due to Secondary Particles

The flux of secondary radiation incident on the detector will produce different effects depending on the nature and energy spectrum of the secondary radiation. Typically one is interested in obtaining the rate of energy deposited (the dose rate) in the detector by a flux of secondary radiation.

6.2.9.1 Dose Rate Due to Secondary Particles Produced by Monoenergetic Primary Electrons.

The dose rate deposited by the secondary flux φ_s of Eq. 6.15 is obtained by integrating this flux weighted by the proper flux-to-dose conversion function (see Appendix C) over the energy spectrum of the secondary radiation. If one assumes an "isotropic" flux of secondary radiation (that is, Eq. 6.16 holds) then the dose rate, d, produced by the secondary radiation in a target material Z' will be

$$d(T, Z, E, Z) = \int_0^E dE' \; K(E', Z') \; J_s^{iso} (E, E', 0, T, Z) \quad , \tag{6.17}$$

where J_S^{iso} is evaluated at zero degrees with respect to the surface normal and $K(E', Z')$ is the flux-to-dose conversion function which is discussed in Appendix C. For electrons, the flux-to-dose conversion function is

$$K(E', Z') = \varkappa \frac{dE}{dX} (E', Z') \quad , \tag{6.18}$$

where $\varkappa$ is the conversion from MeV/g to Rad

$$\varkappa = 1.6 \times 10^{-8} \text{ Rad g/MeV} \tag{6.19}$$

and $\frac{dE}{dX}(E', Z')$ is the rate of energy loss or stopping power in a material Z'. The units of $\frac{dE}{dX}$ are $\left(\frac{\text{MeV cm}^2}{\text{g electrons}}\right)$. For the bremsstrahlung intensity $K(E'Z')$ is defined as

$$K(E'Z') = \varkappa \quad \mu(E', Z') \quad , \tag{6.20}$$

where μ is the mass absorption coefficient in cm^2/g photon for the material Z'. (The quantity $\mu(E', Z')$ is not to be confused with μ, the cosine of the angle to the normal defined in Eq. 6.1.) The quantity $d(T, Z, E, Z')$ therefore has the units of

$$\left(\frac{\text{Rads cm}^2}{\text{Sr}_s \quad \text{incident} \quad \text{electron}}\right) \quad .$$

The limits of the integration in Eq. 6.17 extend only to the energy of the primary electrons since there is no mechanism for producing secondary radiation with energies greater than the primary electron kinetic energy.

6.2.9.2 Dose Rate Due to Secondary Particles Produced by a Spectrum of Isotropic Primary Electrons

The dose rate deposited in a spherical detector of unit cross sectional area which is composed of material Z′ by a spectrum of isotropic primary electrons incident on one side of a differential element of the spacecraft surface of material Z and thickness T which subtend an angle $d\Omega_s$ as viewed by the detector will be given by the expression

$$D(T,Z,Z')\, d\Omega_s = \int_0^\infty dE \; \frac{\Phi(E)}{4} \; d(T,Z,E,Z')\, d\Omega_s \quad . \tag{6.21}$$

The units of $D(T,Z,Z')$ are

$$\left(\frac{\text{Rads}}{\text{Sr}_s \quad \text{Sec}}\right) \quad .$$

The total dose rate will be obtained by summing the contributions from all of the shield sectors of thickness T_i and atomic number Z_i

$$D_{Tot}(Z') = \sum_i D(T_i,Z_i,Z')\, \Delta\Omega_i \quad , \tag{6.22}$$

where $\Delta\Omega_i$ is the solid angle subtended by the i^{th} shield segment which consists of a uniform thickness and chemical composition. The shield seg-

ments can have any shape or actually be composed of different pieces of material at different locations. As long as the thickness and composition of the pieces are the same these pieces can be considered a single segment

The units of $D_{\tau}(Z')$ are $\left(\frac{\text{Rads}}{\text{sec}}\right)$.

6.2.10 Orbital Integrations

In most cases the interest is not in the instantaneous dose rate but in the accumulated dose received by men and materials aboard a spacecraft over extended periods of time. If one defines the total electron flux through which a spacecraft passes in a specific orbit δ as

$$\Phi_{\tau}(\delta, E) \equiv \oint \Phi(B, L, E)\, d\ell \quad , \tag{6.23}$$

where $d\ell$ is a differental element of the orbital path and the symbol $\oint$ represents an integration of $d\ell$ over a complete orbit. Since $\Phi(B, L, E)$ is assumed to be isotropic, $\Phi_{\tau}(\delta, E)$ can be used to replace $\Phi(B, L, E)$ throughout the preceeding section. The units of the resulting quantities will be changed to reflect this substitution by replacing the normalization per second in the units of J_{in}, J_S, δ_S, and D_{τ} by the normalization per orbit.

6.3 DOSE DEPOSITION FROM PRIMARY ELECTRON PENETRATION

There will be some cases where the shielding is not sufficiently thick to stop all of the electrons encountered in the space radiation environment. For these cases, the dose delivered by the electrons typically will be considerably greater than that caused by the secondary photons. In Sect. 3 of this report the parameterization for non-normal incidence electrons gave the probability of electron penetration for targets thicker than 0.3 of the csda range as

$$P(E, E', \theta_e, \theta_\gamma, T)dE'd\omega = S(E, E', T)\, \Phi(\theta_\gamma)\, T_F(E, T, \theta_e)\, dE'd\omega \quad , \tag{6.24}$$

where E is the incident electron energy, E' is the energy of the transmitted radiation, θ_e and θ_γ, are the directions of the incident and transmitted electrons with respect to the normal, and T is the target thickness. The quantities $S(E, E', T)$, $\Phi(\theta_\gamma)$ and $T_F(E, T, \theta_e)$ are, respectively, the differential energy spectrum, angular distribution, and transmitted fraction. (The angular distribution of the transmitted electrons $\Phi(\theta_\gamma)$ is not to be confused with the primary electron flux of Eq. 6.3.)

In this approximation only the transmitted fraction depends on the direction of the incident electron θ_e

$$T_F(E, T, \theta_e) \approx T_F(E, T, 0)[\cos\theta_e]^{\alpha}. \qquad (6.25)$$

where α is defined in terms of E and T in Eq. 5.12.

6.3.1 Secondary Electron Current

The secondary electron current produced by an isotropic primary electron flux J_S^{iso} (defined in Eq. 6.11) can be evaluated analytically to yield

$$J_S^{iso}(E, E', \theta_\gamma, T, Z) = \frac{1}{\pi}\int_0^{2\pi} d\varphi_e \int_0^{\pi/2} [\cos\theta_e]^{\alpha+1} \sin\theta_e \, d\theta_e \, S(E, E', T)$$

$$\Phi(\theta_\gamma)\, T_F(E, T, 0) \qquad (6.26)$$

$$= \frac{2}{(\alpha+2)} S(E, E', T)\, \Phi(\theta_\gamma)\, T_F(E, T, 0)$$

Graphs and parametric representations of the transmitted electron angular distribution, $\Phi(\theta_\gamma)$, and energy spectrum, S, have been discussed in Sections 3 and 5 of this chapter.

6.3.1 Dose Due to Primary Electron Penetration: Parametric Method

One can estimate the dose delivered to a dose point (detector, etc.) on the interior of a spacecraft by using the expression for J_S^{iso} (Eq. 6.26) in Eq. 6.17 along with the expression for the flux-to-dose conversion function for electrons given by Eq. 6.18. The dose $d(T, Z, E, Z')$ (Eq. 6.17) is

$$d(T, Z, E, Z') = \frac{2}{(\alpha+2)} \Phi(\theta_\gamma) T_F(E, T, 0) \int_0^E dE' \, S(E, E', T) \frac{dE}{dX}(E') \, . \qquad (6.27)$$

The electron stopping power $\frac{dE}{dX}(E')$ is a relatively complicated function of the electron energy. At very low electron energies dE/dX is quite large, decreasing to a minimum value around 600 to 1,300 keV and then increasing slowly as the electron energy increases. Instead of evaluating the function, d, numerically a parameterization of the dose calculated using Monte Carlo methods due to Watts and Burrell[56] can be used.

6.3.2 Dose Due to Primary Electron Penetration: Monte Carlo Method.

Watts and Burrell[56] present parametric representations of the results of Monte Carlo calculations of the dose deposited in thin layers of uniform slabs of material. The calculation generates average energy deposited per unit mass per electron at a given depth into a plane, infinitely thick, slab of material by penetrating electrons. The slab is broken up into thin layers and an inventory is kept of the energy deposited in each layer. This total energy deposited is divided by the number of initial incident electrons and the layer thickness to obtain the average energy deposited per unit thickness per initial electron. The quantity so obtained is

$$\rho\,(E, \theta_e, X_j) = \frac{\sum_{i=1}^{N_j} \Delta E_{ij}}{N_o\ \Delta X_j} \quad , \tag{6.28}$$

where ρ is the energy deposition in (MeV/g incident electron), E is the energy of the primary incident electron, θ_e is the angle between the primary electron and the normal to the slab surface, X_j is the depth to the center of the j^{th} layer, ΔE_{ij} is the energy loss in MeV deposited by the i^{th} electron in the j^{th} layer, N_o is the number of incident electrons and ΔX_j is the thickness of the j^{th} layer in g/cm^2. If the directional primary electron flux is isotropic (Eq. 6.4) then the dose deposited at a thin layer located at a distance X in the slab of material will be given by

$$D_{iso}(X) = \frac{\varkappa}{2} \int dE \int_0^{\pi/2} \rho(E, \theta, X) \cos\theta \sin\theta\, d\theta\ \Phi(E)\, dE \quad , \tag{6.29}$$

where $\varkappa$ is the conversion from MeV/g to Rad. It should be pointed out that in this definition $\Phi(E)$ differs by a factor of two from the quantity $\Phi_o(E)$ as used by Watts and Burrell. Watts and Burrell define their primary electron flux only over 2π steradians. Hence their directional electron flux is related to their half-space isotropic flux by

$$\varphi_o\,(E, \bar{\Omega}) = \Phi_o(E)/2\pi \quad . \tag{6.30}$$

The quantity $\Phi(E)$ in Eq. 6.29 is full-space isotropic and related to the directional electron flux by Eq. 6.4. Watts and Burrell define a function ρ_{iso} through the equation

$$\rho_{iso}(E,X) = \int_0^{\pi/2} \rho(E,\theta,X) \cos\theta \sin\theta \, d\theta \qquad (6.31)$$

which they parameterize (the parameterization is given in Sect. 3). The dose $D_{iso}(X)$ thus becomes

$$D_{iso}(X) = \frac{\alpha}{2} \int dE \; \rho_{iso}(E,X) \; \Phi(E) \quad . \qquad (6.32)$$

The formalism described above is very useful in that it eliminates the numerical integration over the secondary electron energies of Eq. 6.27. In its present form it is not, however, readily applicable to the formalism presented in the preceding section. The preceding section developed the formalism necessary to obtain estimates of the dose on the interior of shielded enclosures. It was necessary to retain the angular dependence of the secondary radiation up to the point where the integration over the solid angle subtended by the shielding was to be performed. At that point, an approximation for the angular distribution of the secondary radiation emerging from the shield was made. The results of the Monte Carlo calculations implicitly contain integrations over the energy and angular distributions of the secondary radiation in the function $\rho(E,X)$. Thus the results of Eq. 6.32 cannot be compared directly with results obtained using the formalism of the preceding section. The relationship between the two is discussed in the next section.

6.3.3 Relationship Between Parametric and Monte Carlo Methods

An approximate relationship between the method outlined in Section 6.2.9.1 and the Monte Carlo method outlined above can be obtained by understanding the implications of the Monte Carlo calculation. The slab geometry calculations discussed above can be thought of in a slightly different way where one has a point source of electrons which have a given angular distribution entering a slab of material. The electrons are transported along a line perpendicular to the slab (that is along the normal to the slab) with the directional

aspects of the problem being taken into account with the use of projections onto the slab normal. At a given depth of penetration one has a point source with an angular distribution which is determined by both the initial angular distribution and the transport of the electrons through the material. The electrons from this point source are then allowed to transverse a thin layer of material and the energy deposited is calculated. This gives the quantity $\rho_{iso}(E,X)$ for forward going electrons. This geometry is shown schematically in Fig. 6.5. Watts and Burrell calculate the dose deposited in thin layers of a semi-infinite slab so there will also be a contribution to the dose from backward going electrons in their calculations. In the relationship which we will define here, however, only the forward going component of the electron flux will be considered. The dose deposited by the secondary electron current J_s^{iso} in the thin sheet will be

$$D_{Layer}(T,Z,Z') = \varkappa \int \frac{dE\Phi(E)}{4} \int_0^E dE' \frac{dE}{dX}(E') 2\pi \int_0^{\pi/2} \frac{d\theta \sin\theta}{\cos\theta} J_s^{iso}(E,E',\theta,T,Z) \quad . \tag{6.33}$$

The $\cos\theta$ term is included in the denominator to take into account the dependence of the electron path lengths in the thin slab as a function of electron direction. The integration over $d\theta$ will be taken over the hemisphere subtended by the thin layer. Also J_s^{iso} will be assumed to go as $\cos\theta$. With these approximations the layer dose D_{Layer} will be

$$D_{Layer}(T,Z,Z') = \frac{\pi}{2} \varkappa \int dE \ \Phi(E) \int_0^E dE' \frac{dE}{dX}(E') J_s^{iso}(E,E',0,T,Z), \tag{6.34}$$

where J_s^{iso} is evaluated at zero degrees. A comparison of this equation with Eq. 6.32 shows that $\rho_{iso}(E,T)$ is related to J_s^{iso} through the equation

$$\rho_{iso}(E,T) \approx \pi \int_0^E dE' \frac{dE}{dX}(E') J_s^{iso}(E,E',0,T,Z) \quad . \tag{6.35}$$

This relationship is only approximate, of course, since it depends on the assumptions preceding Eq. 6.34.

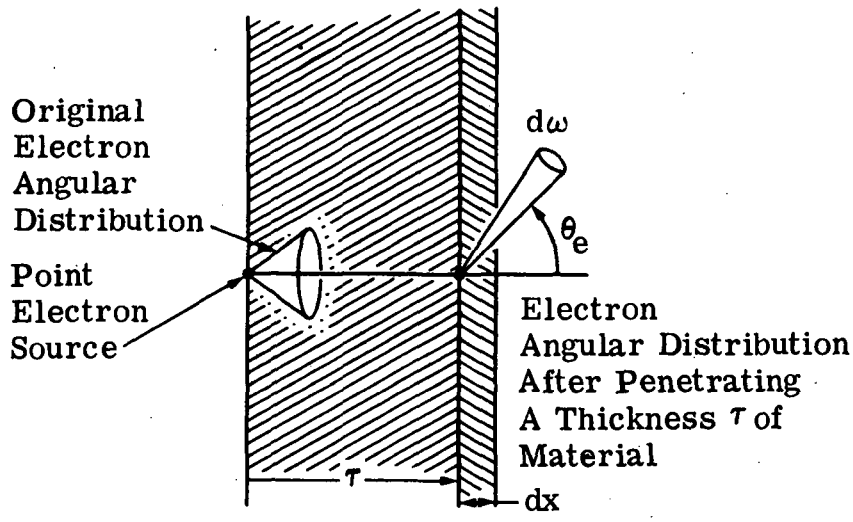

Figure 6.5. Geometry of the calculation for relating parametric and Monte Carlo methods

The function $\rho_{iso}(E, T)$ has been tabulated by Watts and Burrell for energy deposition in Al slabs. They show, however, that since the quantities dE/dX for tissue is 1.3 times dE/dX for aluminum over a very wide energy range that ρ_{iso} for tissue is simply 1.3 times ρ_{iso} for Al.

In the approximation given above the total tissue dose produced by electrons penetrating various Al shield segments is

$$D = 2.08 \times 10^{-8} \sum_i \frac{\Delta \Omega_i}{4\pi} \int_0^\infty dE \; \Phi(E) \, \rho_{iso}(E, T_i) \text{ (Rad/sec)} \quad , \qquad (6.36)$$

where $\Delta\Omega_i$ is the solid angle subtended by the i^{th} shield segment in steradians, $\Phi(E)$ is the full space omnidirectional electron flux in (electrons/MeV cm^2 sec) and E is the electron energy in MeV. The quantity ρ_{iso} (E, T) is tabulated by Watts and Burrell and reproduced in Appendix B for aluminum slabs of various thicknesses.

6.3.4 Dose Due to Primary Electron Penetration for a Spectrum of Electrons

The dose deposited in an isotropic detector by penetrating electrons from a spectrum of electrons incident on a unit solid angle of the shield is given by Eq. 6.21 as

$$D(T, Z, Z') = \int_0^\infty dE \; \frac{\Phi(E)}{4} \; d(T, Z, E, Z') \qquad (6.37)$$

which has the units of (Rad/Sr sec) for an electron flux measured in (electrons/cm^2 sec). Values of $D(T, Z, Z')$ have been calculated using Watts and Burrell's parameterization of the quantity ρ_{iso} (See Sect. 6.3.3) for three types of electron spectra. These are

- A simple exponential function $\Phi(E) = \Phi_0 \, P \quad e^{-PE}$
- Vette's AE2 electron distribution for different values of L; $\Phi(E, B, L) = F_0(B, L) \, N(E, L)$
- Vette's projected 1968 orbital integration electron spectra.

6.3.4.1 Dose Due to Penetrating Electrons; Simple Exponential Electron Spectra

The penetrating electron dose transmitted through an Al shield for an exponential spectrum is shown in Fig. 6.6. In this figure the quantity

$$D = 2.08 \times 10^{-8} \int_0^{7\text{MeV}} dE\, P e^{-PE} \rho_{iso}(E,T) / \pi \qquad (6.38)$$

is plotted which corresponds to the dose per incident electron per cm^2 per unit solid angle subtended by the shield and has the units of

$$\left(\frac{\text{Rad cm}^2}{\text{Sr incident electron}} \right)$$

(The integration is carried out only to seven MeV to be consistent with Vette's electron distributions which only extend to 7 MeV.) The values of D for various thicknesses of Al shield and values of P ranging from 0.5 to 5 are listed in Table 6.1.

6.3.4.2 Dose Due to Penetrating Electrons; Vette's AE2 Electron Spectra

The quantity D has been calculated for several of the electron spectra of Vette's AE2 electron environment. The quantity D in this case is given by the equation

$$D = 2.08 \times 10^{-8} \int_0^{7\text{MeV}} dE\, N(E,L) \rho_{iso}(E,T) / \pi \quad , \qquad (6.39)$$

where N(E, L) is defined in Eq. 6.8. In this case the units of D are

$$\left(\frac{\text{Rad cm}^2}{\text{Sr incident electron } (E > E_0)} \right) .$$

The calculated values of D for various values of the parameter L are shown in Fig. 6.7 as functions of the thickness of Al. These values of D are tabulated in Table 6.2. (It should be pointed out that AE2 electron environment is considered outdated by many since it was obtained from measurements conducted while there were many electrons from the Starfish nuclear detonation.)

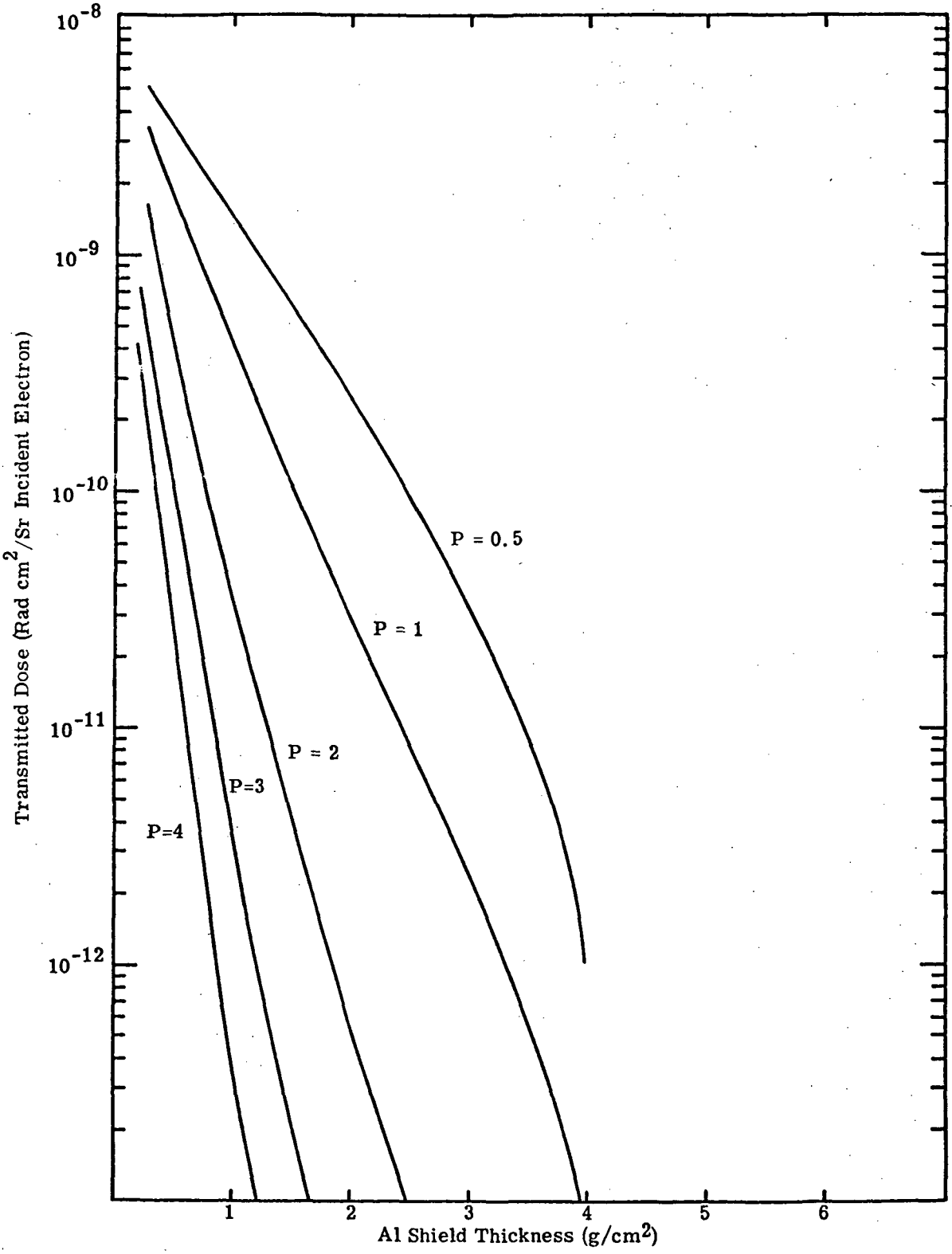

Figure 6.6. Transmitted dose due to penetrating electrons caused by isotropic flux of primary electrons incident on one side of a unit area of shield. The incident electron spectrum is given by $N(E) = Pe^{-PE}$. The curves are normalized per incident electron. The values of P are listed on the figure. The steep fall off with increasing shield thickness for the low P values is due primarily to the integration cut-off of 7 MeV.

TABLE 6.1. TRANSMITTED TISSUE DOSE FROM PENETRATING ELECTRONS CAUSED BY ISOTROPIC FLUX OF ELECTRONS WITH AN ENERGY SPECTRUM GIVEN BY $N = Pe^{-PE}$ INCIDENT ON ONE SIDE OF A UNIT AREA OF AN Al SHIELD. [a]

	Thickness (g/cm^2)									
P	.250	.500	.750	1.000	1.250	1.500	1.750	2.000	4.000	6.000
.5	.554-08	.341-08	.217-09	.141-08	.929-09	.605-09	.390-09	.247-09	.461-12	.000
1.0	.353-08	.162-08	.782-09	.367-09	.210-09	.112-09	.596-10	.320-10	.289-13	.000
1.5	.221-09	.760-09	.280-09	.110-09	.459-10	.197-10	.844-11	.373-11	.136-14	.000
2.0	.141-08	.358-09	.104-09	.318-10	.106-10	.367-11	.126-11	.452-12	.574-16	.000
2.5	.910-09	.184-09	.405-10	.964-11	.257-11	.729-12	.202-12	.585-13	.228-17	.000
3.0	.594-09	.930-10	.161-10	.303-11	.649-12	.152-12	.343-13	.804-14	.868-19	.000
3.5	.391-09	.478-10	.656-11	.979-12	.169-12	.329-13	.610-14	.117-14	.324-20	.000
4.0	.259-09	.249-10	.272-11	.324-12	.452-13	.736-14	.113-14	.176-15	.119-21	.000
4.5	.173-09	.130-10	.115-11	.110-12	.124-13	.169-14	.217-15	.277-16	.429-23	.000
5.0	.116-09	.690-11	.491-12	.380-13	.346-14	.395-15	.429-16	.449-17	.154-24	.000
5.5	.784-10	.369-11	.213-12	.134-13	.997-15	.945-16	.870-17	.748-18	.549-26	.000
6.0	.532-10	.198-11	.931-13	.477-14	.286-15	.229-16	.180-17	.128-18	.195-27	.000
6.5	.363-10	.107-11	.411-13	.173-14	.945-16	.564-17	.379-18	.222-19	.690-29	.000
7.0	.248-10	.579-12	.183-13	.636-15	.353-16	.141-17	.811-19	.395-20	.244-30	.000
7.5	.170-10	.315-12	.824-14	.236-15	.767-17	.355-18	.175-19	.712-21	.860-32	.000
8.0	.117-10	.173-12	.373-14	.889-16	.230-17	.907-19	.383-20	.130-21	.303-33	.000
8.5	.810-11	.948-13	.170-14	.338-16	.731-18	.237-19	.845-21	.241-22	.106-34	.000
9.0	.561-11	.522-13	.778-15	.130-16	.229-18	.804-20	.188-21	.452-23	.374-36	.000
9.5	.390-11	.289-13	.359-15	.504-17	.724-19	.159-20	.419-22	.855-24	.132-37	.000
10.0	.271-11	.160-13	.166-15	.197-17	.230-19	.418-21	.939-23	.163-24	.000	.000

[a] The top heading gives the thickness of Al in g/cm^2. The first column gives the value of P. The remaining columns give the transmitted tissue dose in (Rad cm^2/Sr incident electron).

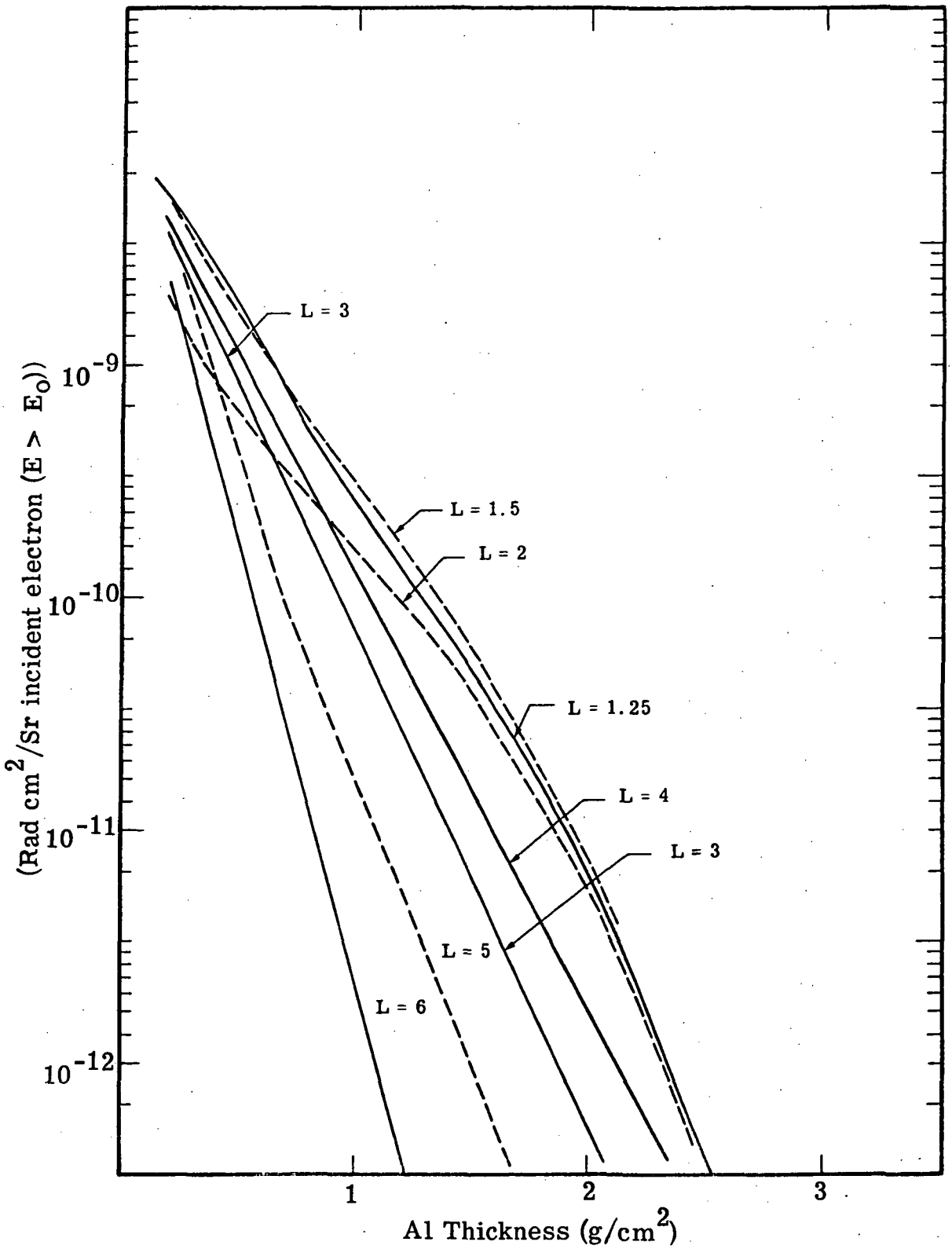

Figure 6.7. Transmitted tissue dose caused by isotropic flux of electrons incident on one side of a unit area of an Al shield. The electron energy spectra are given by Vette's AE2 electron environment. The L values associated with the various electron spectra are shown on the figure. The curves are normalized per unit incident electron. (N.B. The AE2 distribution is considered to be outdated by space scientists.)

TABLE 6.2. TRANSMITTED DOSE DUE TO PENETRATING ELECTRONS CAUSED BY ISOTROPIC FLUXES OF ELECTRONS WITH ENERGY SPECTRA GIVEN BY VETTE'S AE2 ELECTRON DISTRIBUTION INCIDENT ON ONE SIDE OF A UNIT AREA OF AN Al SHIELD.
(Rad cm^2/Sr incident electron)

(N.B. The AE2 Electron environment is considered to be outdated by space scientists.)

	Thickness (g/cm^2)						
L	0.2	0.4	0.6	1.0	1.5	2.0	2.5
1.25	.672-8	.313-8	.145-8	.304-9	.576-10	.808-11	.452-12
1.50	.612-8	.279-8	.138-8	.360-9	.684-10	.908-11	.500-12
2.0	.274-8	.984-9	.560-9	.190-9	.456-10	.700-11	.416-12
2.5	.397-8	.123-8	.473-9	.800-10	.102-10	.101-11	.468-13
3.0	.472-8	.152-8	.532-9	.736-10	.768-11	.648-12	.270-13
3.4	.500-8	.179-8	.704-9	.122-9	.154-10	.150-11	.684-13
4.0	.544-8	.199-8	.804-9	.144-9	.194-10	.201-11	.948-13
5.0	.424-8	.960-9	.257-9	.207-10	.126-11	.696-13	.224-14
6.0	.324-8	.444-9	.756-10	.242-11	.552-13	.127-15	.221-17

6.3.4.3 Dose Due to Penetrating Electrons; Vette's Projected (1968) Orbital Integrated Electron Spectra

The doses for circular orbital integrations were calculated for Vette's projected(1968) orbital integrated electron spectra. The quantity calculated in this case was

$$D_o = 2.08 \times 10^{-8} \int_o^{7MeV} dE \frac{\Phi^o(E)}{4\pi} \rho_{iso}(E,T) \qquad (6.40)$$

where $\Phi^o(E)$ is the total orbital integrated flux averaged over one day. The units of D_o are (Rad/Sr day). The calculated values of the quantity D_o are given in Table 6.3.

6.4 SECONDARY BREMSSTRAHLUNG RADIATION

In cases where all, or most, of the electron energy spectrum is stopped in the shielding material, the dose will be determined by the bremsstrahlung production. Section 5 gives a parametric representation of the bremsstrahlung intensity as a function of photon energy and solid angle. The production probability P defined in Eq. 6.2 can be written for the bremsstrahlung intensity as

$$P_\gamma(E, E', \bar{\Omega}, \bar{\omega}, \xi, T, Z) = I_s(E, E', \theta_{e\gamma}, Z)\, A_T(E', Z, \theta_e, \theta_\gamma, T) \quad , \qquad (6.41)$$

where I_S is the source term defined in Eq. 5.20 of Section 5.3 and A_T is the attenuation term. The angles $\theta_{e\gamma}$, θ_e and θ_γ are shown in Fig. 6.3 and correspond to the angle between the direction of the incident electron and the secondary photon, the angle of the direction of the incident electron with respect to the shield normal and the angle of the direction of the secondary photon with respect to the shield normal. (In Eq. 6.41 the energy of the photon is denoted as E' rather than as k) The units of P_γ are

TABLE 6.3. TRANSMITTED TISSUE DOSE FOR CIRCULAR ORBITS FROM PENETRATING ELECTRONS CAUSED BY AN ISOTROPIC FLUX OF ELECTRONS INCIDENT ON ONE SIDE OF A UNIT SOLID ANGLE OF AN Al SHIELD. [a]

Height (nm)	Inclination (deg)	Thickness (g/cm^2) .250	.500	.750	1.000	1.250	1.500	1.750	2.000	4.000
150.	30.	.141-01	.458-03	.162-03	.112-03	.798-04	.561-04	.387-04	.261-04	.646-07
	60.	.252+01	.572+00	.150+00	.436-01	.143-01	.499-02	.179-02	.695-03	.380-06
300.	0.	.173-03	.787-05	.956-06	.367-06	.160-06	.704-07	.304-07	.130-07	.000
	30.	.982+00	.397+00	.356+00	.319+00	.283+00	.247+00	.210+00	.171+00	.572-04
	60.	.459+01	.903+00	.236+00	.712-01	.254-01	.103-01	.461-02	.233-02	.392-05
450.	0.	.309+00	.131-01	.207-02	.102-02	.568-03	.327-03	.191-03	.113-03	.172-06
	30.	.724+01	.241+00	.804-01	.551-01	.388-01	.270-01	.186-01	.125-01	.304-04
	60.	.128+02	.207+01	.525+00	.164+00	.638-01	.295-01	.154-01	.891-02	.180-04
600.	0.	.152+02	.596+00	.125+00	.732-01	.465-01	.299-01	.192-01	.122-01	.241-04
	30.	.262+02	.861+00	.296+00	.205+00	.145+00	.101+00	.698-01	.469-01	.115-03
	60.	.348+02	.523+01	.138+01	.453+00	.186+00	.901-01	.490-01	.289-01	.602-04
800.	0.	.126+03	.438+01	.126+01	.841+00	.577+00	.393+00	.264+00	.174+00	.388-03
	30.	.113+03	.359+01	.133+01	.937+00	.669+00	.472+00	.326+00	.220+00	.542-03
	60.	.900+02	.102+02	.282+01	.107+01	.516+00	.289+00	.175+00	.110+00	.252-03
1000.	0.	.461+03	.151+02	.515+01	.359+01	.253+01	.177+01	.121+01	.808+00	.191-02
	30.	.299+03	.908+01	.373+01	.268+01	.194+01	.138+01	.963+00	.655+00	.166-02
	60.	.196+03	.171+02	.505+01	.219+01	.120+01	.736+00	.474+00	.310+00	.748-03
1250.	0.	.125+04	.376+02	.155+02	.112+02	.809+01	.577+01	.403+01	.274+01	.693-02
	30.	.587+03	.172+02	.749+01	.559+01	.408+01	.293+01	.206+01	.141+01	.366-02
	60.	.381+03	.294+02	.921+01	.431+01	.251+01	.160+01	.106+01	.706+00	.177-02
1500.	0.	.187+04	.528+02	.247+02	.181+02	.133+02	.961+01	.678+01	.466+01	.124-01
	30.	.704+03	.202+02	.969+01	.711+01	.523+01	.378+01	.267+01	.183+01	.493-02
	60.	.495+03	.402+02	.128+02	.593+01	.349+01	.221+01	.147+01	.975+00	.251-02
1750.	0.	.155+04	.421+02	.215+02	.160+02	.119+02	.866+01	.617+01	.427+01	.120-01
	30.	.504+03	.148+02	.756+01	.552+01	.404+01	.293+01	.207+01	.143+01	.392-02
	60.	.448+03	.470+02	.140+02	.580+01	.309+01	.188+01	.122+01	.804+00	.211-02
2000.	0.	.593+03	.188+02	.990+01	.727+01	.534+01	.386+01	.272+01	.187+01	.508-02
	30.	.239+03	.859+01	.449+01	.321+01	.231+01	.165+01	.116+01	.790+00	.210-02
	60.	.354+03	.546+02	.153+02	.543+01	.245+01	.130+01	.762+00	.474+00	.113-02
2250.	0.	.202+03	.105+02	.607+01	.432+01	.309+01	.218+01	.150+01	.101+01	.251-02
	30.	.892+02	.603+01	.304+01	.194+01	.131+01	.885+00	.596+00	.396+00	.959-03
	60.	.313+03	.618+02	.168+02	.544+01	.214+01	.974+00	.495+00	.277+00	.523-03
2500.	0.	.867+02	.488+01	.280+01	.198+01	.141+01	.987+00	.679+00	.456+00	.111-02
	30.	.548+02	.663+01	.290+01	.157+01	.944+00	.593+00	.378+00	.241+00	.520-03
	60.	.339+03	.709+02	.187+02	.578+01	.212+01	.874+00	.396+00	.200+00	.290-03
2750.	0.	.528+02	.360+01	.212+01	.147+01	.102+01	.708+00	.481+00	.319+00	.727-03
	30.	.573+02	.108+02	.420+01	.194+01	.101+01	.571+00	.334+00	.201+00	.363-03
	60.	.367+03	.785+02	.207+02	.633+01	.226+01	.896+00	.383+00	.181+00	.203-03

The numbers represent the dose received per day per solid angle for circular orbits using Vette's projected AE2 electron environment. The top heading gives the Al thickness in g/cm^2. The first column gives the orbital height in nautical miles, the second gives the orbital inclination in degrees. The remaining columns give the tissue dose in (Rad/Sr day) for various thickness of the Al shield.

TABLE 6.3. (CONTINUED)

Height (nm)	Inclination (deg)	Thickness (g/cm^2) .250	.500	.750	1.000	1.250	1.500	1.750	2.000	4.000
3000.	0.	.402+02	.313+01	.188+01	.126+01	.861+00	.583+00	.389+00	.264+00	.543-03
	30.	.803+02	.186+02	.681+01	.285+01	.135+01	.693+00	.373+00	.210+00	.315-03
	60.	.913+03	.891+02	.235+02	.716+01	.259+01	.990+00	.412+00	.189+00	.176-03
3500.	0.	.362+02	.396+01	.234+01	.149+01	.971+00	.629+00	.402+00	.254+00	.467-03
	30.	.184+03	.979+02	.164+02	.629+01	.268+01	.129+01	.598+00	.307+00	.335-03
	60.	.481+03	.105+03	.284+02	.885+01	.319+01	.126+01	.521+00	.235+00	.179-03
4000.	0.	.584+02	.776+01	.433+01	.262+01	.169+01	.103+01	.644+00	.397+00	.655-03
	30.	.360+03	.941+02	.311+02	.115+02	.478+01	.212+01	.982+00	.481+00	.416-03
	60.	.560+03	.124+03	.343+02	.109+02	.404+01	.162+01	.684+00	.310+00	.220-03
4500.	0.	.163+03	.215+02	.101+02	.535+01	.300+01	.171+01	.980+00	.565+00	.748-03
	30.	.648+03	.177+03	.511+02	.183+02	.743+01	.319+01	.142+01	.664+00	.437-03
	60.	.655+03	.148+03	.421+02	.138+02	.519+01	.210+01	.879+00	.392+00	.226-03
5000.	0.	.286+03	.587+02	.241+02	.114+02	.572+01	.291+01	.148+01	.766+00	.575-03
	30.	.892+03	.233+03	.748+02	.269+02	.108+02	.455+01	.197+01	.893+00	.453-03
	60.	.764+03	.176+03	.511+02	.170+02	.644+01	.260+01	.108+01	.473+00	.218-03
5500.	0.	.563+03	.135+03	.503+02	.221+02	.105+02	.518+01	.256+01	.129+01	.866-03
	30.	.122+04	.325+03	.103+03	.365+02	.143+02	.591+01	.249+01	.110+01	.488-03
	60.	.884+03	.212+03	.625+02	.210+02	.799+01	.322+01	.133+01	.580+00	.250-03
6000.	0.	.966+03	.258+03	.903+02	.369+02	.158+02	.715+01	.325+01	.152+01	.757-03
	30.	.156+04	.421+03	.132+03	.454+02	.172+02	.686+01	.277+01	.117+01	.404-03
	60.	.100+04	.245+03	.726+02	.242+02	.903+01	.355+01	.142+01	.599+00	.210-03
7000.	0.	.200+04	.603+03	.199+03	.697+02	.263+02	.102+02	.395+01	.158+01	.367-03
	30.	.211+04	.578+03	.176+03	.587+02	.220+02	.894+01	.390+01	.184+01	.197-03
	60.	.117+04	.299+03	.876+02	.280+02	.986+01	.361+01	.133+01	.509+00	.967-04
8000.	0.	.267+04	.792+03	.250+03	.822+02	.294+02	.108+02	.394+01	.149+01	.258-03
	30.	.221+04	.565+03	.161+03	.499+02	.171+02	.608+01	.216+01	.803+00	.128-03
	60.	.116+04	.285+03	.799+02	.245+02	.833+01	.296+01	.105+01	.388+00	.619-04
9000.	0.	.266+04	.720+03	.211+03	.668+02	.231+02	.831+01	.297+01	.111+01	.176-03
	30.	.194+04	.445+03	.116+03	.335+02	.109+02	.370+01	.126+01	.452+00	.621-04
	60.	.100+04	.223+03	.577+02	.167+02	.591+01	.185+01	.636+00	.229+00	.324-04
10000.	0.	.228+04	.519+03	.130+03	.351+02	.105+02	.332+01	.104+01	.347+00	.231-04
	30.	.158+04	.307+03	.688+02	.172+02	.486+01	.147+01	.441+00	.139+00	.993-05
	60.	.793+03	.154+03	.346+02	.869+01	.248+01	.753+00	.227+00	.719-01	.496-05

$$\left(\frac{\text{photons} \quad \text{MeV}_s}{\text{MeV}_s \ \text{Sr}_s \ \text{electron}_p} \right) \quad .$$

For an isotropic primary electron flux one obtains a secondary photon energy current J_s^{iso} defined in Eq. 6.11 as

$$J_s^{iso}(E, E', \theta_\gamma, T, Z) = \frac{1}{\pi} \int_0^{2\pi} d\varphi_e \int_0^{\pi/2} \sin\theta_e \cos\theta_e \ I_s(E, E', \theta_e\gamma, Z)$$

$$A_T(E', Z\theta_e, \theta_\gamma, T) \, d\theta_e \quad , \qquad (6.42)$$

which has the units of

$$\left(\frac{\text{photons MeV}_s}{\text{MeV}_s \quad \text{Sr}_s \quad \text{incident electron}} \right) \quad .$$

Figures 6.8 through 6.11 show the energy spectra and angular distributions of the bremsstrahlung energy current J_s^{iso} calculated using the parameterization of Sect. 5.3. The curves are normalized for unit incident electron. The thicknesses of the shields for the examples shown in Figures 6.8 and 6.9 are equal to the ranges (csda) of the incident electrons.

Figures 6.12 and 6.13 show the photon intensity spectra for normally emerging photons ($\theta_\gamma = 0^o$) for different electron energies incident on shields of Al and Pb. These photon energy currents are tabulated in Tables 6.4 and 6.5.

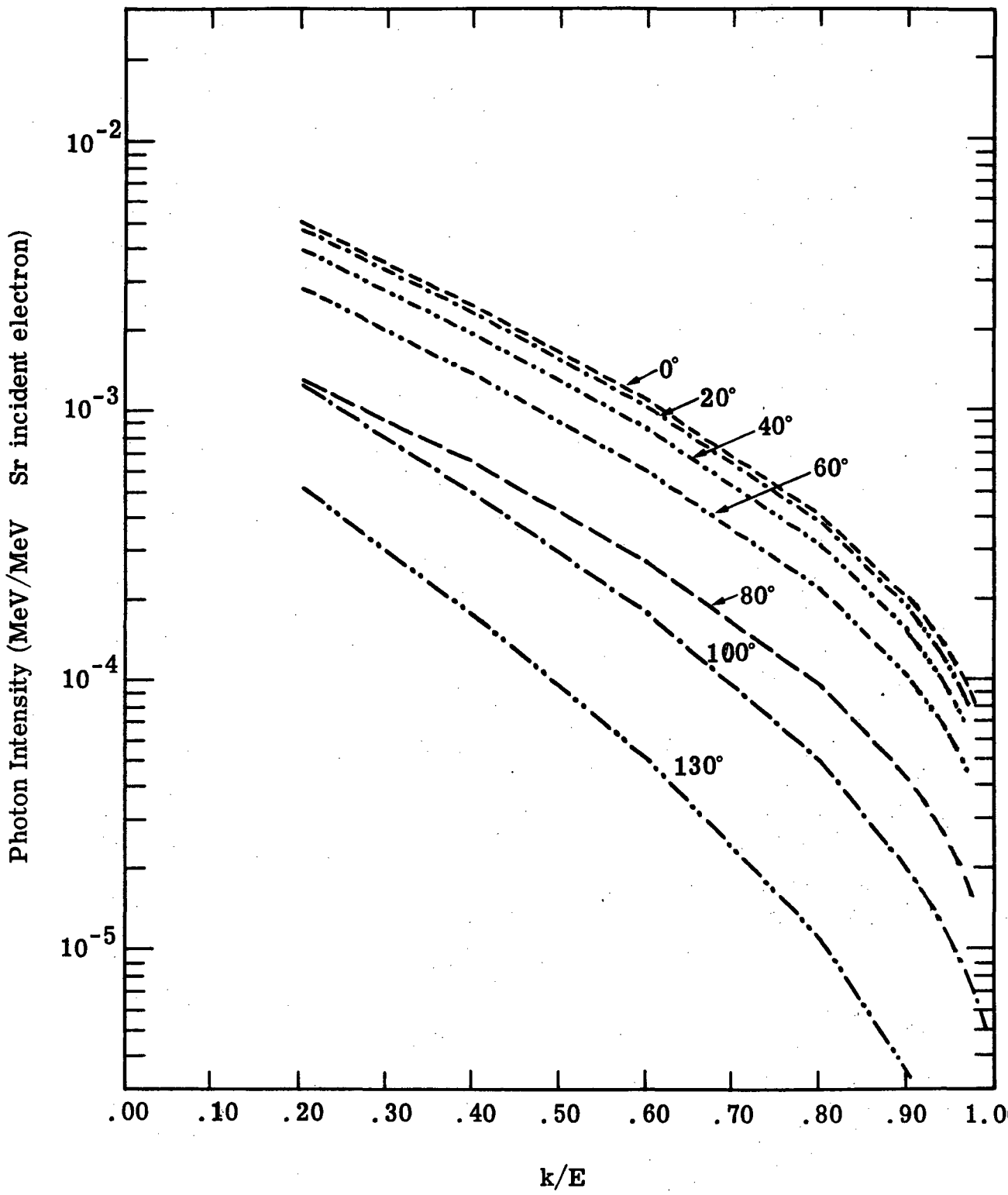

Figure 6.8. Bremsstrahlung intensity energy distribution due to an isotropic flux of 2-MeV electrons incident on one side of a unit area of an Al shield. The target thickness is 1.21 g/cm^2. The curves are normalized per unit incident electron. The photon emission angles are listed on the figure.

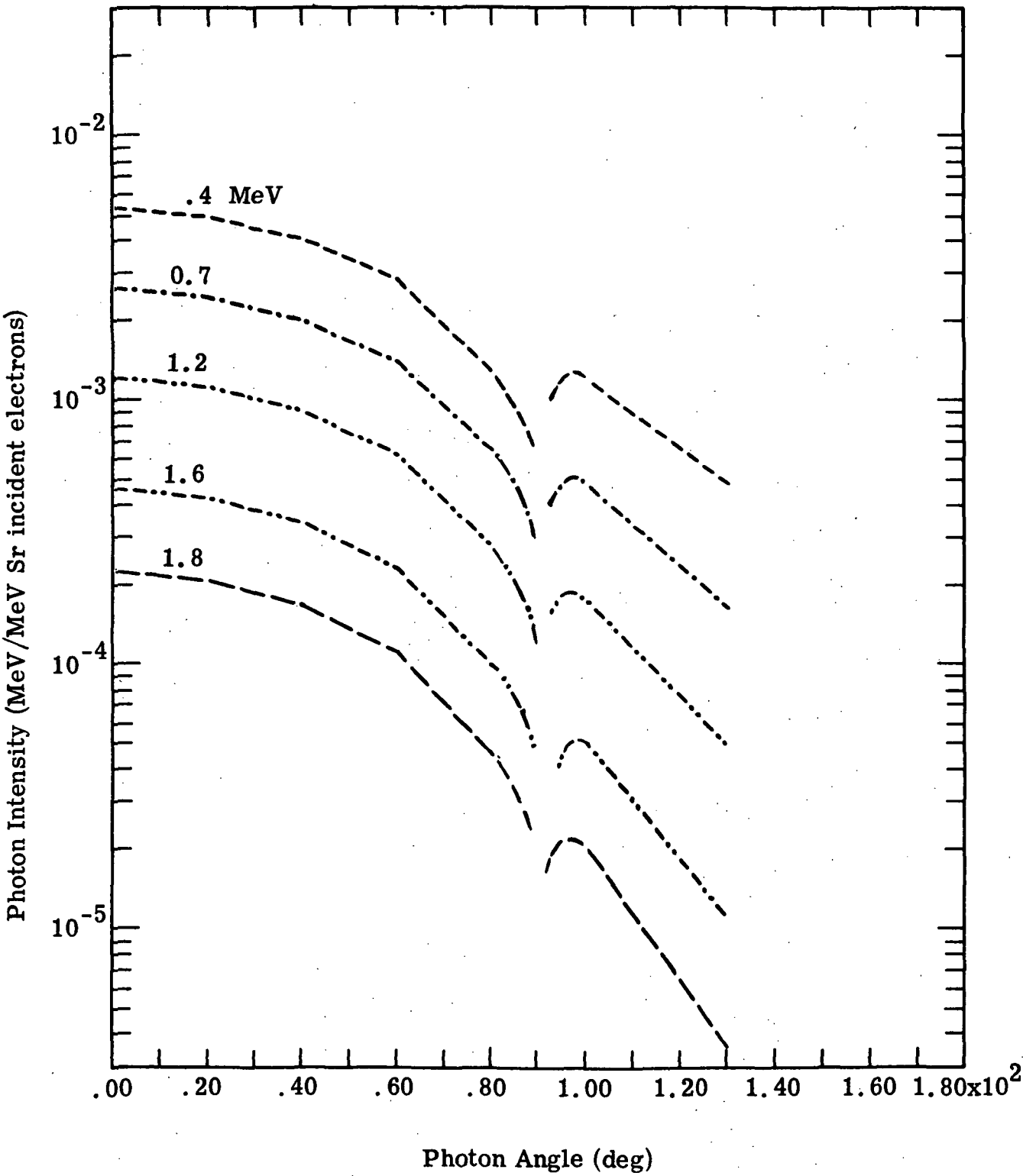

Figure 6.9. Bremsstrahlung intensity angular distributions due to an isotropic flux of 2-MeV electrons incident on one side of a unit area of an Al shield. The Al thickness is 1.21 g/cm^2. The angular distributions are normalized per unit incident electron. The photon energies are listed on the figure in MeV.

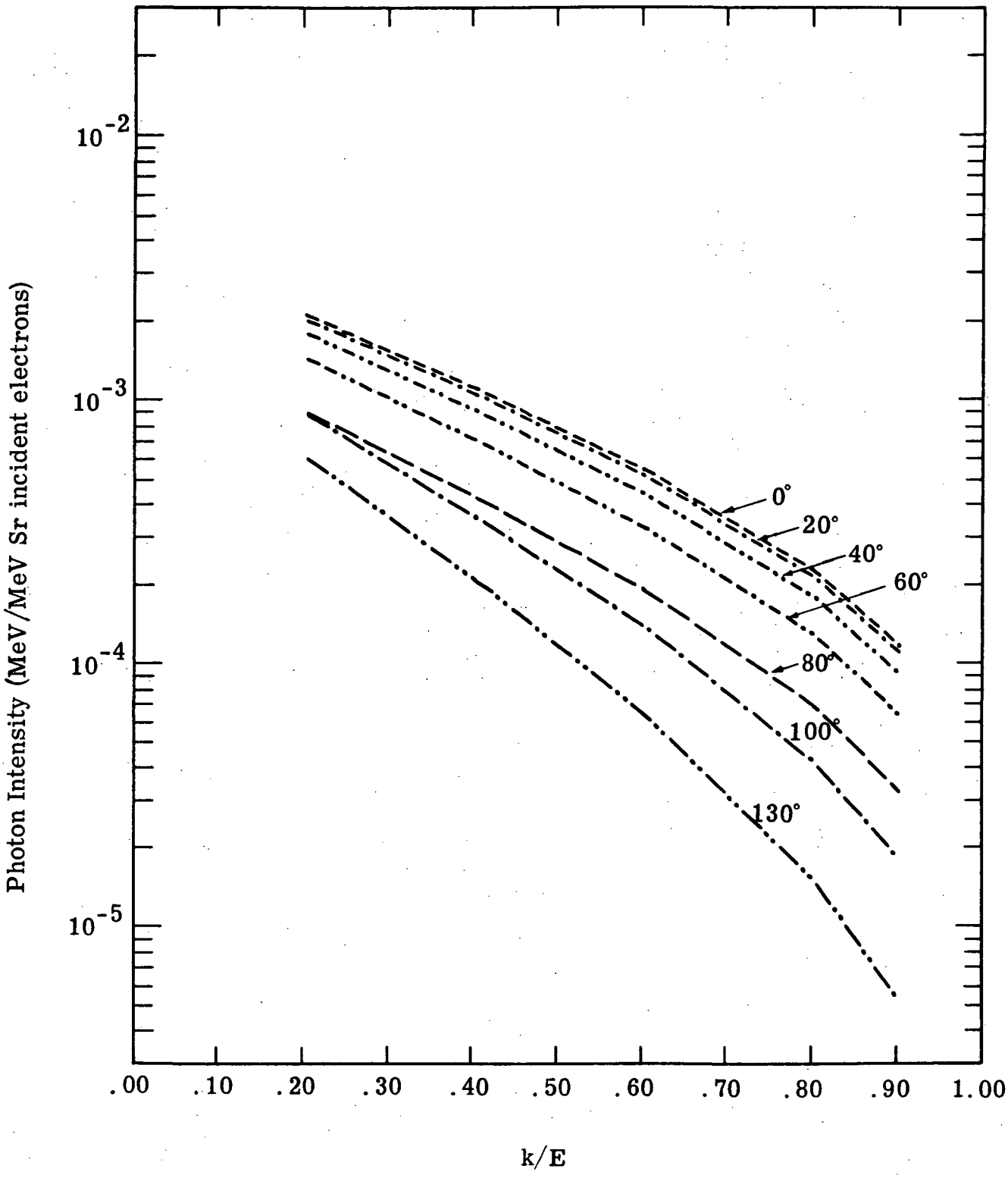

Figure 6.10. Bremsstrahlung intensity energy distribution due to an isotropic flux of 3-MeV electrons incident on one side of a unit area of an Fe target. The target thickness is 1.85 g/cm^2. The curves are normalized per unit incident electron. The photon emission angles are listed on the figure.

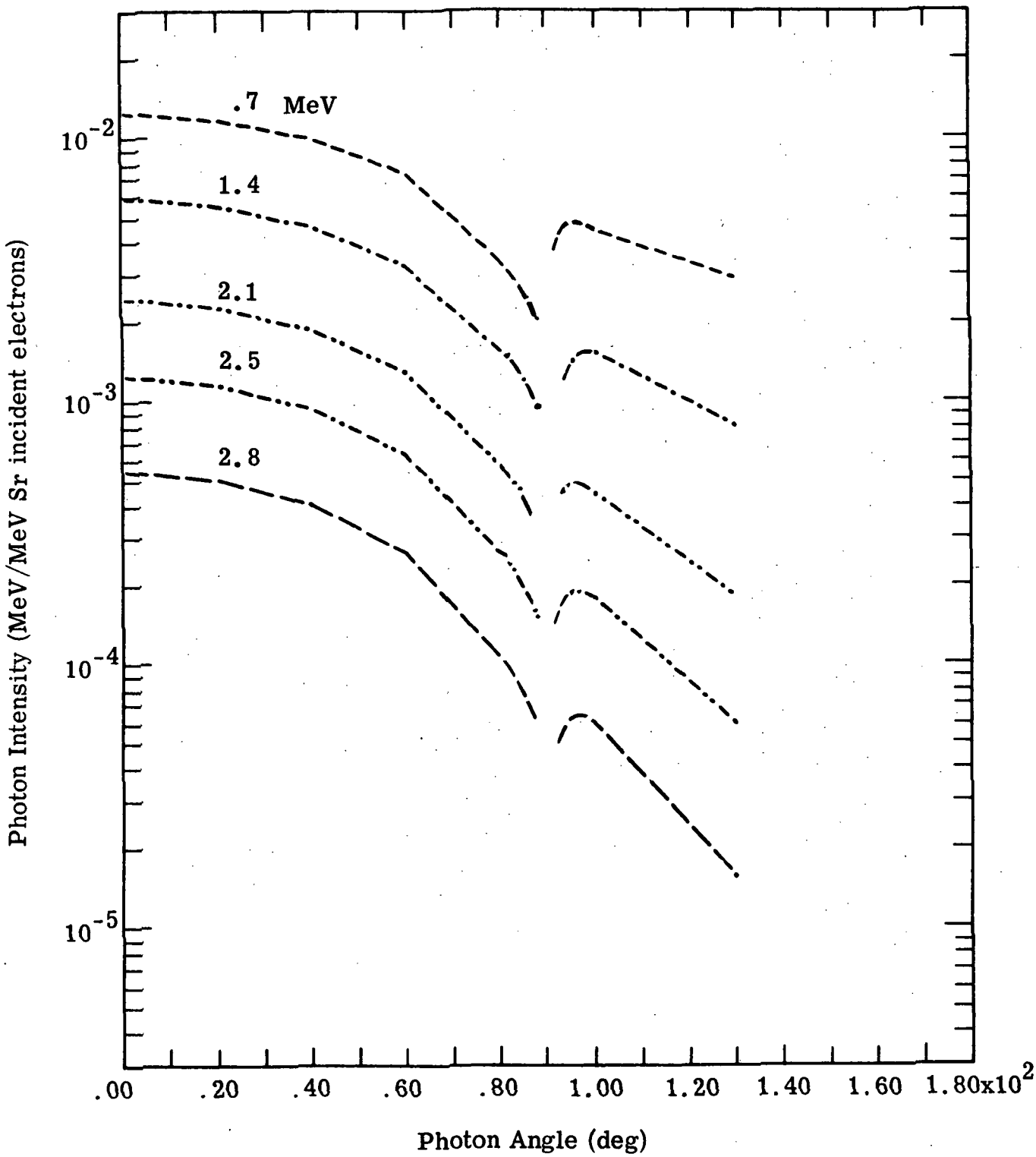

Figure 6.11. Bremsstrahlung intensity angular distribution due to an isotropic flux of 3-MeV electrons incident on one side of a unit area of an Fe shield. The shield thickness is 1.85 g/cm^2. The curves are normalized per unit incident electron. The photon energies are listed on the figure.

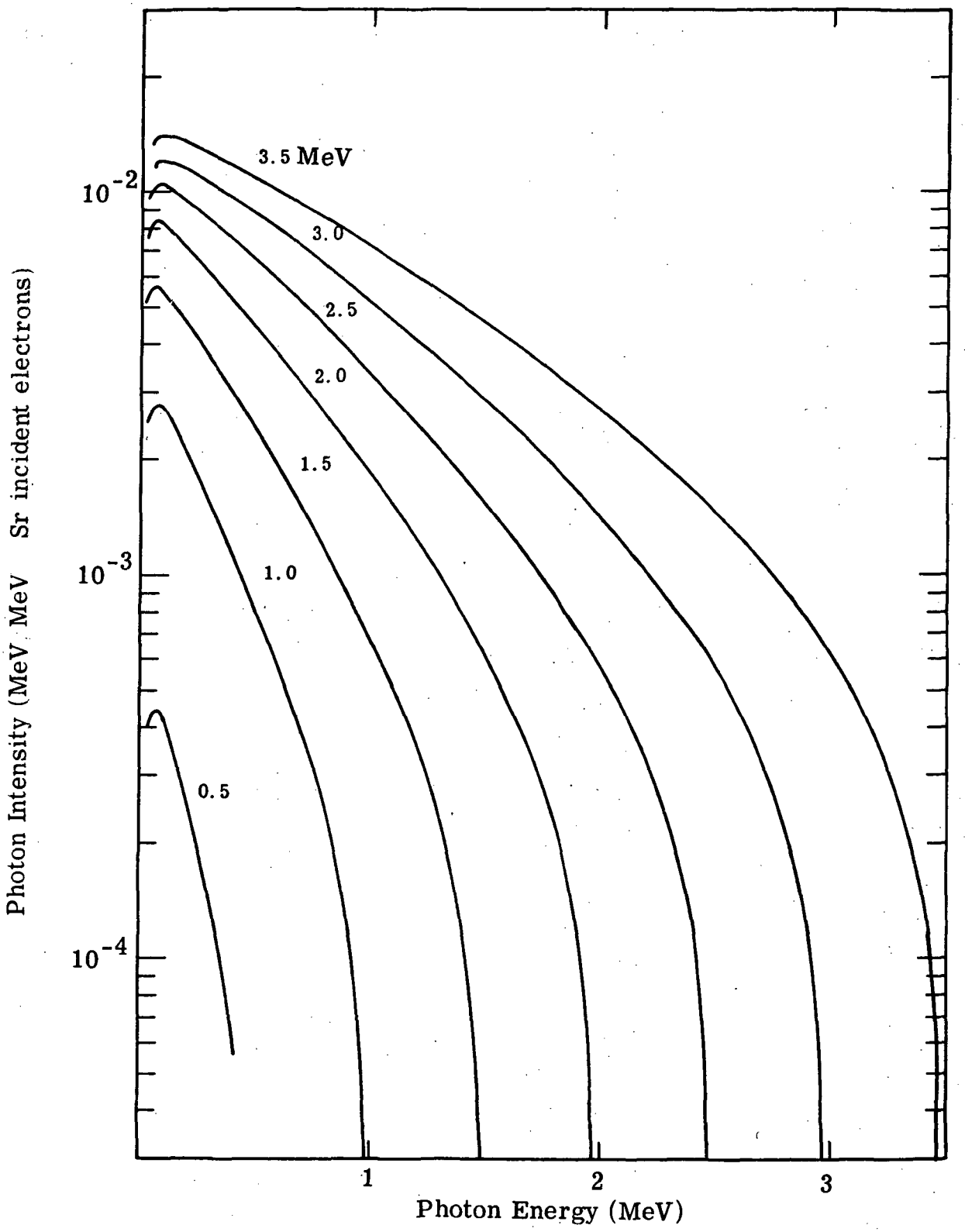

Figure 6.12. Bremsstrahlung intensity energy spectra for a monoenergetic isotropic electron flux incident one side of an Al shield. Spectra are for photons emerging normal to the target. Kinetic energy of incident electrons is given in MeV. Curves are normalized per incident electron (calculated from Eq. 6.42).

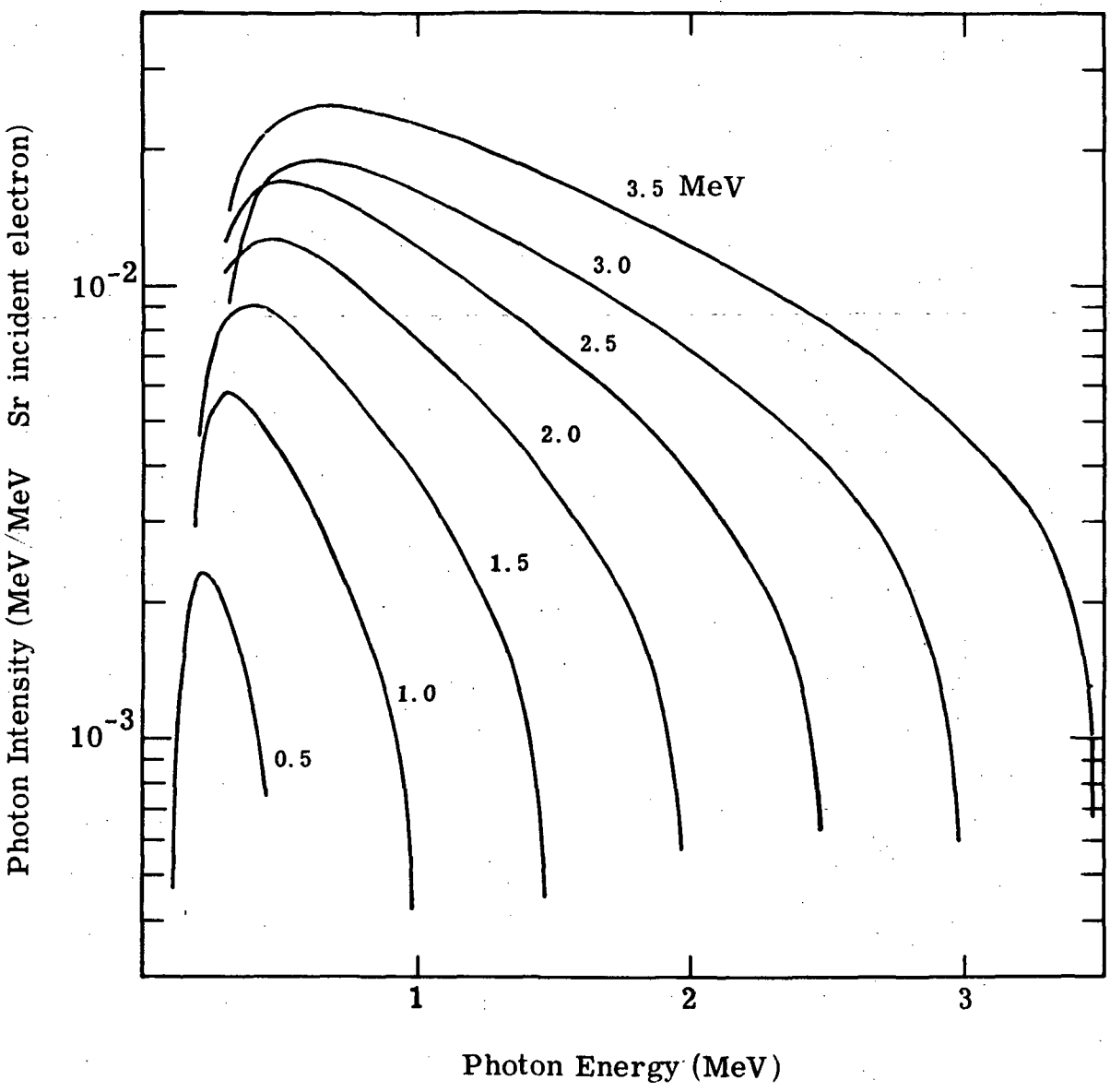

Figure 6.13. Bremsstrahlung intensity energy spectra for a monoenergetic isotropic electron flux incident on one side of an Au shield. Spectra are for photons emerging normal to the target. Kinetic energy of incident electrons is listed in MeV. Curves are normalized per incident electron (calculated from Eq. 6.42).

TABLE 6.4. BREMSSTRAHLUNG INTENSITY SPECTRA CAUSED BY A MONOENERGETIC, ISOTROPIC FLUX OF ELECTRONS INCIDENT ON ONE SIDE OF AN Al SHIELD.[a]

(MeV/MeV Sr incident electron)

	E(MeV)												
K(MeV)	.5000	1.0000	1.5000	2.0000	2.5000	3.0000	3.5000	4.0000	4.5000	5.0000	5.5000	6.0000	6.5000
.100	.423-03	.273-02	.541-02	.802-02	.103-01	.122-01	.138-01	.150-01	.159-01	.164-01	.169-01	.172-01	.177-01
.200	.250-03	.206-02	.496-02	.697-02	.936-02	.114-01	.132-01	.147-01	.159-01	.167-01	.174-01	.179-01	.185-01
.300	.137-03	.152-02	.360-02	.595-02	.828-02	.104-01	.124-01	.140-01	.153-01	.163-01	.172-01	.178-01	.185-01
.400	.873-04	.111-02	.281-02	.506-02	.732-02	.945-02	.115-01	.132-01	.147-01	.159-01	.168-01	.176-01	.184-01
.500	.000	.739-03	.233-02	.427-02	.643-02	.856-02	.107-01	.125-01	.141-01	.154-01	.164-01	.173-01	.181-01
.600	.000	.556-03	.196-02	.360-02	.563-02	.773-02	.984-02	.118-01	.135-01	.148-01	.160-01	.169-01	.178-01
.700	.000	.376-03	.167-02	.304-02	.493-02	.697-02	.907-02	.110-01	.128-01	.143-01	.155-01	.165-01	.175-01
.800	.000	.235-03	.115-02	.254-02	.430-02	.627-02	.834-02	.103-01	.122-01	.137-01	.150-01	.161-01	.171-01
.900	.000	.123-03	.895-03	.212-02	.376-02	.563-02	.767-02	.958-02	.115-01	.131-01	.145-01	.156-01	.166-01
1.000	.000	.000	.672-03	.176-02	.325-02	.503-02	.703-02	.891-02	.109-01	.125-01	.140-01	.151-01	.162-01
1.100	.000	.000	.493-03	.144-02	.279-02	.446-02	.640-02	.834-02	.102-01	.119-01	.133-01	.145-01	.156-01
1.200	.000	.000	.350-03	.118-02	.241-02	.398-02	.582-02	.777-02	.964-02	.113-01	.128-01	.140-01	.151-01
1.300	.000	.000	.229-03	.949-03	.206-02	.353-02	.532-02	.719-02	.907-02	.108-01	.122-01	.135-01	.146-01
1.400	.000	.000	.120-03	.758-03	.176-02	.314-02	.484-02	.668-02	.853-02	.102-01	.117-01	.130-01	.142-01
1.500	.000	.000	.000	.592-03	.149-02	.277-02	.436-02	.618-02	.799-02	.970-02	.112-01	.125-01	.137-01
1.600	.000	.000	.000	.449-03	.126-02	.244-02	.395-02	.570-02	.751-02	.919-02	.107-01	.121-01	.132-01
1.700	.000	.000	.000	.325-03	.105-02	.214-02	.357-02	.525-02	.703-02	.871-02	.102-01	.116-01	.128-01
1.800	.000	.000	.000	.218-03	.866-03	.186-02	.321-02	.484-02	.656-02	.823-02	.977-02	.111-01	.123-01
1.900	.000	.000	.000	.120-03	.703-03	.162-02	.289-02	.446-02	.614-02	.778-02	.931-02	.107-01	.119-01
2.000	.000	.000	.000	.000	.566-03	.139-02	.259-02	.407-02	.573-02	.734-02	.886-02	.102-01	.114-01
2.100	.000	.000	.000	.000	.433-03	.119-02	.231-02	.372-02	.532-02	.692-02	.842-02	.977-02	.110-01
2.200	.000	.000	.000	.000	.321-03	.101-02	.206-02	.341-02	.493-02	.651-02	.800-02	.934-02	.105-01
2.300	.000	.000	.000	.000	.217-03	.850-03	.182-02	.310-02	.458-02	.612-02	.759-02	.892-02	.101-01
2.400	.000	.000	.000	.000	.126-03	.700-03	.160-02	.281-02	.427-02	.575-02	.720-02	.852-02	.972-02
2.500	.000	.000	.000	.000	.000	.567-03	.140-02	.255-02	.392-02	.539-02	.682-02	.813-02	.932-02
2.600	.000	.000	.000	.000	.000	.446-03	.121-02	.230-02	.363-02	.504-02	.645-02	.775-02	.894-02
2.700	.000	.000	.000	.000	.000	.331-03	.104-02	.206-02	.336-02	.471-02	.609-02	.738-02	.856-02
2.800	.000	.000	.000	.000	.000	.227-03	.882-03	.184-02	.306-02	.440-02	.575-02	.702-02	.819-02
2.900	.000	.000	.000	.000	.000	.125-03	.735-03	.164-02	.280-02	.410-02	.542-02	.667-02	.783-02
3.000	.000	.000	.000	.000	.000	.000	.602-03	.145-02	.255-02	.381-02	.510-02	.633-02	.748-02
3.100	.000	.000	.000	.000	.000	.000	.477-03	.126-02	.232-02	.353-02	.480-02	.601-02	.714-02
3.200	.000	.000	.000	.000	.000	.000	.360-03	.109-02	.210-02	.327-02	.450-02	.569-02	.681-02
3.300	.000	.000	.000	.000	.000	.000	.246-03	.936-03	.189-02	.302-02	.422-02	.538-02	.649-02
3.400	.000	.000	.000	.000	.000	.000	.135-03	.789-03	.169-02	.277-02	.394-02	.509-02	.618-02
3.500	.000	.000	.000	.000	.000	.000	.000	.649-03	.150-02	.254-02	.368-02	.480-02	.588-02
3.600	.000	.000	.000	.000	.000	.000	.000	.516-03	.132-02	.232-02	.342-02	.453-02	.559-02
3.700	.000	.000	.000	.000	.000	.000	.000	.388-03	.115-02	.211-02	.318-02	.426-02	.530-02
3.800	.000	.000	.000	.000	.000	.000	.000	.268-03	.990-03	.191-02	.294-02	.400-02	.502-02
3.900	.000	.000	.000	.000	.000	.000	.000	.146-03	.837-03	.172-02	.272-02	.375-02	.476-02
4.000	.000	.000	.000	.000	.000	.000	.000	.000	.694-03	.153-02	.250-02	.351-02	.450-02
4.100	.000	.000	.000	.000	.000	.000	.000	.000	.554-03	.136-02	.229-02	.327-02	.424-02
4.200	.000	.000	.000	.000	.000	.000	.000	.000	.417-03	.119-02	.209-02	.305-02	.400-02
4.300	.000	.000	.000	.000	.000	.000	.000	.000	.287-03	.102-02	.190-02	.283-02	.376-02
4.400	.000	.000	.000	.000	.000	.000	.000	.000	.156-03	.869-03	.171-02	.262-02	.353-02
4.500	.000	.000	.000	.000	.000	.000	.000	.000	.000	.720-03	.153-02	.241-02	.331-02
4.600	.000	.000	.000	.000	.000	.000	.000	.000	.000	.575-03	.136-02	.221-02	.309-02
4.700	.000	.000	.000	.000	.000	.000	.000	.000	.000	.435-03	.119-02	.202-02	.288-02
4.800	.000	.000	.000	.000	.000	.000	.000	.000	.000	.298-03	.103-02	.184-02	.268-02
4.900	.000	.000	.000	.000	.000	.000	.000	.000	.000	.160-03	.876-03	.166-02	.248-02
5.000	.000	.000	.000	.000	.000	.000	.000	.000	.000	.000	.725-03	.149-02	.229-02
5.100	.000	.000	.000	.000	.000	.000	.000	.000	.000	.000	.580-03	.132-02	.211-02
5.200	.000	.000	.000	.000	.000	.000	.000	.000	.000	.000	.438-03	.116-02	.193-02
5.300	.000	.000	.000	.000	.000	.000	.000	.000	.000	.000	.298-03	.101-02	.175-02
5.400	.000	.000	.000	.000	.000	.000	.000	.000	.000	.000	.158-03	.855-03	.159-02
5.500	.000	.000	.000	.000	.000	.000	.000	.000	.000	.000	.000	.708-03	.142-02
5.600	.000	.000	.000	.000	.000	.000	.000	.000	.000	.000	.000	.565-03	.126-02
5.700	.000	.000	.000	.000	.000	.000	.000	.000	.000	.000	.000	.426-03	.111-02
5.800	.000	.000	.000	.000	.000	.000	.000	.000	.000	.000	.000	.288-03	.961-03
5.900	.000	.000	.000	.000	.000	.000	.000	.000	.000	.000	.000	.151-03	.816-03
6.000	.000	.000	.000	.000	.000	.000	.000	.000	.000	.000	.000	.000	.675-03
6.100	.000	.000	.000	.000	.000	.000	.000	.000	.000	.000	.000	.000	.538-03
6.200	.000	.000	.000	.000	.000	.000	.000	.000	.000	.000	.000	.000	.404-03
6.300	.000	.000	.000	.000	.000	.000	.000	.000	.000	.000	.000	.000	.272-03
6.400	.000	.000	.000	.000	.000	.000	.000	.000	.000	.000	.000	.000	.141-03
6.500	.000	.000	.000	.000	.000	.000	.000	.000	.000	.000	.000	.000	.000
6.600	.000	.000	.000	.000	.000	.000	.000	.000	.000	.000	.000	.000	.000
6.700	.000	.000	.000	.000	.000	.000	.000	.000	.000	.000	.000	.000	.000
6.800	.000	.000	.000	.000	.000	.000	.000	.000	.000	.000	.000	.000	.000
6.900	.000	.000	.000	.000	.000	.000	.000	.000	.000	.000	.000	.000	.000

[a]The intensity spectra are calculated for photons emerging normal to the shield and are normalized per incident electron.

TABLE 6.5. BREMSSTRAHLUNG INTENSITY SPECTRA CAUSED BY A MONOENERGETIC, ISOTROPIC FLUX OF ELECTRONS INCIDENT ON ONE SIDE OF A Pb SHIELD.[a]
(MeV/MeV Sr incident electron)

E(MeV)

K(MeV)	.5000	1.0000	1.5000	2.0000	2.5000	3.0000	3.5000	4.0000	4.5000	5.0000	5.5000	6.0000	6.5000
.100	.459-03	.135-03	.141-04	.222-05	.732-06	.131-09	.110-07	.169-08	.256-09	.910-10	.320-10	.111-10	.346-11
.200	.727-02	.447-02	.955-02	.455-02	.420-02	.125-02	.311-02	.253-02	.202-02	.184-02	.165-02	.147-02	.129-02
.300	.180-02	.567-02	.940-02	.117-01	.125-01	.904-02	.145-01	.147-01	.146-01	.151-01	.153-01	.154-01	.153-01
.400	.105-02	.501-02	.805-02	.124-01	.159-01	.150-01	.214-01	.234-01	.249-01	.267-01	.282-01	.294-01	.303-01
.500	.000	.407-02	.818-02	.134-01	.166-01	.177-01	.243-01	.275-01	.301-01	.330-01	.355-01	.376-01	.394-01
.600	.000	.721-02	.777-02	.136-01	.182-01	.185-01	.251-01	.291-01	.325-01	.362-01	.392-01	.421-01	.445-01
.700	.000	.241-02	.671-02	.136-01	.183-01	.188-01	.250-01	.295-01	.334-01	.376-01	.412-01	.445-01	.473-01
.800	.000	.171-02	.559-02	.135-01	.183-01	.178-01	.248-01	.292-01	.337-01	.381-01	.421-01	.457-01	.489-01
.900	.000	.107-02	.447-02	.130-01	.177-01	.170-01	.235-01	.286-01	.330-01	.380-01	.423-01	.461-01	.496-01
1.000	.000	.000	.337-02	.121-01	.171-01	.161-01	.225-01	.278-01	.328-01	.377-01	.421-01	.462-01	.498-01
1.100	.000	.000	.239-02	.111-01	.161-01	.154-01	.216-01	.268-01	.324-01	.371-01	.418-01	.459-01	.496-01
1.200	.000	.000	.156-02	.101-01	.151-01	.145-01	.207-01	.256-01	.309-01	.351-01	.396-01	.432-01	.466-01
1.300	.000	.000	.107-02	.934-02	.142-01	.135-01	.195-01	.247-01	.296-01	.336-01	.378-01	.414-01	.446-01
1.400	.000	.000	.000	.869-02	.134-01	.126-01	.186-01	.236-01	.284-01	.327-01	.368-01	.404-01	.436-01
1.500	.000	.000	.000	.809-02	.126-01	.117-01	.174-01	.226-01	.277-01	.317-01	.357-01	.394-01	.452-01
1.600	.000	.000	.000	.750-02	.118-01	.109-01	.164-01	.216-01	.267-01	.318-01	.364-01	.407-01	.445-01
1.700	.000	.000	.000	.692-02	.111-01	.102-01	.156-01	.206-01	.258-01	.309-01	.356-01	.399-01	.437-01
1.800	.000	.000	.000	.636-02	.103-01	.954-02	.147-01	.196-01	.249-01	.299-01	.347-01	.390-01	.429-01
1.900	.000	.000	.000	.582-02	.967-02	.890-02	.139-01	.187-01	.238-01	.290-01	.338-01	.381-01	.421-01
2.000	.000	.000	.000	.530-02	.901-02	.830-02	.131-01	.177-01	.229-01	.280-01	.328-01	.372-01	.412-01
2.100	.000	.000	.000	.480-02	.837-02	.767-02	.123-01	.168-01	.219-01	.271-01	.319-01	.363-01	.404-01
2.200	.000	.000	.000	.000	.776-02	.710-02	.116-01	.159-01	.210-01	.261-01	.310-01	.354-01	.395-01
2.300	.000	.000	.000	.000	.718-02	.653-02	.107-01	.150-01	.201-01	.252-01	.301-01	.345-01	.386-01
2.400	.000	.000	.000	.000	.662-02	.596-02	.990-02	.141-01	.192-01	.243-01	.291-01	.336-01	.377-01
2.500	.000	.000	.000	.000	.608-02	.542-02	.916-02	.133-01	.183-01	.234-01	.282-01	.327-01	.368-01
2.600	.000	.000	.000	.000	.000	.488-02	.842-02	.125-01	.174-01	.225-01	.273-01	.318-01	.360-01
2.700	.000	.000	.000	.000	.000	.436-02	.770-02	.117-01	.166-01	.216-01	.264-01	.309-01	.351-01
2.800	.000	.000	.000	.000	.000	.386-02	.699-02	.109-01	.157-01	.207-01	.255-01	.301-01	.342-01
2.900	.000	.000	.000	.000	.000	.337-02	.630-02	.102-01	.149-01	.199-01	.247-01	.292-01	.333-01
3.000	.000	.000	.000	.000	.000	.289-02	.562-02	.945-02	.141-01	.190-01	.238-01	.283-01	.325-01
3.100	.000	.000	.000	.000	.000	.000	.496-02	.875-02	.133-01	.182-01	.230-01	.274-01	.316-01
3.200	.000	.000	.000	.000	.000	.000	.431-02	.805-02	.126-01	.174-01	.221-01	.266-01	.308-01
3.300	.000	.000	.000	.000	.000	.000	.368-02	.735-02	.118-01	.166-01	.213-01	.258-01	.299-01
3.400	.000	.000	.000	.000	.000	.000	.305-02	.668-02	.111-01	.158-01	.205-01	.249-01	.291-01
3.500	.000	.000	.000	.000	.000	.000	.000	.602-02	.103-01	.150-01	.197-01	.241-01	.282-01
3.600	.000	.000	.000	.000	.000	.000	.000	.537-02	.961-02	.142-01	.189-01	.233-01	.274-01
3.700	.000	.000	.000	.000	.000	.000	.000	.473-02	.891-02	.135-01	.181-01	.225-01	.266-01
3.800	.000	.000	.000	.000	.000	.000	.000	.410-02	.819-02	.127-01	.173-01	.217-01	.258-01
3.900	.000	.000	.000	.000	.000	.000	.000	.348-02	.748-02	.120-01	.165-01	.209-01	.250-01
4.000	.000	.000	.000	.000	.000	.000	.000	.286-02	.675-02	.112-01	.157-01	.201-01	.242-01
4.100	.000	.000	.000	.000	.000	.000	.000	.000	.602-02	.105-01	.150-01	.193-01	.234-01
4.200	.000	.000	.000	.000	.000	.000	.000	.000	.525-02	.975-02	.142-01	.185-01	.226-01
4.300	.000	.000	.000	.000	.000	.000	.000	.000	.446-02	.900-02	.135-01	.178-01	.219-01
4.400	.000	.000	.000	.000	.000	.000	.000	.000	.357-02	.825-02	.127-01	.170-01	.211-01
4.500	.000	.000	.000	.000	.000	.000	.000	.000	.249-02	.748-02	.120-01	.163-01	.203-01
4.600	.000	.000	.000	.000	.000	.000	.000	.000	.000	.670-02	.112-01	.155-01	.196-01
4.700	.000	.000	.000	.000	.000	.000	.000	.000	.000	.587-02	.104-01	.148-01	.188-01
4.800	.000	.000	.000	.000	.000	.000	.000	.000	.000	.499-02	.967-02	.140-01	.181-01
4.900	.000	.000	.000	.000	.000	.000	.000	.000	.000	.401-02	.889-02	.132-01	.173-01
5.000	.000	.000	.000	.000	.000	.000	.000	.000	.000	.281-02	.808-02	.125-01	.166-01
5.100	.000	.000	.000	.000	.000	.000	.000	.000	.000	.000	.725-02	.117-01	.158-01
5.200	.000	.000	.000	.000	.000	.000	.000	.000	.000	.000	.638-02	.109-01	.151-01
5.300	.000	.000	.000	.000	.000	.000	.000	.000	.000	.000	.543-02	.102-01	.143-01
5.400	.000	.000	.000	.000	.000	.000	.000	.000	.000	.000	.437-02	.936-02	.136-01
5.500	.000	.000	.000	.000	.000	.000	.000	.000	.000	.000	.307-02	.853-02	.128-01
5.600	.000	.000	.000	.000	.000	.000	.000	.000	.000	.000	.000	.767-02	.121-01
5.700	.000	.000	.000	.000	.000	.000	.000	.000	.000	.000	.000	.675-02	.113-01
5.800	.000	.000	.000	.000	.000	.000	.000	.000	.000	.000	.000	.576-02	.105-01
5.900	.000	.000	.000	.000	.000	.000	.000	.000	.000	.000	.000	.465-02	.967-02
6.000	.000	.000	.000	.000	.000	.000	.000	.000	.000	.000	.000	.326-02	.883-02
6.100	.000	.000	.000	.000	.000	.000	.000	.000	.000	.000	.000	.000	.795-02
6.200	.000	.000	.000	.000	.000	.000	.000	.000	.000	.000	.000	.000	.701-02
6.300	.000	.000	.000	.000	.000	.000	.000	.000	.000	.000	.000	.000	.599-02
6.400	.000	.000	.000	.000	.000	.000	.000	.000	.000	.000	.000	.000	.483-02
6.500	.000	.000	.000	.000	.000	.000	.000	.000	.000	.000	.000	.000	.340-02
6.600	.000	.000	.000	.000	.000	.000	.000	.000	.000	.000	.000	.000	.000
6.700	.000	.000	.000	.000	.000	.000	.000	.000	.000	.000	.000	.000	.000
6.800	.000	.000	.000	.000	.000	.000	.000	.000	.000	.000	.000	.000	.000
6.900	.000	.000	.000	.000	.000	.000	.000	.000	.000	.000	.000	.000	.000

[a] The intensity spectra are calculated for photons emerging normal to the shield and are normalized per incident electron.

6.4.2 Bremsstrahlung Energy Current for Arbitrary Shield Thickness

The results of the preceding section for the production of bremsstrahlung radiation were all obtained for monoenergetic electrons incident on shield thicknesses equal to the ranges of the incident electrons. The photons which are produced in these shield thicknesses often will have to pass through additional shielding material to reach the dose point. The additional shielding affects both the angular distribution and energy spectrum of the bremsstrahlung energy current. The angular distribution of the bremsstrahlung current will tend to become more forward peaked in the direction of the normal to the exit plane. Photons which are originally traveling at large angles with respect to this normal will have a greater probability of being absorbed or scattered than photons traveling in the direction of the normal. Also, the low energy end of the photon energy spectrum will be attenuated much more rapidly than the high energy end of the spectrum because of photoelectric absorption. Finally, Compton scattering will shift photons from higher to lower energies and change their directions. Detailed calculations which treat the entire photon transport problem are possible only with sophisticated gamma-ray transport computer codes. However, space shielding calculations seldom require a complete description of the energy and angular dependence of the bremsstrahlung radiation. Estimates of the dose deposited by bremsstrahlung, for example, can be performed using buildup factors. If an energy spectrum is one of the desired quantities in the calculation, a first approximation can be obtained by neglecting entirely the photon buildup. In this approximation the bremsstrahlung energy current $J^{iso}_{s(0)}(E, E', \theta_\gamma, T, Z)$ will be given by the current determined using the intensity calculated for shield thicknesses equal to the electron range $R_0(E)$ times a simple exponential attenuation term

$$J^{iso}_{s(0)}(E, E', \theta_\gamma, T, Z) = J^{iso}_{s}(E, E', \theta_\gamma, R_0 Z) e^{-\mu(E', Z)(T-R_0)/\cos\theta_\gamma} , \tag{6.43}$$

where $\mu(E', Z)$ is the mass attenuation coefficient for photons of energy E' in a material of atomic number Z. An improvement to this approximation is obtained for the bremsstrahlung emerging normal to the target ($\theta_\gamma = 0$) by using the single Compton scattering model discussed in Section 5.4. In this approximation $J^{iso}_{s}(E, E', 0, T, Z)$ is given as

$$J^{iso}_{s(1)}(E, E', 0, T, Z) = J^{iso}_{s}(E, E', 0, R_0, Z) e^{-\mu(E', Z)(T-R_0)} + \int_{E'}^{E} dE'' J^{iso}_{s}(E', E'', \theta_\gamma, R_0, Z) C^{(1)}(E'', E') , \tag{6.44}$$

where $C^{(1)}(E'', E')$ is the probability of a photon of energy E'' downscattering to an energy E' and is given as

$$C^{(1)}(E'', E') = \frac{N_o Z}{A} \frac{E'}{E''} \frac{d\sigma}{dE'}(E'', E') \left[\frac{e^{-\mu(E')(T-R} - e^{-\mu(E'')(T-R_o)/\cos\theta_\gamma}}{\mu(E'') - \mu(E')\cos\theta_\gamma} \right] \quad (6.45)$$

where N_o is Avogadro's number, Z and A are the atomic number and atomic weight of the shield material, $d\sigma/dE'(E'', E')$ is the Klein-Nishina cross section for Compton scattering from a photon energy of E'' to an energy of E', and $\mu(E')$ and $\mu(E'')$ are, respectively, the mass attenuation coefficients for photons of energy E' and E''.

Examples of the bremsstrahlung spectra emerging at zero degrees with respect to the shield normal are shown for various shield thicknesses in Fig. 6.14. It should be emphasized that this treatment of scattered radiation is still only approximate. Accurate calculations demand the treatment of scattering to all orders and can only be done with photon transport computer codes.

6.4.3 Dose Due to Bremsstrahlung Radiation

For shield thicknesses just equal to the range of the electrons one can use the bremsstrahlung energy current defined in Eq. 6.42 to calculate the dose $d(R_o, Z, E, Z')$ defined in Eq. 6.17 as

$$d(R_o, Z, E, Z') = \varkappa \int_o^E dE' \mu_a(E', Z') J_s^{iso}(E, E', 0, R_o, Z)$$

$$= \varkappa \int_o^E dE' \mu_a(E', Z') \frac{1}{\pi} \int_o^{2\pi} d\varphi_e \int_o^{\pi/2} \sin\theta_e \cos\theta_e$$

$$I_s(E, E', \theta_e, Z) A_T(E', Z, \theta_e, 0, R_o) d\theta_e \quad , \quad (6.46)$$

where $\mu_a(E', Z')$ is the mass absorbtion coefficient for photons of energy E' in the dose material. The quantity d has the units of

$$\left(\frac{\text{Rad cm}^2}{\text{Sr incident electron}} \right) .$$

To obtain the dose for shields thicker than the range of the electrons one must modify Eq. 6.46. This can be done in several ways. First, one

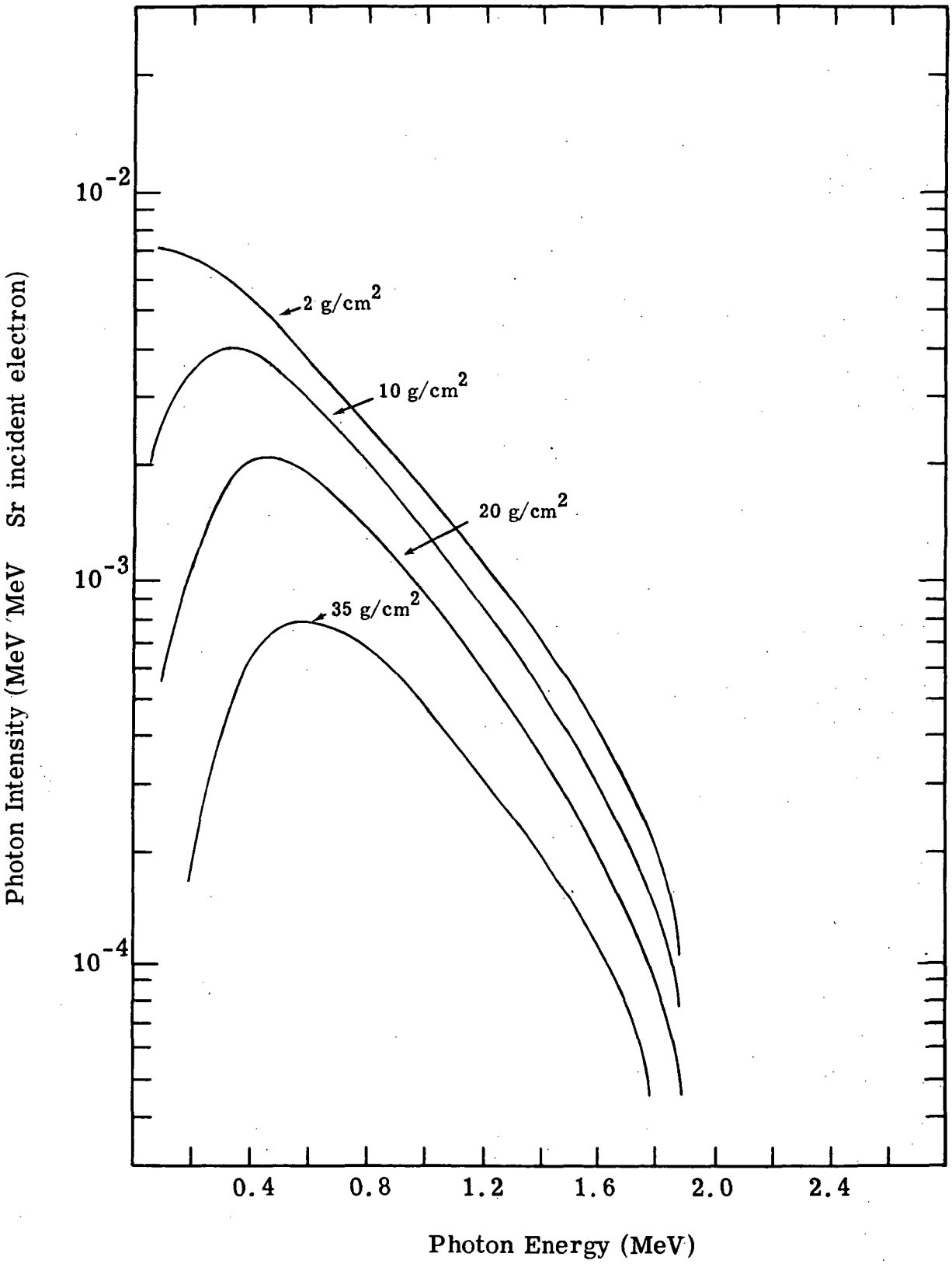

Figure 6.14. Bremsstrahlung intensity spectra due to an isotropic flux of 2 MeV electrons incident on one side of an Al shield. The thickness of the Al shield is shown for the various curves.

might neglect the effect of the scattered photons and calculate the dose due to only the uncollided photons. The quantity d then becomes

$$d(T, Z, E, Z') \approx \varkappa \int_0^E dE' \mu_a (E', Z') J_s^{iso} (E, E', 0, R_o, Z) e^{-\mu(Z)(T-R_o)} \quad . \quad (6.47)$$

For shields only slightly thicker than the range of the electrons this should be an adequate approximation. It will, however, considerably underestimate the true dose for thicker shields, especially if they are of low Z material. A first order analytic correction is obtained by using the single Compton scatter model discussed in Section 6.4.2. The quantity $J_s^{iso} e^{-\mu(Z)(T-R_o)}$ is replaced in Eq. 6.44 by the quantity $J_{s(1)}^{iso} (E, E', 0, T, Z)$ of Eq. 6.41 and the dose is approximated as

$$d(T, Z, E, Z') \approx \varkappa \int_0^E dE' \mu_a (E', Z') \left[J_s^{iso} (E, E', 0, R_o, Z) e^{-\mu(E', Z)(T-R_o)} + \int_{E'}^E dE'' J_s^{iso} (E', E'', \theta_\gamma, R_o, Z) C^{(1)} (E'', E') \right] , \quad (6.48)$$

where $C^{(1)}$ is defined in Eq. 6.45.

For still thicker shields one can use buildup factors and write the dose as

$$d(T, Z, E, Z') = \varkappa \int_0^E dE' \mu_a (E', Z') J_s^{iso} (E, E', 0, R_o, Z) B[\mu(E')(T-R_o)] \cdot G[\mu(E')(T-R_o)] \quad (6.49)$$

where $B(\mu x)$ is a dose buildup factor (for a tissue absorber this quantity is often referred to as an exposure buildup factor) and $G(\mu x)$ is the attenuation kernel. Both the buildup factor and the attenuation kernel depend on the geometry of the problem and are discussed in Section 5.4. In the present problem one is concerned with a source of gamma-rays distributed on some surface which completely surrounds the dose point. The angular distribution of the gamma-ray source varies between $\cos \theta$ for the high energy photons and $\cos^{1/2} \theta$ for the low energy photons. Buildup factors are not tabulated for this problem. A conservative estimate of the dose will be obtained by using the buildup factors calculated for a point isotropic source in an infinite medium and writing the dose received from a differential solid angle as

$$d(T, Z, E, Z') = \kappa \int_0^E dE' \mu_a (E', Z') J_s^{iso}(E, E', 0, R_o, Z) B_{pt}[\mu(E')(T-R_o)] e^{-\mu(E')(T-R_o)} . \quad (6.50)$$

Figures 6.15 and 6.16 show the thickness dependence of the dose $d(T, Z, E, Z')$ for the bremsstrahlung produced by an isotropic flux of monoenergetic electrons incident on one side of shields of Al and Pb. These doses are also listed in Tables 6.6 and 6.7.

6.4.4 Dose Due to Bremsstrahlung Produced by a Spectrum of Electrons

The dose calculated for a spectrum of electrons isotropically incident on one side of a shield is given as

$$D(T, Z, Z') = \int dE \frac{\Phi(E)}{4} d(T, Z, E, Z') \quad , \quad (6.51)$$

where $d(T, Z, E, Z')$ is given by Eq. 6.50 and $\Phi(E)$ is the full space omnidirection flux of electrons. The values of $D(T, Z, Z')$ have been calculated for an electron energy spectra given by simple exponential functions, electron energy spectra given by Vette's AE2 electron environment, and also for Vette's projected (1968) orbital integrated electron spectra and are discussed below.

6.4.4.1 Dose Due to Bremsstrahlung Produced by a Spectrum of Electrons ; Exponential Spectra

The bremsstrahlung dose transmitted through Al and Pb shields for exponential spectra of incident electron are shown in Figs. 6.17 and 6.18. In these figures the quantity

$$D = \int_0^{7\ MeV} dE\ P\ e^{-PE} d(T, Z, E, Z') \quad (6.52)$$

is plotted. This quantity corresponds to the bremsstrahlung dose per incident electron per cm^2 per unit solid angle. The units of D are

$$\left(\frac{\text{Rad cm}^2}{\text{Sr incident electron}} \right)$$

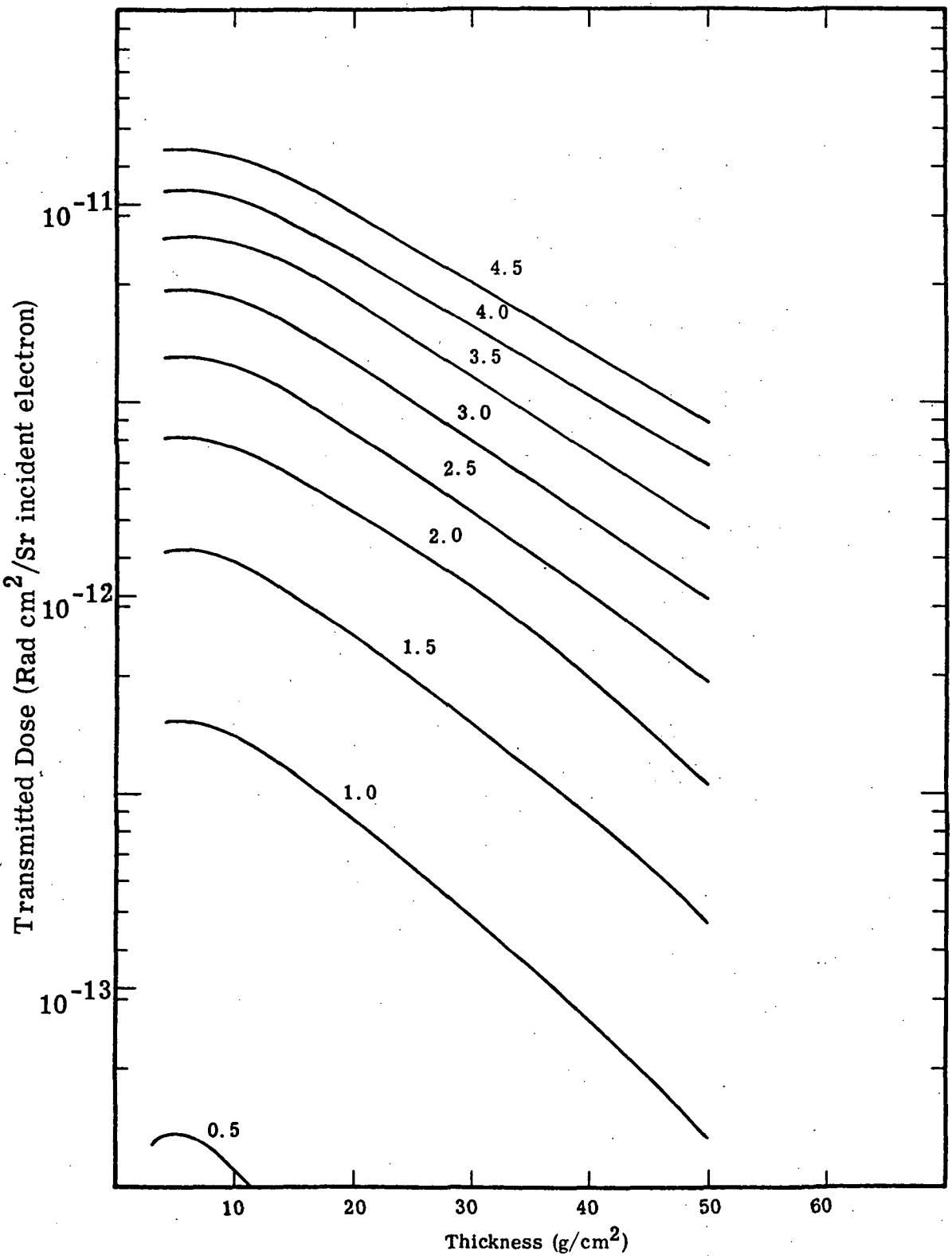

Figure 6.15. Bremsstrahlung tissue dose transmitted through Al shield caused by an isotropic flux of monoenergetic electrons incident on one side of the shield. Curves are normalized per incident electron. The incident electron kinetic energies are listed in MeV on the figure (Calculated from Eq. 6.47).

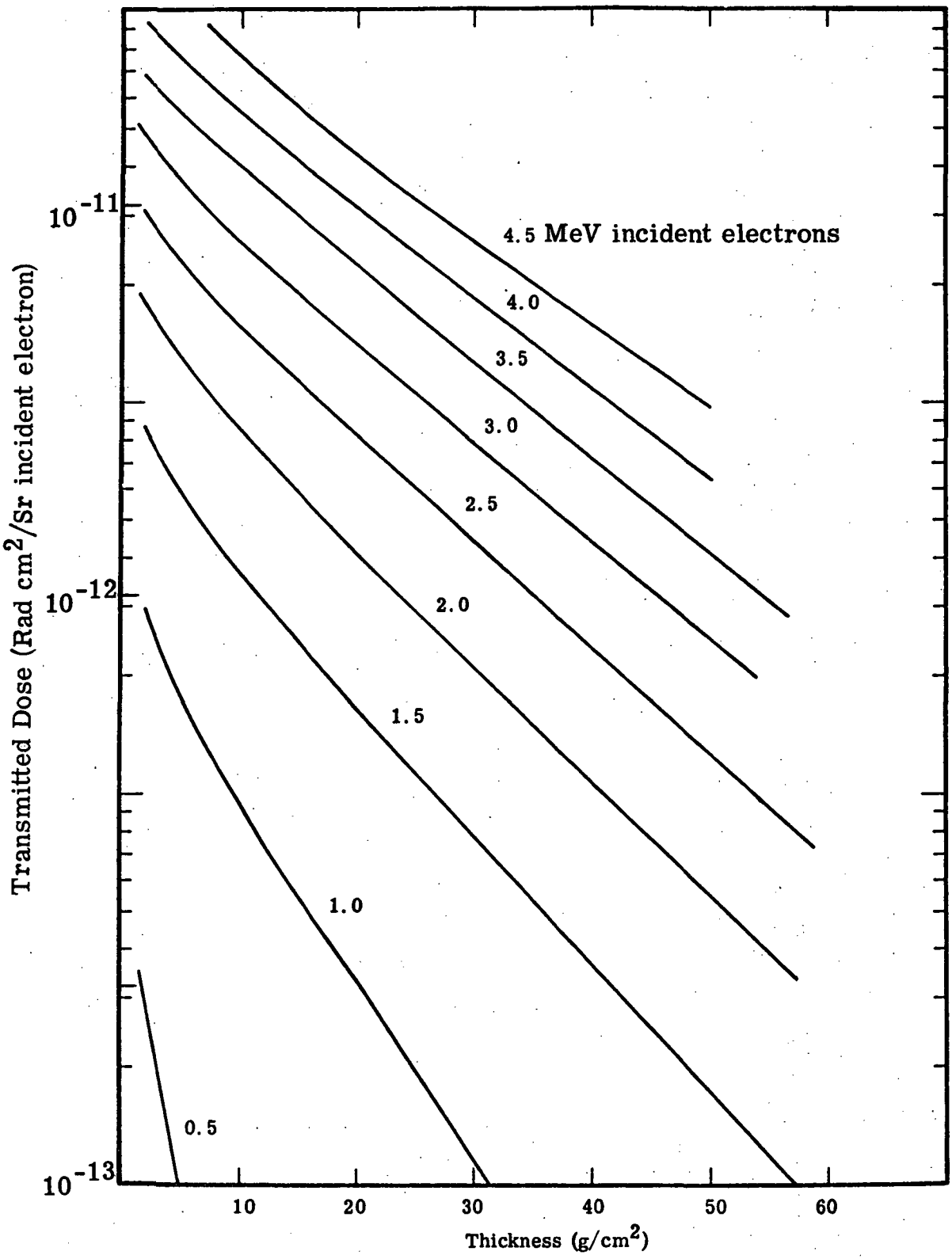

Figure 6.16. Bremsstrahlung tissue dose transmitted through a Pb shield caused by an isotropic flux of monoenergetic electrons incident on one side of a unit area of the shield. The curves are normalized per incident electron. The kinetic energies of the incident electron are listed on the figure.

TABLE 6.6. TRANSMITTED TISSUE DOSE DUE TO BREMSSTRAHLUNG CAUSED BY A MONOENERGETIC, ISOTROPIC FLUX OF ELECTRONS INCIDENT ON ONE SIDE OF AN Al SHIELD.
(Rad cm^2/Sr incident electron)

Thickness (g/cm^2)	Electron Energy (MeV)												
	.500	1.000	1.500	2.000	2.500	3.000	3.500	4.000	4.500	5.000	5.500	6.000	6.500
1.000	.727-13	.397-12	.117-11										
1.250	.717-13	.387-12	.110-11	.217-11									
1.500	.708-13	.373-12	.109-11	.212-11	.351-11								
1.750	.699-13	.367-12	.105-11	.207-11	.343-11	.509-11	.697-11	.907-11	.113-10	.136-10	.158-10	.180-10	.201-10
2.000	.690-13	.888-12	.176-11	.262-11	.424-11	.624-11	.847-11	.108-10	.133-10	.158-10	.182-10	.205-10	.228-10
4.000	.627-13	.492-12	.137-11	.262-11	.422-11	.619-11	.847-11	.110-10	.139-10	.167-10	.196-10	.224-10	.250-10
6.000	.579-13	.496-12	.178-11	.264-11	.425-11	.623-11	.855-11	.112-10	.140-10	.170-10	.199-10	.228-10	.255-10
8.000	.775-13	.450-12	.128-11	.248-11	.405-11	.598-11	.826-11	.108-10	.136-10	.165-10	.194-10	.223-10	.249-10
10.000	.771-13	.441-12	.125-11	.241-11	.392-11	.579-11	.798-11	.105-10	.132-10	.160-10	.188-10	.216-10	.242-10
15.000	.784-13	.353-12	.102-11	.200-11	.330-11	.493-11	.696-11	.908-11	.115-10	.141-10	.166-10	.192-10	.216-10
20.000	.710-13	.272-12	.801-12	.160-11	.267-11	.401-11	.564-11	.751-11	.958-11	.118-10	.140-10	.162-10	.183-10
35.000	.769-14	.114-12	.359-12	.750-12	.130-11	.202-11	.292-11	.400-11	.522-11	.656-11	.794-11	.937-11	.107-10
50.000	.245-14	.432-13	.149-12	.332-12	.606-12	.988-12	.148-11	.210-11	.281-11	.360-11	.444-11	.532-11	.617-11

TABLE 6.7. TRANSMITTED TISSUE DOSE DUE TO BREMSSTRAHLUNG CAUSED BY A MONOENERGETIC, ISOTROPIC FLUX OF ELECTRONS INCIDENT ON ONE SIDE OF A Pb SHIELD. (Rad cm^2/Sr incident electron)

Thickness (g/cm^2)	Electron Energy (MeV)												
	.500	1.000	1.500	2.000	2.500	3.000	3.500	4.000	4.500	5.000	5.500	6.000	6.500
2.000	.969-13	.952-12	.278-11	.560-11	.953-11	.128-10	.198-10	.263-10	.336-10	.418-10	.503-10	.589-10	.674-10
4.000	.459-13	.691-12	.221-11	.466-11	.814-11	.130-10	.188-10	.260-10	.343-10	.434-10	.530-10	.629-10	.721-10
10.000	.733-14	.296-12	.116-11	.266-11	.492-11	.817-11	.122-10	.173-10	.233-10	.300-10	.372-10	.446-10	.521-10
20.000	.580-15	.106-12	.526-12	.133-11	.263-11	.459-11	.711-11	.104-10	.144-10	.189-10	.237-10	.286-10	.337-10
40.000	.407-17	.164-13	.115-12	.335-12	.732-12	.137-11	.226-11	.347-11	.499-11	.677-11	.870-11	.107-10	.128-10
50.000	.356-18	.713-14	.571-13	.176-12	.400-12	.776-12	.131-11	.206-11	.303-11	.420-11	.548-11	.681-11	.818-11

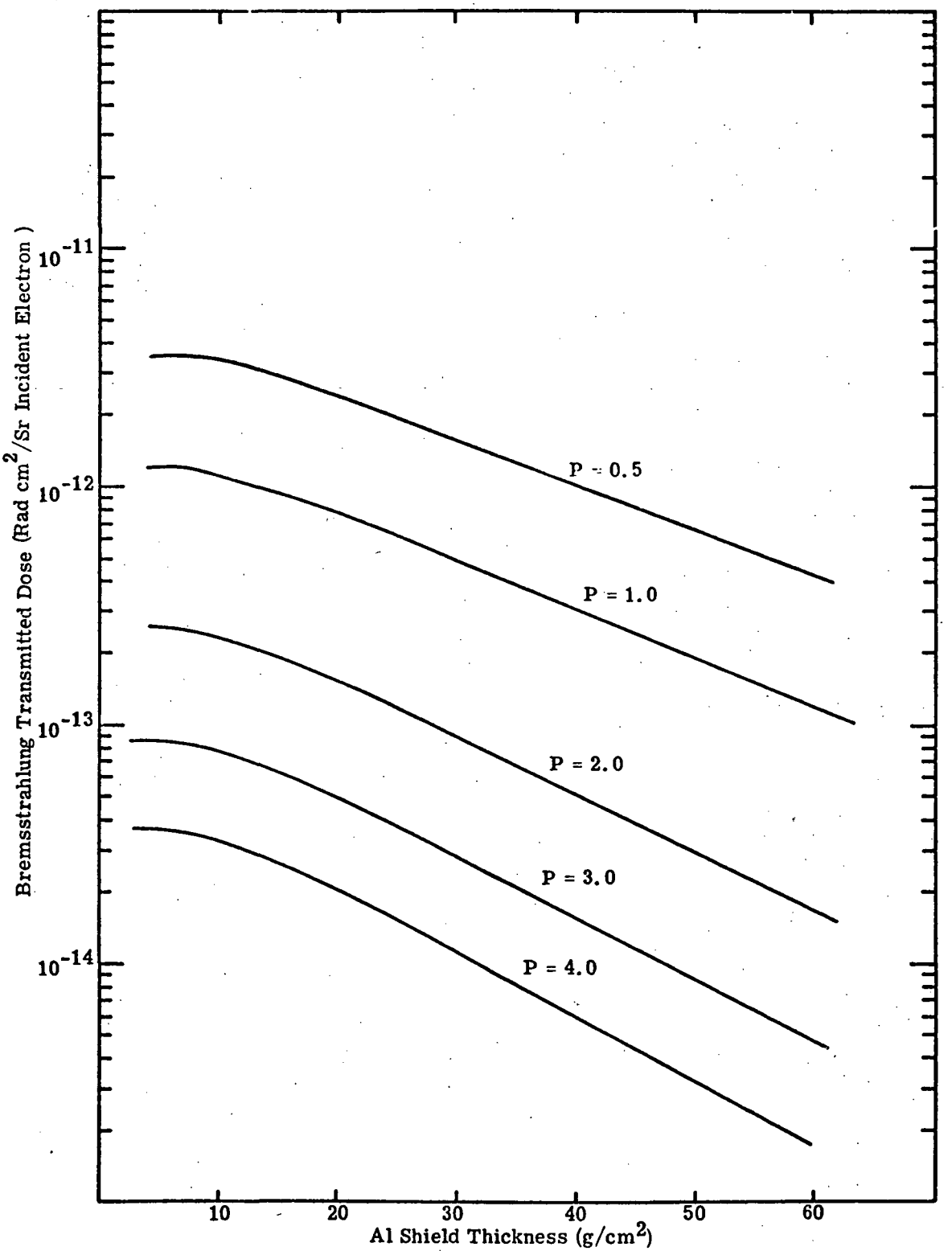

Figure 6.17. Bremsstrahlung tissue dose transmitted through an Al shield caused by an isotropic flux of electrons incident on a unit area of one side of the shield. The electron energy spectra are given by $N(E) = Pe^{-PE}$. The values of P are listed on the figure.

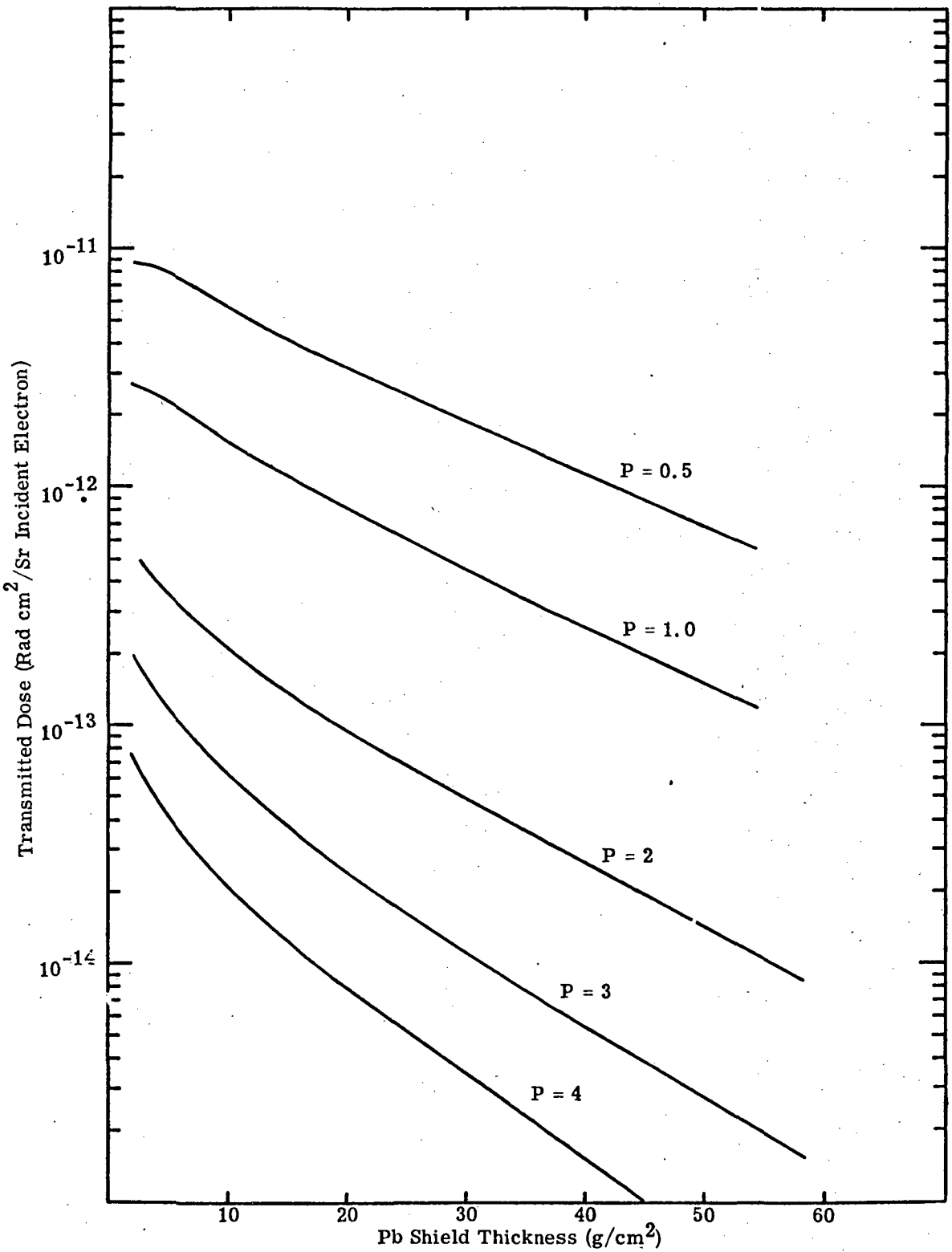

Figure 6.18. Bremsstrahlung tissue dose transmitted through a Pb shield caused by an isotropic flux of electrons incident on a unit area of one side of the shield. The electron energy spectra are given by $N(E) = Pe^{-PE}$. The values of P are listed in the figure.

The values of D for the transmitted bremsstrahlung are listed in Tables 6.8* and 6.9 for shields of Al and Pb.

6.4.4.2 Dose Due to Bremsstrahlung Produced by a Spectrum of Electrons; Vette's AE2 Electron Distribution

The bremsstrahlung dose transmitted through Al and Pb shields has been calculated for several of the spectra given by Vette in his AE2 electron environment. The transmitted dose is given for this case by the equation

$$D(T) = \varkappa \int_0^{7\ \mathrm{MeV}} dE\ N(E, L) d(T, Z, E, Z') \qquad (6.53)$$

which as the units of

$$\left(\frac{\mathrm{Rad\ cm}^2}{\mathrm{Sr\ incident\ electron\ (E\ E_o)}} \right) .$$

Graphs of the transmitted bremsstrahlung dose through Al and Pb shields are shown in Figs. 6.19 and 6.20 for several values of the spatial parameter L. Lists of these doses are given in Tables 6.10 and 6.11. (N.B. The AE2 Electron Environment is considered to be outdated by space scientists.)

6.4.4.3 Dose Due to Bremsstrahlung Produced by Vette's Projected (1968) Orbital Integration Data

The bremsstrahlung doses were calculated for Vette's projected (1968) orbital integration electron spectra. The bremsstrahlung dose in this case is given as

$$D_o = \int_0^{7\ \mathrm{MeV}} dE\ \frac{\Phi^o(H, \lambda)}{4}\ d(T, Z, E, Z') \qquad (6.54)$$

*It should be pointed out that these values differ from the values calculated by Watts and Burrell [56] for a similar electron source for two reasons. First, Watts and Burrell calculate the dose behind a slab of material assuming that the photon source is a plane of isotropic emitters. As was pointed out in Sect. 5.4. the dose due to the uncollided photons from such a source falls off as E1 (μx) rather than $e^{-\mu x}$. This produces a change in the shape of the dose transmission vs material thickness relative to the shape calculated by Eq. 6.52. Second, they normalize their source strength to the total number of photons produced rather than the intensity at zero degrees as is done in the present treatment. If one modifies the above equations to apply to a plane source, attenuates the uncollided doses as E1 (μx), and normalizes the calculations to the total photon source strength, the results of the present calculation and those of Watts and Burrell for a "half-space isotropic" photon source agree remarkably well.

TABLE 6.8. TRANSMITTED TISSUE DOSE FROM BREMSSTRAHLUNG CAUSED BY AN ISOTROPIC FLUX OF ELECTRONS WITH AN ENERGY SPECTRUM GIVEN BY $N = Pe^{-PE}$ INCIDENT ON ONE SIDE OF A UNIT AREA OF AN Al SHIELD. [a]

	Thickness (g/cm^2)							
P	4.000	6.000	8.000	10.000	15.000	20.000	35.000	50.000
.5	.357-11	.362-11	.349-11	.338-11	.293-11	.242-11	.129-11	.674-12
1.0	.122-11	.123-11	.117-11	.114-11	.982-12	.781-12	.390-12	.190-12
1.5	.510-12	.515-12	.483-12	.470-12	.391-12	.312-12	.147-12	.668-13
2.0	.257-12	.259-12	.241-12	.235-12	.192-12	.152-12	.690-13	.296-13
2.5	.145-12	.147-12	.135-12	.132-12	.107-12	.838-13	.369-13	.152-13
3.0	.886-13	.895-13	.817-13	.799-13	.644-13	.501-13	.216-13	.861-14
3.5	.569-13	.575-13	.522-13	.511-13	.410-13	.317-13	.134-13	.520-14
4.0	.380-13	.384-13	.347-13	.340-13	.271-13	.209-13	.867-14	.330-14
4.5	.261-13	.264-13	.238-13	.233-13	.185-13	.142-13	.581-14	.217-14
5.0	.184-13	.186-13	.167-13	.164-13	.129-13	.988-14	.400-14	.147-14
5.5	.132-13	.134-13	.119-13	.117-13	.923-14	.703-14	.281-14	.102-14
6.0	.963-14	.975-14	.867-14	.852-14	.669-14	.508-14	.202-14	.722-15
6.5	.711-14	.720-14	.639-14	.629-14	.492-14	.372-14	.147-14	.519-15
7.0	.531-14	.538-14	.476-14	.468-14	.366-14	.276-14	.108-14	.378-15
7.5	.400-14	.406-14	.358-14	.352-14	.275-14	.207-14	.804-15	.279-15
8.0	.304-14	.308-14	.271-14	.267-14	.208-14	.157-14	.604-15	.208-15
8.5	.233-14	.236-14	.207-14	.204-14	.159-14	.119-14	.457-15	.156-15
9.0	.179-14	.182-14	.159-14	.157-14	.122-14	.914-15	.349-15	.118-15
9.5	.139-14	.141-14	.123-14	.121-14	.941-15	.705-15	.268-15	.901-16
10.0	.108-14	.109-14	.955-15	.947-15	.730-15	.546-15	.207-15	.691-16

[a] The top heading gives the thickness of Al in g/cm^2. The first column gives the value of P. The remaining columns give the transmitted tissue dose in (Rad cm^2/Sr incident electron).

TABLE 6.9. TRANSMITTED TISSUE DOSE FROM BREMSSTRAHLUNG CAUSED BY AN ISOTROPIC FLUX OF ELECTRONS WITH AN ENERGY SPECTRUM GIVEN BY $N = Pe^{-PE}$ INCIDENT ON ONE SIDE OF A UNIT AREA OF A Pb SHIELD. [a]

	Thickness (g/cm^2)					
P	2.000	4.000	10.000	20.000	40.000	50.000
.5	.856-11	.839-11	.558-11	.335-11	.114-11	.696-12
1.0	.274-11	.249-11	.154-11	.860-12	.265-12	.154-12
1.5	.110-11	.926-12	.527-12	.272-12	.750-13	.416-13
2.0	.539-12	.429-12	.226-12	.108-12	.270-13	.143-13
2.5	.300-12	.228-12	.112-12	.502-13	.115-13	.590-14
3.0	.182-12	.133-12	.613-13	.257-13	.543-14	.272-14
3.5	.117-12	.822-13	.357-13	.141-13	.278-14	.136-14
4.0	.785-13	.532-13	.218-13	.813-14	.150-14	.716-15
4.5	.545-13	.356-13	.138-13	.487-14	.844-15	.394-15
5.0	.388-13	.245-13	.896-14	.300-14	.491-15	.224-15
5.5	.283-13	.173-13	.597-14	.190-14	.293-15	.131-15
6.0	.210-13	.124-13	.406-14	.122-14	.178-15	.783-16
6.5	.158-13	.902-14	.280-14	.804-15	.111-15	.476-16
7.0	.121-13	.665-14	.197-14	.535-15	.699-16	.295-16
7.5	.937-14	.497-14	.140-14	.361-15	.447-16	.185-16
8.0	.733-14	.375-14	.100-14	.246-15	.289-16	.118-16
8.5	.578-14	.285-14	.727-15	.170-15	.189-16	.756-17
9.0	.461-14	.219-14	.532-15	.118-15	.125-16	.490-17
9.5	.370-14	.169-14	.393-15	.828-16	.832-17	.321-17
10.0	.299-14	.131-14	.292-15	.585-16	.558-17	.212-17

[a] The top heading gives the thickness of Pb in g/cm^2. The first column gives the value of P. The remaining columns give the transmitted tissue dose in (Rad cm^2/Sr incident electron).

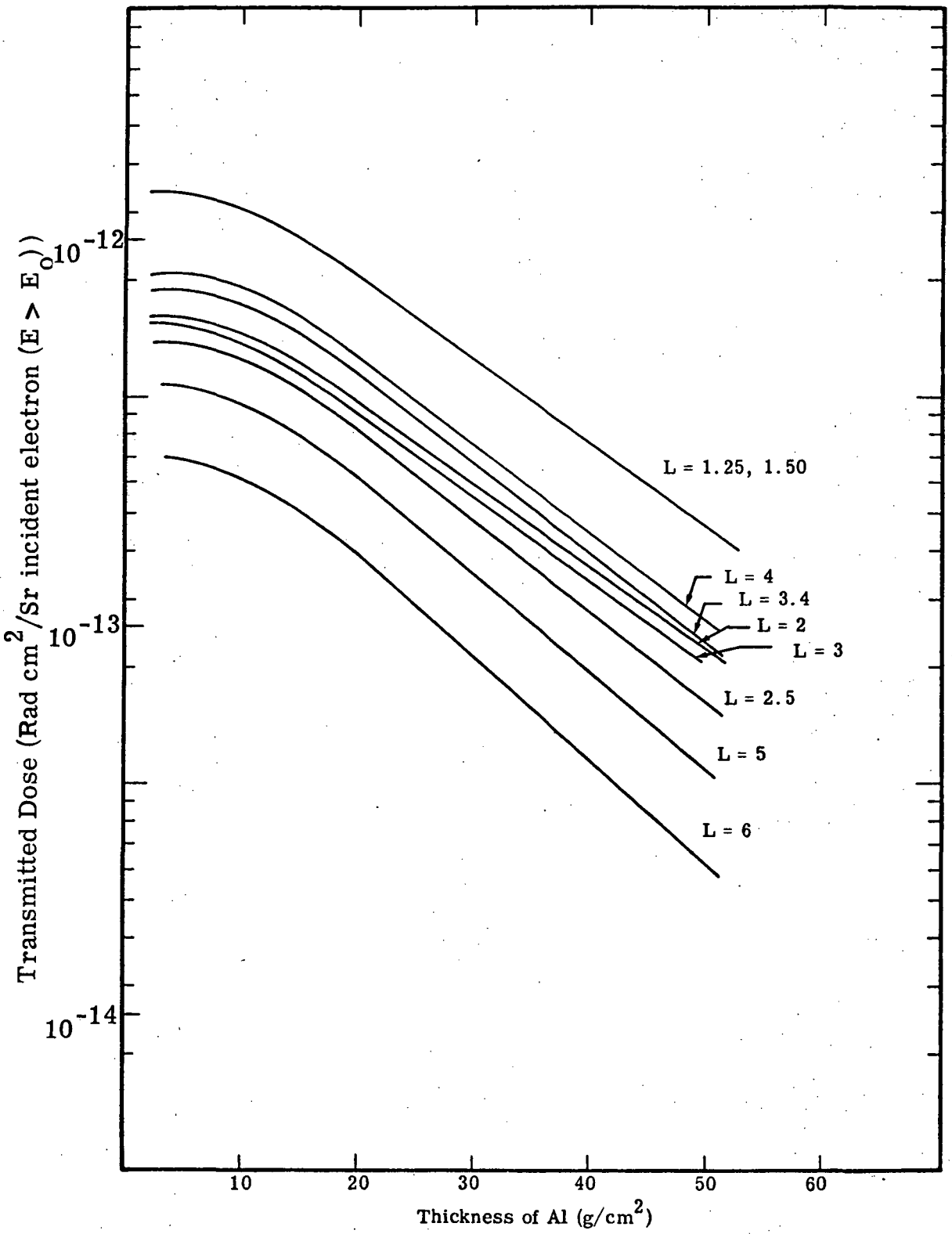

Figure 6.19. Bremsstrahlung tissue dose transmitted through an Al shield caused by an isotropic flux of electrons incident on a unit area of one side of the shield. The electron energy spectra are given by Vette's AE2 electron environment. The L values associated with the electron spectra are shown on the Figure. The curves are normalized per incident electron. (N. B. The AE2 Electron environment is considered to be outdated by space scientists.)

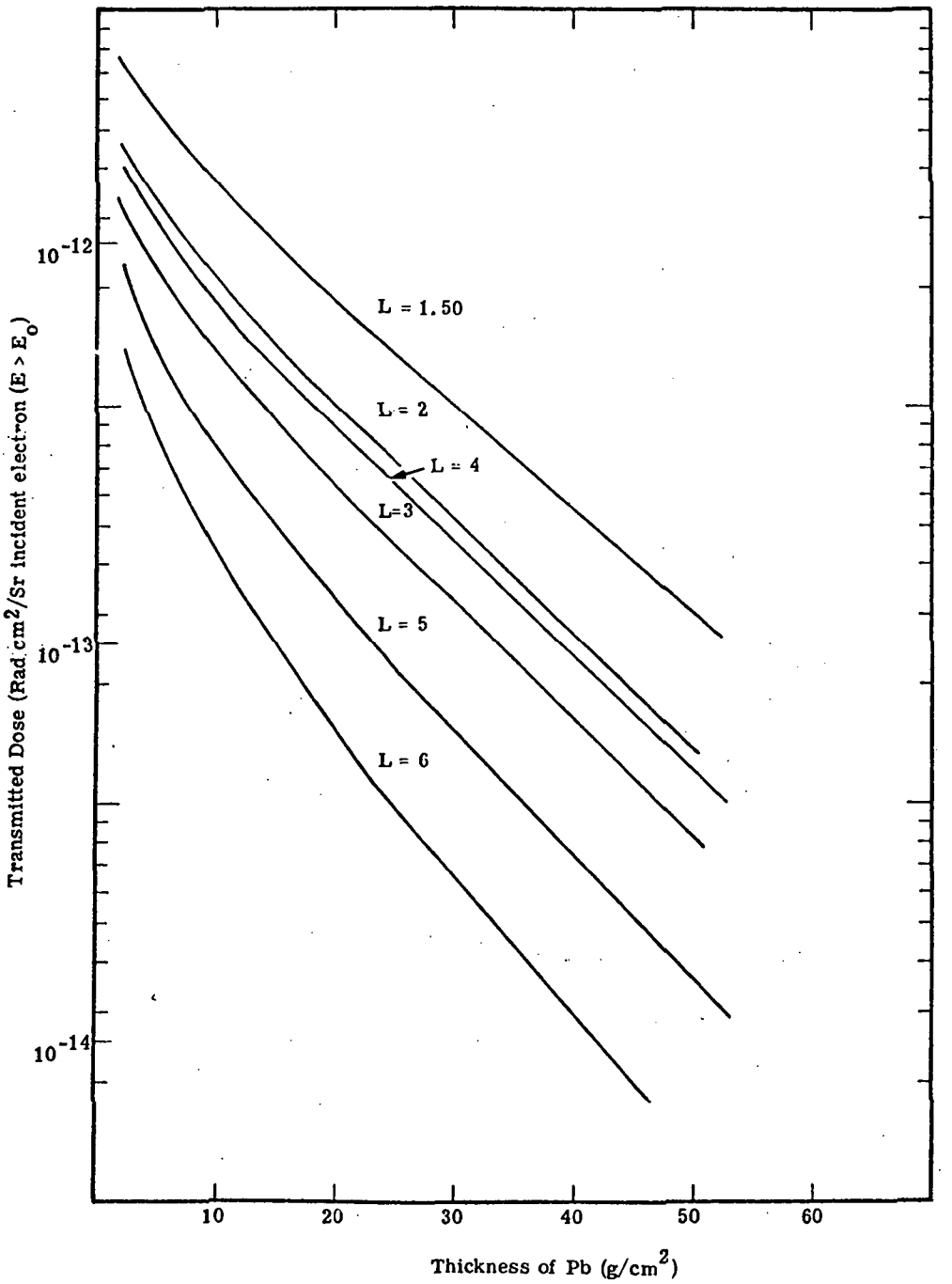

Figure 6.20. Bremsstrahlung tissue dose transmitted through a Pb shield caused by an isotropic flux of electrons incident on a unit area of one side of the shield. The electron energy spectra are given by Vette's AE2 electron environment. The L values associated with the electron spectra are shown on the Figure. The curves are normalized per incident electron. (N.B. The AE 2 electron environment is considered to be outdated.)

TABLE 6.10. TRANSMITTED BREMSSTRAHLUNG TISSUE DOSE CAUSED BY ISOTROPIC FLUXES OF ELECTRONS WITH ENERGY SPECTRA GIVEN BY VETTE'S AE2 ELECTRON DISTRIBUTION INCIDENT ON ONE SIDE OF A UNIT AREA OF AN Al SHIELD.
(Rad cm^2/Sr incident electron)

(N.B. The AE2 Electron environment is considered to be outdated by space scientists.)

L	Thickness (g/cm^2)							
	4	6	8	10	15	20	35	50
1.25	.136-11	.137-11	.128-11	.125-11	.104-11	.832-12	.396-12	.181-12
1.50	.132-11	.134-11	.126-11	.123-11	.102-11	.824-12	.395-12	.183-12
2.0	.652-12	.660-12	.616-12	.600-12	.500-12	.400-12	.192-12	.892-13
2.5	.560-12	.568-12	.524-12	.512-12	.420-12	.332-12	.151-12	.652-13
3.0	.628-12	.636-12	.588-12	.576-12	.472-12	.371-12	.168-12	.716-13
3.4	.756-12	.764-12	.712-12	.692-12	.572-12	.452-12	.208-12	.912-13
4.0	.848-12	.856-12	.800-12	.780-12	.644-12	.508-12	.236-12	.104-12
5.0	.436-12	.440-12	.404-12	.394-12	.319-12	.248-12	.108-12	.436-13
6.0	.281-12	.284-12	.257-12	.252-12	.200-12	.147-12	.640-13	.244-13

TABLE 6.11. TRANSMITTED BREMSSTRAHLUNG TISSUE DOSE CAUSED BY ISOTROPIC FLUXES OF ELECTRONS WITH ENERGY SPECTRA GIVEN BY VETTE'S AE2 ELECTRON DISTRIBUTION INCIDENT ON ONE SIDE OF A UNIT AREA OF AN Pb SHIELD.

(Rad cm^2/Sr incident electron)

(N.B. The AE2 Electron environment is considered to be outdated by space scientists.)

	Shield Thickness (g/cm^2)					
L	2	4	10	20	40	50
1.25	.302-11	.249-11	.144-11	.748-12	.207-12	.115-12
1.50	.300-11	.249-11	145-11	.772-12	.219-12	.122-12
2.0	.154-11	.122-11	.692-12	.372-12	.110-12	.628-13
2.50	.122-11	.940-12	.496-12	.239-12	.608-13	.326-13
3.0	.134-11	.104-12	.544-12	.258-12	.636-13	.337-13
3.4	.163-11	.130-11	.704-12	.346-12	.896-13	.484-13
4.0	.184-11	.147-11	.804-12	.399-12	.104-12	.564-13
5.0	.900-12	.668-12	.164-12	.136-12	.299-13	.152-13
6.0	.580-12	.394-12	.161-12	.604-13	.111-13	.532-14

where $\Phi^{o}(H, \lambda)$ is the orbital integrated electron flux for a circular orbit of height H and inclination λ averaged over one day with units of

$$\left(\frac{\text{electrons}}{\text{MeV cm}^2 \text{ day}} \right)$$

The units of D_o are

$$\left(\frac{\text{Rad}}{\text{Sr day}} \right).$$

The values of D_o are listed in Tables 6.12 and 6.13 for Al and Pb shields. Figure 6.21 shows the values of D_o for 30° orbital inclination for shield thickness of 1 and 10 g/cm^2 as a function of orbital height.

6.5 UNCERTAINTIES AND ERRORS

There have been several assumptions made in the development of the formalism of Section 6. The errors and uncertainties these assumptions can introduce into the final results will be discussed here. The assumptions which have been made are:

- The primary electron flux is isotropic.
- The shielding material is thin compared to other dimensions in the problem.
- The effect of interior shielding can be replaced by selectively increasing the thickness of the surface shielding. This is a complex geometry problem and requires the use of sophisticated computer codes to analysis.
- The angular distribution of the radiation which reaches the interior surface of the shield is emitted from a differential area of that surface with a cosine distribution with respect to the surface normal (this assumption is equivalent to assuming that the geometry of the shield is spherically symmetric about the point of interest).

The possible errors introduced by the use of these assumptions will be discussed below.

6.5.1 Isotropic Electron Flux

The electron flux encountered in space is not isotropic. At any point in space where there is trapped radiation more electrons will be moving perpendicular to the magnetic field lines than in any other direction. Also, there will be no electrons traveling in the direction of the magnetic field line within the electron loss cone. One expects that the assumption of isotropic electron fluxes will lead to errors in the instantaneous dose rates.

TABLE 6.12. TRANSMITTED TISSUE DOSE FOR CIRCULAR ORBITS FROM BREMSSTRAHLUNG CAUSED BY AN ISOTROPIC FLUX OF ELECTRONS INCIDENT ON ONE SIDE OF A UNIT SOLID ANGLE OF AN Al SHIELD. [a]

Inclination (deg)	Thickness (g/cm^2) 1.750	2.000	4.000	6.000	8.000	10.000	15.000	20.000	35.000	50.000
30.	.243-05	.333-05	.336-05	.341-05	.303-05	.298-05	.235-05	.179-05	.728-06	.273-06
60.	.345-03	.449-03	.451-03	.455-03	.420-03	.410-03	.334-03	.262-03	.117-03	.489-04
0.	.219-07	.303-07	.302-07	.305-07	.272-07	.268-07	.211-07	.161-07	.647-08	.236-08
30.	.941-03	.110-02	.119-02	.121-02	.117-02	.114-02	.997-03	.833-03	.470-03	.263-03
60.	.651-03	.856-03	.860-03	.869-03	.796-03	.778-03	.630-03	.491-03	.215-03	.886-04
0.	.411-04	.562-04	.567-04	.573-04	.512-04	.503-04	.396-04	.302-04	.122-04	.449-05
30.	.122-02	.167-02	.169-02	.171-02	.153-02	.150-02	.118-02	.902-03	.366-03	.137-03
60.	.184-02	.244-02	.246-02	.248-02	.226-02	.221-02	.178-02	.138-02	.594-03	.239-03
0.	.217-02	.296-02	.299-02	.302-02	.270-02	.265-02	.209-02	.159-02	.646-03	.240-03
30.	.446-02	.610-02	.616-02	.624-02	.556-02	.546-02	.431-02	.328-02	.133-02	.501-03
60.	.516-02	.687-02	.692-02	.699-02	.635-02	.621-02	.499-02	.386-02	.165-02	.663-03
0.	.196-01	.267-01	.270-01	.273-01	.244-01	.240-01	.189-01	.144-01	.586-02	.220-02
30.	.196-01	.269-01	.272-01	.275-01	.245-01	.241-01	.190-01	.145-01	.588-02	.222-02
60.	.142-01	.191-01	.192-01	.194-01	.175-01	.172-01	.137-01	.106-01	.444-02	.175-02
0.	.766-01	.105+00	.106+00	.107+00	.955-01	.939-01	.740-01	.565-01	.230-01	.865-02
30.	.545-01	.745-01	.753-01	.763-01	.679-01	.668-01	.527-01	.401-01	.163-01	.614-02
60.	.327-01	.442-01	.446-01	.452-01	.405-01	.398-01	.316-01	.243-01	.101-01	.391-02
0.	.226+00	.310+00	.313+00	.317+00	.282+00	.278+00	.219+00	.167+00	.678-01	.255-01
30.	.112+00	.153+00	.154+00	.156+00	.139+00	.137+00	.108+00	.821-01	.333-01	.126-01
60.	.669-01	.908-01	.917-01	.928-01	.831-01	.816-01	.647-01	.496-01	.205-01	.791-02
0.	.363+00	.497+00	.503+00	.509+00	.453+00	.445+00	.351+00	.267+00	.108+00	.408-01
30.	.140+00	.191+00	.194+00	.196+00	.174+00	.171+00	.135+00	.103+00	.417-01	.157-01
60.	.896-01	.122+00	.123+00	.124+00	.111+00	.109+00	.866-01	.664-01	.275-01	.106-01
0.	.320+00	.439+00	.444+00	.450+00	.399+00	.393+00	.309+00	.235+00	.953-01	.358-01
30.	.105+00	.143+00	.145+00	.147+00	.130+00	.128+00	.101+00	.769-01	.312-01	.118-01
60.	.798-01	.108+00	.109+00	.110+00	.988-01	.970-01	.772-01	.593-01	.247-01	.965-02
0.	.128+00	.175+00	.178+00	.180+00	.160+00	.157+00	.124+00	.944-01	.384-01	.145-01
30.	.524-01	.716-01	.725-01	.734-01	.653-01	.642-01	.506-01	.386-01	.157-01	.599-02
60.	.584-01	.780-01	.786-01	.795-01	.720-01	.705-01	.566-01	.438-01	.187-01	.750-02

(a) The top heading gives the thickness of Al in g/cm^2. The first column gives the value of P. The remaining columns give the transmitted tissue dose in (Rad/Sr day).

TABLE 6.12 (CONTINUED)

Height (nm)	Inclination (deg)	Thickness (g/cm^2) 1.750	2.000	4.000	6.000	8.000	10.000	15.000	20.000	35.000	50.000
2250	0°	.528-01	.718-01	.728-01	.738-01	.657-01	.646-01	.511-01	.391-01	.161-01	.628-02
	30°	.220-01	.299-01	.302-01	.306-01	.274-01	.269-01	.213-01	.163-01	.678-02	.266-02
	60°	.475-01	.626-01	.629-01	.636-01	.582-01	.568-01	.460-01	.359-01	.157-01	.646-02
2500	0°	.231-01	.315-01	.319-01	.323-01	.288-01	.283-01	.224-01	.171-01	.710-02	.277-02
	30°	.134-01	.179-01	.182-01	.184-01	.165-01	.162-01	.129-01	.998-02	.424-02	.171-02
	60°	.484-01	.636-01	.638-01	.645-01	.592-01	.578-01	.469-01	.367-01	.162-01	.673-02
2750	0°	.151-01	.204-01	.207-01	.210-01	.187-01	.184-01	.146-01	.112-01	.467-02	.185-02
	30°	.126-01	.167-01	.169-01	.171-01	.155-01	.152-01	.123-01	.954-02	.417-02	.174-02
	60°	.515-01	.674-01	.677-01	.683-01	.628-01	.614-01	.499-01	.391-01	.173-01	.721-02
3000	0°	.118-01	.160-01	.163-01	.165-01	.147-01	.145-01	.115-01	.882-02	.369-02	.147-02
	30°	.161-01	.213-01	.212-01	.214-01	.196-01	.192-01	.156-01	.122-01	.544-02	.232-02
	60°	.575-01	.752-01	.755-01	.762-01	.702-01	.685-01	.557-01	.436-01	.194-01	.809-02
3500	0°	.109-01	.147-01	.149-01	.151-01	.135-01	.133-01	.106-01	.818-02	.349-02	.143-02
	30°	.324-01	.420-01	.422-01	.426-01	.394-01	.384-01	.314-01	.248-01	.112-01	.486-02
	60°	.672-01	.877-01	.881-01	.889-01	.819-01	.799-01	.651-01	.510-01	.227-01	.953-02
4000	0°	.154-01	.205-01	.209-01	.211-01	.191-01	.187-01	.150-01	.117-01	.513-02	.217-02
	30°	.598-01	.773-01	.777-01	.784-01	.726-01	.708-01	.581-01	.458-01	.208-01	.903-02
	60°	.793-01	.103+00	.104+00	.105+00	.966-01	.943-01	.769-01	.603-01	.269-01	.113-01
4500	0°	.312-01	.412-01	.417-01	.422-01	.384-01	.376-01	.304-01	.237-01	.104-01	.440-02
	30°	.102+00	.132+00	.133+00	.134+00	.124+00	.121+00	.994-01	.784-01	.357-01	.154-01
	60°	.939-01	.122+00	.123+00	.124+00	.114+00	.111+00	.910-01	.715-01	.320-01	.135-01
5000	0°	.518-01	.673-01	.678-01	.686-01	.632-01	.617-01	.505-01	.398-01	.181-01	.788-02
	30°	.141+00	.181+00	.182+00	.184+00	.171+00	.166+00	.137+00	.108+00	.492-01	.213-01
	60°	.110+00	.143+00	.144+00	.145+00	.134+00	.131+00	.107+00	.842-01	.378-01	.161-01
5500	0°	.976-01	.126+00	.127+00	.128+00	.119+00	.116+00	.950-01	.751-01	.345-01	.152-01
	30°	.191+00	.246+00	.247+00	.249+00	.231+00	.225+00	.185+00	.146+00	.668-01	.290-01
	60°	.130+00	.168+00	.169+00	.170+00	.158+00	.154+00	.126+00	.989-01	.446-01	.191-01
6000	0°	.163+00	.209+00	.210+00	.212+00	.197+00	.192+00	.158+00	.125+00	.577-01	.254-01
	30°	.242+00	.311+00	.312+00	.315+00	.293+00	.285+00	.234+00	.185+00	.845-01	.366-01
	60°	.147+00	.190+00	.191+00	.193+00	.179+00	.174+00	.142+00	.112+00	.507-01	.217-01
7000	0°	.329+00	.422+00	.423+00	.427+00	.398+00	.387+00	.319+00	.253+00	.116+00	.510-01
	30°	.324+00	.417+00	.419+00	.422+00	.392+00	.382+00	.314+00	.248+00	.113+00	.492-01
	60°	.172+00	.222+00	.223+00	.225+00	.208+00	.203+00	.166+00	.131+00	.592-01	.253-01
8000	0°	.422+00	.542+00	.543+00	.548+00	.510+00	.497+00	.409+00	.324+00	.148+00	.646-01
	30°	.319+00	.412+00	.414+00	.417+00	.387+00	.377+00	.309+00	.243+00	.110+00	.469-01
	60°	.165+00	.214+00	.214+00	.216+00	.200+00	.195+00	.160+00	.126+00	.565-01	.240-01
9000	0°	.393+00	.507+00	.508+00	.513+00	.476+00	.464+00	.381+00	.300+00	.137+00	.588-01
	30°	.263+00	.343+00	.344+00	.347+00	.320+00	.313+00	.255+00	.200+00	.893-01	.375-01
	60°	.134+00	.175+00	.175+00	.177+00	.163+00	.159+00	.130+00	.102+00	.453-01	.190-01
10000	0°	.303+00	.395+00	.396+00	.400+00	.369+00	.360+00	.293+00	.230+00	.102+00	.427-01
	30°	.198+00	.260+00	.261+00	.264+00	.242+00	.236+00	.192+00	.150+00	.655-01	.268-01
	60°	.997-01	.131+00	.132+00	.133+00	.122+00	.119+00	.964-01	.753-01	.330-01	.135-01

TABLE 6.13. TRANSMITTED TISSUE DOSE FOR CIRCULAR ORBITS FROM BREMSSTRAHLUNG CAUSED BY AN ISOTROPIC FLUX OF ELECTRONS INCIDENT ON ONE SIDE OF A UNIT SOLID ANGLE OF A Pb SHIELD.[a]

Height (nm)	Inclination (deg)	Thickness (g/cm^2) 2.000	4.000	10.000	20.000	40.000	50.000
150	30.	.783-05	.454-05	.157-05	.582-06	.139-06	.786-07
	60.	.952-03	.724-03	.363-03	.168-03	.406-04	.214-04
300	0.	.649-07	.397-07	.139-07	.457-08	.773-09	.365-09
	30.	.315-02	.314-02	.217-02	.138-02	.520-03	.333-03
	60.	.185-02	.134-02	.635-03	.286-03	.689-04	.366-04
450	0.	.123-03	.751-04	.264-04	.895-05	.167-05	.836-06
	30.	.392-02	.228-02	.792-03	.291-03	.687-04	.386-04
	60.	.537-02	.369-02	.165-02	.716-03	.170-03	.908-04
600	0.	.661-02	.399-02	.141-02	.497-03	.103-03	.545-04
	30.	.143-01	.831-02	.290-02	.107-02	.254-03	.143-03
	60.	.152-01	.103-01	.450-02	.193-02	.463-03	.248-03
800	0.	.610-01	.364-01	.129-01	.470-02	.107-02	.591-03
	30.	.632-01	.367-01	.128-01	.475-02	.115-02	.651-03
	60.	.433-01	.276-01	.113-01	.467-02	.113-02	.615-03
1000	0.	.243+00	.143+00	.503-01	.186-01	.443-02	.249-02
	30.	.178+00	.102+00	.352-01	.132-01	.325-02	.186-02
	60.	.102+00	.629-01	.243-01	.980-02	.239-02	.133-02
1250	0.	.737+00	.423+00	.147+00	.548-01	.135-01	.775-02
	30.	.367+00	.209+00	.716-01	.268-01	.673-02	.387-02
	60.	.213+00	.128+00	.482-01	.192-01	.476-02	.267-02
1500	0.	.120+01	.678+00	.231+00	.865-01	.218-01	.126-01
	30.	.466+00	.261+00	.889-01	.334-01	.851-02	.492-02
	60.	.286+00	.172+00	.646-01	.259-01	.649-02	.365-02
1750	0.	.108+01	.598+00	.201+00	.751-01	.193-01	.112-01
	30.	.353+00	.196+00	.663-01	.251-01	.649-02	.378-02
	60.	.254+00	.155+00	.604-01	.248-01	.620-02	.346-02
2000	0.	.436+00	.241+00	.822-01	.316-01	.835-02	.489-02
	30.	.179+00	.991-01	.342-01	.133-01	.357-02	.209-02
	60.	.179+00	.117+00	.501-01	.218-01	.542-02	.297-02
2250	0.	.186+00	.102+00	.366-01	.153-01	.440-02	.262-02
	30.	.761-01	.429-01	.158-01	.669-02	.190-02	.112-02
	60.	.139+00	.978-01	.459-01	.208-01	.515-02	.278-02
2500	0.	.817-01	.451-01	.163-01	.688-02	.199-02	.119-02
	30.	.453-01	.269-01	.108-01	.486-02	.139-02	.808-03
	60.	.138+00	.101+00	.488-01	.223-01	.546-02	.291-02
2750	0.	.537-01	.297-01	.110-01	.478-02	.141-02	.845-03
	30.	.408-01	.263-01	.118-01	.557-02	.156-02	.895-03
	60.	.145+00	.108+00	.528-01	.243-01	.592-02	.315-02

(a) The top heading gives the thickness of Pb in g/cm^2. The first column gives the value of P. The remaining columns give the transmitted tissue dose in (Rad/Sr day).

TABLE 6.13 (CONTINUED)

Height (nm)	Inclination (deg)	Thickness (g/cm^2) 2.000	4.000	10.000	20.000	40.000	50.000
	0.	.424-01	.236-01	.884-02	.390-02	.116-02	.694-03
3000	30.	.494-01	.343-01	.165-01	.799-02	.220-02	.124-02
	60.	.161+00	.120+00	.595-01	.274-01	.667-02	.354-02
	0.	.387-01	.223-01	.898-02	.417-02	.126-02	.751-03
3500	30.	.939-01	.704-01	.361-01	.177-01	.475-02	.263-02
	60.	.187+00	.141+00	.705-01	.326-01	.802-02	.427-02
	0.	.526-01	.328-01	.145-01	.702-02	.213-02	.126-02
4000	30.	.169+00	.130+00	.679-01	.332-01	.881-02	.484-02
	60.	.221+00	.167+00	.839-01	.391-01	.968-02	.518-02
	0.	.966-01	.659-01	.304-01	.144-01	.407-02	.235-02
4500	30.	.285+00	.223+00	.117+00	.567-01	.148-01	.804-02
	60.	.261+00	.199+00	.101+00	.473-01	.118-01	.635-02
	0.	.149+00	.113+00	.581-01	.288-01	.806-02	.456-02
5000	30.	.390+00	.307+00	.162+00	.788-01	.206-01	.113-01
	60.	.306+00	.235+00	.120+00	.566-01	.143-01	.766-02
	0.	.274+00	.217+00	.115+00	.575-01	.159-01	.894-02
5500	30.	.527+00	.417+00	.221+00	.108+00	.281-01	.153-01
	60.	.358+00	.278+00	.143+00	.681-01	.173-01	.930-02
	0.	.452+00	.361+00	.194+00	.964-01	.261-01	.145-01
6000	30.	.665+00	.527+00	.279+00	.136+00	.351-01	.190-01
	60.	.405+00	.315+00	.163+00	.779-01	.197-01	.106-01
	0.	.904+00	.727+00	.393+00	.195+00	.511-01	.278-01
6500	30.	.890+00	.707+00	.376+00	.183+00	.473-01	.256-01
	60.	.472+00	.368+00	.192+00	.913-01	.229-01	.123-01
	0.	.116+01	.926+00	.498+00	.244+00	.629-01	.340-01
7000	30.	.874+00	.683+00	.355+00	.169+00	.420-01	.224-01
	60.	.453+00	.351+00	.181+00	.851-01	.211-01	.112-01
	0.	.108+01	.850+00	.448+00	.216+00	.544-01	.291-01
7500	30.	.723+00	.554+00	.280+00	.129+00	.312-01	.165-01
	60.	.368+00	.281+00	.141+00	.652-01	.157-01	.825-02
	0.	.831+00	.634+00	.318+00	.146+00	.347-01	.181-01
8000	30.	.546+00	.405+00	.195+00	.863-01	.197-01	.102-01
	60.	.275+00	.204+00	.981-01	.434-01	.991-02	.511-02

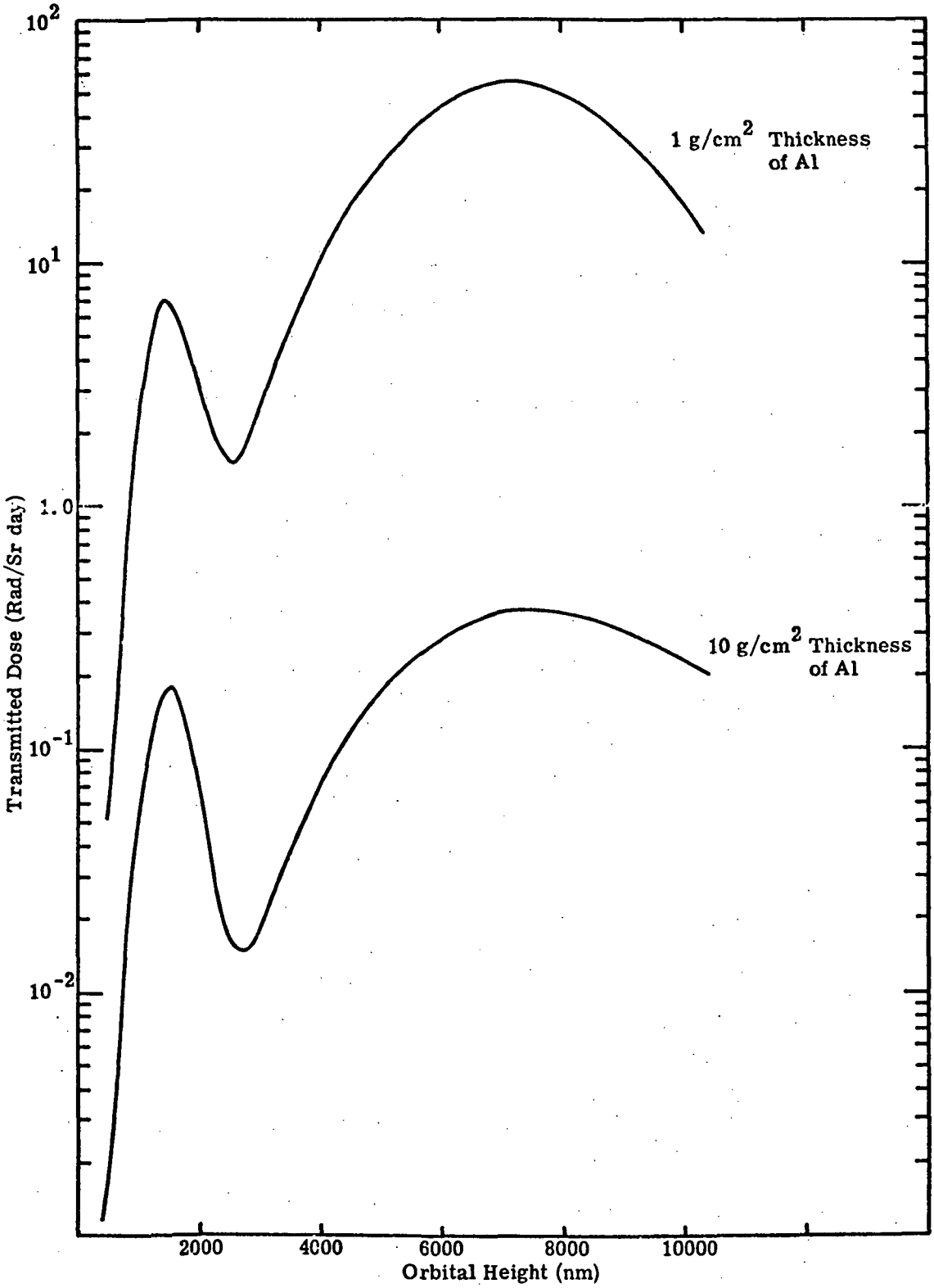

Figure 6.21. Tissue dose transmitted through an Al shield for circular orbital integrations at 30^{o} inclination as a function of orbital height in nautical miles. The top curve is for a shield of $1 g/cm^2$ the bottom for a shield of $10 g/cm^2$.

A simple example will serve to illustrate the uncertainty in instantaneous measurements introduced by the assumption of isotropic electron fluxes. Consider, for example, a spherical Al spacecraft which has considerable shielding (10 g/cm^2) everywhere except for a small window which subtends 0.1 Sr and whose thickness is 0.5 g/cm^2. If the window is directed into the electron loss cone one would expect a much lower dose rate than if the window were randomly oriented with respect to the magnetic field lines. For a 2000 nm circular orbit at a 30-degree inclination the dose for the first case would be due entirely to bremsstrahlung, and from Table 6.12 would be

$$D\left(\frac{\text{Rad}}{\text{day}}\right) = 0.075\ (4\pi - .1) = 0.125\ \text{R/day} \quad . \tag{6.55}$$

For the second case the dose would be mainly due to electron penetration, and from Tables 6.3 and 6.12 would be

$$D\left(\frac{\text{Rad}}{\text{day}}\right) = 54.6 \times 0.1 + 0.075\ (4\pi - 0.1) = 5.5\ \text{R/day} \tag{6.56}$$

or a factor of 40 higher than the first case.

Thus, instantaneous dose rates may be substantially in error if one assumes an isotropic primary electron flux. Average doses or doses for orbital integrations should be substantially more accurate, however.

6.5.2 Thin Shields

For most applications the assumption that the shields are thin with respect to other dimensions in the problem should be valid since the range of 6-MeV electrons in Al is less than one inch. The physical dimensions of the entire system will be typically on the order of several feet so little error will be introduced in assuming a thin shield. Also, shielding on the order of feet of material will produce enough attenuation so that the radiation from other portions of the shield will dominate the problem and only small errors will be introduced.

6.5.3 Assumption of Spherical Geometry (or of a cos θ distribution for the penetrating radiation)

The errors introduced by assuming a spherical shield geometry surrounding the dose point (or equivalently, assuming a cos θ distribution of the penetrating radiation) cannot be calculated unless the actual geometry of the problem is known. An estimate of the error for a shield thickness less than about 10 g/cm^2 can be obtained by assuming a uniform spherical geometry and calculating the flux of particles through a spherical isotropic detector at different positions inside the sphere. The number of particles through

this detector, as a function of the distance from the center of the sphere, will be given by the expression

$$N(r) = 2\pi \int_0^{\pi} \frac{J_s^{iso}(\theta_n) \sin \theta d\theta}{\cos \theta_n} \qquad (6.57)$$

where $J_s^{iso}(\theta_n)$ is the actual angular distribution of the radiation emerging from a unit differential area of the surface, θ_n is the angle between the direction to the detector from an element of the surface and the surface normal at that point. The geometry is shown in Fig. 6.22. The relationship between θ and θ_n is given by

$$\sin \theta_n = \frac{r}{R} \sin \theta \quad , \qquad (6.58)$$

where r is the displacement of the detector from the center of the sphere and R is the radius of the sphere. For electron penetration $I(\theta_n)$ is given as $I(\theta_n) = 0.23\ (0.717 + \cos \theta_n) \cos \theta_n$ and $N(r)$ reduces to

$$N(r) = 2\pi\,(0.717) \cdot 2 + 2\pi \int_0^{\pi} \left[1 - \frac{r^2}{R^2} \sin^2 \theta\right]^{1/2} \sin \theta\, d\theta \qquad (6.59)$$

which can be integrated to yield

$$N(r) = .92\pi\,(0.717) + .46\pi \left[1 + \frac{1}{2}\left(\frac{R}{r} - \frac{r}{R}\right) \ln\left(\frac{R+r}{R-r}\right)\right] . \qquad (6.60)$$

Thus for electron penetration $N(r)$ decreases from a value of

$$N(0) = .92\pi\,(1.717) = 4.95 \qquad (6.61)$$

at $r = 0$ (the center of the sphere) to a value of

$$N(R) = .46\pi\,(2.434) = 3.52 \qquad (6.62)$$

at $r = R$ or the surface of the sphere. This corresponds to intensities approximately 40 percent higher at the center of the sphere than at the edges. The angular distribution for bremsstrahlung produced in electron range thick targets by an isotropic flux of electrons incident on one side of the target range can be calculated assuming a $\cos \theta_n$ distribution for the high energy photons and a $\cos^{1/2} \theta_n$ distribution for the low energy photons. The photon intensity for a geometry such as shown in Fig. 6.22 will be constant as a function of r for a $\cos \theta_n$ distribution and will be given by the expression

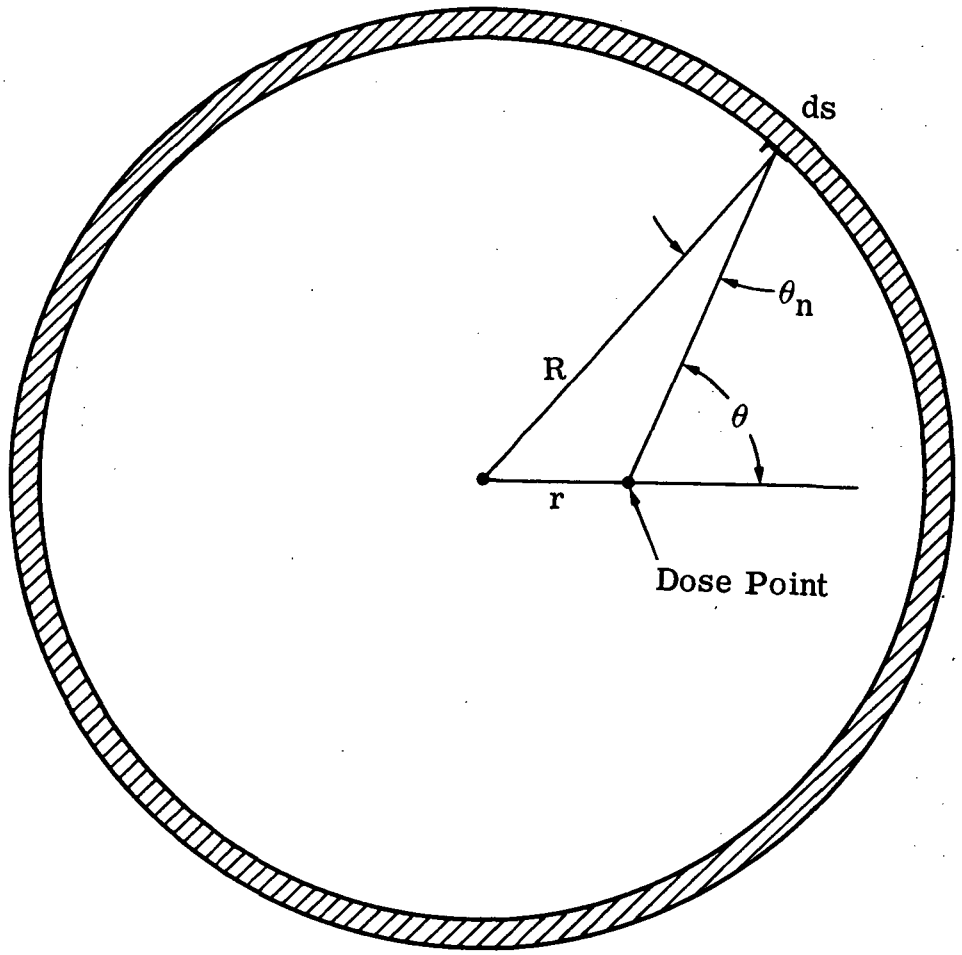

Figure 6.22. Geometry for calculation of error introduced by assuming spherical dose point centered geometry.

$$N(r) = 2\pi \int_0^{\pi} \sin\theta \, d\theta \left[1 - \frac{r^2}{R^2} \sin^2\theta \right]^{1/4}$$

for a $\cos^{1/2}\theta_n$ distribution. The function N(r) for this case increases by a factor of two as one increases r from zero to R.

For shields thicker than about 6 g/cm^2 only the bremsstrahlung will be important. As the shield thickness increases, the transported photon angular distribution will become progressively more forward peaked. For shields thicker than about one mean free path the assumption of a $\cos\theta_n$ distribution will become progressively worse and substantial errors will result. Problems such as these (unless they are spherically symmetric to begin with) are best done with photon transport codes.

6.6 ELECTRON TRANSPORT USING THE STRAIGHT-AHEAD AND CONTINUOUS SLOWING-DOWN APPROXIMATIONS

Most problems which deal with the penetration of protons and other heavy charged particles through material use the straight-ahead approximation. The particles are assumed to slow down in a straight line, losing energy continuously as they stop. The angular distributions of the particles from their original lines of travel caused by multiple electron or nuclear scattering are assumed to be small. For protons and other heavy charged particles this approximation is very good. Electrons, on the other hand, can suffer large deviation from their original lines of travel as they slow down and can suffer large energy losses in any given collision. It would seem, then, that the straight-ahead-continuous slowing approximation would not be good for electrons. Nevertheless, this approximation offers distinct advantages for complex geometry calculations and is useful for obtaining order of magnitude estimates for these types of problems.

6.6.1 Straight-Ahead Approximation For Electrons

It is assumed in this approximation that the electrons have a well defined range; that is all of the electrons of a given energy are assumed to traverse the same thickness of material before they are stopped. It is also assumed that the energy of the electrons after traversing a given thickness of material is given by a function which depends on the energy of incident electrons, the atomic number of the material, and the thickness

of the material along the electron's line of motion. These assumptions should be contrasted with the experimental observations that the transmitted fraction is a smoothly varying function of the material thickness (See Fig. 3.3) and not a step function, that the energy spectrum of the transmitted electrons (See Fig. 3.6) is smeared and not a delta function and that the angular distribution of originally monodirectional electrons is quite broad after penetrating fairly small thicknesses of material (See Fig. 3.7), and not a delta function. Obviously, the straight-ahead-continuous slowing down model is a very poor approximation for monodirectional beams of monoenergetic electrons incident on a material. For problems dealing with electrons which have a broad spectrum of energies many of the errors introduced by the model cancel, however, and reasonable results are obtained.

6.6.2 Space Applications of the Straight-Ahead Approximation For Electron Transport

If a coordinate system is set up at a dose point on the interior of a space craft, the penetrating flux of electrons from the direction $\bar{\Omega}$ in the solid angle $d\Omega$ with energies between E' and $E' + dE'$ will be given in the straight-ahead approximation as

$$\varphi(E',\bar{\Omega})\, dE' = \varphi(E,\bar{\Omega})\, dE \quad , \tag{6.64}$$

if the "range" of the electrons of energy E is greater than the shield thickness along the direction $\bar{\Omega}$ and

$$\varphi(E',\bar{\Omega})\, dE' = 0 \quad , \tag{6.65}$$

if the "range" of the electrons of energy E is less than the shield thickness along the direction $\bar{\Omega}$. In Eq. 6.64 $\varphi(E, \bar{\Omega})$ is the primary electron flux between the energies E and $E + dE$ in the direction $\bar{\Omega}$ about the solid angle $d\Omega$. The energy of the penetrating electrons E' is assumed to be a function of the initial energy E and the shield thickness $t(\bar{\Omega})$ along the direction $\bar{\Omega}$

$$E' = F(E, t(\bar{\Omega})) \tag{6.66}$$

The dose at the point is given by weighting the transmitted flux $\varphi(E', \bar{\Omega})$ by the flux to dose conversion function (See Appendix C) and integrating over the transmitted energy dE' and the solid angle $d\Omega$ Thus the dose is

$$D_{Tot}(Z') = \int_{4\pi} d\Omega \int dE' \; \varphi(E', \bar{\Omega}) \; \kappa \frac{dE}{dX}(E', Z') \qquad (6.67)$$

where $\kappa \frac{dE}{dX}(E', Z')$ is the flux to dose conversion function for the dose material Z'. Equation 6.67 can be solved if the primary flux $\varphi(E, \bar{\Omega})$, the transmitted energy function $F(E, t(\bar{\Omega}))$ and the thickness $t(\bar{\Omega})$ are known.

One method of obtaining an analytic expression for Eq. 6.67 is given by Watts and Burrell (58) who use a parameterization for the extrapolated electron range (See Sec. 5.2.2) in Al to obtain a functional form for $F(E, t(\Omega))$. They use a parameterization of the extrapolated range

$$r_{ex}(E) = \left[\frac{E^2}{a^2} + b^2 \right]^{1/2} - b \quad (g/cm^2) \quad , \qquad (6.68)$$

where E is the electron kinetic energy in MeV, a is 1.92, and b is 0.11. The degraded electron energy after traversing a thickness of material, t, can be obtained from the relationship

$$r_{ex}(E) = r_{ex}(E') + t \qquad (6.69)$$

and is given in this parameterization as

$$E'^2 = a^2 \left\{ \left[\frac{E^2}{a^2} + b^2 \right]^{1/2} - t \right]^2 - b^2 \right\} \qquad (6.70)$$

they also obtain an expression for the instantaneous stopping power $\frac{dE}{dX}(E', Z')$ from the range formula since

$$\frac{dE}{dX} = - \frac{1}{\frac{dr}{dE}} \qquad (6.71)$$

Using these approximations the dose of Eq. 6.67 becomes

$$D_{Tot} = \kappa \int_{4\pi} d\Omega \int_{E_{min}(\Omega)}^{\infty} dE \quad \varphi(\bar{\Omega}, E)\, a \frac{\left[E'(\Omega)^2 + b^2\right]^{1/2}}{E'(\Omega)} \qquad (6.72)$$

where $\varphi(\bar{\Omega}, E)$ is the differential primary electron flux and $E'(\Omega)$ is given for different thickness of material $t(\Omega)$ by Eq. 6.70. The minimum energy limit on the integral $E_{min}(\Omega)$ is the minimum electron energy for which penetration will occur and is given as

$$E_{min}(\Omega) = a\left[2\,b\,t(\Omega) + t^2(\Omega)\right]^{1/2} \qquad (6.73)$$

Alternatively, Eq. 6.72 could have been written as an integral over the degraded energy E'. The equations seem to be equally complex.

6.6.3 Comparison of Straight-Ahead Approximation to Other Methods

The simplest comparison for a broad beam situation is to compare the doses one would obtain for a broad parallel monoenergetic beam of electrons normally incident on a slab of material using the parameterization of Sec. 5 and the straight ahead approximation. For the parameterization of Sec. 5 the dose at a point detector behind the slab would be given by

$$D = \kappa \int_{2\pi} d\Omega \int_{0}^{E} dE' \quad T(Z,E,t)\ \phi(\theta)\, S(E,E',T) \qquad (6.74)$$

$$\times \frac{dE}{dX}(E',Z')\ \frac{1}{\cos\theta}$$

where $T(Z,E,t)$, $\phi(\theta)$, and $S(E, E', t)$ are the transmitted fraction, angular distribution (not to be confused with primary or secondary flux) and transmitted energy spectrum defined in Sec. 5.2. The $\cos\theta$ factor in the denominator of Eq. 6.74 converts the angular distribution which is a current to a flux. Using the expression for $\phi(\theta)$ given by Eq. 5.9 for shield thickness greater than 0.3

the extrapolated range

$$\varphi = 0.23\,(0.717 + \cos\theta)\,\cos\theta \tag{6.75}$$

yields a total dose given for the parameterization as

$$D_{Par} = 1.75\,T\,(Z,E,t)\;\kappa\int_{o}^{E} dE'\,\frac{dE}{dX}\;(E',Z')\,S(E,E',t) \tag{6.76}$$

The dose calculated using the straight ahead model for the similar geometry is given as

$$D_{SA} = \kappa\int_{o}^{E} dE''\;\frac{dE''}{dX}\;\delta(E'',\,E'(t)) \tag{6.77}$$

where E' (t) is determined by Eq. 6.70. If it is assumed that the energy spectrum of the transmitted electrons S(E, E', t) is close to a delta function or that $\frac{dE}{dX}$ is a very slowly varying function, the integrals over energy for Eq. 6.76 and 6.77 will be similar. It is seen that the doses calculated by the two methods are approximately related by the equation

$$D_{SA} \approx D_{Par}/1.75\;T\;(Z,\,E,\,t) \tag{6.78}$$

The transmitted fraction T(Z, E, t) is unity for small values of t implying that D_{SA} will underestimate the dose for thin shields. For thicker materials the transmitted fraction will drop below a value of 0.55 and D_{SA} will be an over estimate of the actual dose. For a spectrum of electron energies these effects tend to cancel.

Watts and Burrell[58] compare the doses calculated by the straight-ahead approximation with those calculated by Monte Carlo methods for electrons with exponential energy spectra incident on slabs of Al. They find that for both normally incident and isotropic electron fluxes, the comparisons are quite good. This would seem to indicate that, for these cases, most of the errors have canceled. This leads to the expectation that space shielding studies using the straight-ahead continuous slowing down model will yield reasonable results.

APPENDIX A

COMPARISON OF EXPERIMENTAL THICK TARGET BREMSSTRAHLUNG DATA WITH PARAMETERIC FITS

INTRODUCTION

The parametric representation of the thick target bremsstrahlung data discussed in Section 5 is compared with the experimental data in this appendix. The data were obtained with beams of electrons normally incident on targets equal in thickness to the range of the incident electrons. The curves have been displaced to allow a better comparison between the data and the parametric representation. In the figures the top curves (experiment and fit) are normalized correctly. Each of the other pairs of curves have been multiplied by a factor of one-half from the normalization of the curve above it. Thus, the top spectrum is correctly normalized, the spectrum at the next angle has been multiplied by one-half, the spectrum at the third angle has been multiplied by a factor of one-fourth, and so forth.

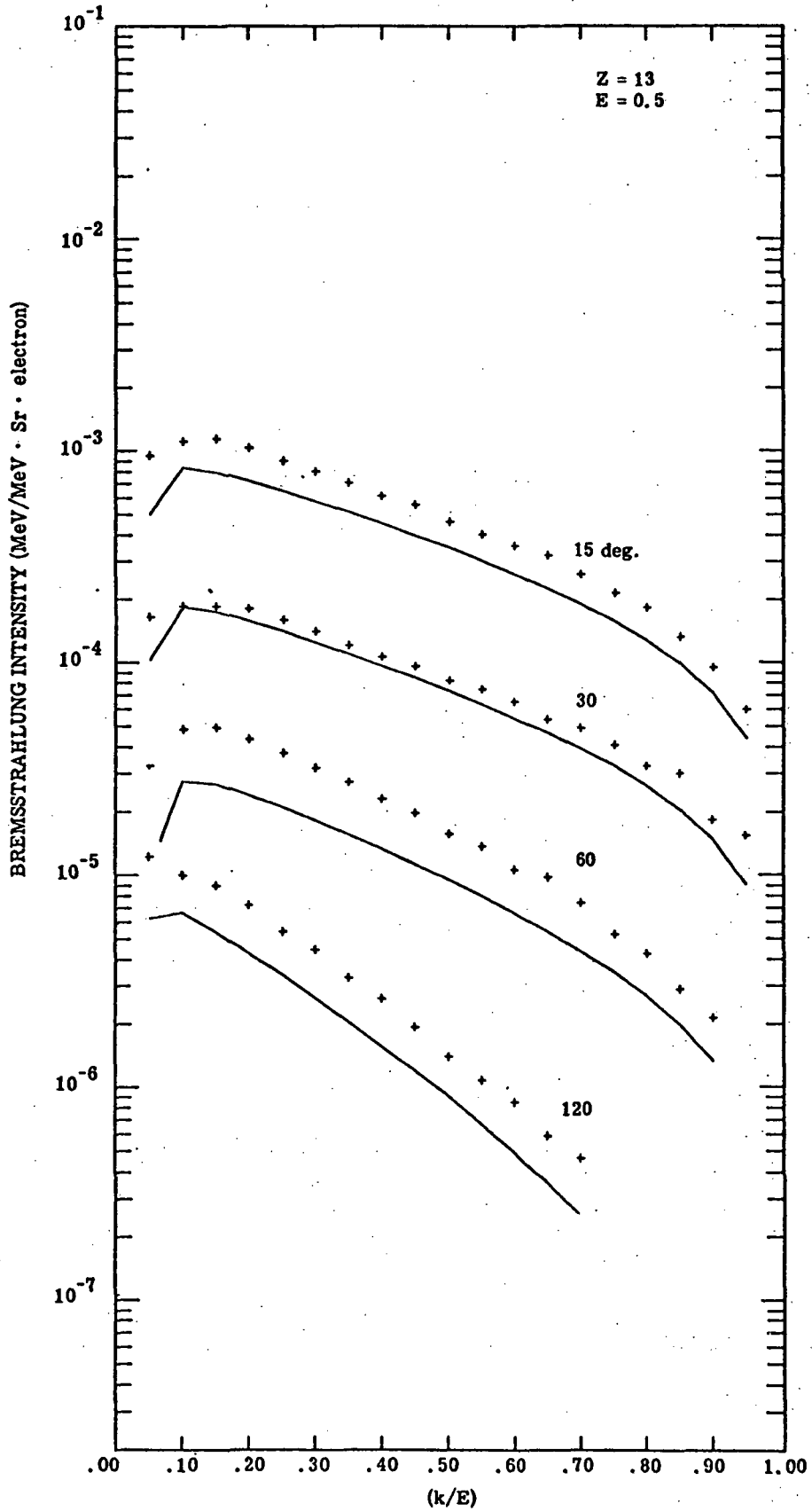

See Introduction to Appendix A for normalization

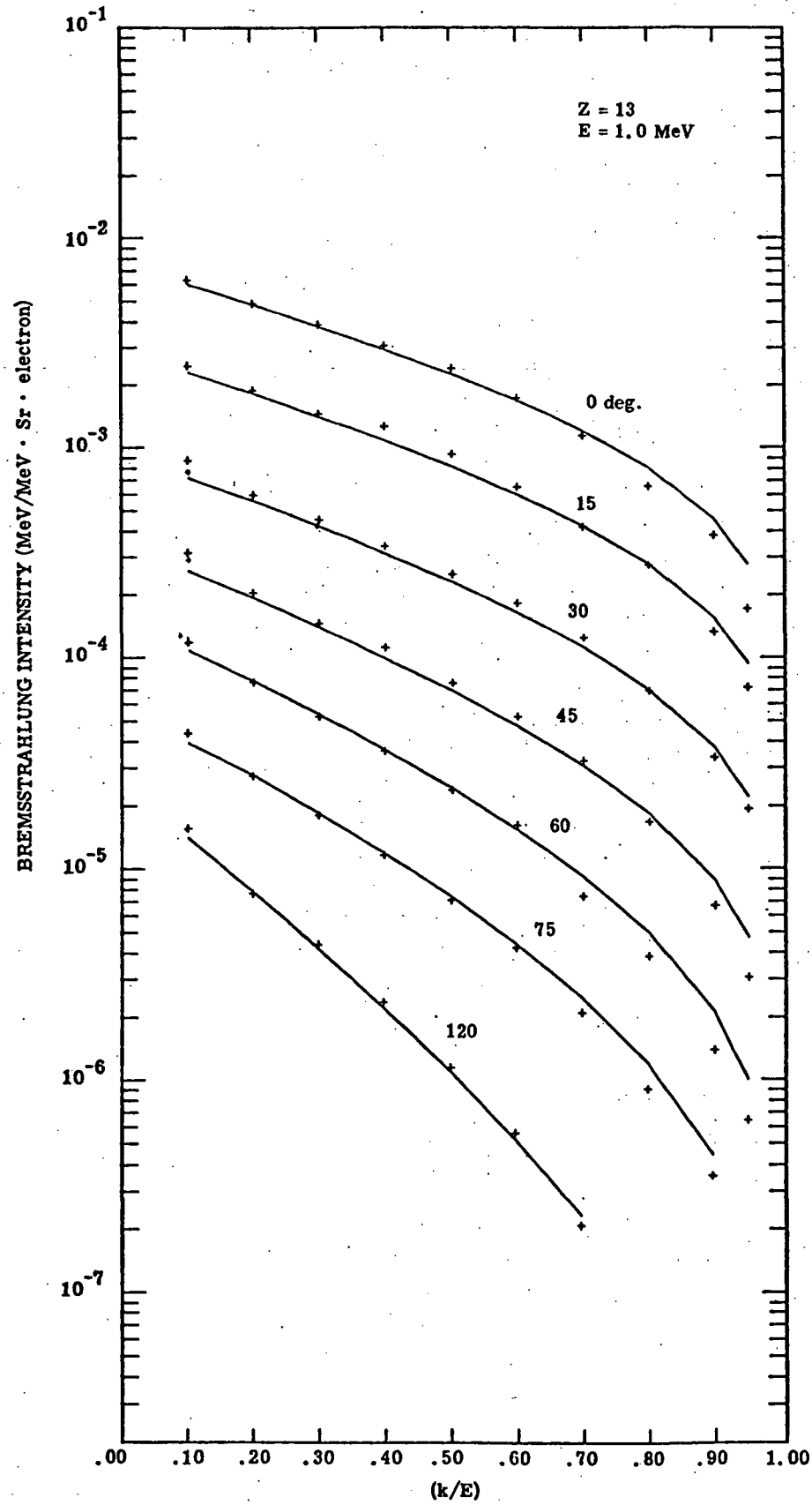

See Introduction to Appendix A for normalization

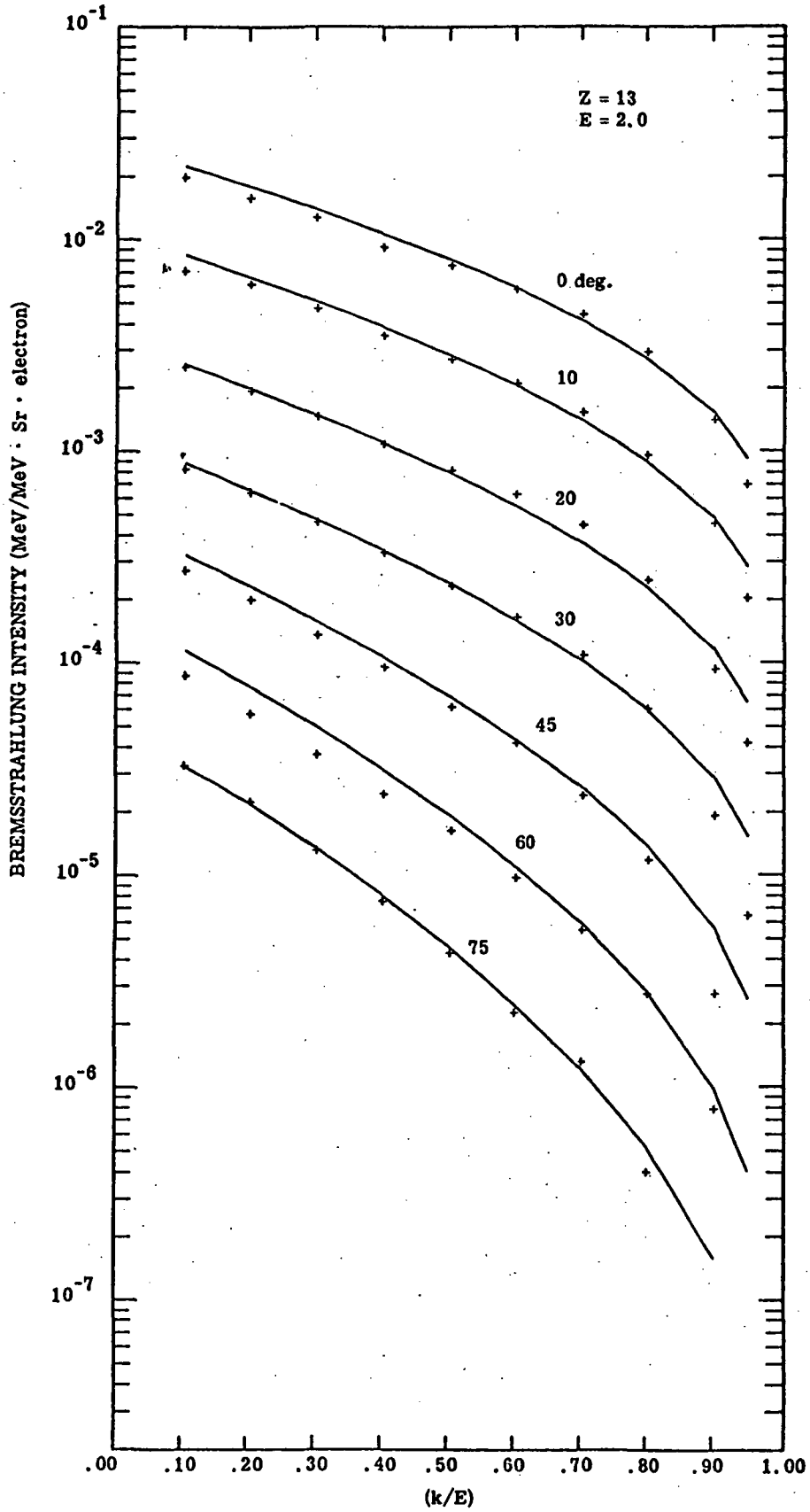

See Introduction to Appendix A for normalization

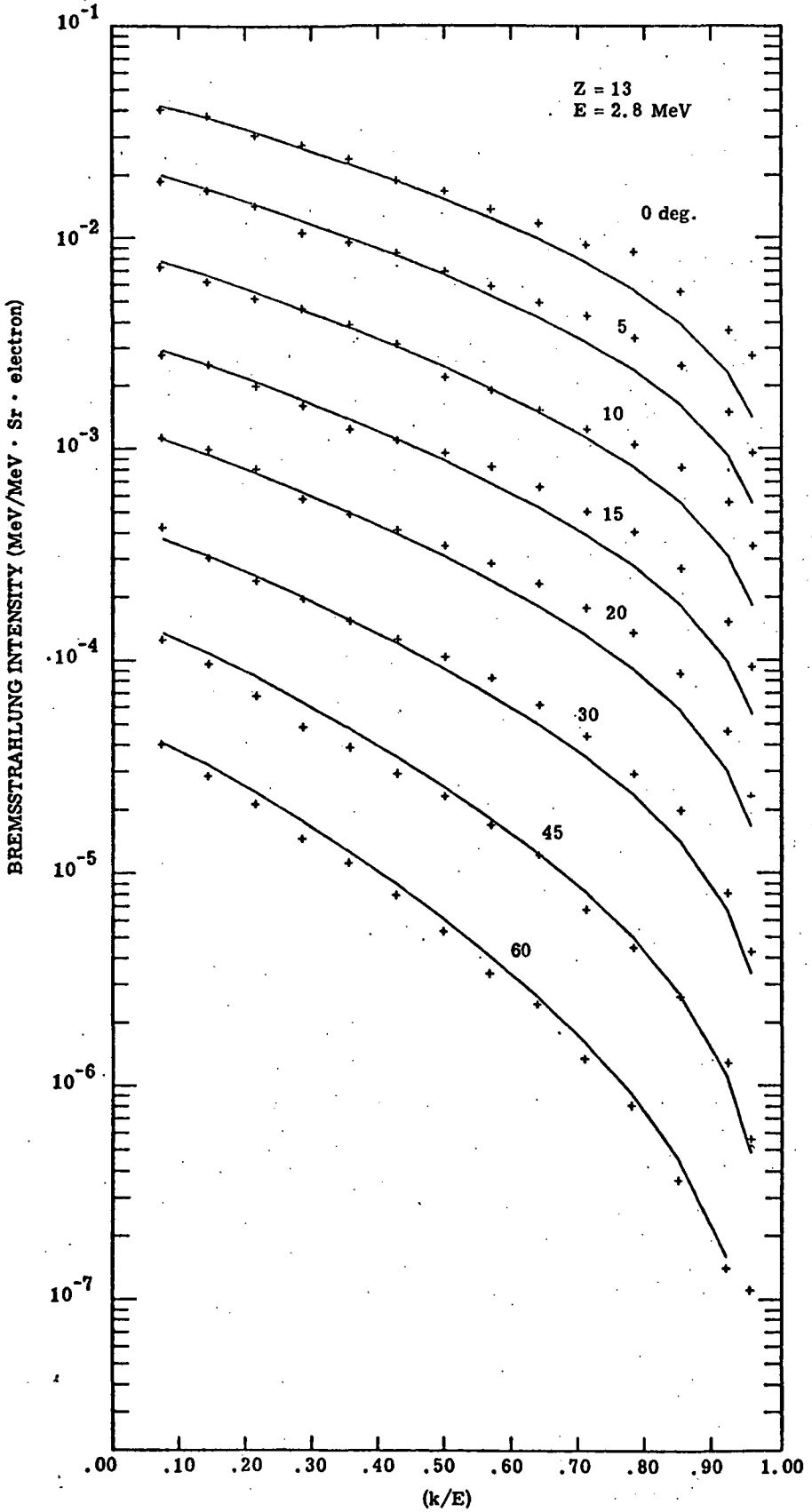

See Introduction to Appendix A for normalization

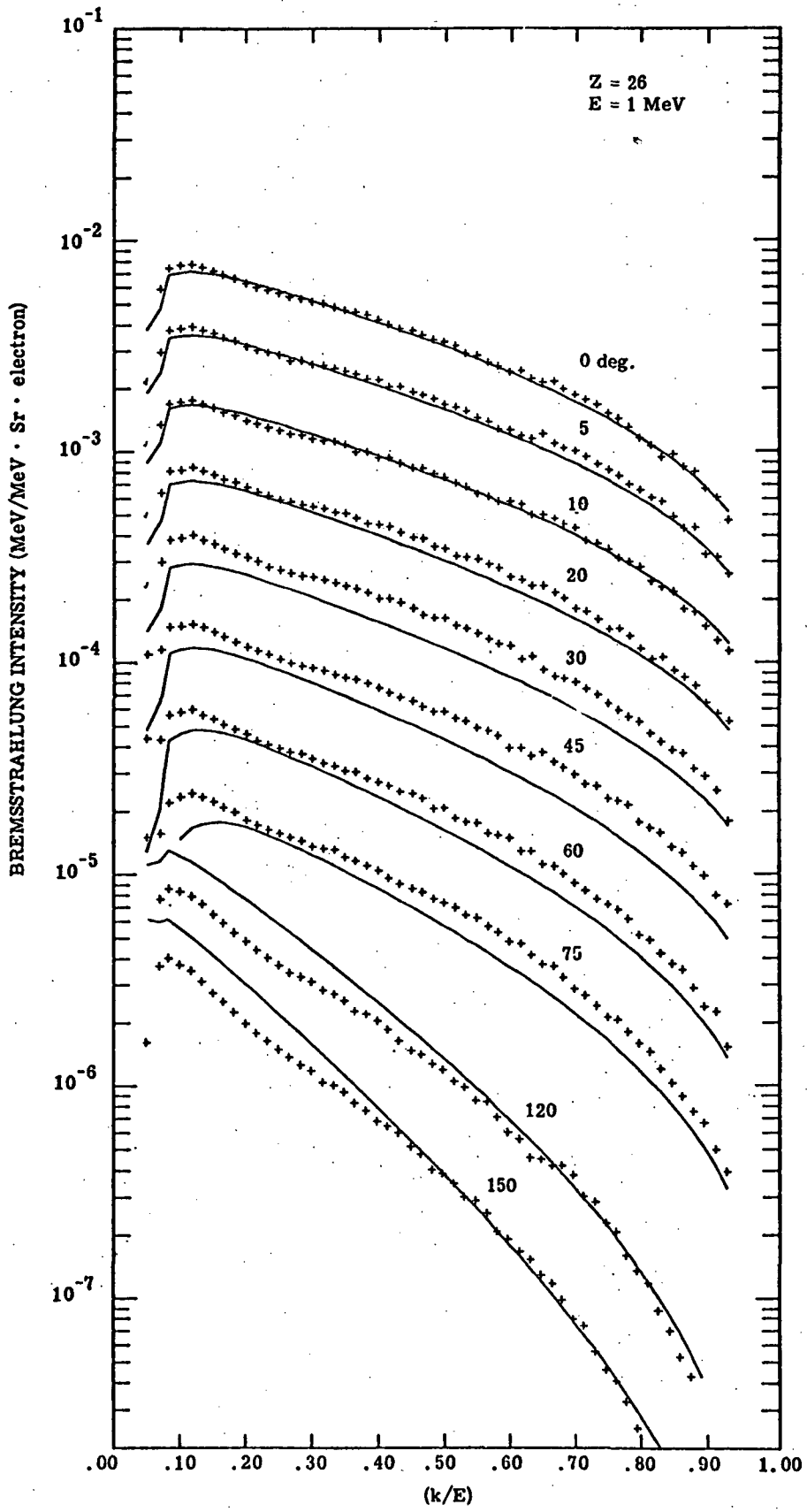

See Introduction to Appendix A for normalization

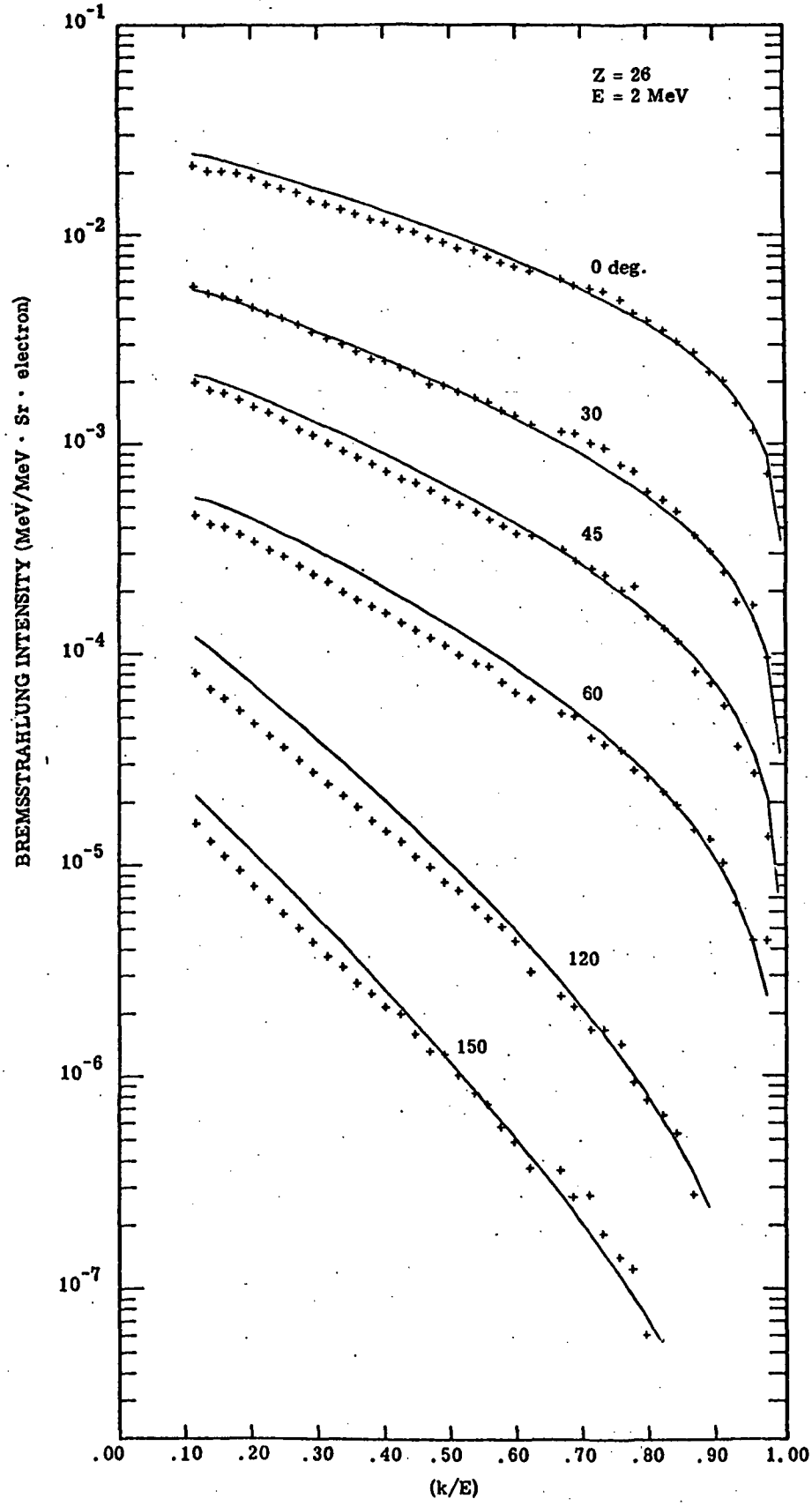

See Introduction to Appendix A for normalization

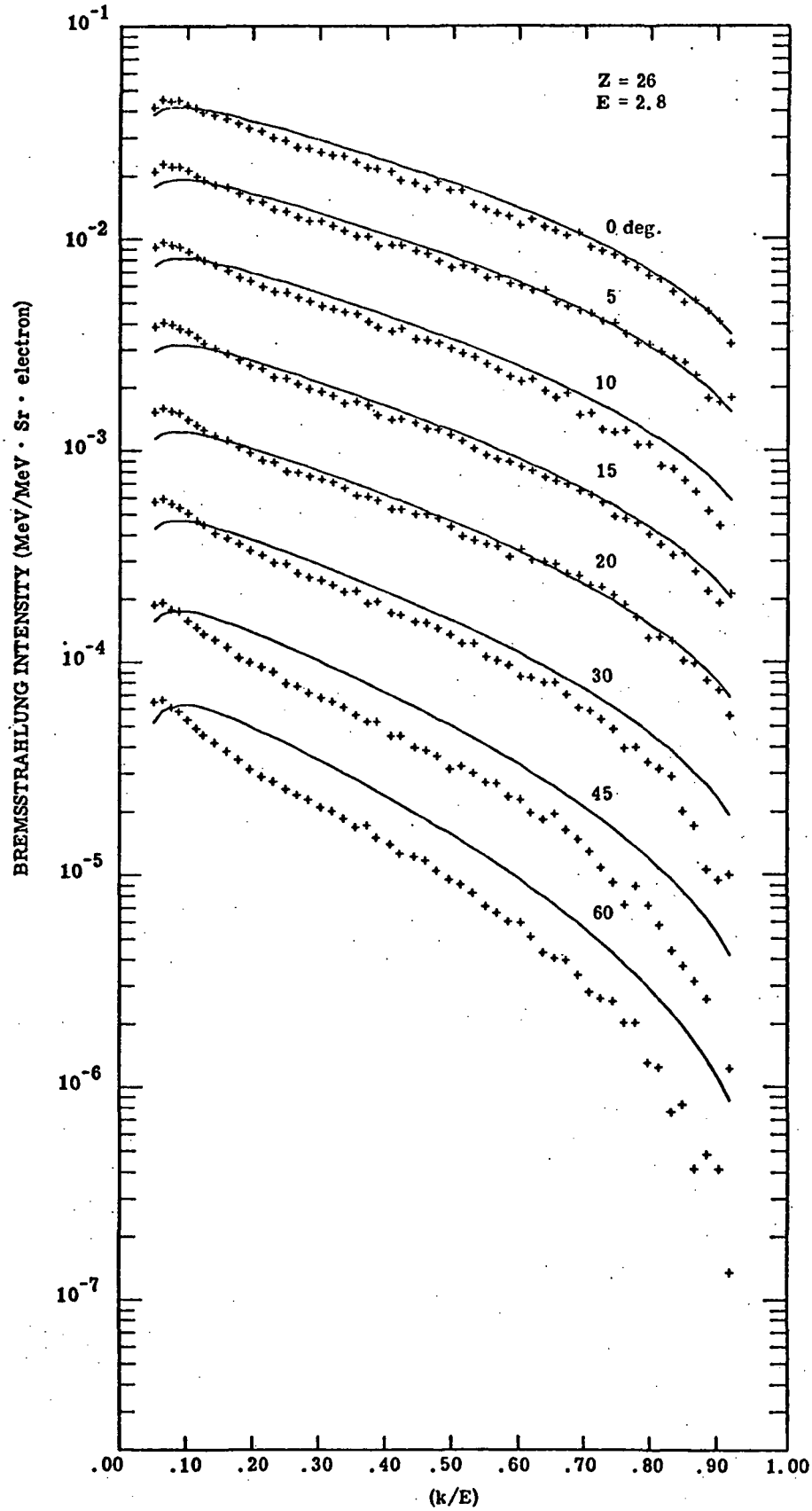

See Introduction to Appendix A for normalization

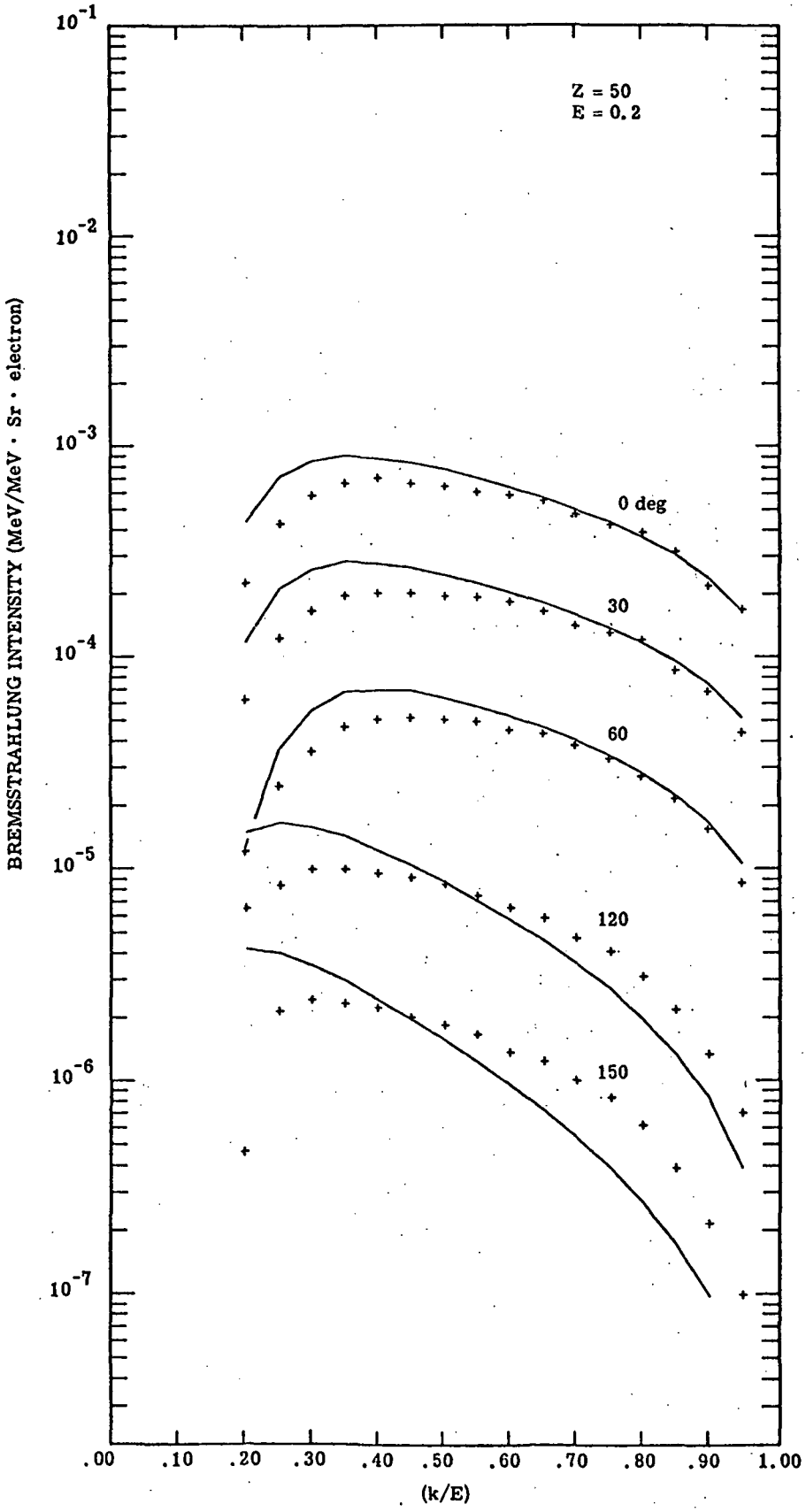

See Introduction to Appendix A for normalization

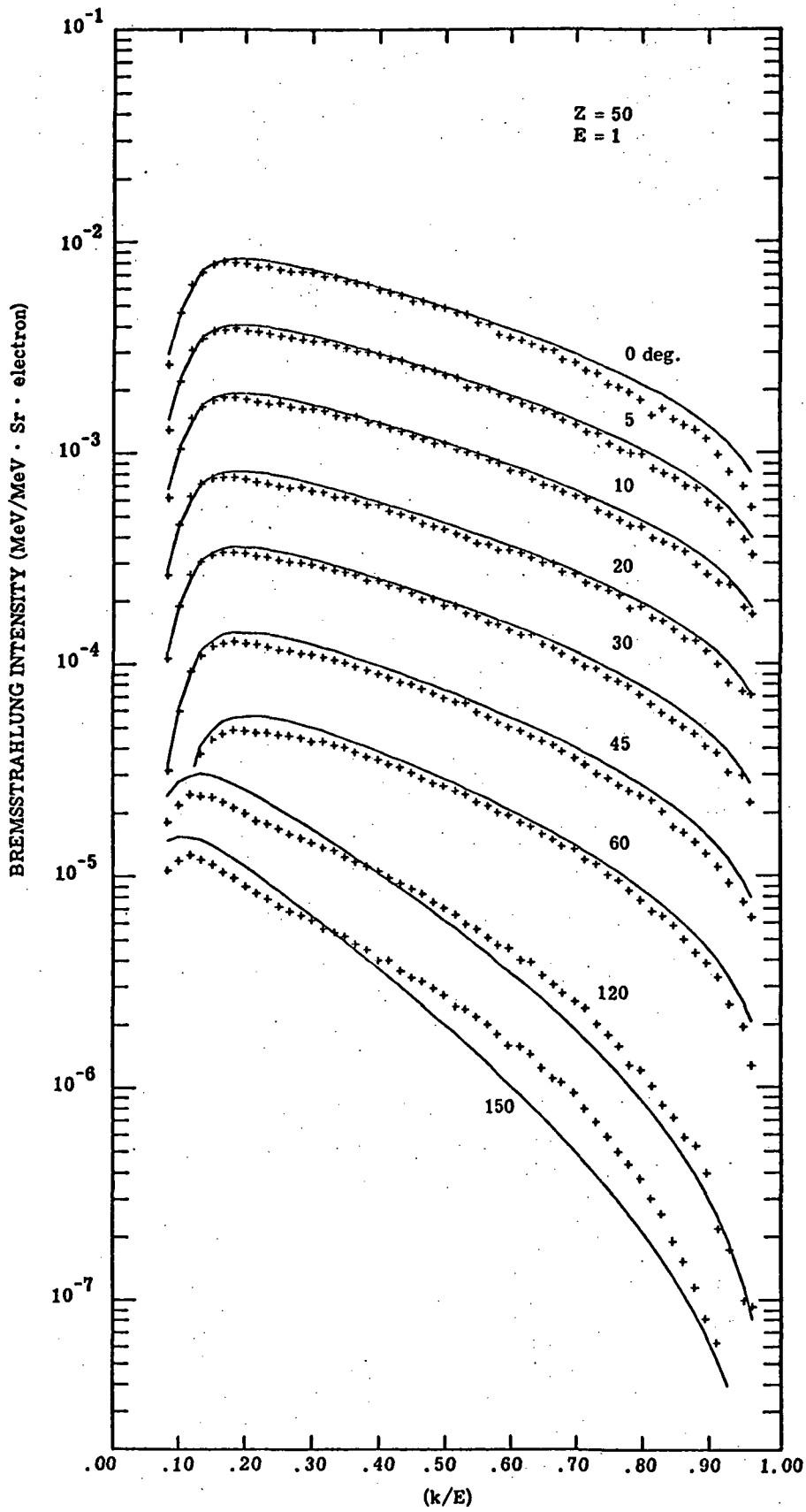

See Introduction to Appendix A for normalization

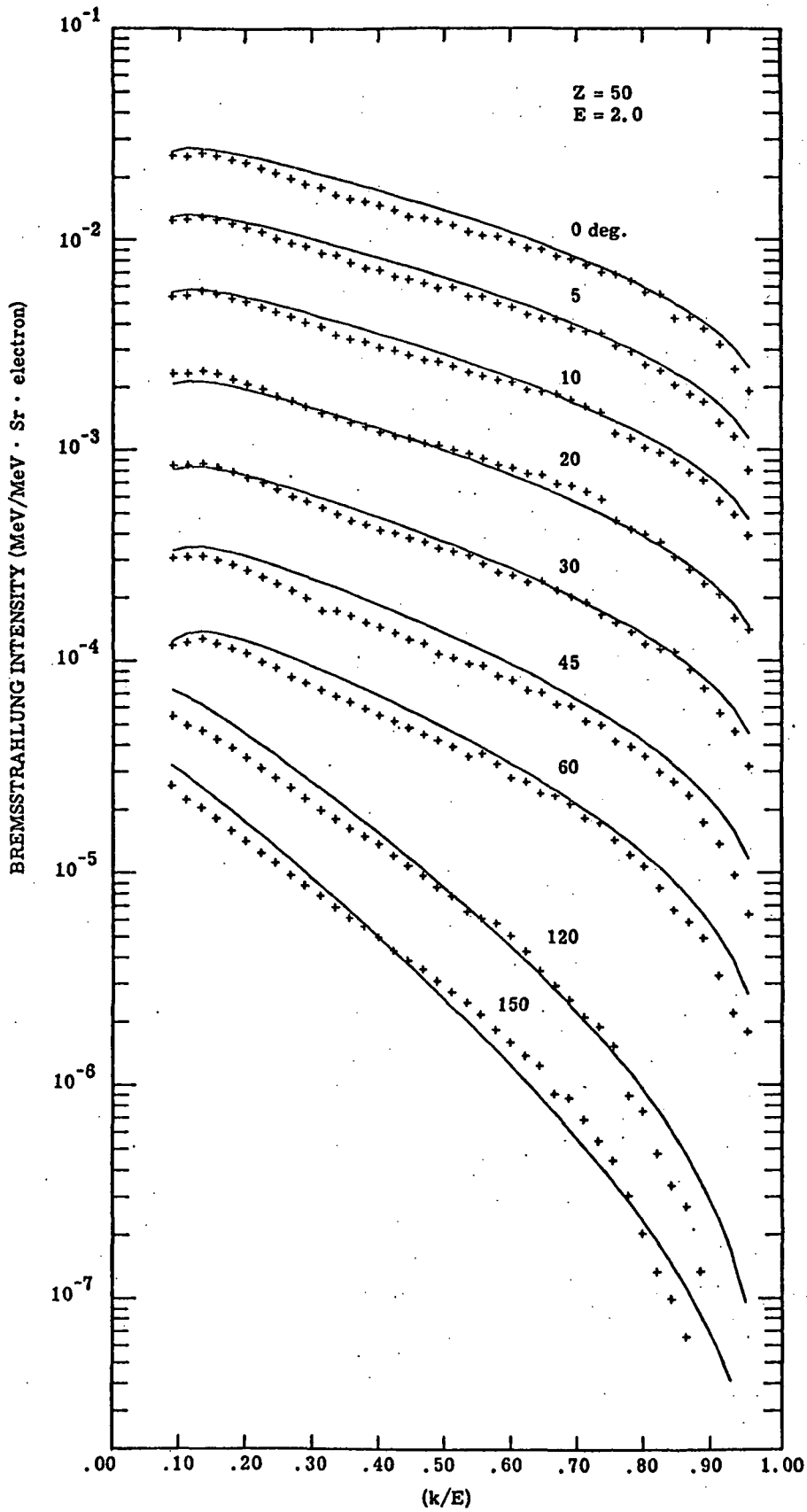

See Introduction to Appendix A for normalization

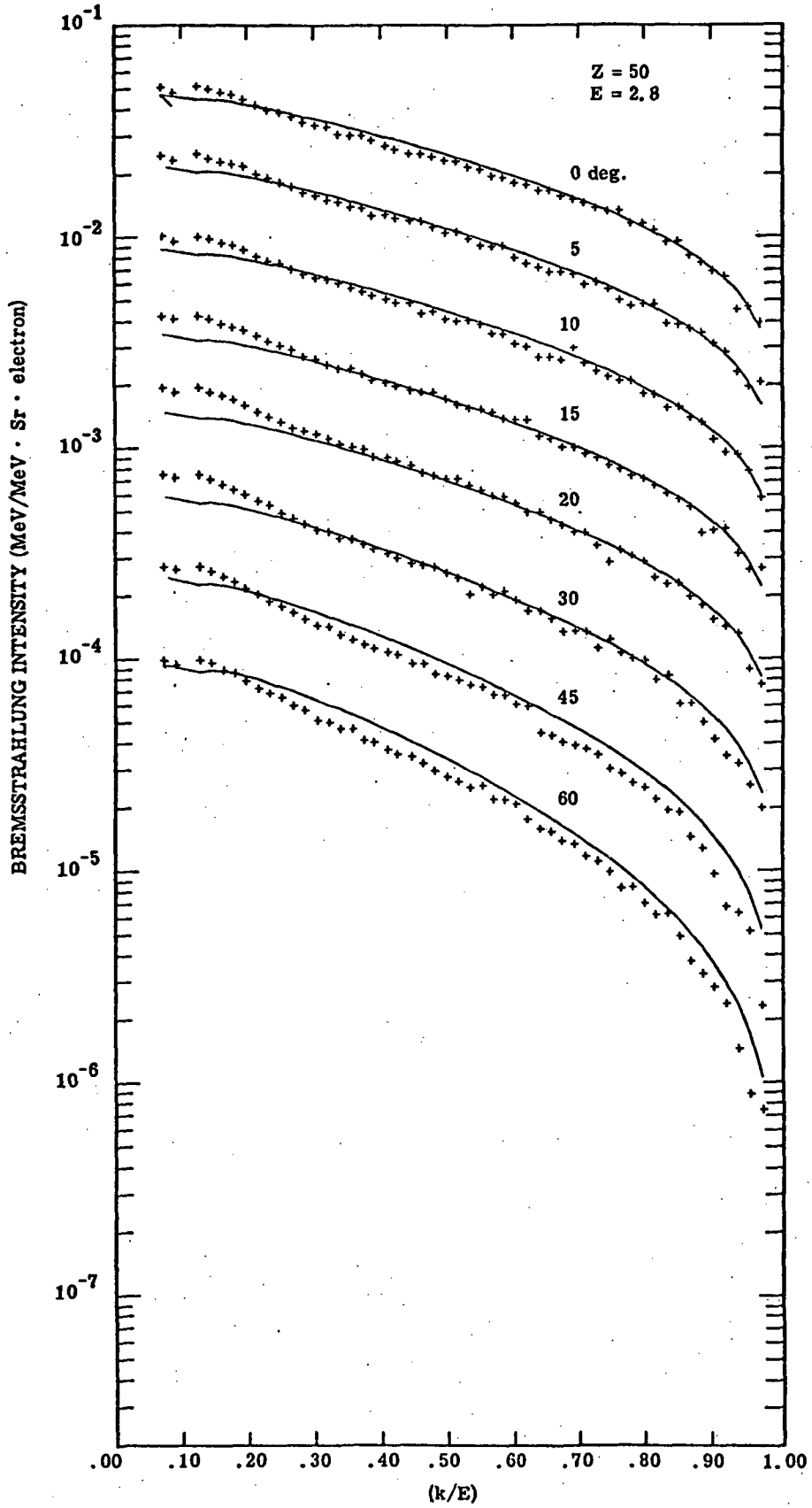

See Introduction to Appendix A for normalization

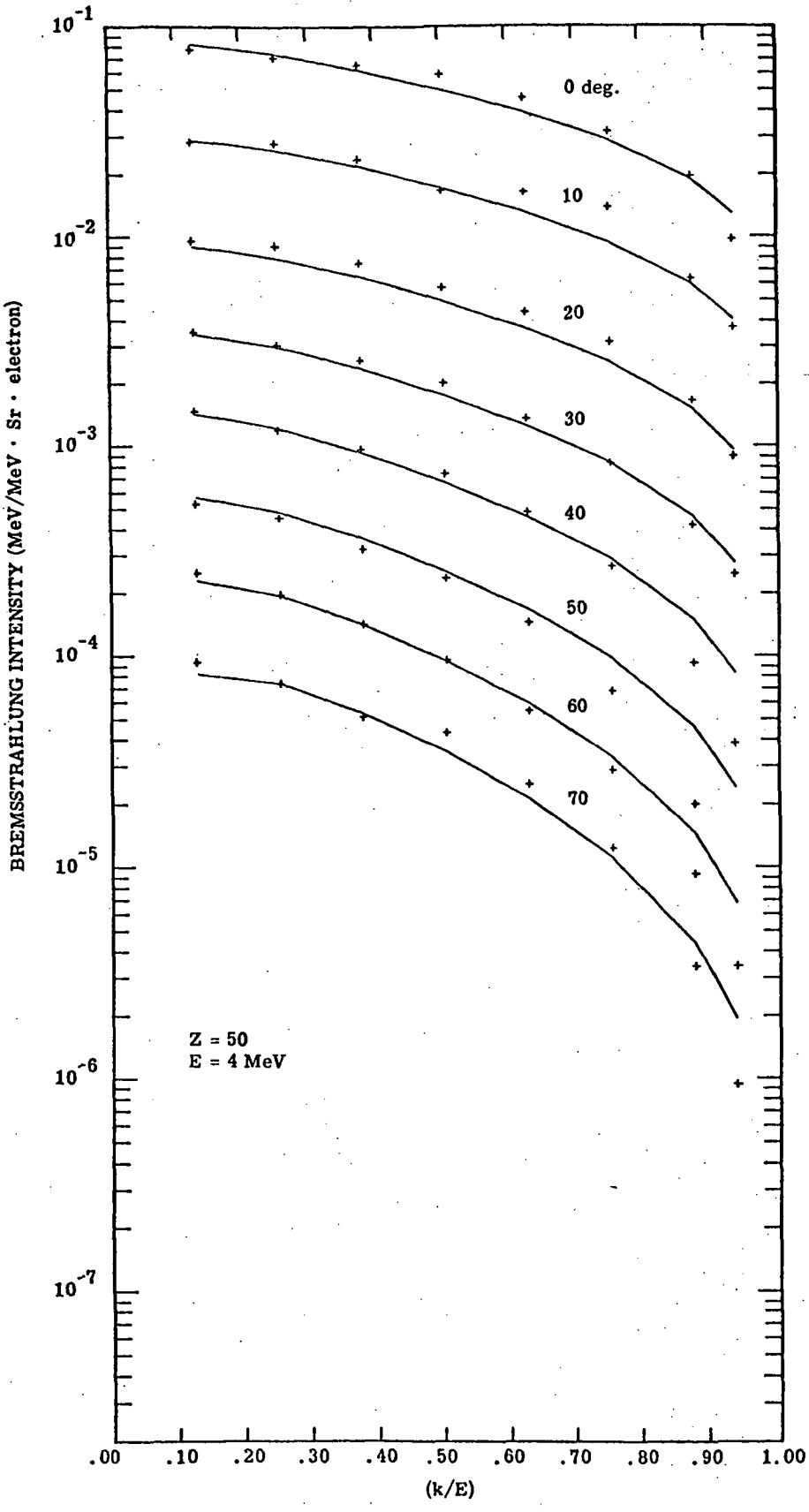

See Introduction to Appendix A for normalization

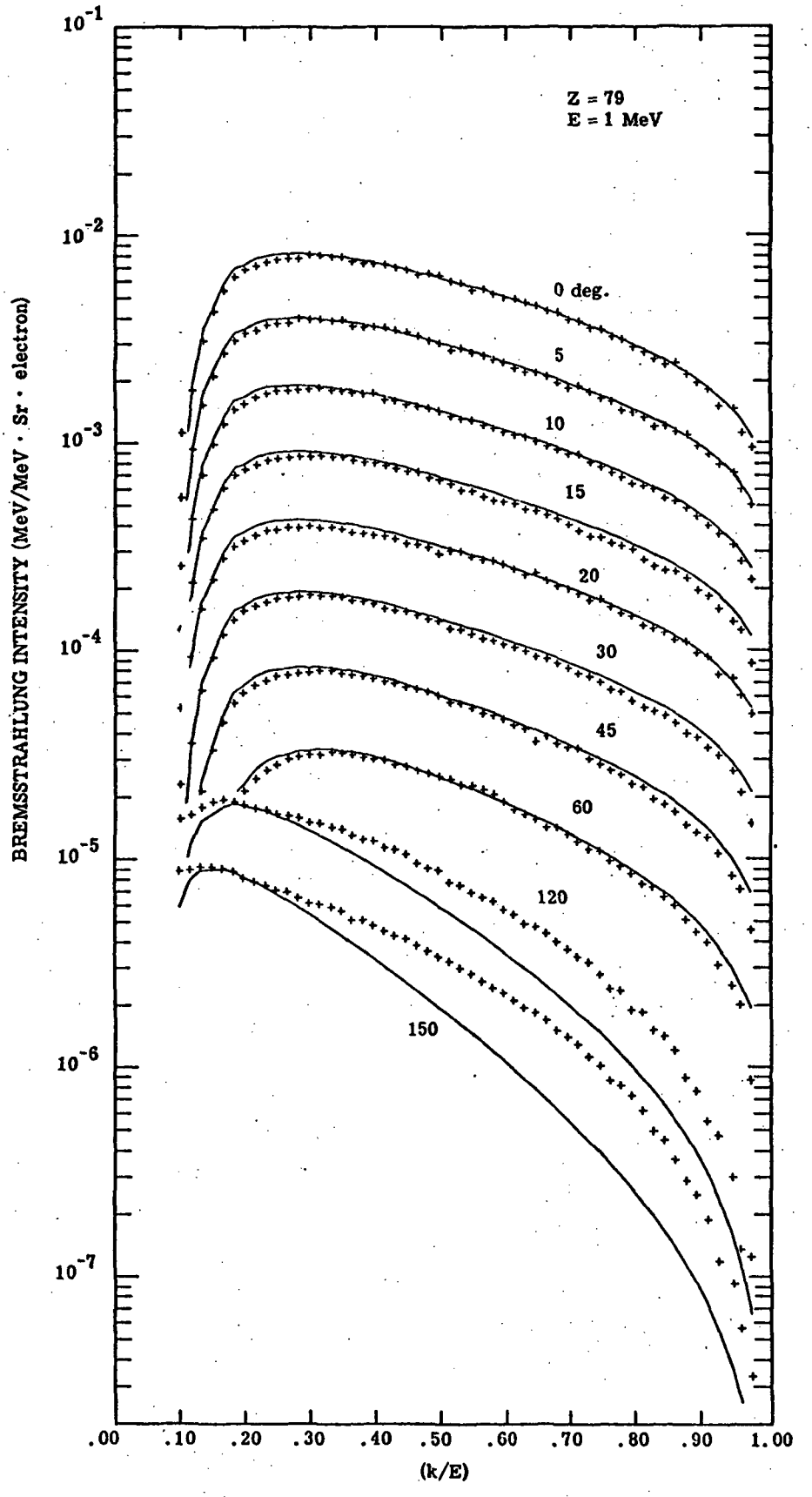

See Introduction to Appendix A for normalization

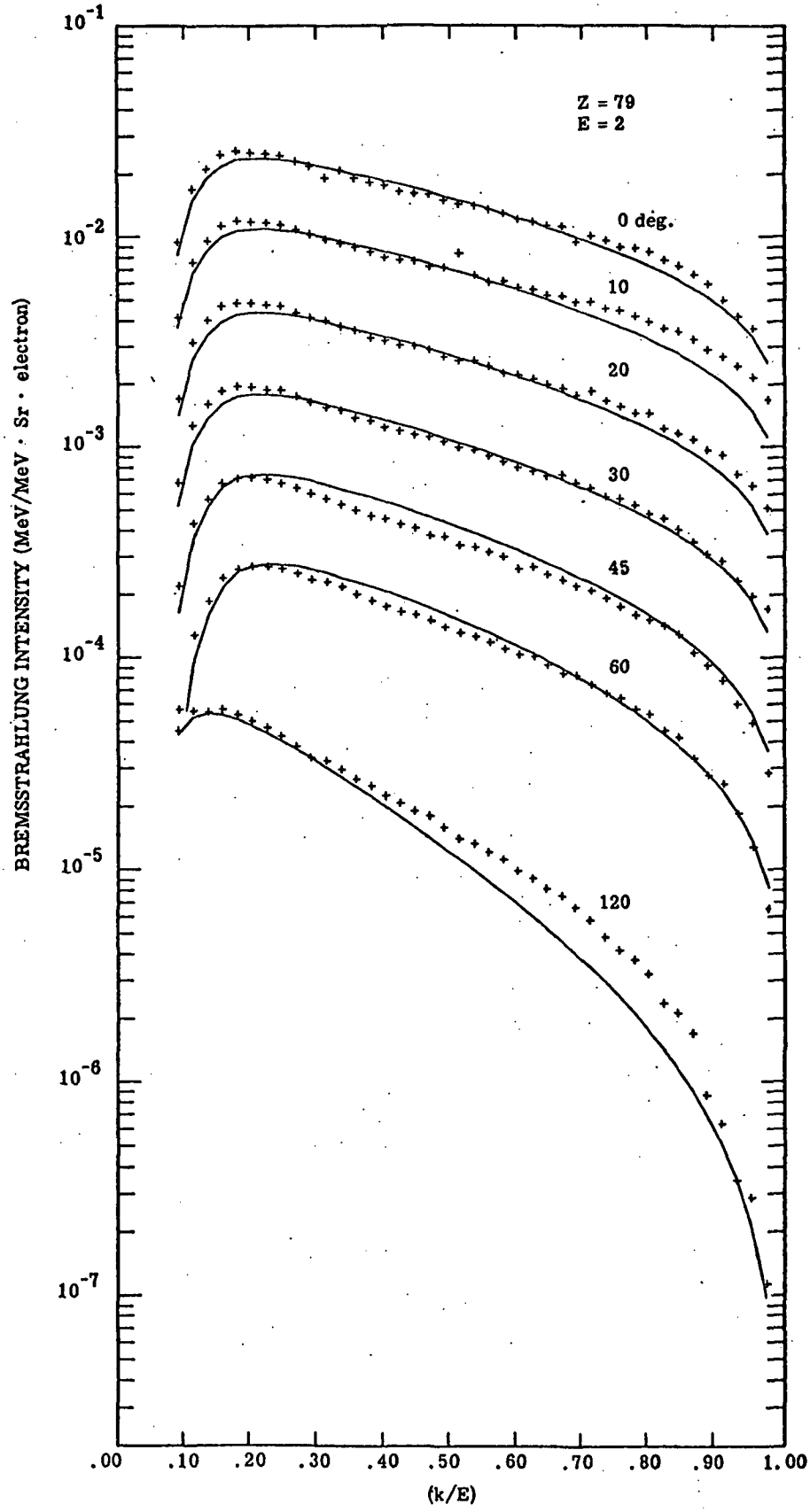

See Introduction to Appendix A for normalization

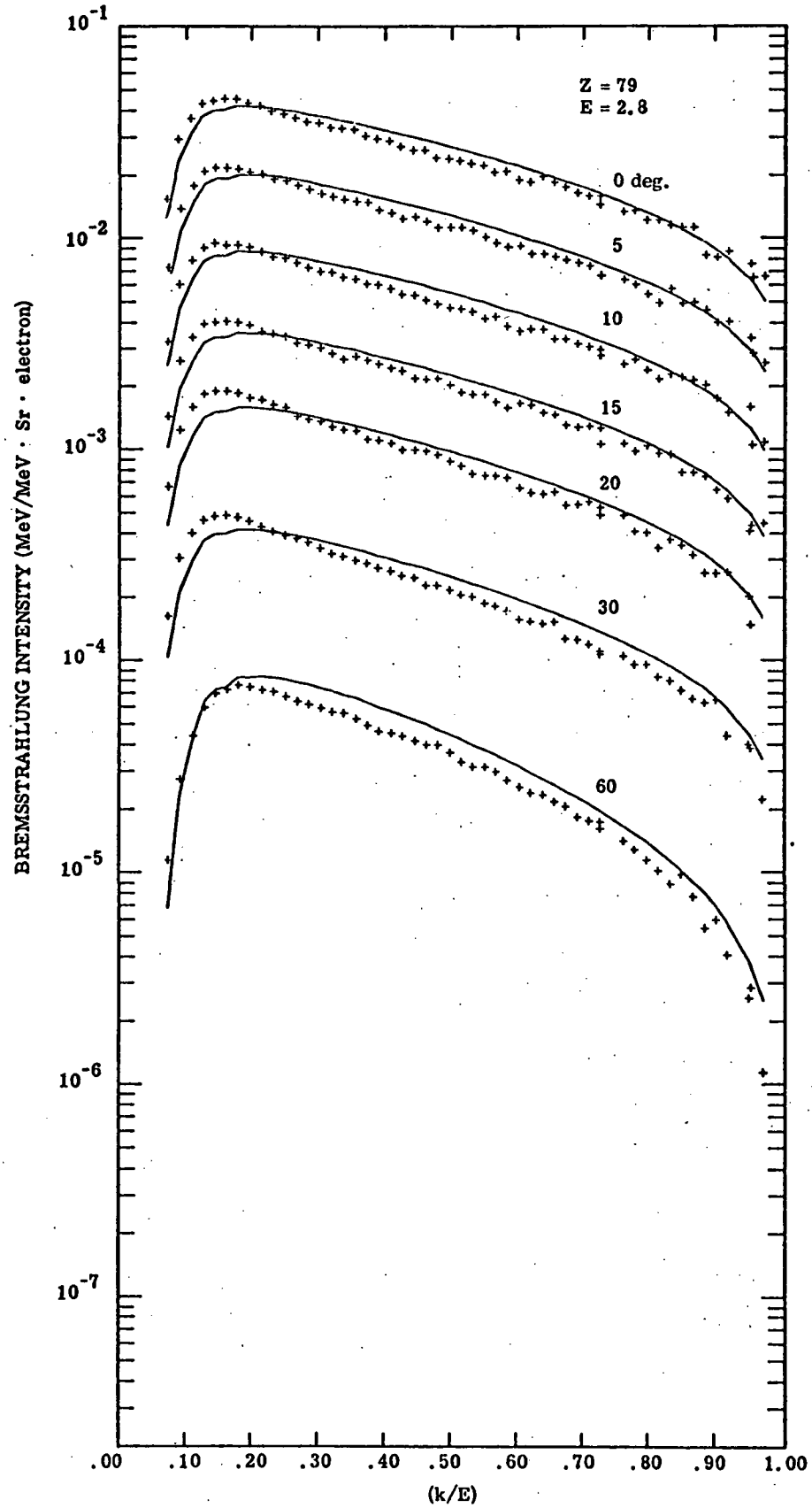

See Introduction to Appendix A for normalization

APPENDIX B

RESULTS OF ETRAN MONTE CARLO CALCULATIONS

INTRODUCTION

The results of ETRAN Monte Carlo[57] Calculation by Watts and Burrell[56] are reproduced here. Electrons with energies of 0.5-, 1.0-, 2.0-, 3.0-, 4.0-, 5.0-, 6.0- and 10.0- MeV were directed at slabs of aluminum. The transmitted fraction, backscatter coefficient, energy transmission coefficient, energy reflection coefficient and energy deposition for both monodirectional beam and half-space isotropic sources are tabulated as a function of incident energy and direction and slab thickness. Thicknesses are expressed as T/R_o where T is the thickness in g/cm^2 and R_o is the appropriate csda range in g/cm^2.

TABLE B-1. ELECTRON TRANSMITTED FRACTION FOR AN ALUMINUM PLANE SHIELD

(Energy = 0.5 MeV)

Shield Thickness (T/R)	Incident Angle (deg) 0	30	45	60	75	89.9
0.1	0.9912	0.9696	0.9120	0.7657	0.5600	0.2162
0.2	0.9188	0.8540	0.7557	0.5963	0.4227	0.1675
0.3	0.7732	0.6960	0.5853	0.4437	0.3003	0.1125
0.4	0.6004	0.5072	0.4060	0.2837	0.1793	0.0667
0.5	0.4012	0.3236	0.2323	0.1527	0.0856	0.0290
0.6	0.2032	0.1512	0.0953	0.0563	0.0313	0.0095
0.7	0.0752	0.0500	0.0270	0.0150	0.0060	0.0032
0.8	0.0164	0.0064	0.0006	0.0013	0.0003	0.0000
0.9	0.0008	0.0012	0.0023	0.0000	0.0000	0.0000
1.0	0.0000	0.0004	0.0000	0.0000	0.0000	0.0000

(Energy = 1.0 MeV)

Shield Thickness (T/R)	Incident Angle (deg) 0	30	45	60	75	89.9
0.1	0.9976	0.9797	0.9208	0.7900	0.5780	0.2114
0.2	0.9436	0.8767	0.7763	0.6286	0.4411	0.1626
0.3	0.8176	0.7183	0.6189	0.4699	0.3104	0.1116
0.4	0.6432	0.5433	0.4429	0.3107	0.1884	0.0651
0.5	0.4428	0.3560	0.2709	0.1678	0.0937	0.0284
0.6	0.2424	0.1763	0.1237	0.1036	0.0333	0.0092
0.7	0.1028	0.0613	0.0397	0.0207	0.0077	0.0028
0.8	0.0232	0.0123	0.0000	0.0028	0.0002	0.0005
0.9	0.0024	0.0010	0.0077	0.0000	0.0000	0.0000
1.0	0.0000	0.0000	0.0000	0.0000	0.0000	0.0000

(Energy = 2.0 MeV)

Shield Thickness (T/R)	Incident Angle (deg) 0	30	45	60	75	89.9
0.1	1.0120	0.9980	0.9531	0.8295	0.5969	0.2060
0.2	0.9772	0.9213	0.8188	0.6650	0.4518	0.1577
0.3	0.8892	0.7833	0.6683	0.4962	0.3251	0.1077
0.4	0.7388	0.6110	0.4946	0.3415	0.2027	0.0671
0.5	0.5380	0.4253	0.3154	0.1880	0.1022	0.0308
0.6	0.3284	0.2323	0.1491	0.0845	0.0384	0.0177
0.7	0.1460	0.0926	0.5286	0.0235	0.0082	0.0027
0.8	0.0348	0.0223	0.0005	0.0032	0.0011	0.0001
0.9	0.0044	0.0020	0.0108	0.0002	0.0002	0.0000
1.0	0.0008	0.0000	0.0000	0.0000	0.0000	0.0000

TABLE B-1. (CONTINUED)

(Energy = 3.0 MeV)

Shield Thickness (T/R)	Incident Angle (deg) 0	30	45	60	75	89.9
0.1	1.0180	1.0100	0.9797	0.8790	0.6282	0.2020
0.2	1.0010	0.9530	0.8548	0.6977	0.4653	0.1537
0.3	0.9424	0.8387	0.7123	0.5285	0.3336	0.1071
0.4	0.7968	0.6727	0.5343	0.3620	0.2098	0.0638
0.5	0.6092	0.4960	0.3563	0.2122	0.1053	0.0334
0.6	0.3900	0.2803	0.1843	0.0972	0.0406	0.0121
0.7	0.1928	0.1237	0.0731	0.0300	0.0111	0.0025
0.8	0.0588	0.0300	0.0014	0.0050	0.0013	0.0002
0.9	0.0060	0.0023	0.0134	0.0000	0.0000	0.0000
1.0	0.0004	0.0000	0.0000	0.0000	0.0000	0.0000

(Energy = 4.0 MeV)

Shield Thickness (T/R)	Incident Angle (deg) 0	30	45	60	75	89.9
0.1	1.0260	1.0200	0.9906	0.8925	0.6453	0.1980
0.2	1.0150	0.9723	0.8777	0.7195	0.4756	0.1473
0.3	0.9624	0.8703	0.7383	0.5542	0.3456	0.1027
0.4	0.8441	0.7103	0.5543	0.3787	0.2169	0.0652
0.5	0.6769	0.5350	0.3789	0.2325	0.1144	0.0354
0.6	0.4605	0.3380	0.2149	0.1140	0.0440	0.0137
0.7	0.2449	0.1570	0.0880	0.0355	0.0117	0.0024
0.8	0.0899	0.0510	0.0025	0.0060	0.0024	0.0007
0.9	0.0159	0.0066	0.0231	0.0005	0.0004	0.0000
1.0	0.0007	0.0003	0.0000	0.0000	0.0000	0.0000

(Energy = 5.0 MeV)

Shield Thickness (T/R)	Incident Angle (deg) 0	30	45	60	75	89.9
0.1	1.0330	1.0220	1.0020	0.9237	0.6593	0.1924
0.2	1.0240	0.9880	0.9057	0.7515	0.4862	0.1409
0.3	0.9852	0.9007	0.7660	0.5795	0.3444	0.0940
0.4	0.8856	0.7497	0.5897	0.4075	0.2156	0.0618
0.5	0.7132	0.5657	0.4097	0.2400	0.1167	0.0328
0.6	0.5032	0.3703	0.2394	0.1145	0.0488	0.0127
0.7	0.2812	0.1917	0.0985	0.0400	0.0146	0.0032
0.8	0.1024	0.0593	0.0045	0.0085	0.0024	0.0002
0.9	0.0216	0.0100	0.0277	0.0010	0.0004	0.0000
1.0	0.0004	0.0000	0.0000	0.0000	0.0000	0.0000

TABLE B-1. (CONTINUED)

(Energy = 6.0 MeV)

Shield Thickness (T/R)	Incident Angle (deg) 0	30	45	60	75	89.9
0.1	1.0320	1.0250	1.0150	0.9380	0.6778	0.1894
0.2	1.0340	1.0010	0.9200	0.7605	0.4929	0.1380
0.3	0.9896	0.9120	0.7828	0.5875	0.3542	0.0918
0.4	0.9092	0.7830	0.6129	0.4212	0.2236	0.0567
0.5	0.7548	0.6033	0.4263	0.2525	0.1242	0.0284
0.6	0.5576	0.4090	0.2520	0.1235	0.0515	0.0110
0.7	0.3232	0.2180	0.1169	0.0465	0.0140	0.0031
0.8	0.1268	0.0773	0.0051	0.0102	0.0026	0.0002
0.9	0.0272	0.0140	0.0314	0.0015	0.0002	0.0000
1.0	0.0000	0.0000	0.0000	0.0000	0.0000	0.0000

(Energy = 10.0 MeV)

Shield Thickness (T/R)	Incident Angle (deg) 0	30	45	60	75	89.9
0.1	1.0480	1.0420	1.0280	0.9830	0.7378	0.1540
0.2	1.0460	1.0320	0.9834	0.8282	0.5553	0.1103
0.3	1.0210	0.9787	0.8583	0.6532	0.3804	0.0737
0.4	0.9648	0.8473	0.7143	0.4712	0.2338	0.0437
0.5	0.8700	0.6930	0.5314	0.3040	0.1178	0.0200
0.6	0.6820	0.4987	0.3457	0.1600	0.0488	0.0072
0.7	0.4480	0.2987	0.1746	0.0665	0.0135	0.0018
0.8	0.2240	0.1307	0.0697	0.0180	0.0026	0.0002
0.9	0.0688	0.0313	0.0122	0.0025	0.0006	0.0000
1.0	0.0084	0.0020	0.0011	0.0000	0.0000	0.0000

TABLE B-2. ELECTRON BACKSCATTER COEFFICIENTS FOR AN ALUMINUM PLANE SLAB

(Energy = 0.5 MeV)

Shield Thickness (T/R)	Incident Angle (deg)					
	0	30	45	60	75	89.9
0.1	0.0176	0.0396	0.0970	0.2493	0.4510	0.7892
0.2	0.0656	0.1180	0.1910	0.3417	0.5160	0.8115
0.3	0.0984	0.1516	0.2177	0.3597	0.5267	0.8142
0.4	0.1020	0.1548	0.2203	0.3610	0.5267	0.8145
0.5	0.1020	0.1548	0.2203	0.3610	0.5267	0.8145
0.6	0.1020	0.1548	0.2203	0.3610	0.5267	0.8145
0.7	0.1020	0.1548	0.2203	0.3610	0.5267	0.8145
0.8	0.1020	0.1548	0.2203	0.3610	0.5267	0.8145
0.9	0.1020	0.1548	0.2203	0.3610	0.5267	0.8145
1.0	0.1020	0.1548	0.2203	0.3610	0.5267	0.8145

(Energy = 1.0 MeV)

Shield Thickness (T/R)	Incident Angle (deg)					
	0	30	45	60	75	89.9
0.1	0.0132	0.0350	0.0962	0.2347	0.4533	0.8157
0.2	0.0556	0.1103	0.1874	0.3253	0.5187	0.8371
0.3	0.0868	0.1440	0.2143	0.3433	0.5302	0.8418
0.4	0.0920	0.1470	0.2160	0.3446	0.5309	0.8418
0.5	0.0920	0.1470	0.2160	0.3446	0.5309	0.8418
0.6	0.0920	0.1470	0.2160	0.3446	0.5309	0.8418
0.7	0.0920	0.1470	0.2160	0.3446	0.5309	0.8418
0.8	0.0920	0.1470	0.2160	0.3610	0.5309	0.8418
0.9	0.0920	0.1470	0.2160	0.3446	0.5309	0.8418
1.0	0.0920	0.1470	0.2160	0.3446	0.5309	0.8418

(Energy = 2.0 MeV)

Shield Thickness (T/R)	Incident Angle (deg)					
	0	30	45	60	75	89.9
0.1	0.0100	0.0246	0.0714	0.2015	0.4420	0.8261
0.2	0.0332	0.0813	0.1577	0.2935	0.5064	0.8435
0.3	0.0548	0.1067	0.1789	0.3102	0.5160	0.8463
0.4	0.0592	0.1107	0.1806	0.3115	0.5162	0.8464
0.5	0.0592	0.1107	0.1806	0.3115	0.5162	0.8464
0.6	0.0592	0.1107	0.1806	0.3115	0.5162	0.8464
0.7	0.0592	0.1107	0.1806	0.3115	0.5162	0.8464
0.8	0.0592	0.1107	0.1806	0.3446	0.5162	0.8464
0.9	0.0592	0.1107	0.1806	0.3115	0.5162	0.8464
1.0	0.0592	0.1107	0.1806	0.3115	0.5162	0.8464

TABLE B-2. (CONTINUED)

(Energy = 3.0 MeV)

Shield Thickness (T/R)	Incident Angle (deg) 0	30	45	60	75	89.9
0.1	0.0052	0.0163	0.0565	0.1705	0.4389	0.8470
0.2	0.0180	0.0650	0.1351	0.2650	0.5058	0.8643
0.3	0.0312	0.0860	0.1577	0.2830	0.5151	0.8665
0.4	0.0352	0.0890	0.1586	0.2840	0.5153	0.8665
0.5	0.0352	0.0890	0.1586	0.2840	0.5153	0.8665
0.6	0.0352	0.0890	0.1586	0.2840	0.5153	0.8665
0.7	0.0352	0.0890	0.1586	0.2840	0.5153	0.8665
0.8	0.0352	0.0890	0.1586	0.3115	0.5153	0.8665
0.9	0.0352	0.0890	0.1586	0.2840	0.5153	0.8665
1.0	0.0352	0.0890	0.1586	0.2840	0.5153	0.8665

(Energy = 4.0 MeV)

Shield Thickness (T/R)	Incident Angle (deg) 0	30	45	60	75	89.9
0.1	0.0050	0.0146	0.0491	0.1590	0.4364	0.8667
0.2	0.0146	0.0523	0.1151	0.2540	0.5040	0.8833
0.3	0.0267	0.0746	0.1329	0.2710	0.5122	0.8853
0.4	0.0299	0.0760	0.1343	0.2722	0.5124	0.8854
0.5	0.0301	0.0760	0.1343	0.2722	0.5124	0.8854
0.6	0.0301	0.0760	0.1343	0.2722	0.5124	0.8854
0.7	0.0301	0.0760	0.1343	0.2722	0.5124	0.8854
0.8	0.0301	0.0760	0.1343	0.2840	0.5124	0.8854
0.9	0.0301	0.0760	0.1343	0.2722	0.5124	0.8854
1.0	0.0301	0.0760	0.1343	0.2722	0.5124	0.8854

(Energy = 5.0 MeV)

Shield Thickness (T/R)	Incident Angle (deg) 0	30	45	60	75	89.9
0.1	0.0048	0.0090	0.0397	0.1390	0.4271	0.8885
0.2	0.0108	0.0370	0.0985	0.2287	0.4929	0.9038
0.3	0.0192	0.0506	0.1151	0.2450	0.5018	0.9055
0.4	0.0228	0.0520	0.1157	0.2457	0.5018	0.9055
0.5	0.0228	0.0520	0.1157	0.2457	0.5018	0.9055
0.6	0.0228	0.0520	0.1157	0.2457	0.5018	0.9055
0.7	0.0228	0.0520	0.1157	0.2457	0.5018	0.9055
0.8	0.0228	0.0520	0.1157	0.2722	0.5018	0.9055
0.9	0.0228	0.0520	0.1157	0.2457	0.5018	0.9055
1.0	0.0228	0.0520	0.1157	0.2457	0.5018	0.9055

TABLE B-2. (CONTINUED)

(Energy = 6.0 MeV)

Shield Thickness (T/R)	Incident Angle (deg) 0	30	45	60	75	89.9
0.1	0.0056	0.0103	0.0302	0.1310	0.4240	0.8995
0.2	0.0096	0.0283	0.0842	0.2130	0.4878	0.9155
0.3	0.0176	0.0397	0.1000	0.2292	0.4962	0.9165
0.4	0.0204	0.0416	0.1003	0.2300	0.4962	0.9167
0.5	0.0204	0.0416	0.1003	0.2300	0.4962	0.9167
0.6	0.0204	0.0416	0.1003	0.2300	0.4962	0.9167
0.7	0.0204	0.0416	0.1003	0.2300	0.4962	0.9167
0.8	0.0204	0.0416	0.1003	0.2300	0.4962	0.9167
0.9	0.0204	0.0416	0.1003	0.2300	0.4962	0.9167
1.0	0.0204	0.0416	0.1003	0.2300	0.4962	0.9167

(Energy = 10.0 MeV)

Shield Thickness (T/R)	Incident Angle (deg) 0	30	45	60	75	89.9
0.1	0.0052	0.0106	0.0254	0.1012	0.3831	0.9437
0.2	0.0088	0.0166	0.0565	0.1665	0.4449	0.9556
0.3	0.0120	0.0233	0.0680	0.1810	0.4502	0.9558
0.4	0.0132	0.0246	0.0682	0.1817	0.4502	0.9558
0.5	0.0132	0.0250	0.0682	0.1817	0.4502	0.9558
0.6	0.0132	0.0250	0.0682	0.1817	0.4502	0.9558
0.7	0.0132	0.0250	0.0682	0.1817	0.4502	0.9558
0.8	0.0132	0.0250	0.0682	0.1817	0.4502	0.9558
0.9	0.0132	0.0250	0.0682	0.1817	0.4502	0.9558
1.0	0.0132	0.0250	0.0682	0.1817	0.4502	0.9558

TABLE B-3. ELECTRON ENERGY TRANSMISSION COEFFICIENT FOR AN ALUMINUM PLANE SHIELD

(Energy = 0.5 MeV)

Shield Thickness (T/R)	Incident Angle (deg) 0	30	45	60	75	89.9
0.1	0.9097	0.8772	0.7917	0.6326	0.4407	0.1653
0.2	0.7444	0.6667	0.5586	0.4174	0.2746	0.1061
0.3	0.5379	0.4692	0.3666	0.2620	0.1655	0.0605
0.4	0.3509	0.2861	0.2134	0.1405	0.0825	0.0297
0.5	0.1937	0.1487	0.1005	0.0623	0.0335	0.0107
0.6	0.0814	0.0585	0.0349	0.0197	0.0099	0.0031
0.7	0.0257	0.0156	0.0081	0.0041	0.0016	0.0007
0.8	0.0040	0.0018	0.0007	0.0002	0.0000	0.0000
0.9	0.0001	0.0002	0.0001	0.0000	0.0000	0.0000
1.0	0.0000	0.0000	0.0000	0.0000	0.0000	0.0000

(Energy = 1.0 MeV)

Shield Thickness (T/R)	Incident Angle (deg) 0	30	45	60	75	89.9
0.1	0.9063	0.8700	0.7868	0.6355	0.4310	0.1532
0.2	0.7508	0.6637	0.5551	0.4142	0.2680	0.0957
0.3	0.5497	0.4564	0.3686	0.2581	0.1574	0.0553
0.4	0.3603	0.2867	0.2202	0.1415	0.0794	0.0266
0.5	0.2035	0.1510	0.1093	0.0630	0.0325	0.0099
0.6	0.0896	0.0603	0.0403	0.0235	0.0095	0.0028
0.7	0.0298	0.0165	0.0107	0.0049	0.0017	0.0006
0.8	0.0051	0.0023	0.0015	0.0005	0.0000	0.0000
0.9	0.0005	0.0001	0.0000	0.0000	0.0000	0.0000
1.0	0.0000	0.0000	0.0000	0.0000	0.0000	0.0000

(Energy = 2.0 MeV)

Shield Thickness (T/R)	Incident Angle (deg) 0	30	45	60	75	89.9
0.1	0.9064	0.8745	0.7997	0.6442	0.4264	0.1398
0.2	0.7654	0.6821	0.5656	0.4121	0.2571	0.0864
0.3	0.5840	0.4827	0.3794	0.2553	0.1529	0.0492
0.4	0.4007	0.3109	0.2316	0.1427	0.0785	0.0246
0.5	0.2342	0.1719	0.1194	0.0644	0.0326	0.0092
0.6	0.1126	0.0740	0.0458	0.0231	0.0099	0.0027
0.7	0.0385	0.0232	0.0129	0.0052	0.0017	0.0005
0.8	0.0071	0.0043	0.0021	0.0004	0.0001	0.0000
0.9	0.0007	0.0003	0.0000	0.0000	0.0000	0.0000
1.0	0.0000	0.0000	0.0000	0.0000	0.0000	0.0000

TABLE B-3. (CONTINUED)

(Energy = 3.0 MeV)

Shield Thickness (T/R)	Incident Angle (deg) 0	30	45	60	75	89.9
0.1	0.9048	0.8798	0.8132	0.6643	0.4260	0.1300
0.2	0.7784	0.6992	0.5814	0.4197	0.2492	0.0778
0.3	0.6140	0.5092	0.3955	0.2591	0.1471	0.0444
0.4	0.4296	0.3354	0.2420	0.1451	0.0745	0.0223
0.5	0.2594	0.1943	0.1288	0.0687	0.0301	0.0095
0.6	0.1317	0.0859	0.0534	0.0247	0.0094	0.0026
0.7	0.0490	0.0289	0.0158	0.0060	0.0018	0.0004
0.8	0.0111	0.0053	0.0021	0.0007	0.0001	0.0000
0.9	0.0008	0.0003	0.0002	0.0000	0.0000	0.0000
1.0	0.0000	0.0000	0.0000	0.0000	0.0000	0.0000

(Energy = 4.0 MeV)

Shield Thickness (T/R)	Incident Angle (deg) 0	30	45	60	75	89.9
0.1	0.9035	0.8804	0.8169	0.6694	0.4275	0.1228
0.2	0.7800	0.7064	0.5904	0.4254	0.2482	0.0727
0.3	0.6232	0.5219	0.4020	0.2630	0.1459	0.0412
0.4	0.4473	0.3476	0.2460	0.1470	0.0747	0.0214
0.5	0.2837	0.2081	0.1342	0.0719	0.0318	0.0093
0.6	0.1437	0.1021	0.0598	0.0274	0.0100	0.0028
0.7	0.0607	0.0366	0.0189	0.0065	0.0020	0.0004
0.8	0.0163	0.0086	0.0035	0.0008	0.0003	0.0000
0.9	0.0021	0.0008	0.0003	0.0000	0.0000	0.0000
1.0	0.0000	0.0000	0.0000	0.0000	0.0000	0.0000

(Energy = 5.0 MeV)

Shield Thickness (T/R)	Incident Angle (deg) 0	30	45	60	75	89.9
0.1	0.9033	0.8821	0.8281	0.6852	0.4280	0.1149
0.2	0.7866	0.7187	0.6026	0.4341	0.2427	0.0655
0.3	0.6428	0.5376	0.4133	0.2688	0.1408	0.0369
0.4	0.4751	0.3643	0.2558	0.1508	0.0719	0.0192
0.5	0.3054	0.2189	0.1412	0.0721	0.0318	0.0082
0.6	0.1686	0.1119	0.0647	0.0274	0.0106	0.0025
0.7	0.0711	0.0441	0.0205	0.0075	0.0026	0.0005
0.8	0.0186	0.0099	0.0044	0.0010	0.0004	0.0000
0.9	0.0027	0.0010	0.0005	0.0001	0.0000	0.0000
1.0	0.0000	0.0000	0.0000	0.0000	0.0000	0.0000

TABLE B-3. (CONTINUED)

(Energy = 6.0 MeV)

Shield Thickness (T/R)	Incident Angle (deg) 0	30	45	60	75	89.9
0.1	0.9027	0.8810	0.8327	0.6911	0.4279	0.1106
0.2	0.7891	0.7247	0.6078	0.4354	0.2386	0.0626
0.3	0.6488	0.5458	0.4181	0.2666	0.1397	0.0340
0.4	0.4877	0.3778	0.2619	0.1521	0.0726	0.0169
0.5	0.3212	0.2348	0.1456	0.0745	0.0316	0.0069
0.6	0.1856	0.1240	0.0678	0.0287	0.0106	0.0021
0.7	0.0808	0.0503	0.0232	0.0081	0.0022	0.0004
0.8	0.0229	0.0130	0.0048	0.0013	0.0003	0.0000
0.9	0.0037	0.0015	0.0006	0.0002	0.0000	0.0000
1.0	0.0000	0.0000	0.0000	0.0000	0.0000	0.0000

(Energy = 10.0 MeV)

Shield Thickness (T/R)	Incident Angle (deg) 0	30	45	60	75	89.9
0.1	0.8991	0.8773	0.8374	0.7114	0.4448	0.0821
0.2	0.7844	0.7329	0.6349	0.4516	0.2479	0.0440
0.3	0.6587	0.5714	0.4464	0.2787	0.1336	0.0226
0.4	0.5200	0.4050	0.2936	0.1626	0.0656	0.0108
0.5	0.3716	0.2634	0.1756	0.0824	0.0268	0.0040
0.6	0.2271	0.1500	0.0902	0.0354	0.0089	0.0012
0.7	0.1144	0.0679	0.0350	0.0115	0.0020	0.0002
0.8	0.0413	0.0210	0.0098	0.0022	0.0003	0.0000
0.9	0.0087	0.0039	0.0013	0.0001	0.0000	0.0000
1.0	0.0007	0.0001	0.0000	0.0000	0.0000	0.0000

TABLE B-4. ELECTRON ENERGY REFLECTION COEFFICIENT FOR AN ALUMINUM PLANE SHIELD

(Energy = 0.5 MeV)

Shield Thickness (T/R)	Incident Angle (deg) 0	30	45	60	75	89.9
0.1	0.0120	0.0263	0.0686	0.1802	0.3593	0.7318
0.2	0.0373	0.0659	0.1159	0.2239	0.3894	0.7415
0.3	0.0502	0.0785	0.1248	0.2298	0.3924	0.7425
0.4	0.0511	0.0793	0.1255	0.2302	0.3926	0.7425
0.5	0.0511	0.0793	0.1255	0.2302	0.3926	0.7425
0.6	0.0511	0.0793	0.1255	0.2302	0.3926	0.7425
0.7	0.0511	0.0793	0.1255	0.2302	0.3926	0.7425
0.8	0.0511	0.0793	0.1255	0.2302	0.3926	0.7425
0.9	0.0511	0.0793	0.1255	0.2302	0.3926	0.7425
1.0	0.0511	0.0793	0.1255	0.2302	0.3926	0.7425

(Energy = 1.0 MeV)

Shield Thickness (T/R)	Incident Angle (deg) 0	30	45	60	75	89.9
0.1	0.0083	0.0214	0.0630	0.1603	0.3403	0.7376
0.2	0.0285	0.0570	0.1051	0.1997	0.3667	0.7459
0.3	0.0395	0.0681	0.1131	0.2051	0.3700	0.7471
0.4	0.0406	0.0689	0.1135	0.2053	0.3701	0.7471
0.5	0.0406	0.0689	0.1135	0.2053	0.3701	0.7471
0.6	0.0406	0.0689	0.1135	0.2053	0.3701	0.7471
0.7	0.0406	0.0689	0.1135	0.2053	0.3701	0.7471
0.8	0.0406	0.0689	0.1135	0.2053	0.3701	0.7471
0.9	0.0406	0.0689	0.1135	0.2053	0.3701	0.7471
1.0	0.0406	0.0689	0.1135	0.2053	0.3701	0.7471

(Energy = 2.0 MeV)

Shield Thickness (T/R)	Incident Angle (deg) 0	30	45	60	75	89.9
0.1	0.0040	0.0130	0.0422	0.1252	0.3081	0.7409
0.2	0.0140	0.0375	0.0784	0.1607	0.3310	0.7471
0.3	0.0201	0.0446	0.0839	0.1648	0.3336	0.7477
0.4	0.0211	0.0454	0.0842	0.1650	0.3336	0.7477
0.5	0.0211	0.0454	0.0842	0.1650	0.3336	0.7477
0.6	0.0211	0.0454	0.0842	0.1650	0.3336	0.7477
0.7	0.0211	0.0454	0.0842	0.1650	0.3336	0.7477
0.8	0.0211	0.0454	0.0842	0.1650	0.3336	0.7477
0.9	0.0211	0.0454	0.0842	0.1650	0.3336	0.7477
1.0	0.0211	0.0454	0.0842	0.1650	0.3336	0.7477

TABLE B-4 (CONTINUED)

(Energy = 3.0 MeV)

Shield Thickness (T/R)	Incident Angle (deg) 0	30	45	60	75	89.9
0.1	0.0023	0.0068	0.0288	0.0963	0.2791	0.7424
0.2	0.0077	0.0259	0.0587	0.1293	0.2998	0.7478
0.3	0.0116	0.0313	0.0642	0.1332	0.3018	0.7482
0.4	0.0125	0.0319	0.0644	0.1334	0.3018	0.7482
0.5	0.0125	0.0319	0.0644	0.1334	0.3018	0.7482
0.6	0.0125	0.0319	0.0644	0.1334	0.3018	0.7482
0.7	0.0125	0.0319	0.0644	0.1334	0.3018	0.7482
0.8	0.0125	0.0319	0.0644	0.1334	0.3018	0.7482
0.9	0.0125	0.0319	0.0644	0.1334	0.3018	0.7482
1.0	0.0125	0.0319	0.0644	0.1334	0.3018	0.7482

(Energy = 4.0 MeV)

Shield Thickness (T/R)	Incident Angle (deg) 0	30	45	60	75	89.9
0.1	0.0016	0.0053	0.0227	0.0829	0.2616	0.7462
0.2	0.0051	0.0193	0.0466	0.1136	0.2816	0.7509
0.3	0.0081	0.0245	0.0508	0.1169	0.2832	0.7512
0.4	0.0086	0.0248	0.0511	0.1172	0.2832	0.7512
0.5	0.0086	0.0248	0.0511	0.1172	0.2832	0.7512
0.6	0.0086	0.0248	0.0511	0.1172	0.2832	0.7512
0.7	0.0086	0.0248	0.0511	0.1172	0.2832	0.7512
0.8	0.0086	0.0248	0.0511	0.1172	0.2832	0.7512
0.9	0.0086	0.0248	0.0511	0.1172	0.2832	0.7512
1.0	0.0086	0.0248	0.0511	0.1172	0.2832	0.7512

(Energy = 5.0 MeV)

Shield Thickness (T/R)	Incident Angle (deg) 0	30	45	60	75	89.9
0.1	0.0013	0.0033	0.0158	0.0660	0.2400	0.7474
0.2	0.0042	0.0131	0.0349	0.0933	0.2584	0.7515
0.3	0.0065	0.0162	0.0385	0.0965	0.2599	0.7517
0.4	0.0072	0.0162	0.0386	0.0966	0.2599	0.7517
0.5	0.0072	0.0162	0.0386	0.0966	0.2599	0.7517
0.6	0.0072	0.0162	0.0386	0.0966	0.2599	0.7517
0.7	0.0072	0.0162	0.0386	0.0966	0.2599	0.7517
0.8	0.0072	0.0162	0.0386	0.0966	0.2599	0.7517
0.9	0.0072	0.0162	0.0386	0.0966	0.2599	0.7517
1.0	0.0072	0.0162	0.0386	0.0966	0.2599	0.7517

TABLE B-4. (CONTINUED)

(Energy = 6.0 MeV)

Shield Thickness (T/R)	Incident Angle (deg) 0	30	45	60	75	89.9
0.1	0.0013	0.0026	0.0120	0.0577	0.2252	0.7483
0.2	0.0031	0.0089	0.0294	0.0818	0.2418	0.7520
0.3	0.0053	0.0118	0.0327	0.0850	0.2432	0.7522
0.4	0.0060	0.0118	0.0328	0.0851	0.2432	0.7522
0.5	0.0060	0.0118	0.0328	0.0851	0.2432	0.7522
0.6	0.0060	0.0118	0.0328	0.0851	0.2432	0.7522
0.7	0.0060	0.0118	0.0328	0.0851	0.2432	0.7522
0.8	0.0060	0.0118	0.0328	0.0851	0.2432	0.7522
0.9	0.0060	0.0118	0.0328	0.0851	0.2432	0.7522
1.0	0.0060	0.0118	0.0328	0.0851	0.2432	0.7522

(Energy = 10.0 MeV)

Shield Thickness (T/R)	Incident Angle (deg) 0	30	45	60	75	89.9
0.1	0.0005	0.0029	0.0076	0.0382	0.1779	0.7905
0.2	0.0014	0.0049	0.0162	0.0543	0.1920	0.7928
0.3	0.0022	0.0065	0.0181	0.0566	0.1927	0.7929
0.4	0.0024	0.0067	0.0181	0.0567	0.1927	0.7929
0.5	0.0024	0.0067	0.0181	0.0567	0.1927	0.7929
0.6	0.0024	0.0067	0.0181	0.0567	0.1927	0.7929
0.7	0.0024	0.0067	0.0181	0.0567	0.1927	0.7929
0.8	0.0024	0.0067	0.0181	0.0567	0.1927	0.7929
0.9	0.0024	0.0067	0.0181	0.0567	0.1927	0.7929
1.0	0.0024	0.0067	0.0181	0.0567	0.1927	0.7929

TABLE B-5. ELECTRON ENERGY DEPOSITION COEFFICIENTS IN MeV/g FOR MONODIRECTIONAL BEAMS INCIDENT AT SEVERAL ANGLES ON AN ALUMINUM SEMI-INFINITE PLANE SHIELD

(Energy = 0.5 MeV)

Shield Thickness (T/R)	Incident Angle (deg)					
	0	30	45	60	75	89.9
0.01	2.0000	2.5400	3.3100	5.2900	8.7800	6.3700
0.03	2.3400	3.0100	4.1000	6.0900	5.7700	2.0700
0.05	2.7100	3.5300	4.6400	5.5100	4.3400	1.7000
0.07	2.9300	3.6300	4.9800	4.9500	3.8800	1.4900
0.09	3.1000	3.8500	4.7100	4.5000	3.5300	1.2900
0.11	3.4500	3.9400	4.6400	4.3100	3.2400	1.2200
0.13	3.5800	4.1300	4.3200	3.9300	2.9000	1.1200
0.15	3.8000	4.2700	4.2900	3.7900	2.8500	1.0900
0.17	4.0500	4.0400	4.1100	3.5700	2.6200	1.0600
0.19	4.1000	4.4000	4.0300	3.4100	2.6200	1.0000
0.21	4.2900	4.2000	3.8000	3.1300	2.3500	0.9900
0.23	4.1300	4.2100	3.7500	3.0200	2.3000	0.9100
0.25	4.2100	3.9100	3.7800	3.0600	2.1800	0.8900
0.27	4.0600	4.0100	3.5300	2.9200	1.9800	0.7900
0.29	3.9200	3.8000	3.3700	2.6200	1.9600	0.7900
0.31	3.9400	3.7900	3.2200	2.5700	1.8400	0.7000
0.33	3.6800	3.6600	3.0400	2.4500	1.6800	0.6100
0.35	3.7400	3.2900	3.0900	2.2900	1.6200	0.6400
0.37	3.4800	3.3600	3.0000	2.1900	1.3900	0.5300
0.39	3.4200	3.2800	2.8800	2.0700	1.3300	0.5000
0.41	3.4300	3.0600	2.5000	1.9100	1.1700	0.4800
0.43	3.1800	2.7300	2.2400	1.6700	1.0900	0.3800
0.45	3.0800	2.6100	2.0900	1.4300	0.8800	0.3500
0.47	3.0300	2.4100	2.0200	1.3100	0.8300	0.3000
0.49	2.9900	2.3200	1.8600	1.1700	0.6900	0.2500
0.51	2.7100	2.1700	1.6700	1.0900	0.6800	0.2100
0.53	2.2700	1.9800	1.3500	0.8400	0.5900	0.1900
0.55	2.2100	1.7200	1.2700	0.8400	0.4000	0.1600
0.57	1.9100	1.4700	1.1200	0.7400	0.4100	0.1200
0.59	1.7200	1.1600	0.8900	0.5600	0.3200	0.1000
0.61	1.5400	1.1000	0.7700	0.4300	0.2700	0.0800
0.63	1.2200	0.9500	0.5600	0.3600	0.1800	0.0600
0.65	0.9700	0.7600	0.4400	0.2800	0.1300	0.0600
0.67	0.7400	0.6400	0.3800	0.2100	0.0900	0.0400
0.69	0.6900	0.5800	0.3000	0.1500	0.0700	0.0300
0.71	0.5500	0.4100	0.2200	0.1400	0.0500	0.0300
0.73	0.5000	0.2800	0.1800	0.1200	0.0500	0.0300
0.75	0.4300	0.2500	0.1200	0.0800	0.0200	0.0100
0.77	0.3500	0.1500	0.0700	0.0400	0.0100	0.0100
0.79	0.2400	0.1500	0.0400	0.0300	0.0100	0.0000
0.81	0.1800	0.1000	0.0200	0.0200	0.0000	0.0000
0.83	0.0900	0.0300	0.0100	0.0000	0.0000	0.0000
0.85	0.0600	0.0200	0.0100	0.0000	0.0000	0.0000
0.87	0.0200	0.0100	0.0100	0.0000	0.0000	0.0000
0.89	0.0100	0.0100	0.0100	0.0000	0.0000	0.0000
0.91	0.0000	0.0100	0.0100	0.0000	0.0000	0.0000
0.93	0.0000	0.0000	0.0100	0.0000	0.0000	0.0000

TABLE B-5. (CONTINUED)

(Energy = 1.0 MeV)

Shield Thickness (T/R)	Incident Angle (deg) 0	30	45	60	75	89.9
0.01	1.7700	2.0900	2.9000	4.4700	7.9500	5.4100
0.03	1.8700	2.3900	3.3000	5.2000	5.2500	1.8600
0.05	2.1800	2.7900	3.7800	4.8700	4.0300	1.4600
0.07	2.3100	3.0200	3.9700	4.3400	3.3600	1.2200
0.09	2.4200	3.2600	3.8800	3.9100	3.0600	1.0600
0.11	2.6500	3.3400	3.7500	3.7000	2.7200	0.9800
0.13	2.9600	3.4100	3.6000	3.3900	2.5000	0.9000
0.15	3.1100	3.5100	3.7000	3.1300	2.3500	0.8600
0.17	3.1600	3.6600	3.5300	3.0000	2.2100	0.8000
0.19	3.4300	3.5900	3.4300	2.8100	2.1000	0.7900
0.21	3.3700	3.4000	3.1900	2.7400	2.0600	0.7200
0.23	3.3000	3.3800	3.0500	2.5800	1.7400	0.6500
0.25	3.3500	3.2000	2.8800	2.5500	1.7400	0.6200
0.27	3.3400	3.1600	2.7700	2.3400	1.6600	0.5600
0.29	3.2900	3.1100	2.7500	2.2000	1.5300	0.5500
0.31	3.1700	2.9500	2.6100	2.0200	1.4400	0.5500
0.33	3.1600	2.8000	2.4100	1.9700	1.2500	0.5100
0.35	3.0200	2.7100	2.3800	1.7800	1.2100	0.4600
0.37	3.0200	2.7300	2.2100	1.7200	1.0900	0.4600
0.39	2.9400	2.6800	2.1000	1.6300	1.0500	0.4100
0.41	2.7400	2.4500	2.0900	1.4900	0.9100	0.3300
0.43	2.6800	2.3500	1.9300	1.3600	0.8400	0.2800
0.45	2.4900	2.0800	1.7400	1.2400	0.7100	0.2600
0.47	2.4600	2.0200	1.6300	1.0800	0.6000	0.2100
0.49	2.3400	1.8700	1.5800	0.9800	0.5800	0.1800
0.51	2.1100	1.7500	1.3800	0.9200	0.5100	0.1400
0.53	1.9800	1.5300	1.1500	0.7700	0.4500	0.1300
0.55	1.7100	1.4500	1.1400	0.6600	0.3900	0.1000
0.57	1.5600	1.2700	1.0100	0.5600	0.3000	0.0900
0.59	1.4000	1.1400	0.8100	0.4800	0.2200	0.0800
0.61	1.1300	0.9000	0.6200	0.3700	0.1800	0.0500
0.63	1.1100	0.7600	0.5300	0.2900	0.1700	0.0400
0.65	1.0400	0.7000	0.4700	0.2500	0.1000	0.0300
0.67	0.7500	0.5500	0.3500	0.1900	0.0800	0.0200
0.69	0.7400	0.4600	0.2900	0.1600	0.0600	0.0200
0.71	0.5700	0.3500	0.2300	0.1400	0.0500	0.0200
0.73	0.4900	0.2800	0.1700	0.0900	0.0300	0.0200
0.75	0.3600	0.2000	0.1500	0.0600	0.0400	0.0000
0.77	0.2900	0.1500	0.1100	0.0400	0.0200	0.0000
0.79	0.2000	0.1000	0.0700	0.0200	0.0100	0.0000
0.81	0.1500	0.0900	0.0400	0.0200	0.0000	0.0000
0.83	0.0900	0.0500	0.0300	0.0100	0.0000	0.0000
0.85	0.0600	0.0300	0.0300	0.0100	0.0000	0.0000
0.87	0.0400	0.0200	0.0100	0.0000	0.0000	0.0000
0.89	0.0200	0.0100	0.0000	0.0000	0.0000	0.0000
0.91	0.0100	0.0000	0.0000	0.0000	0.0000	0.0000
0.93	0.0100	0.0000	0.0000	0.0000	0.0000	0.0000
0.95	0.0100	0.0000	0.0000	0.0000	0.0000	0.0000

TABLE B-5. (CONTINUED)

(Energy = 2.0 MeV)

Shield Thickness (T/R)	Incident Angle (deg)					
	0	30	45	60	75	89.9
0.01	1.5300	1.9100	2.6100	4.1600	7.8700	5.2400
0.03	1.6300	2.1200	3.0100	4.9200	5.3300	1.7600
0.05	1.8300	2.3500	3.3400	4.7900	4.1100	1.3200
0.07	1.9200	2.5600	3.4500	4.2100	3.4600	1.0800
0.09	2.0300	2.7100	3.4600	3.8200	2.9600	0.9800
0.11	2.2700	2.9100	3.5100	3.5400	2.6900	0.8400
0.13	2.4200	2.9000	3.3000	3.3000	2.4200	0.7800
0.15	2.4400	3.1000	3.1900	3.1800	2.1700	0.7600
0.17	2.5900	3.1700	3.2400	2.9100	2.0000	0.7000
0.19	2.7100	3.0900	3.0900	2.6500	1.9300	0.6400
0.21	2.8500	3.1600	2.8300	2.5800	1.7700	0.6100
0.23	2.9200	2.9900	2.8400	2.4100	1.5900	0.6200
0.25	2.8600	2.9400	2.7400	2.1800	1.4700	0.5500
0.27	2.9000	2.8800	2.7600	2.0100	1.4100	0.5000
0.29	2.8800	2.7400	2.5200	2.0000	1.3300	0.4600
0.31	2.6800	2.7100	2.4300	1.8700	1.2400	0.4000
0.33	2.8100	2.6700	2.3100	1.7300	1.1500	0.4000
0.35	2.8100	2.5500	2.1900	1.6100	1.0900	0.3600
0.37	2.6400	2.4200	2.1100	1.5400	0.9800	0.3300
0.39	2.8100	2.4300	2.0700	1.4000	0.9500	0.2900
0.41	2.6600	2.3500	1.8900	1.3400	0.8000	0.2800
0.43	2.6300	2.1900	1.7600	1.2500	0.7500	0.2600
0.45	2.4300	2.0200	1.6400	1.1900	0.7000	0.2300
0.47	2.4400	1.8900	1.5100	1.0700	0.5700	0.2000
0.49	2.3600	1.8000	1.4600	0.8700	0.5100	0.1500
0.51	2.0900	1.6600	1.3200	0.8100	0.4400	0.1300
0.53	1.9200	1.5400	1.1600	0.6900	0.3700	0.1200
0.55	1.7100	1.3700	1.0500	0.5800	0.3200	0.0800
0.57	1.6400	1.2900	0.8900	0.4900	0.2800	0.0700
0.59	1.5400	1.1500	0.7800	0.4100	0.2300	0.0700
0.61	1.2900	0.9500	0.6000	0.3800	0.1700	0.0500
0.63	1.2000	0.8500	0.5600	0.3200	0.1500	0.0300
0.65	0.9900	0.7400	0.5100	0.2600	0.1000	0.0300
0.67	0.8700	0.6800	0.4000	0.1800	0.0700	0.0200
0.69	0.7700	0.5000	0.3200	0.1400	0.0500	0.0100
0.71	0.6000	0.4100	0.2500	0.1200	0.0300	0.0100
0.73	0.5300	0.3400	0.1900	0.0900	0.0200	0.0100
0.75	0.4700	0.2600	0.1400	0.0700	0.0100	0.0100
0.77	0.3900	0.2200	0.1200	0.0600	0.0100	0.0100
0.79	0.2700	0.1900	0.0700	0.0300	0.0000	0.0000
0.81	0.1700	0.1100	0.0600	0.0100	0.0000	0.0000
0.83	0.1200	0.0800	0.0300	0.0100	0.0000	0.0000
0.85	0.0700	0.0400	0.0200	0.0000	0.0000	0.0000
0.87	0.0500	0.0200	0.0200	0.0000	0.0000	0.0000
0.89	0.0500	0.0200	0.0100	0.0000	0.0000	0.0000
0.91	0.0100	0.0100	0.0000	0.0000	0.0000	0.0000
0.93	0.0100	0.0100	0.0000	0.0000	0.0000	0.0000
0.95	0.0100	0.0000	0.0000	0.0000	0.0000	0.0000

TABLE B-5. (CONTINUED)

(Energy = 3.0 MeV)

Shield Thickness (T/R)	Incident Angle (deg)					
	0	30	45	60	75	89.9
0.01	1.4300	1.8300	2.4600	3.9200	8.1500	5.4500
0.03	1.5200	1.9300	2.8500	4.7900	5.7400	1.8200
0.05	1.7300	2.1800	3.0900	4.8000	4.5200	1.3200
0.07	1.7700	2.2800	3.3400	4.4400	3.6500	1.1100
0.09	1.8800	2.4900	3.3300	3.9400	3.2600	0.9300
0.11	2.0100	2.6500	3.3100	3.7900	2.7700	0.8000
0.13	2.0500	2.6500	3.3400	3.5600	2.4400	0.7800
0.15	2.2100	2.7500	3.2800	3.2000	2.2600	0.7000
0.17	2.3700	2.8000	3.2200	2.9500	2.0900	0.6700
0.19	2.4500	2.8600	3.0000	2.7400	1.8500	0.6100
0.21	2.5800	2.9000	2.9400	2.5100	1.7000	0.5600
0.23	2.6600	2.9700	2.7000	2.3500	1.5900	0.5100
0.25	2.5800	2.9300	2.6800	2.2500	1.4600	0.4800
0.27	2.6700	2.7800	2.5800	2.0900	1.3800	0.4200
0.29	2.7500	2.8000	2.5400	1.9600	1.3000	0.4200
0.31	2.8200	2.5600	2.3600	1.8800	1.1800	0.3900
0.33	2.7900	2.7200	2.3000	1.7400	1.1400	0.3600
0.35	2.8000	2.5800	2.2500	1.6200	1.0100	0.3000
0.37	2.8600	2.5200	2.1500	1.4600	0.9400	0.2700
0.39	2.8800	2.4600	1.9900	1.4000	0.8700	0.2500
0.41	2.7200	2.2700	1.8200	1.3000	0.8000	0.2300
0.43	2.5500	2.1500	1.8000	1.1900	0.7300	0.1900
0.45	2.4400	2.0600	1.6400	1.1200	0.6100	0.1800
0.47	2.3100	2.0100	1.5800	1.0200	0.5500	0.1700
0.49	2.2500	1.8800	1.4500	0.8800	0.4800	0.1500
0.51	2.0900	1.7500	1.3100	0.8000	0.4100	0.1400
0.53	1.9200	1.6800	1.2600	0.7200	0.3300	0.1200
0.55	1.7900	1.5800	1.1200	0.6500	0.2700	0.1000
0.57	1.7000	1.3400	0.9300	0.5100	0.2200	0.0800
0.59	1.6100	1.2300	0.8400	0.4700	0.1900	0.0700
0.61	1.4400	1.0700	0.7000	0.3900	0.1600	0.0600
0.63	1.3100	0.9500	0.5800	0.2900	0.1200	0.0300
0.65	1.1600	0.8400	0.5200	0.2800	0.1100	0.0300
0.67	1.0500	0.6800	0.4600	0.2000	0.0800	0.0200
0.69	0.8900	0.5500	0.3800	0.1700	0.0700	0.0200
0.71	0.8000	0.4900	0.3300	0.1200	0.0400	0.0100
0.73	0.5800	0.4200	0.2700	0.0900	0.0400	0.0100
0.75	0.5100	0.3300	0.1600	0.0800	0.0200	0.0000
0.77	0.4300	0.2500	0.1100	0.0600	0.0200	0.0000
0.79	0.3800	0.1900	0.0800	0.0300	0.0100	0.0000
0.81	0.2500	0.1500	0.0600	0.0200	0.0000	0.0000
0.83	0.2000	0.0900	0.0400	0.0200	0.0000	0.0000
0.85	0.1200	0.0700	0.0200	0.0100	0.0000	0.0000
0.87	0.0900	0.0300	0.0100	0.0100	0.0000	0.0000
0.89	0.0500	0.0100	0.0100	0.0000	0.0000	0.0000
0.91	0.0200	0.0100	0.0100	0.0000	0.0000	0.0000
0.93	0.0100	0.0100	0.0000	0.0000	0.0000	0.0000
0.95	0.0200	0.0100	0.0000	0.0000	0.0000	0.0000
0.97	0.0100	0.0000	0.0000	0.0000	0.0000	0.0000

TABLE B-5. (CONTINUED)

(Energy = 4.0 MeV)

Shield Thickness (T/R)	Incident Angle (deg)					
	0	30	45	60	75	89.9
0.01	1.4400	1.7800	2.4000	3.9500	8.3100	5.5600
0.03	1.5500	1.9000	2.7100	4.6900	5.9900	1.8300
0.05	1.6100	2.0500	3.0100	4.8300	4.6700	1.3000
0.07	1.7100	2.1900	3.2100	4.4800	3.8700	1.0800
0.09	1.7900	2.3700	3.3300	4.0800	3.3800	0.9000
0.11	1.8800	2.4300	3.3300	3.7200	2.8200	0.8000
0.13	1.9900	2.6100	3.3200	3.4400	2.5600	0.7100
0.15	2.0400	2.6500	3.2600	3.2200	2.3300	0.7000
0.17	2.1700	2.7600	3.1900	2.8900	2.0400	0.6500
0.19	2.2700	2.8500	3.1300	2.7400	1.8500	0.5700
0.21	2.3600	2.7800	2.9800	2.6000	1.7000	0.4900
0.23	2.4300	2.8800	2.8200	2.4100	1.5500	0.4700
0.25	2.5200	2.8200	2.7900	2.2500	1.3700	0.4500
0.27	2.6100	2.7900	2.6300	2.1000	1.3800	0.4300
0.29	2.6700	2.7100	2.5500	1.9700	1.2600	0.4000
0.31	2.6600	2.6000	2.4600	1.8700	1.1700	0.3500
0.33	2.7100	2.6600	2.3100	1.7900	1.0800	0.3100
0.35	2.6500	2.5900	2.2000	1.6300	1.0000	0.2800
0.37	2.6700	2.5000	2.1400	1.6100	0.9500	0.2600
0.39	2.6300	2.4200	2.0000	1.4400	0.8900	0.2300
0.41	2.5700	2.2800	1.8800	1.2600	0.7700	0.2300
0.43	2.5400	2.0800	1.7500	1.1600	0.6700	0.1800
0.45	2.4700	2.0400	1.6500	1.1400	0.6300	0.1800
0.47	2.3400	1.9900	1.5000	0.9900	0.5200	0.1600
0.49	2.2900	1.9200	1.4600	0.9200	0.4700	0.1500
0.51	2.2100	1.8500	1.2900	0.7900	0.4200	0.1300
0.53	2.1000	1.6800	1.1800	0.7400	0.3400	0.1100
0.55	1.9700	1.4900	1.0800	0.6800	0.3200	0.0900
0.57	1.8400	1.3700	0.9700	0.5800	0.2800	0.0800
0.59	1.6900	1.2900	0.8700	0.4700	0.2000	0.0500
0.61	1.5800	1.1600	0.7600	0.4400	0.1700	0.0500
0.63	1.4500	1.0400	0.6300	0.3600	0.1300	0.0400
0.65	1.3000	0.9400	0.5700	0.3200	0.1100	0.0300
0.67	1.1600	0.8200	0.5100	0.2200	0.0900	0.0300
0.69	1.0000	0.7300	0.4000	0.1700	0.0700	0.0200
0.71	0.8600	0.5500	0.3200	0.1400	0.0400	0.0100
0.73	0.7500	0.5000	0.2500	0.1000	0.0300	0.0100
0.75	0.6400	0.4000	0.2300	0.0700	0.0200	0.0000
0.77	0.5400	0.3000	0.1600	0.0500	0.0100	0.0000
0.79	0.4300	0.2200	0.1200	0.0500	0.0100	0.0000
0.81	0.3500	0.2000	0.0800	0.0200	0.0100	0.0000
0.83	0.2600	0.1400	0.0700	0.0100	0.0100	0.0000
0.85	0.1900	0.1100	0.0400	0.0100	0.0000	0.0000
0.87	0.1300	0.0700	0.0300	0.0000	0.0000	0.0000
0.89	0.0900	0.0400	0.0200	0.0000	0.0000	0.0000
0.91	0.0600	0.0300	0.0100	0.0000	0.0000	0.0000
0.93	0.0400	0.0200	0.0100	0.0000	0.0000	0.0000
0.95	0.0300	0.0100	0.0000	0.0000	0.0000	0.0000
0.97	0.0100	0.0000	0.0000	0.0000	0.0000	0.0000
0.99	0.0100	0.0000	0.0000	0.0000	0.0000	0.0000

TABLE B-5. (CONTINUED)

(Energy = 5.0 MeV)

Shield Thickness (T/R)	Incident Angle (deg)					
	0	30	45	60	75	89.9
0.01	1.4300	1.7200	2.3100	3.7800	8.4400	5.8500
0.03	1.5100	1.8800	2.6100	4.5300	6.5000	1.8900
0.05	1.6300	1.9400	2.8600	4.7700	5.0000	1.2900
0.07	1.6200	2.1100	3.1000	4.5300	4.1700	1.0700
0.09	1.6700	2.2400	3.1900	4.2100	3.5400	0.9200
0.11	1.7800	2.3300	3.2000	3.8900	2.9700	0.7900
0.13	1.7500	2.4100	3.2900	3.5400	2.6200	0.7200
0.15	1.8400	2.6000	3.3900	3.3200	2.3800	0.6800
0.17	2.0200	2.7900	3.2900	3.0800	2.1200	0.5800
0.19	2.1100	2.7900	3.1700	2.8500	1.9200	0.5800
0.21	2.1600	2.6700	2.9900	2.6300	1.7300	0.4800
0.23	2.2400	2.7400	2.8300	2.5000	1.5700	0.4500
0.25	2.3200	2.7500	2.8700	2.3500	1.4400	0.4200
0.27	2.5300	2.7700	2.6800	2.2000	1.2900	0.3800
0.29	2.4300	2.7100	2.5800	2.0600	1.2200	0.3400
0.31	2.4800	2.6600	2.5000	1.9200	1.1300	0.2900
0.33	2.6000	2.6700	2.3900	1.8100	1.1100	0.2800
0.35	2.6200	2.5300	2.3000	1.7300	1.0100	0.2600
0.37	2.6900	2.5900	2.1900	1.7000	0.8900	0.2200
0.39	2.7100	2.6500	2.1000	1.5300	0.7900	0.2400
0.41	2.6200	2.2700	1.9300	1.4100	0.7500	0.2000
0.43	2.4900	2.2700	1.8300	1.2400	0.6400	0.1800
0.45	2.5800	2.1500	1.7100	1.2000	0.5600	0.1500
0.47	2.4200	2.0100	1.5400	1.0500	0.5200	0.1300
0.49	2.4100	1.9300	1.4400	0.9100	0.4600	0.1400
0.51	2.2900	1.8600	1.3800	0.8300	0.4100	0.1100
0.53	2.1800	1.7100	1.1900	0.7400	0.3600	0.0900
0.55	2.0800	1.6000	1.0600	0.6600	0.2900	0.0800
0.57	1.9400	1.4500	1.0100	0.5600	0.2500	0.0700
0.59	1.8300	1.3200	0.9600	0.4800	0.2100	0.0600
0.61	1.6400	1.2700	0.8500	0.4100	0.1900	0.0500
0.63	1.5300	1.0800	0.7000	0.3200	0.1400	0.0300
0.65	1.4100	0.9700	0.6000	0.1200	0.1100	0.0300
0.67	1.2800	0.8600	0.5300	0.0800	0.0800	0.0200
0.69	1.1400	0.7400	0.4300	0.0700	0.0600	0.0200
0.71	1.0500	0.6800	0.3300	0.0500	0.0600	0.0100
0.73	0.8400	0.5900	0.2600	0.0300	0.0400	0.0100
0.75	0.7200	0.5000	0.2300	0.0200	0.0400	0.0100
0.77	0.6100	0.3900	0.1900	0.0100	0.0200	0.0000
0.79	0.5000	0.2900	0.1600	0.0000	0.0100	0.0000
0.81	0.4000	0.2300	0.1000	0.0000	0.0100	0.0000
0.83	0.2900	0.1900	0.0700	0.0000	0.0100	0.0000
0.85	0.2000	0.1200	0.0400	0.0000	0.0000	0.0000
0.87	0.1600	0.0800	0.0500	0.0000	0.0000	0.0000
0.89	0.1000	0.0600	0.0300	0.0000	0.0000	0.0000
0.91	0.0800	0.0400	0.0100	0.0000	0.0000	0.0000
0.93	0.0500	0.0100	0.0100	0.0000	0.0000	0.0000
0.95	0.0500	0.0100	0.0100	0.0000	0.0000	0.0000
0.97	0.0300	0.0000	0.0000	0.0000	0.0000	0.0000

TABLE B-5. (CONTINUED)

(Energy = 6.0 MeV)

Shield Thickness (T/R)	Incident Angle (deg) 0	30	45	60	75	89.9
0.01	1.4200	1.7300	2.3000	3.6900	8.5400	5.9500
0.03	1.4900	1.8900	2.5700	4.4600	6.7900	1.8900
0.05	1.5900	1.9700	2.7400	4.7400	5.2700	1.3700
0.07	1.6100	2.0600	2.9800	4.5500	4.3400	1.1300
0.09	1.6200	2.1200	3.1100	4.3500	3.6500	0.9000
0.11	1.7000	2.2600	3.1800	4.0900	3.0700	0.7900
0.13	1.7100	2.4200	3.2900	3.6700	2.7300	0.7400
0.15	1.8500	2.4600	3.2500	3.4500	2.4300	0.6400
0.17	1.9300	2.6500	3.3400	3.0900	2.2300	0.5800
0.19	2.0500	2.7400	3.1500	2.9300	1.9200	0.5200
0.21	2.1200	2.6900	3.0200	2.6900	1.6300	0.5000
0.23	2.1800	2.6800	2.8600	2.5200	1.5500	0.4600
0.25	2.3100	2.6800	2.9100	2.3700	1.4400	0.3900
0.27	2.3900	2.7500	2.7800	2.2000	1.2800	0.3700
0.29	2.4900	2.6600	2.5400	2.0700	1.2000	0.3600
0.31	2.3500	2.5600	2.4700	1.8600	1.1400	0.3000
0.33	2.5100	2.5900	2.3600	1.7900	1.0700	0.2700
0.35	2.5000	2.6500	2.3200	1.7400	1.0200	0.2500
0.37	2.5300	2.5600	2.2100	1.6200	0.9000	0.2100
0.39	2.6900	2.4400	2.1000	1.5400	0.8400	0.2100
0.41	2.5900	2.2900	1.9500	1.4000	0.7100	0.1800
0.43	2.5300	2.2800	1.8400	1.2600	0.6500	0.1700
0.45	2.3900	2.1300	1.7400	1.1500	0.6000	0.1600
0.47	2.4400	2.0200	1.5800	1.0100	0.5600	0.1300
0.49	2.3400	1.9200	1.4900	0.9000	0.4700	0.1100
0.51	2.2700	1.8100	1.3700	0.8300	0.4200	0.0900
0.53	2.2000	1.7800	1.3000	0.7600	0.3500	0.0700
0.55	2.0400	1.6500	1.1700	0.6900	0.3000	0.0700
0.57	1.9600	1.6500	1.0800	0.5800	0.2400	0.0600
0.59	1.9600	1.4700	1.0000	0.5000	0.2300	0.0400
0.61	1.8000	1.3600	0.8600	0.4300	0.1700	0.0400
0.63	1.6300	1.1100	0.7100	0.3600	0.1600	0.0300
0.65	1.5200	1.0900	0.6400	0.2800	0.1300	0.0300
0.67	1.3800	1.0100	0.5200	0.2400	0.1000	0.0200
0.69	1.2200	0.8700	0.4500	0.2100	0.0700	0.0100
0.71	1.1100	0.7300	0.4100	0.1500	0.0500	0.0100
0.73	0.9400	0.6500	0.3200	0.1300	0.0300	0.0100
0.75	0.8600	0.5200	0.2500	0.0800	0.0300	0.0100
0.77	0.7300	0.4400	0.2100	0.0700	0.0100	0.0000
0.79	0.6400	0.3600	0.1500	0.0600	0.0100	0.0000
0.81	0.4700	0.2800	0.1100	0.0300	0.0100	0.0000
0.83	0.3200	0.2100	0.0600	0.0200	0.0100	0.0000
0.85	0.2600	0.1600	0.0500	0.0100	0.0000	0.0000
0.87	0.1900	0.1000	0.0400	0.0000	0.0000	0.0000
0.89	0.1300	0.0600	0.0200	0.0000	0.0000	0.0000
0.91	0.1000	0.0600	0.0100	0.0000	0.0000	0.0000
0.93	0.0600	0.0400	0.0200	0.0000	0.0000	0.0000
0.95	0.0400	0.0200	0.0200	0.0000	0.0000	0.0000
0.97	0.0300	0.0100	0.0100	0.0000	0.0000	0.0000
0.99	0.0200	0.0000	0.0000	0.0000	0.0000	0.0000

TABLE B-5. (CONTINUED)

(Energy = 10.0 MeV)

Shield Thickness (T/R)	Incident Angle (deg)					
	0	30	45	60	75	89.9
0.01	1.4500	1.6900	2.2100	3.5500	8.6400	5.1000
0.03	1.4800	1.8100	2.3800	4.2400	7.6200	1.7600
0.05	1.5200	1.8300	2.5400	4.4500	5.9000	1.2700
0.07	1.5900	2.0300	2.7200	4.5600	4.6500	1.0200
0.09	1.6700	2.0000	2.9000	4.4900	3.7200	0.8200
0.11	1.6400	2.1000	2.9800	4.1100	3.3100	0.7200
0.13	1.7600	2.2400	3.0500	3.9000	2.9700	0.5900
0.15	1.7700	2.2500	3.0800	3.6500	2.6600	0.5000
0.17	1.7800	2.3200	3.1400	3.4300	2.4100	0.4700
0.19	1.8300	2.3600	3.1000	3.2000	2.2600	0.4100
0.21	1.9600	2.4500	2.9700	2.9500	2.0300	0.3800
0.23	1.9300	2.5000	2.9200	2.7400	1.7900	0.3700
0.25	1.9700	2.5600	2.7900	2.4600	1.6500	0.3300
0.27	2.0700	2.6200	2.7600	2.3100	1.4600	0.2800
0.29	2.0800	2.6100	2.7200	2.1900	1.3000	0.2400
0.31	2.0700	2.6500	2.6100	2.0300	1.2300	0.2300
0.33	2.1500	2.6100	2.4400	1.9000	1.1500	0.2000
0.35	2.1900	2.6300	2.3200	1.7800	1.0500	0.1800
0.37	2.3200	2.4500	2.1500	1.6600	0.9500	0.1700
0.39	2.2700	2.3700	2.0700	1.5600	0.8400	0.1600
0.41	2.3900	2.2400	2.0400	1.4400	0.7200	0.1400
0.43	2.4300	2.2600	1.9200	1.3700	0.6700	0.1100
0.45	2.3400	2.2500	1.8000	1.2500	0.5900	0.1000
0.47	2.3200	2.1600	1.7400	1.0900	0.5200	0.0900
0.49	2.3400	2.0400	1.6500	0.9800	0.4400	0.0800
0.51	2.4500	1.9800	1.5700	0.9200	0.3700	0.0600
0.53	2.3400	1.8600	1.4500	0.7900	0.3200	0.0500
0.55	2.2800	1.7700	1.3200	0.7000	0.2700	0.0400
0.57	2.1800	1.6400	1.2500	0.6300	0.2300	0.0400
0.59	2.0700	1.6000	1.1300	0.5200	0.1800	0.0300
0.61	1.9400	1.4900	1.0700	0.4600	0.1500	0.0200
0.63	1.8900	1.4100	0.9500	0.4500	0.1200	0.0200
0.65	1.7700	1.2600	0.8900	0.3900	0.1000	0.0100
0.67	1.6200	1.1400	0.7600	0.2900	0.0900	0.0100
0.69	1.5100	1.0400	0.6200	0.2700	0.0600	0.0100
0.71	1.3800	0.9400	0.5500	0.2100	0.0400	0.0100
0.73	1.3600	0.8500	0.4400	0.1700	0.0400	0.0100
0.75	1.1700	0.6900	0.3700	0.1500	0.0300	0.0000
0.77	0.9700	0.6100	0.3000	0.1000	0.0100	0.0000
0.79	0.8700	0.5300	0.2800	0.0700	0.0100	0.0000
0.81	0.7000	0.3800	0.2300	0.0600	0.0100	0.0000
0.83	0.6000	0.3300	0.1900	0.0400	0.0100	0.0000
0.85	0.4600	0.2600	0.1100	0.0400	0.0000	0.0000
0.87	0.3900	0.1900	0.0800	0.0200	0.0000	0.0000
0.89	0.3100	0.1700	0.0600	0.0100	0.0000	0.0000
0.91	0.2200	0.1000	0.0400	0.0100	0.0000	0.0000
0.93	0.1500	0.0800	0.0200	0.0100	0.0000	0.0000
0.95	0.1000	0.0500	0.0100	0.0000	0.0000	0.0000
0.97	0.0700	0.0400	0.0100	0.0000	0.0000	0.0000
0.99	0.0400	0.0200	0.0100	0.0000	0.0000	0.0000

TABLE B-6. ELECTRON ENERGY DEPOSITION COEFFICIENTS IN MeV/g FOR A HALF-SPACE ISOTROPIC BEAM INCIDENT ON AN ALUMINUM SEMI-INFINITE PLANE SHIELD

Shield Thickness (Pathlengths)	Incident Energy (MeV)							
	0.5	1	2	3	4	5	6	10
0.01	2.1151	1.8368	1.7236	1.6841	1.6854	1.6567	1.6544	1.6312
0.03	2.1534	1.8064	1.6960	1.6611	1.6489	1.6532	1.6632	1.6672
0.05	2.1410	1.8097	1.6726	1.6446	1.6250	1.6103	1.6148	1.5833
0.07	2.1133	1.7640	1.6082	1.5869	1.5760	1.5748	1.5672	1.5539
0.09	2.0430	1.7225	1.5557	1.5369	1.5399	1.5243	1.5183	1.4976
0.11	2.0211	1.67[illegible]	1.5509	1.5095	1.4711	1.4655	1.4784	1.4461
0.13	1.9466	1.6354	1.4837	1.4652	1.4504	1.4222	1.4441	1.4339
0.15	1.9542	1.6299	1.4668	1.4269	1.4095	1.4239	1.4048	1.3889
0.17	1.9698	1.6071	1.4481	1.3941	1.3647	1.4010	1.3927	1.3641
0.19	1.8955	1.5688	1.3903	1.3376	1.3439	1.3500	1.3462	1.3308
0.21	1.8020	1.4981	1.3542	1.3056	1.2928	1.2745	1.2730	1.2887
0.23	1.7683	1.4325	1.3028	1.2633	1.2581	1.2417	1.2348	1.2470
0.25	1.7289	1.3848	1.2463	1.2305	1.2192	1.2259	1.2228	1.2001
0.27	1.6721	1.3360	1.2194	1.1777	1.1836	1.1872	1.1695	1.1788
0.29	1.5832	1.2990	1.1611	1.1592	1.1420	1.1408	1.1312	1.1466
0.31	1.5492	1.2267	1.1246	1.0862	1.0969	1.1041	1.0742	1.1131
0.33	1.4704	1.1598	1.0784	1.0836	1.0733	1.0840	1.0593	1.0729
0.35	1.4057	1.1130	1.0268	1.0351	1.0233	1.0376	1.0530	1.0419
0.37	1.3632	1.0787	0.9762	0.9943	0.9980	1.0230	1.0056	0.9807
0.39	1.3164	1.0411	0.9634	0.9547	0.9441	0.9951	0.9695	0.9377
0.41	1.2083	0.9720	0.9042	0.8826	0.8778	0.8997	0.8995	0.8993
0.43	1.0848	0.9154	0.8502	0.8378	0.8133	0.8541	0.8616	0.8775
0.45	1.0022	0.8213	0.7911	0.7828	0.7864	0.8159	0.8054	0.8375
0.47	0.9460	0.7718	0.7340	0.7465	0.7295	0.7477	0.7539	0.7936
0.49	0.8853	0.7262	0.6849	0.6884	0.7006	0.7036	0.7048	0.7453
0.51	0.8172	0.6611	0.6227	0.6307	0.6477	0.6679	0.6594	0.7232
0.53	0.6949	0.5740	0.5590	0.5941	0.5930	0.6039	0.6301	0.6660
0.55	0.6307	0.5320	0.4953	0.5413	0.5393	0.5531	0.5762	0.6225
0.57	0.5520	0.4653	0.4477	0.4602	0.4884	0.5051	0.5445	0.5799
0.59	0.4438	0.3992	0.3967	0.4224	0.4393	0.4635	0.4996	0.5380
0.61	0.3936	0.3134	0.3259	0.3630	0.3962	0.4243	0.4466	0.4999
0.63	0.3161	0.2719	0.2944	0.3108	0.3449	0.3597	0.3759	0.4677
0.65	0.2496	0.2428	0.2522	0.2786	0.3101	0.3019	0.3479	0.4252
0.67	0.2034	0.1845	0.2131	0.2323	0.2666	0.2647	0.3081	0.3730
0.69	0.1744	0.1590	0.1669	0.1921	0.2253	0.2258	0.2663	0.3315
0.71	0.1310	0.1248	0.1335	0.1653	0.1776	0.1981	0.2282	0.2943
0.73	0.1031	0.0965	0.1087	0.1340	0.1513	0.1628	0.1937	0.2624
0.75	0.0812	0.0740	0.0853	0.1014	0.1254	0.1394	0.1572	0.2189
0.77	0.0519	0.0548	0.0722	0.0778	0.0947	0.1110	0.1320	0.1822
0.79	0.0417	0.0355	0.0518	0.0592	0.0730	0.0859	0.1078	0.1603
0.81	0.0274	0.0271	0.0323	0.0429	0.0591	0.0651	0.0800	0.1236
0.83	0.0098	0.0162	0.0219	0.0295	0.0429	0.0503	0.0555	0.1045
0.85	0.0069	0.0119	0.0115	0.0192	0.0307	0.0316	0.0424	0.0770
0.87	0.0036	0.0060	0.0077	0.0109	0.0199	0.0253	0.0283	0.0578
0.89	0.0031	0.0023	0.0064	0.0056	0.0125	0.0170	0.0172	0.0475
0.91	0.0026	0.0004	0.0018	0.0036	0.0093	0.0107	0.0145	0.0306
0.93	0.0012	0.0004	0.0018	0.0018	0.0060	0.0050	0.0110	0.0221
0.95	0.0000	0.0004	0.0000	0.0023	0.0028	0.0050	0.0072	0.0131
0.97	0.0000	0.0000	0.0000	0.0000	0.0004	0.0014	0.0041	0.0102
0.99	0.0000	0.0000	0.0000	0.0000	0.0004	0.0000	0.0009	0.0060

APPENDIX C

FLUX TO DOSE RELATIONSHIPS

INTRODUCTION

In general, in practical shielding problems the end result is a prediction of the effect the radiation will have on some object or person located behind a shield. A good measure of the effect of a radiation field is the energy that the field deposits in an object or person. In the case of electrons and photons most of the effects of interest on both object and man can be related completely to the energy deposited. There are important exceptions, however, for example films at low photon energies. The effects are independent of how the energy is deposited and do not depend on whether the radiation is in the form of electrons or photons. The energy deposited per unit mass of a medium is referred to as the absorbed dose or simply the dose and is usually quoted in units of rads. The rad is defined as 100 ergs of energy absorbed per gram, which is also equal to 0.624×10^8 MeV per gram. The dose is a measure of the absorbed energy and is therefore not a unique measure of the radiation field that deposited the energy. In fact the relation between the intensity of either photon or electron radiation and the energy it deposits is a function of the energy of the radiation, whether it is composed of electrons or photons and the atomic number of the absorber. There are any number of combinations of electron or photon spectra and absorber atomic number that will deposit the same dose.

In the case where the object receiving the dose is inanimate the effect of the energy deposition is tied directly to the dose. For example, the photocurrents generated in transistors is often peculiar to the transistor type and is established by measurement in terms of dose or dose rate. The discharge induced in a capacitor is usually measured at several different dose levels and then the discharge due to an arbitrary field is predicted by extrapolating or interpolating the measured data with the dose the field deposits. A large amount of effort has been devoted to the study of the effects of radiation on electronic components; it is conveniently summarized in several documents.[71, 72] Effects of nonelectronic hardware have also been studied extensively; the results of such studies can usually be found in the literature specific to the hardware of interest.

Several quantities have been introduced to relate absorbed energy to biological effects on man and animals. Two of these, the RBE and Quality factor (QF), will be discussed here. The Relative Biological Effectiveness (RBE) relates the response of a human organ to different types of radiation. Because a rad of energy deposited by neutrons or alpha particles will produce a different response in a human organ than a rad of electrons or photons the RBE was defined to correlate these effects. The unit of rem was defined as a standard of human response and is quantitatively defined

as that response which is induced by one rad of 250 keV-radiation. The dose in rads deposited by a specific radiation is converted to rem by weighting the rad dose with the RBE. For electrons and photons the RBE is 1. Historically the RBE has been tied to specific human organ responses. This has proven to be limiting and recently another but similar quantity called the Quality Factor (QF) has been defined in terms a physical quantity, the linear rate of energy transfer (LET). Again for electrons and photons the absorbed dose is weighted by the QF to obtain the total biological response in rem. For electrons and photons the QF is 1 like the RBE. The utility of the Dose Equivalent (dose weighted by QF) becomes apparent when comparisons of the radiation effects on man are made betweel electron or photon radiation and other radiations. Heavy elements can have QF's exceeding 20.

FLUX-DOSE CONVERSION METHODS FOR ELECTRONS

Much of the energy lost by electrons as they pass through a material is the result of ionization along the path. As the energy of the electron increases and/or the atomic number of the stopping medium increases the energy lost to bremsstrahlung becomes increasingly important. Since there is a good probability that the photons emitted in bremsstrahlung will not be reabsorbed near the site of emission, they typically are not included in dose calculations. The energy loss due to ionization can be calculated from the theory of Bethe and has been tabulated for different elements and chemical compounds by Berger and Seltzer[15] and more recently by L. Pages, et al.[24] The dose due to a flux of electrons can be calculated with the expression:

$$D\left(\frac{\text{rad}}{\text{sec}}\right) = 1.6 \times 10^{-8} \int_E (dE/dx)\phi(E)\, dE \quad ,$$

where dE/dx is the stopping power (MeV cm^2/g) due to ionization collisions in the stopping medium, $\phi(E)$ is the energy-dependent flux (electrons/$cm^2 \cdot$ sec $\cdot$ MeV), and the integration is over the spectrum of incident electrons. Values of the stopping power for aluminum, air, muscle, and bone are listed in Table C1.

A simple method of calculating the dose due to monoenergetic electrons has been suggested by Hill[73] in the following parametric form:

$$D(\text{Rad cm}^2/\text{electron}) = 1.6 \times 10^{-8} \frac{\alpha F}{\alpha X} = 6 \times 10^{-9} + 2.5 \times 10^{-8} E^{0.15}$$

where E is the electron energy in MeV. This expression is accurate to within 30 percent for most materials over the energy range from 100 keV to 10 MeV. Another expression for the tissue dose due to monoenergetic electrons is given by

$$D\ (\text{Rad cm}^2/\text{electron}) = 1.6 \times 10^{-8}\ [A \cdot E + B + C/E]$$

where E is in MeV

$$A = 0.0617$$

$$B = 1.612$$

and

$$C = 0.246$$

This expression is accurate to within 4% from 25 keV to 10 MeV.

TABLE C1. ELECTRON COLLISION STOPPING POWER

Electron Energy	Al	Air	Muscle	Bone
0.010	1.657E 01	1.970E 01	2.292E 01	2.101E 01
0.015	1.225E 01	1.441E 01	1.670E 01	1.536E 01
0.020	9.885E 00	1.155E 01	1.334E 01	1.231E 01
0.025	8.372E 00	9.733E 00	1.123E 01	1.037E 01
0.030	7.316E 00	8.475E 00	9.763E 00	9.030E 00
0.035	6.535E 00	7.548E 00	8.686E 00	8.041E 00
0.040	5.932E 00	6.835E 00	7.859E 00	7.281E 00
0.045	5.451E 00	6.269E 00	7.202E 00	6.678E 00
0.050	5.059E 00	5.808E 00	6.669E 00	6.186E 00
0.055	4.733E 00	5.425E 00	6.225E 00	5.778E 00
0.060	4.456E 00	5.101E 00	5.851E 00	5.434E 00
0.065	4.220E 00	4.824E 00	5.531E 00	5.139E 00
0.070	4.014E 00	4.585E 00	5.254E 00	4.883E 00
0.075	3.834E 00	4.375E 00	5.012E 00	4.660E 00
0.080	3.676E 00	4.190E 00	4.799E 00	4.463E 00
0.085	3.534E 00	4.026E 00	4.609E 00	4.288E 00
0.090	3.408E 00	3.879E 00	4.440E 00	4.131E 00
0.095	3.294E 00	3.747E 00	4.287E 00	3.990E 00
0.100	3.191E 00	3.627E 00	4.149E 00	3.862E 00
0.150	2.526E 00	2.856E 00	3.261E 00	3.041E 00
0.200	2.188E 00	2.466E 00	2.811E 00	2.623E 00
0.250	1.986E 00	2.233E 00	2.543E 00	2.374E 00
0.300	1.848E 00	2.081E 00	2.367E 00	2.210E 00
0.350	1.757E 00	1.975E 00	2.245E 00	2.097E 00
0.400	1.691E 00	1.899E 00	2.157E 00	2.015E 00
0.450	1.641E 00	1.843E 00	2.092E 00	1.953E 00
0.500	1.603E 00	1.800E 00	2.041E 00	1.906E 00
0.550	1.574E 00	1.766E 00	2.003E 00	1.869E 00
0.600	1.551E 00	1.740E 00	1.972E 00	1.840E 00
0.650	1.532E 00	1.720E 00	1.948E 00	1.817E 00
0.700	1.517E 00	1.704E 00	1.929E 00	1.799E 00
0.750	1.505E 00	1.691E 00	1.914E 00	1.784E 00
0.800	1.496E 00	1.681E 00	1.902E 00	1.772E 00
0.850	1.488E 00	1.673E 00	1.892E 00	1.763E 00
0.900	1.482E 00	1.667E 00	1.884E 00	1.755E 00

TABLE C1. (CONTINUED)

Electron Energy	Al	Air	Muscle	Bone
0.950	1.477E 00	1.662E 00	1.878E 00	1.749E 00
1.000	1.473E 00	1.659E 00	1.874E 00	1.744E 00
1.100	1.468E 00	1.655E 00	1.868E 00	1.738E 00
1.200	1.465E 00	1.653E 00	1.865E 00	1.734E 00
1.300	1.463E 00	1.654E 00	1.864E 00	1.733E 00
1.400	1.463E 00	1.656E 00	1.866E 00	1.734E 00
1.500	1.464E 00	1.659E 00	1.868E 00	1.735E 00
1.600	1.466E 00	1.663E 00	1.872E 00	1.737E 00
1.700	1.468E 00	1.667E 00	1.876E 00	1.741E 00
1.800	1.470E 00	1.672E 00	1.881E 00	1.744E 00
1.900	1.473E 00	1.677E 00	1.886E 00	1.748E 00
2.000	1.476E 00	1.683E 00	1.891E 00	1.752E 00
2.200	1.482E 00	1.694E 00	1.902E 00	1.761E 00
2.400	1.489E 00	1.705E 00	1.913E 00	1.770E 00
2.600	1.495E 00	1.716E 00	1.925E 00	1.779E 00
2.800	1.502E 00	1.728E 00	1.936E 00	1.788E 00
3.000	1.508E 00	1.738E 00	1.948E 00	1.797E 00
3.500	1.523E 00	1.764E 00	1.974E 00	1.819E 00
4.000	1.537E 00	1.789E 00	1.999E 00	1.839E 00
4.500	1.549E 00	1.811E 00	2.022E 00	1.858E 00
5.000	1.561E 00	1.831E 00	2.043E 00	1.875E 00
5.500	1.571E 00	1.851E 00	2.063E 00	1.890E 00
6.000	1.581E 00	1.868E 00	2.082E 00	1.905E 00
6.500	1.590E 00	1.885E 00	2.099E 00	1.919E 00
7.000	1.598E 00	1.901E 00	2.115E 00	1.932E 00
7.500	1.606E 00	1.915E 00	2.130E 00	1.943E 00
8.000	1.613E 00	1.929E 00	2.144E 00	1.955E 00
8.500	1.620E 00	1.942E 00	2.158E 00	1.965E 00
9.000	1.626E 00	1.955E 00	2.171E 00	1.975E 00
9.500	1.632E 00	1.966E 00	2.183E 00	1.985E 00
10.000	1.637E 00	1.978E 00	2.194E 00	1.994E 00

This stopping power corresponds to the energy lost by collision and excitation only. Radiative processes are excluded. The numbers were taken from the tabulations by Berger and Seltzer[15] and are quoted in units of (MeV · Cm^2/g).

FLUX-TO-DOSE CONVERSION FACTORS FOR PHOTONS

In the preceding section it was mentioned that the flux-to-dose conversion for electrons is relatively independent of the material in question. This occurs because the transport properties of electrons scale roughly with the material thickness in g/cm^2. Low energy photons interact mainly through the photoelectric effect which is strongly Z dependent. Flux-to-dose relationships for photons will, therefore, also be strongly Z dependent in the low energy region. Since photons undergo fewer interactions than electrons as they pass through matter and do not have the diffusive character of electrons, the conversion from flux to dose is less complicated.

One complication does arise, however, in the case of photon flux-to-dose relationships since photons must interact with electrons before ionization is produced. Consequently, the dose deposited at one point can be produced by electrons arriving from a photon interaction at another point. This means that the energy deposited at a given point depends on the amount and atomic number of material surrounding that point. Consider the case where a slab of material is exposed to a photon beam. Secondary electrons produced at the back edge of the material will leave the material producing little or no ionization in the volume of interest. Consider next, the case where the slab of material has additional material in front of it and the same flux of photons, as in the previous case. If the number of electrons which escape from the additional front material into the slab of interest is equal to the flux escaping from the back the situation is said to be in equilibrium. The dose in the slab of interest is higher in the second case where equilibrium exists. Energy absorption coefficients for photons are calculated for the equilibrium case since that assumes that if an electron recoils with a given amount of energy this energy will be deposited in the material. No correction for electrons leaving the volume of interest is made.

The conversion of flux to dose for several materials can be calculated using the tabulated energy absorption coefficients given in Table C2. The dose produced by monoenergetic photons of energy k in a material with atomic number Z is given by

$$D(k, Z) = kN(k) \cdot \mu_a(k, Z)\, 1.6 \times 10^{-8} \quad \text{(Rads)}$$

where k is the photon energy in MeV, N(k) is the photon flux (number of photons/cm^2 and μ_a (k, Z) is the energy absorption coefficient in cm^2/g. Again 1.6×10^{-8} is the conversion from MeV/g to rads.

TABLE C2. VALUES OF THE MASS ABSORPTION COEFFICIENT, μ_a, UNITS ARE cm^2/g[a]

Photon Energy [MeV]	$_1H$ μ_a/ρ	Al μ_a/ρ	$_{14}Si$ μ_a/ρ	Air μ_a/ρ	H_2O μ_a/ρ
0.01	0.00991	25.6	33.4	4.63	4.79
0.015	0.0110	7.48	9.78	1.27	1.28
0.02	0.0136	3.06	4.02	0.512	0.512
0.03	0.0186	0.868	1.14	0.148	0.149
0.04	0.0231	0.357	0.473	0.0669	0.0678
0.05	0.0271	0.184	0.241	0.0406	0.0419
0.06	0.0305	0.111	0.144	0.0305	0.0320
0.08	0.0362	0.0562	0.0701	0.0243	0.0262
0.10	0.0406	0.0386	0.0459	0.0234	0.0256
0.15	0.0481	0.0286	0.0312	0.0250	0.0277
0.2	0.0525	0.0276	0.0293	0.0268	0.0297
0.3	0.0569	0.0283	0.0294	0.0288	0.0319
0.4	0.0586	0.0287	0.0298	0.0295	0.0328
0.5	0.0590	0.0288	0.0298	0.0297	0.0330
0.6	0.0587	0.0286	0.0296	0.0296	0.0329
0.8	0.0574	0.0279	0.0289	0.0289	0.0321
1.0	0.0555	0.0270	0.0279	0.0280	0.0311
1.5	0.0507	0.0248	0.0257	0.0257	0.0285
2	0.0465	0.0233	0.0241	0.0238	0.0264
3	0.0400	0.0213	0.0221	0.0212	0.0234
4	0.0355	0.0201	0.0211	0.0194	0.0214
5	0.0320	0.0194	0.0204	0.0182	0.0200
6	0.0294	0.0190	0.0201	0.0174	0.0190
8	0.0255	0.0186	0.0197	0.0162	0.0176
10	0.0229	0.0185	0.0197	0.0156	0.0168

[a]From Ref. 65

The energy deposited in a given material is computed sufficiently accurately with the methods described above for most cases of interest to the space shielding community, with one possible exception. This occurs at the interface between two materials of very different atomic numbers. At such interfaces the secondary electrons produced by photons interacting with one material can leave that material and penetrate to the adjacent material where they come to rest. Photons lose energy more readily in high Z materials per unit mass so that more electrons are generated there than in lower Z materials. Consequently, the energy deposited per unit mass in the lower Z material is greater due to the increased flux of secondary electrons from the higher Z materials. A compensatory effect is observed in the high Z material where the dose is lower at the interface due to the decrease in current of secondary electrons from the low Z material.

In addition, the probability for the generation of secondary electrons is related to the angle between the photon and the emergent electron in that there are more electrons produced in the direction of the photon motion than in the other directions. This results in the dose perturbations at the interface being dependent on the direction that the photon crosses the interface. The dose at the interface of dissimilar materials has been studied experimentally by Wall and Burke[74] and further by Frederickson and Burke.[75] Examples of the dose deposition profiles they have measured at several interfaces are shown in Fig. C1 for different arrangements of materials and beam directions.

From these data it is apparent that the dose at a tungsten-aluminum interface can be increased by a factor of two in the low Z material. This effect occurs within 300 microns of the interface for 1.3 MeV photons. Consequently, the effect is only important where small dimensions are of interest. Examples of cases where the effect should be considered are: solid state electronic components where gold is sometimes bonded to silicon or iron-like surfaces, and the front surfaces of solar cells or solid state light detectors where a high Z conduction surface is frequently evaporated on to a low Z substrate.

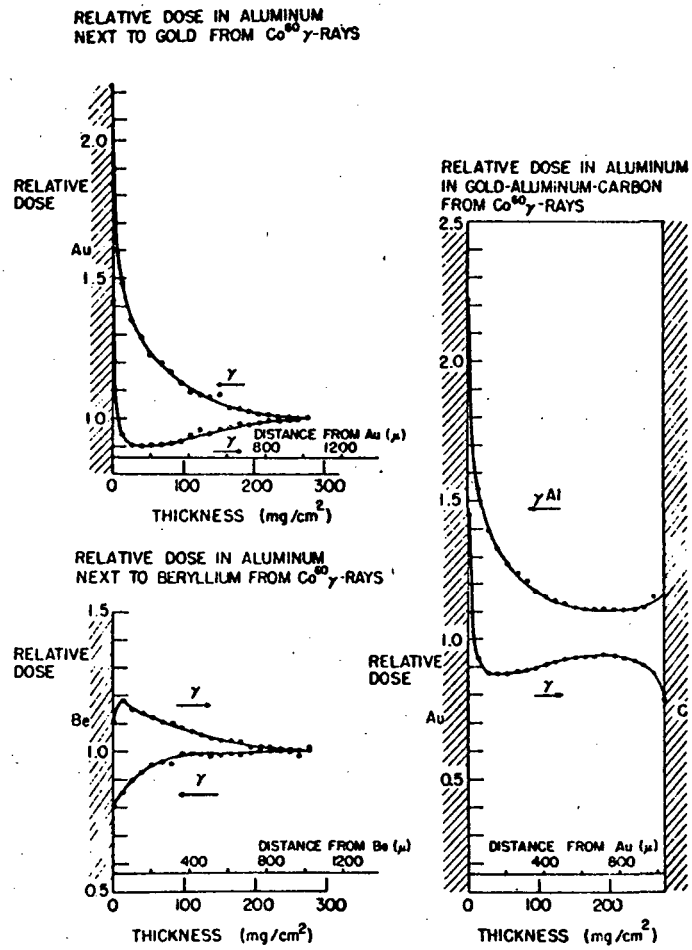

Figure C1. Air ionization measurements of the relative dose in aluminum next to gold, beryllium, and a gold-carbon combination.

REFERENCES

1. J. A. Van Allen, G. H. Ludwig, E. C. Ray and C. E. McIlwain, "Observations of High Intensity Radiation by Satellites 1958, Alpha and Gamma," Jet Propulsion 28, 1 (1958).

2. B. McCormac, Radiation Trapped in the Earth's Magnetic Field, D. Reidel Publishing Company, Dolrecht Holland (1966).

3. Treco, "An Orbital Integration Computer Program For Trapped Radiation," Documented by A. B. Lucero, Jan. 1968. Distributed by Radiation Shielding Information Center Oak Ridge National Laboratory.

4. H. Liemohn, "Radiation Belt Particle Orbits," Boeing Scientific Research Laboratories Report No. DI-82-0116, June 1961.

5. W. N. Hess, The Radiation Belts and Magnetosphere, Bliesdell Publishing Co. Waltham Mass. (1968).

6. C. E. McIlwain, "Coordinates for Mapping the Distribution of Magnetically Trapped Particles," J. Geophys. Res. 66, 3681 (1961).

7. W. N. Hess, Introduction to Space Science, Gordon and Breach Science Publishers, New York (1965).

8. Handbook of Geophysics and Space Environments, Editor S. L. Valley McGraw-Hill Book Company Inc. New York (1965).

9. J. I. Vette, A. B. Lucero and J. A. Wright, "Models of the Trapped Radiation Environment Vol. II Inner and Outer Zone Electrons," NASA SP - 3024 (1966).

10. E. G. Stassinopoulos, "World Maps of Constant B, L, and Flux Contours," NASA SP-3054 (1970).

11. J. I. Vette, "Models of the Trapped Radiation Environment Vol I Inner Zone Protons and Electrons," NASA SP-3042 (1966).

12. J. I. Vette, A. B. Lucero, "Models of the Trapped Radiation Environment Vol III Electrons at Synchronous Alitudes," NASA SP-3024 (1967).

13. C. Møller, "On the Theory of the Penetration of Fast Electrons through Matter," Ann Physik 14, 531 (1932).

14. R. D. Birkhoff, Handbuch der Physik, "The Passage of Fast Electrons through Matter," S. Flugge, ed. Springer-Verlag Berlin, Vol. 34 (1958).

15. M. J. Berger and S. M. Seltzer, "Tables of Energy Losses and Ranges of Electrons and Positrons," NASA SP-3012 (1964).

16. R. B. Leighton, Principles of Modern Physics, McGraw-Hill Book Compnay Inc. New York (1959).

17. W. C. Dickinson and E. M. Lent, "Calculation of Forward Bremsstrahlung Spectra from Thick Targets," UCRL-50442 June 1968.

18. L. Landau, "On the Energy Loss of Fast Particles by Ionization," J. Phys. USSR 8, 201 (1944).

19. T. Tabata, "Backscattering of Electrons from 3.2 to 14 MeV," Phys. Rev. 162, 336 (1967).

20. G. Moliere, Z. Naturforsch 3a, 78 (1948).

21. F. N. Huffman, J. S. Cheka, B. G. Saunders, R. H. Ritchie and R. D. Birkhoff, "Spatial Distribution of Energy Absorbed from an Electron Beam Penetrating Aluminum," Phys. Rev. 106, 435 (1957).

22. L. V. Spencer. "Energy Dissipation by Fast Electrons," NBS Monograph 2 National Bureau of Standards (1959).

23. J. A. Lonergan, C. P. Jupiter and G. Merkel, "Electron Energies Straggling Measurements for Thick Targets of Be, Al and Au at 4.0 and 8.0 MeV," J. Appl. Phys. 41, 678 (1970).

24. L. Pages, E. Bertel, H. Joffre and L. Sklavenitis, "Energy, Losses, Range, and Bremsstrahlung Yield for 10 keV to 100 MeV Electrons in Some Simple Elements and Some Chemical Compounds," ORNL-tr-2331, CEA-R-3942 (1970).

25. Engineering Compendium on Radiation Shielding Vol. 1, R. G. Jaeger, ed. Springer-Verlag New York Inc. (1968).

26. H. Bethe and W. Heitler, "On the Stopping of Fast Particles and the Creation of Positive Electrons," Proc. Roy. Soc. A146, 83 (1934).

27. D. H. Rester and W. E. Dance, "Electron-Bremsstrahlung Cross Section Measurements at Incident Electron Energies of 0.2, 1.0, 1.7 and 2.5 MeV," NAS8-21055, LTV Report 0-71000/8R-2 Part II, Feb. 1968.

28. W. E. Dance and D. H. Rester, "Electron Bremsstrahlung Produced in Thick Targets at Incident Energies of 0.2, 1.0, 2.0 and 2.8 MeV," NAS8-21055, LTV Report 0-71000/8R-2 Part III, Feb. 1968.

29. H. A. Bethe and J. Ashkin, Experimental Nuclear Physics, "Passage of Radiation through Matter," John Wiley and Sons Inc. New York (1953)

30. C. D. Zerby and F. L. Keller, "Electron Transport Theory, Calculations and Experiment," Nucl. Sci. and Eng. 27, 190 (1967).

31. Messiah, Quantin Mechanics Vol. II.

32. N. F. Mott, Proc. Roy. Soc. London Ser. A124, 425 (1929). A135, 429 (1932).

33. H. A. Bethe, "On the Theory of Penetration of Fast Corpuscular Radiation through Material," Ann. Physick 5, 325 (1930).

34. E. C. Bullard and H. S. Massey, "Remarks on the Scattering of Electrons by Atomic Fields," Proc. Cambridge Phil. Soc. 26, 556 (1930).

35. G. A. Goudsmit and J. L. Saunderson, "Theory of Electron Penetration," Phys. Rev. 57, 24 (1940) and Phys. Rev. 58, 36 (1940).

36. J. W. Motz, H. Olsen, and H. W. Koch, "Electron Scattering without Atomic or Nuclear Excitation,". Rev. Mod. Phys. 36, 881 (1964).

37. H. W. Koch and J. W. Motz, "Bremsstrahlung Cross-Section Formulas and Related Data," Rev. Mod. Phys. 31, 920 (1959).

38. H. Brysk, C. D. Zerby, and S. K. Penny, "Bremsstrahlung Cross Sections at Moderate Energies," Phys. Rev. 180, 104 (1969).

39. H. K. Tseng and R. H. Pratt, "Comments on the Calculation of Relativistic Bremsstrahlung Cross Sections," Phys. Rev. A1, 528 (1970).

40. G. Elwert and E. Haug, "Calculation of Bremsstrahlung Cross Section with Sommerfeld-Maua Eigenfunctions," Phys. Rev. 183, 90 (1969).

41. J. Blunck and S. Leisegang, "Zum Energiererlust Schneller Elektronen in Dunnen Schichten," Z. Physik 128, 500 (1950).

42. H. Snyder and W. T. Scott, "Multiple Scattering of Fast Charged Particles," Phys. Rev. 76, 220 (1949).

43. W. T. Scott, "The Theory of Small-Angle Multiple Scattering of Fast Charged Particles," Rev. Mod. Phys. 35, 231 (1963).

44. A. Sirlin, "Spectrum of Target Bremsstrahlung at Small Angles," Phys. Rev. 106, 637 (1957).

45. G. Ialongo, "Thick-Target Bremsstrahlung from Electrons with an Energy Spectrum and an Angular Distribution," Aerospace Report No. TR-0066(5260-20)-2 Dec. 1969.

46. C. Robert Emigh, "Thick Target Bremsstrahlung Theory," Los Alamos Scientific Laboratory Report LA-4097-MS (1970).

47. H. Ferdinade, G. Knuyt, R. Van De Vijver and R. Jacobs, Numerical Calculation of Absolute Forward Thick-Target Bremsstrahlung Spectra," Nucl. Instr. and Methods 91, 135 (1971).

48. W. W. Scott, "Electron-Bremsstrahlung Differential Cross Sections for Thin and Thick Targets," NASA TN D-2659 March 1965.

49. W. W. Scott, "Angular Distributions of Thick Target Bremsstrahlung Compared with Experiment in Protection against Space Radiation," A. Reetz Jr. ed. NASA SP-169, p. 339 (1968).

50. L. V. Spencer, "Theory of Electron Penetration," Phys. Rev. Second Ser. 98, 1597 (1955).

51. C. D. Zerby and H. S. Moran, "Studies of the Longitudinal Development of Electron-Photon Cascade Showers," J. Appl. Phys. 34, 2445 (1963).

52. J. F. Perkins, "Monte Carlo Calculation of Transport of Fast Electrons," Phys. Rev. 126, 1781 (1962).

53. M. J. Berger and S. M. Seltzer, "Monte Carlo Code System for Electron and Photon Transport through Extended Media," National Bureau of Standards Reports NBS-9836 (1968) and NBS-9837 (1968).

54. L. D. Buxton, "The Electron Transport Computer Code ZEBRA I," HDL-TR-1536, June 1971.

55. P. E. Bartine et al., "Low-Energy Electron Transport by the Method of Discrete Ordinates," ORNL-TM-3438 (1971).

56. P. J. Ebert, A. F. Lanzon and E. M. Lent, "Transmission and Backscatter of 4.0 to 12.0 MeV Electrons," Lawrence Radiation Laboratory Report No. UCRL-71462, Dec. 1968.

57. B. W. Mar, American Nuclear Society Transactions, "Electron Shielding for Space Vehicles," 7, 322 (1964).

58. J. W. Watts Jr. and M. O. Burrell, "Electron and Bremsstrahlung Penetration and Dose Calculations," NASA TMX-2440 and NASA TND 6385.

59. ETRAN, "Monte Carlo Code System for Electron and Photon Transport Through Extended Media," Available through RSIC CCC-107.

60. L. Katz and A. S. Penfold, "Range-Energy Relations for Electrons and the Determinations of Beta-Ray End-Point Energies by Absorption," Rev. Mod. Phys. 24, 28, (1952).

61. D. G. Costello, H. Weber and J. A. Lonergan, "Electron Shielding Studies," Gulf General Atomic Report GA 9907 (1970).

62. D. H. Rester and W. J. Rainwater Jr., "Measurement of Electron Scattering at 1 MeV for Non-Normal Incidence," Ling-Temco-Vought Report No. 0-71000/8R-2 Part I, Feb. 1968.

63. H. A. Bethe, M. E. Rose and L. P. Smith, "The Multiple Scattering of Electrons," Proc. Amer. Phil. Soc. 78, 573 (1938).

64. D. H. Rester, "Bremsstrahlung Production and Electron Transmission Studies for Electron Beams of Non-Normal Incidence," Ling-Temco-Vought Report No. 0-71100/9R-1, Part I Feb. 1969.

65. M. J. Berger and S. M. Seltzer, "Penetration of Electrons and Associated Bremsstrahlung Through Aluminum Targets," in Protection Against Space Radiation, NASA SP-169, p. 285 (1968).

66. Alpha-Beta-Gamma-Ray Spectroscopy, Vol. 1, Ed. K. Siegbahm, North Holland Pub. Co. (1968).

67. J. H. Hubbell and M. J. Berger, "Attenuation Coefficients, Energy Absorption Coefficients, and Related Quantities," Engineering Compendium on Radiation Shielding, Vol. I Chapter 4, R. G. Jaeger ed. Springer-Verlag New York Inc. (1968).

68. R. T. Berger, "The X- or Gamma-Ray Energy Absorption or Transfer Coefficient: tabulations and discussion," Radiation Research 15, 1 (1961).

69. A. B. Chilton,"Broad Beam Attenuation," in Engineering Compendium on Radiation Shielding, Vol. I. R. G. Jaeger ed. Springer-Verlag New York Inc. (1968).

70. M. O. Burrell and J. W. Watts, "Plane Isotropic Buildup Factors for Bremsstrahlung Calculations," NASA TN D-4096 Aug. 1967.

71. O. Klein and Y. Nishina, "On the Scattering of Radiation by Free Electrons according to the Relativistic Quantum Mechanics of Dirac," Z. Physik 52, 853 (1929).

72. J. W. Motz, Quarterly Progress Report, Dec. 1969-Mar. 1970, Applied Radiation Division Center for Radiation Research, National Bureau of Standards, Washington, D.C.

73. TREE (Transient-Radiation Effects on Electronics) Handbook, Ed. J. J. Kalinowski and R. K. Thatcher, DASA 1420, Sept. 1969.

74. Radiation Effects Information Center, Battelle Memorial Institute, 505 King Ave., Columbus, Ohio.

75. C. W. Hill, W. B. Ritchie, and K. M. Simpson Jr., "Data Compilation and Evaluation of Spare Shielding Problems," Vol. III, Radiation Hazards in Space, Lockheed Report, ER 7777, April 1966.

76. J. W. Wall and E. A. Burke, "Gamma Dose Distribution at and Near the Interface of Different Materials," IEEE Nucl. Sci. Trans., Dec. 1970, p. 305.

77. A. R. Frederickson and E. A. Burke, "Ionization, Secondary Emission and Compton Currents at Gamma Irradiated Interface," IEEE Nucl. Sci. Trans., Dec. 1971, p. 162.